ACTIVE VIBRATION CONTROL AT MACHINERY FEET

Michael Wai Shing Lau

Doctor of Philosophy

ASTON UNIVERSITY

January 2000.

ASTON UNIVERSITY

ACTIVE VIBRATION CONTROL AT MACHINERY FEET

By

Michael Wai Shing Lau

A thesis submitted for the degree of Doctor of Philosophy, 2000

The unmitigated transmission of undesirable vibration can result in problems by way of causing human discomfort, machinery and equipment failure, and affecting the quality of a manufacturing process. When identifiable transmission paths are discernible, vibrations from the source can be isolated from the rest of the system and thus prevents or minimises the problems. The approach proposed here for vibration isolation is active force cancellation at points close to the vibration source. It uses force feedback for multiple-input and multiple-output control at the mounting locations. This is particularly attractive for rigid mounting of machine on relative flexible base where machine alignment and motions are to be restricted.

The force transfer function matrix is used as a disturbance rejection performance specification for the design of MIMO controllers. For machine soft-mounted via flexible isolators, a model for this matrix has been derived. Under certain condition, a simple multiplicative uncertainty model is obtained that shows the amount of perturbation a flexible base has on the machine-isolator-rigid base transmissibility matrix. Such a model is very suitable for use with robust control design paradigm. A different model is derived for the machine on hard-mounts without the flexible isolators. With this model, the level of force transmitted from a machine to a final mounting structure using the measurements for the machine running on another mounting structure can be determined. The two mounting structures have dissimilar dynamic characteristics. Experiments have verified the usefulness of the expression. The model compares well with other methods in the literature. The disadvantage lies with the large amount of data that have to be collected.

Active force cancellation is demonstrated on an experimental rig using an AC industrial motor hard-mounted onto a relative flexible structure. The force transfer function matrix, determined from measurements, is used to design $\mathcal{H}_\infty$ and Static Output Feedback controllers. Both types of controllers are stable and robust to modelling errors within the identified frequency range. They reduce the RMS of transmitted force by between 30~80% at all mounting locations for machine running at 1340 rpm. At the rated speed of 1440 rpm only the static gain controller is able to provide 30~55 % reduction at all locations. The $\mathcal{H}_\infty$ controllers on the other hand could only give a small reduction at one mount location. This is due in part to the deficient of the model used in the design. Higher frequency dynamics has been ignored in the model. This can be resolved by the use of a higher order model that can result in a high order controller. A low order static gain controller, with some tuning, performs better. But it lacks the analytical framework for analysis and design.

Keywords

Vibration isolation, Active Force Cancellation, MIMO Robust Vibration Control.

TO JENNY, KRISTEN, ALEX, DAD AND MUM
FOR YOUR PATIENCE AND ENCOURAGEMENT
TO PERSERVE AND COMPLETE THIS PIECE OF WORK

ACKNOWLEDGEMENT

The author wishes to thank all those who have in many ways provided assistance and moral support during the period of the project. They are many friends who have given their precious time and attention in helping me to sort out some difficult problem.

In particular, my gratitude to my supervisor Dr. S.D. Garvey who has given me much encouragement and enlightenment derived from the many discussions we had. Also to Dr. JET Penny who had helped me to get started in Aston University, and Dr. N. Sundararajan of NTU for his advice.

Technical assistance especially during the late hours is most cherished. In such instance, I have to thank in particular Wai Mun, Hock Tee, Han Woon and the other staff members and friends.

Special thanks to my friends, Gerald, Eicher and Sean for their unwavering support and for having to suffer the agony of proof reading my draft thesis. Last but not least, not to forget the unforgettable and sometimes painful words of wisdom from G.R. and Ted.

CONTENTS

		Page
Summary		ii
Dedication		iii
Acknowledgement		iv
List of Contents		v
List of Figures		x
List of Tables		xv
Nomenclature		xvi
1	**Introduction**	
	1.1 Vibration control problems	2
	1.2 Active force cancellation for soft-mounted machine	7
	1.3 Determining the force transmitted from a machine on hard-mounts.	8
	1.4 An experimental demonstration of active force cancellation using hard mounts	9
2	**A Review of Selected Active Vibration Control Topics and Results of Preliminary Experiments.**	
	2.1 Introduction	13
	2.2 Active Vibration Control	13
	2.2.1 Active vibration control of the disturbance source	15
	2.2.2 Active vibration control of the receiver region	16
	2.2.3 Active vibration control of the transmission paths	21
	2.3 A Review of Sensors and Control Devices in Active Vibration Control	
	2.3.1 Dynamic vibration absorbers	29
	2.3.2 Proof-mass actuators	30
	2.3.3 Actuators used in active vibration isolation	31
	2.4 Sensed Variables and Plant Model	33
	2.5 Preliminary Works	37
	2.6 Summary	41

3 **Modelling and Control of Active Vibration Isolation of a Machine Soft-mounted on a Flexible Base Structure at Multiple Points.**

3.1 Introduction 44

3.2 Motivation 45

3.3 The Classical 1-DoF Model 48

3.4 Extension to m-DoF

3.4.1 Machine model mounted on n-isolators on a rigid base 50

3.4.2 Effect of base flexibility when disturbance is applied at the machine c.g. 52

3.4.3 A more useful model 55

3.5 Discussion 57

3.5.1 The spectral norm as a measure of magnitude of force transmissibility matrix 57

3.5.2 The effect of the coupled stiffness term ($\mathbb{D}_f$+$\mathbb{K}$) on Δ_M 58

3.5.3 The spectral norm of the perturbation term Δ_M 59

3.5.4 The implication of the term $\delta \cdot \mathbb{R}_{em}$ 61

3.6 Example of a Machine on a Flexible Beam 63

3.7 Reduction to 1-DoF and Comparison with Blackwood and von Flotow's work 66

3.8 Implication on Control Design 70

3.9 Summary 74

4 **The Determination of Transmitted Force of a Machine Hard-mounted onto a Final Structure using a Dissimilar Test Structure.**

4.1 Introduction 77

4.2 The need for machine to be hard-mounted 78

4.3 The set of equivalent forces at the feet 79

4.4 The force transmitted to the mounting 82

4.5 The combined dynamic stiffness and the combined receptance matrices 85

4.6 An example: A single DoF mounting using (4.14) 86

4.7 Experimental set-up to determine the force transmitted 88

4.8 Results of an experiment using the proposed Method 1 93
4.9 Results using Method 2 and Method 3 99
4.10 General comments on the proposed method (Method 1) 104
4.11 Summary 108

5 **Identification of the Force Transmissibility Matrix of a Machine Hard-mounted onto a Structure.**
5.1 Introduction 111
5.2 Active control of machine hard-mounted onto a foundation 112
5.3 Experimental Model
5.3.1 The hardware description 115
5.3.2 Plant identification 118
5.3.3 The Maximum Likelihood Estimator 120
5.3.4 Input signal for excitation 121
5.3.5 Estimation of the system disturbance transfer function matrix 124
5.3.6 Conversion to State-space model {**A**,**B**,**C**,**D**} 130
5.4 Model reduction 130
5.5 Comparing $\mathbf{G}_{12}$ model time responses with measured time responses. 140
5.6 Actuator Model 147
5.7 Summary 148

6 **Active Vibration Control of a Machine Hard-mounted onto a Structure using Force Cancellation and Force Transmissibility Matrix as a Performance Specification**
6.1 Introduction 152
6.2 Controller Design Objectives 152
6.3 Force transmissibility function as a performance objective 153
6.4 The H-infinity ($\mathcal{H}_\infty$) design approach 157
6.5 The design of a $\mathcal{K}_{28}$ controller using the $\mathbf{G}_{12}$ model 161
6.6 The design of a $\mathcal{K}_8$ controller using the $\mathbf{G}_{154}$ model 166
6.7 Static Output Feedback design 169

6.8 Controller Implementation 178
6.9 Experimental results 179
6.9.1 Experimental results using the $\mathcal{Z}_{28}$ controller 180
6.9.2 Experimental results using the $\mathcal{Z}_{8}$ controller 182
6.9.3 Experimental results using the $\mathcal{Z}_{optim1}$ and the $\mathcal{Z}_{4}$ controller 182
6.10 Discussions 186
6.11 Analogue controllers 192
6.12 Hybrid implementation – the use of thermoplastic material as a passive element 193
6.13 Summary 194

7 **Conclusions and Recommendations**
7.1 Conclusion 197
7.2 Recommendations and suggestions for future work 201

8 **References** 204

APPENDICES

A Model of a Passive Isolator
A.1 Introduction 213
A.2 Mount 4-pole parameter
A.2.1 General case 213
A.2.2 Special case 214
A.3 A general model of a mount or isolator with 6-DoFs 215
A.4 Model of a 3 DoF isolator 216
A.5 Summary 217

B **Model of a Machine Mounted on a Flexible Beam at Two Points**
B.1 Example model 219
B.2 Model parameters 219
B.3 Model equations 220
B.4 Summary 222

C **Transfer Function Frequency Response Plots of Measured and Estimated G_p** 223

D **Small Gain Theorem**

D.1 Introduction 241

D.2 Theorem D.1 Generalised (MIMO) Nyquist Theorem 241

D.3 Theorem D.2 The Small Gain Theorem (one version) 242

D.4 Equivalence of robust stability and $\mathcal{H}_\infty$ control problem 243

D.5 Application to the vibration problem of chapter three 244

D.6 Summary 245

E **Analogue Controller Circuit and the Responses at 1330 and 1440 rpm.** 246

LIST OF FIGURES

Figures	Title	Page
2.1	Region for which vibration control can be implemented	14
2.2	Vibration control at the receiver region	16
2.3	Vibration control along the transmission paths	21
2.4	Active vibration control in a car model	23
2.5	Active vibration isolation: local feedback	24
2.6	Principle of active force cancellation	27
2.7	Types of dampers	30
2.8	Dynamic response of an ideal proof mass actuator	32
2.9	Actuators arrangement	33
2.10	Arrangement of actuators, sensors and mounts	35
2.11	Active force cancellation at the feet of a machine	36
2.12	Active pendulum DVA for an unbalanced rotor	37
2.13	Calibration for rod length versus frequency	37
Photo 2.1	Machine vibrating at point indicated	38
Photo 2.2	Effect of the active DVA on the vibrating machine	38
2.14	The effect of active DVA on measured RMS	39
2.15	A rig for a 1-DoF AVC using motion feedback and force actuation	39
2.16	Time response of a 1-DoF active vibration experiment	40
3.1	System definition and symbols	45
3.2	Forces and displacements on a rigid machine	50
3.3	Interpretations of $\mathbf{R}_{em}$ and $\mathbf{R}_{mf}$	63
3.4a	Plots of $\overline{\sigma}(\delta \cdot R_{em})$, $\overline{\sigma}(\Delta_M)$ & $\overline{\sigma}(K \cdot R_{mf})$ for soft isolators	64
3.4b	Perturbed model versus actual plant model for soft isolators	64
3.5a	Plots of $\overline{\sigma}(\delta \cdot R_{em})$, $\overline{\sigma}(\Delta_M)$ & $\overline{\sigma}(K \cdot R_{mf})$ for stiffer isolators	65
3.5b	Perturbed model versus actual plant model for stiffer isolators	65
3.6	A block diagram for equation (3.26)	71
3.7	Equivalent LFT block diagram for Figure 3.6	71
3.8	The M-Δ block diagram	73
4.1	Model of the machine and the test-bed	87
4.2	Model of the final mounting	87

4.3	Forces, Q_{e1}, at test-bed and Q_{e2}, at final mounting	89
4.4	Displacements, q_{e1}, at test-bed and q_{e2}, at final mounting	89
4.5	Ratio of Q_{e2}/q_{e1} and R_{f1}	90
4.6	Set-up for the measurement of $\mathbf{R}_e$ and $\mathbf{q}_e^0$	90
4.7	Set-up for the measurement of $\mathbf{R}_{ef1}$ and $\mathbf{q}_{e1}$	92
4.8	Set-up for the measurement of $\mathbf{R}_{f2}$ and $\mathbf{R}_{ef2}$	92
4.9a	Measurement of element (1) and (2) of vector $\mathbf{q}_{e1}$ of displacements at the works for motor running at 1440 rpm	94
4.9b	Measurement of element (3) and (4) of vector $\mathbf{q}_{e1}$ of displacements at the works for motor running at 1440 rpm	95
4.10	Load cell measurement of Q_{e2} for motor running at 1440 rpm	97
4.11	Calculated Q_{e2} using Method 1 for motor running at 1440 rpm	97
4.12	Normalised measured Q_{e2} for motor running at 1440 rpm	98
4.13	Normalised calculated Q_{e2} using Method 1 for motor running at 1440 rpm	98
4.14	Calculated Q_{e2} using $[(\mathbf{R}_{f2})^{-1}+(\mathbf{R}_e)^{-1}]^{-1}$ for motor running at 1440 rpm	100
4.15	Normalised calculated Q_{e2} using $[(\mathbf{R}_{f2})^{-1}+(\mathbf{R}_e)^{-1}]^{-1}$ for motor running at 1440 rpm	100
4.16a	Elements (1) and (2) of vector $\mathbf{q}_e^0$ of displacements measured at the four feet of the machine operating at 1440 rpm.	101
4.16b	Elements (3) and (4) of vector $\mathbf{q}_e^0$ of displacements measured at the four feet of the machine operating at 1440 rpm.	102
4.17	Calculated Q_{e2} using Method 2 for motor running at 1440 rpm	103
4.18	Calculated Q_{e2} using Method 3 for motor running at 1440 rpm	103
4.19	Product of norms of matrices of the right side of (4.14)	107
4.20	Norm of $\mathbf{Q}_{e2}$ of (4.14)	107
5.1	Side view of the plant or system used in the experiment	115
Photo 5.1	Side view of the motor on the plate	116
Photo 5.2	Front view of the motor on the plate	116
5.2	Hard mount design	117
5.3	Frequency response of rigid mount, measured at its centre	117
5.4	Block diagram of the target system	118

5.5	A system model for the control of the rig shown in Figure 5.1	119
5.6	Spectrum of the multi-sine and periodic chirp	122
5.7	One period of the multi-sine excitation signal	124
5.8	System identification set-up	125
5.9a	Bode plots of ICATS fitted curves with measured g_{i2} curves	126
5.9b	Bode plots of ICATS fitted curves with measured g_{i2} curves	127
5.10	Bode plot of element g_{32} before reduction to lower order	129
5.11	Bar graph of the Hankel singular values in descending order	134
5.12	Plots of $\bar{\sigma}(\mathbf{G}_{12})$, $\bar{\sigma}(\mathbf{G}_{154})$ and (factor$\cdot \sum_{i,j=1}^{4} \lvert g_{ij} \rvert$)	135
5.13	Magnitude plots of measured g_{i1} and g_{i1} of $\mathbf{G}_{12}$.	136
5.14	Magnitude plots of measured g_{i2} and g_{i2} of $\mathbf{G}_{12}$.	136
5.15	Magnitude plots of measured g_{i3} and g_{i3} of $\mathbf{G}_{12}$.	137
5.16	Magnitude plots of measured g_{i4} and g_{i4} of $\mathbf{G}_{12}$.	137
5.17	Time response plot of $\mathbf{G}_{12}$ to sine input of 1440 rpm	141
5.18	Time response plot of $\mathbf{G}_{12}$ to sine input of 1320 rpm	141
5.19	Time response plot of $\mathbf{G}_{12}$ to a 1440 rpm sine wave with band limited noise	143
5.20	Measured response of system at 1440 rpm.	143
5.21	Time response plot of $\mathbf{G}_{12}$ to a 1340 rpm sine wave with band limited noise	144
5.22	Measured response of system at 1340 rpm.	144
5.23	Spectral plot of mount #2 sensor at 1460 rpm	146
5.24	Frequency response plot of the GWV4 shaker with 0.25 kg mass	147
6.1	Block diagram of the target system	154
6.2	$\mathbf{W}_2$ as a disturbance rejection performance specification	155
6.3	Block diagram of the weighted system model	158
6.4	Maximum singular values of $\mathbf{G}_p$ and $\mathbf{T}_{yd}$	163
6.5	Weighting function w_{ii} of $\mathbf{W}_2^{-1}$ against g_{ii} of $\mathbf{G}_p$ for case I	164
6.6	Maximum singular values of $\mathbf{G}_p$ and $\mathbf{T}_{yd}$ using $\mathcal{K}_{28\_I}$	164
6.7	Weighting function w_{ii} of $\mathbf{W}_2^{-1}$ against g_{ii} of $\mathbf{G}_p$ for case II	165
6.8	Maximum singular values of $\mathbf{G}_p$ and $\mathbf{T}_{yd}$ using $\mathcal{K}_{28\_II}$	165
6.9	Maximum singular values of $\mathbf{G}_p$ and $\mathbf{T}_{yd}$ using $\mathcal{K}_8$	168
6.10	Maximum singular values of $\mathbf{G}_p$ and $\mathbf{T}_{yd}$ using $\mathcal{K}_{12}$	168

6.11	Responses at 1440 rpm with $\mathcal{K}$=-0.72$\mathbf{D}_p^{-1}$ w/o actuators' dynamics	171
6.12	Maximum singular values of $\mathbf{G}_p$ and $\mathbf{T}_{yd}$ using $\mathcal{K}$=-$\mathbf{D}_p^{-1}$	173
6.13	Singular values of the sensitivity function $\mathbf{S}$ for α=1.5	177
6.14	Maximum singular values of $\mathbf{G}_p$ and $\mathbf{T}_{yd}$ using $\mathcal{K}_{optim1}$	177
6.15	Control Loop Schematic	179
6.16	Responses using $\mathcal{K}_{28}$ for motor running at 1340 rpm	181
6.17	Responses using $\mathcal{K}_{28}$ for motor running at 1440 rpm	181
6.18	Responses using $\mathcal{K}_8$ for motor running at 1300 rpm	183
6.19	Responses using $\mathcal{K}_8$ for motor running at 1340 rpm	183
6.20	Maximum singular values of $\mathbf{G}_p$ and $\mathbf{T}_{yd}$ using $\mathcal{K}_4$	184
6.21	Responses using $\mathcal{K}_4$ for various speeds	185
6.22	Maximum singular values of $\mathbf{G}_p$ and $(\mathbf{T}_{yd})_4$ for $\mathcal{K}_4$ and $(\mathbf{T}_{yd})_{28}$ for $\mathcal{K}_{28}$	188
6.23	Power spectrum of mount #3 using $\mathcal{K}_{28}$ at 1340 rpm	190
6.24	Power spectrum of mount #3 using $\mathcal{K}_8$ at 1320 rpm	190
6.25	Power spectrum of mount #3 using $\mathcal{K}_4$ at 1320 rpm	191
6.26	Power spectrum of mount #3 using $\mathcal{K}_4$ at 1440 rpm	191
6.27	Active (analogue controller) at mount #4 for motor at 1440 rpm	193
6.28	Active plus passive element at mount #4 for motor at 1440 rpm	194
A.1	Forces and displacements of an isolator	213
A.2	Displacements and angular displacements of an isolator	215
B.1	A model of a machine mounted at two points on a flexible beam	219
C.1a	Bode plots of g_{11} and g_{21} of measured and ICATS fit	224
C.1b	Bode plots of g_{31} and g_{41} of measured and ICATS fit	225
C.2a	Bode plots of g_{12} and g_{22} of measured and ICATS fit	226
C.2b	Bode plots of g_{32} and g_{42} of measured and ICATS fit	227
C.3a	Bode plots of g_{13} and g_{23} of measured and ICATS fit	228
C.3b	Bode plots of g_{33} and g_{43} of measured and ICATS fit	229
C.4a	Bode plots of g_{14} and g_{24} of measured and ICATS fit	230
C.4b	Bode plots of g_{34} and g_{44} of measured and ICATS fit	231
C.5a	Bode plots of g_{11}, g_{21} of Measured, $\mathbf{G}_{154}$ and $\mathbf{G}_{12}$	232
C.5b	Bode plots of g_{31}, g_{41} of Measured, $\mathbf{G}_{154}$ and $\mathbf{G}_{12}$	233
C.6a	Bode plots of g_{12}, g_{22} of Measured, $\mathbf{G}_{154}$ and $\mathbf{G}_{12}$	234

C.6b	Bode plots of g_{32}, g_{42} of Measured, $\mathbf{G}_{154}$ and $\mathbf{G}_{12}$	235
C.7a	Bode plots of g_{13}, g_{23} of Measured, $\mathbf{G}_{154}$ and $\mathbf{G}_{12}$	236
C.7b	Bode plots of g_{33}, g_{43} of Measured, $\mathbf{G}_{154}$ and $\mathbf{G}_{12}$	237
C.8a	Bode plots of g_{14}, g_{24} of Measured, $\mathbf{G}_{154}$ and $\mathbf{G}_{12}$	238
C.8b	Bode plots of g_{34}, g_{44} of Measured, $\mathbf{G}_{154}$ and $\mathbf{G}_{12}$	239
D.1	A unity feedback system	241
D.2	The $\mathbf{M}$-Δ block	243
D.3	General LFT framework	244
E.1	The variable phase shifter circuit used as a local analogue controller in active vibration isolation experiment	247
E.2	Responses at mount locations using analogue controller at 1340 rpm	248
E.3	Responses at mount locations using analogue controller at 1440 rpm	249

LIST OF TABLES

Tables	Title	Page
2.1	Various combinations of input variables and output variables	34
3.1	Comparison of $\delta \cdot R_{em}$, Δ_M and $k \cdot R_f$	69
4.1	Machine variables	87
4.2	Test-bed and final mount parameters	87
4.3	Comparison between measured and calculated Q_{e2} at selected peaks	96
5.1	Modal frequencies and damping factors of $\mathbf{G}_{12}$	139
5.2	Comparison of a damping value of the ICATS and MLE model	140
6.1	Values of w_{ii} defined for $\mathbf{W}_2$	167
6.2	Results of $\mathcal{Z}_{28}$ and $\mathcal{Z}_8$ at four mounts for motor speed of 1340 rpm	187
6.3	Results of $\mathcal{Z}_4$ at two speeds for the four mounting locations	188
A.1	Values of stiffness of an isotropic isolator	216
B.1	Model parameters	219

NOMENCLATURE

The list summarises the notations used through out the thesis. In some chapters, typically Chapter Three and Chapter Four some notations are redefined to best represent their meanings. Alternative definitions are given in brackets. In general, symbols in **CAPITAL BOLD** letters denote matrices and vectors. In some cases, small letters with underscore and in italic are used to represent vectors. This is to conform to the standard notations found in the respective vibration, modal analysis and control literature.

$\mathbf{A}$	State matrix of a state space model realisation ($\mathbf{A}$,$\mathbf{B}$,$\mathbf{C}$,$\mathbf{D}$) of $\mathbf{G}$.
$\mathbf{B}$	Input matrix
$\mathbf{C}$	Damping matrix (Output matrix)
$\mathbf{D}$	Dynamic stiffness matrix (Direct input matrix)
$\mathbf{G}$	Transfer function or Force transmissibility matrix
$\mathbf{I}$	Identity Matrix (dimension to be defined)
$\mathbf{J}$	Mass inertia matrix
$\mathcal{K}$	Controller matrix
$\mathbf{K}$	Stiffness matrix
$\mathbf{M}$	Mass matrix
$\mathbf{P}$	Matrix containing the location of isolators
$\mathcal{P}$	Generalised plant model
$\mathbf{R}$	Receptance matrix equals to the inverse of [$\mathbf{D}$]
$\mathbf{S}$	Sensitivity Function matrix
$\mathbf{L}$	Loop transfer function matrix
$\mathbf{F}$	Return difference matrix
$\mathbf{T}$	Closed loop transfer function matrix
$\mathbf{Y}$	Mobility matrix
Δ	Error or perturbation matrix
$\mathbf{Q}$	Vector of force and moments
$\mathbf{X}$	Vector of linear displacements

m	Mass of a rigid body
c	Damping factor
$\underline{d}$	Vector of disturbances
$\underline{y}$	Vector of outputs of a system
$\underline{z}$	Vector of outputs of a system
$\underline{u}$	Controller's output
f	frequency, Hz
j	Imaginary number = $\sqrt{-1}$
k	Spring (dissipative) stiffness
n	Isolator loss factor
$\mathbf{q}$	Vector of displacements and rotations
s	Laplace variable
t	Time variable, sec
Ξ	Vector of angular displacements
υ,ϖ,ω	Angular velocities in the x-, y- and z-directions respectively
ω	Angular frequency, rad/sec
ϕ	Mass normalised mode shapes
ζ	Modal damping factor or damping factor
$\mathbf{A}^T$ and $\mathbf{A}^*$	Transpose and complex conjugate transpose of $\mathbf{A}$
$\lambda(\mathbf{A})$	Eigenvalues of matrix $\mathbf{A}$
$\rho(\mathbf{A})$	Spectral radius of $\mathbf{A}$
$\kappa(\mathbf{A})$	Condition number of $\mathbf{A}$
$\bar{\sigma}(\mathbf{A})$ & $\underline{\sigma}(\mathbf{A})$	Largest and smallest singular values of $\mathbf{A}$
$\|\mathbf{A}\|_s$	Spectral norm of a matrix $\mathbf{A}$: $\|\mathbf{A}\|_s = \bar{\sigma}(\mathbf{A})$

CHAPTER ONE

INTRODUCTION

1.1 Vibration Control Problems

In some instances vibration is intentionally generated to move and orientates machine parts in a vibratory bowl and to rock a bucking horse in a shopping mall for example. In most cases, vibration is a problem when as an undesirable or unintended motion, it causes human discomfort, machinery and equipment failure, poor yield in a manufacturing process, and possibly loss of lives, for example if a submarine fails to evade detection because it is has undesirable vibratory motions. In these cases it is necessary to control vibratory motion. It is almost impossible to stop vibratory responses in some cases, as the causes of vibration are usually a by-product of a primary process. A machine in operation generates a continuous disturbance that causes undesirable vibratory responses in other parts of the system. It can only be completely reduced to zero when the machine is stopped. Vibration control is then applied to reduce the undesirable vibratory responses to some acceptable levels. A space structure is manoeuvred into position by firing selected rocket thrusters. The desired rigid body response is accompanied by undesirable flexible mode responses because the space structure has to be designed to be relatively light using trusses and beams. The vibration control problem here is to decide how to effect a rapid reduction of vibratory responses in the shortest time possible. Unlike the former example, the disturbance normally occurs as discrete events.

The case of continuous disturbances can be regarded as a steady-state vibration control problem whereas the case of discrete event disturbances is very much a transient or impulse response problem. The amount of reduction and the speed of reduction depend very much on the cost of implementing the control versus the cost of failing to implement the control that can result in the loss of equipment and lives. Control techniques for continuous time disturbance may not be suitable for discrete event type disturbance.

For continuous time disturbance, the primary cause of vibration produced by machines can be traced to inertia forces produced by reciprocating or unbalanced rotating masses. Vibration control can be implemented by attaching counter weights in the machine or inertia actuators to the machine body to generate forces opposite to those inertia forces causing vibration. In many practical problems, the source of the disturbance is inaccessible, or the suppression of the disturbance at source is impractical. For vibration arising from vehicle manoeuvres, suppressing the disturbance at source is to suppress the

excitation needed to execute a manoeuvre. Vibration control means dissipating the energy injected into the system or injecting energy into the system to counter the disturbance. In dissipation of energy, it can be done by the addition of damping material or dampers to the parts of the vehicle or system. The idea is to absorb and dissipate the energy associated with the vibration motion and to prevent the propagation of the energy. The system natural frequencies and mode shapes can also be modified by the addition of mass and stiffness elements at selected locations to shift the system natural frequencies away from the frequency of the external disturbances. These are typical control methods for vibration control associated with space structures or vehicle structures such as cars, ships, and aeroplanes. In the literature, these are also called *vibration suppression* techniques.

Another way to control vibration is to isolate vibration from one part of the system, where vibration is to be small, from another, typically the source. This is referred to as *vibration isolation*. It involves reducing the transmission of the vibration along known or identifiable paths in which energy is passed along. The characteristic of the paths is modified. Its (mechanical) impedance can be reduced. The most commonly used isolation technique is to install flexible spring and damper elements in the transmission paths from disturbance to regions of vibration control. The ubiquitous car suspensions comprising a shock absorber tube in parallel with a coil spring or layers of leaf springs for heavy-duty vehicles are relevant examples.

In both cases of vibration control - either suppression or isolation - the examples mentioned above are regarded as passive control. The term passive is taken to mean that the design or the solution is based on some pertinent assumptions made about the systems where vibration control is needed. The effectiveness of the design is very much dependent on the getting the assumptions right. By and large many of such passive vibration control solutions are robust enough to accommodate the errors or the differences between the model or assumptions and the actual system behaviour. This is of the course the result of having a better understanding and experience in using passive vibration control and the inherent robustness of some passive vibration control elements (whose designs are again the result of experience and knowledge) used in passive control.

Examinations of some of these passive techniques will however reveal areas in which improved and perhaps more cost effective (with respect to the cost of the system being

protected) solutions can be found. For example in passive vibration suppression, a simple solution is to modify the affected part of the structure, accepting some comprises between weights and stiffness. Once the design is built, any subsequent modifications may be expensive. Dampers may be tuned and the mounting locations identified. However, when the vehicle has been launched and is beyond reach as in a space structure, it would not be possible to re-tune the damper.

Passive isolation in a car suspension system is a compromise between providing for passengers' comfort when designed to be "soft" and providing for good road handling characteristic when designed to be "hard". As a machine mounting, passive isolation is a compromise between having a higher frequency range for which the transmissibility is sufficiently reduced and keeping the static deflection acceptably small. For a given mass, m, it means properly selecting the stiffness, k, and the damping, c, of the isolation element. If k is small, then reduction in the transmissibility is achieved for a wider frequency range. This means that there will be a larger static deflection, and it may not be acceptable. Increasing c will reduce the amplitude at resonant frequency but increases (compared with smaller c) the transmissibility for frequencies beyond $\sqrt{2k/m}$.

A general term to describe the limitations imposed or the constraints of passive vibration control is inflexibility to meet conflicting requirements or to effectively adjust to actual operating conditions. In describing some passive techniques as being robust, it is usually taken to mean that robustness is achieved at the reduction of effectiveness in the sense that if the model used to design the passive vibration control has no errors, then it will have the optimal performance. With errors, the performance will deviate from being optimal. With rapid development in high precision manufacturing, high performance cars and spaceships and structures, and the like, there is less tolerance to errors and deviation from desired performance. The term active vibration control (AVC) begins to take on a life of its own. It may yet be the alternative solution but it definitely is a complementary solution to passive vibration control.

Active vibration control can be characterised by the use of externally supplied energy to achieve the same objectives as passive vibration control and in some cases objectives that cannot be achieved by the use of passive vibration control. It can be applied in lieu of

passive control at the same locations. More importantly it can use measurements from other parts of the system to enhance the suppression or isolation of vibration at those parts where it replaces or complements passive methods. The actuation can either be effected as a force or as a displacement to counter the undesirable vibratory motions. A controller is normal complement of an AVC system. It treats the vibration measurements as error signals and drives the actuators to reduce the measured vibrations until they reach a specified acceptable level. With a digital computer, the AVC is in a sense truly flexible compared with passive vibration control. Even if the arrangements of actuators and sensors are designed and already in place, it will still be possible to change or optimise the control system in response to actual operating conditions, and with advances made in signal telemetry, this can be done remotely and on the fly. Of course, nothing is gained without having to pay a price. AVC is firstly more expensive and more importantly less forgiving than passive methods. If it is poorly designed or wrongly implemented, it can cause far more harm than if it is not in use or when passive technique is used. This is because energy is added into the system instead of being removed from it, and this energy wrongly directed can make vibration more severe. As a compromise (again) AVC is sometimes used in conjunction with passive elements. This partnership can also give a more cost-effective solution when optimal combinations of passive and active vibration control techniques exist. There is a great performance potential in using AVC either by itself or in combination with passive vibration control.

A brief review of the literature on AVC in Chapter Two will provide some insights and possible answers on how to exploit this potential and a better understanding of the use of AVC so that desired results can be achieved. As in the passive case, active vibration control can be either active vibration suppression or active vibration isolation. In active vibration suppression, models of the plant become more important in understanding and determining the location of sensors and actuators. Using ideal beam and plate models and newer developments in control theory, different configurations and control algorithms are obtained. Most of these works are driven in part by the surge in funding and interest in flexible space structures control and active structural control to suppress noise propagation. Current work in these areas involves finding the best controller algorithm to achieve the desired results. The control architecture varies very little: global feedback using multiple-input-multiple-output (MIMO) controller or local feedback with local control authority. As always simple configurations and algorithms provide useful

solutions and insights to the design and implementation of active vibration suppression. Not all these methods and configurations are necessarily appropriate for vibration isolation, which is the focus of this thesis.

In the area of active vibration isolation, low frequency active control is used to complement passive mount high frequency attenuation. This has been very successful to the extent that active mounts (a self-contained unit of actuator, sensor and interface to external controller) have been commercialised. Developments of active vibration isolation components or equipment are already in an advanced stage, but there is still room for advancing both the theory and the application of control theory to active vibration isolation. For in most of this equipment, classical controllers and filters designed using single-input-single-output (SISO) control concepts are still very much the order of the day with a few exceptions. Several suggestions and studies have been done to use MIMO control and multi-channel filtering theory in active vibration isolation although few relate directly to recent developments in robust control design methods. Adaptive feedforward and feedback controllers are robust, but they do not admit a formal and quantifiable model to deal with modelling errors or perturbations.

Another interesting outcome of the review is the use of piezo-ceramic material in active isolation. It is inherently very stiff (comparable to aluminium) and is very much a hard-mount. Active vibration isolation using hard-mounts has limited literature and is certainly worthy of exploration. When compared with active vibration in conjunction with soft-mounts, machine motion during controlled actuation is limited or restraint for a machine on hard mounts.

The basic configuration of the complete dynamic system for AVC design is the same as that used in the design of a passive vibration control system. The addition of active elements only serves to provide greater flexibility and potential in controlling undesirable vibration. A greater part of the improvement is obtained from the application of appropriate control to the active elements. For example in active dampers, the damping and the stiffness are continuously adjusted according to some control law to minimise the sensed vibration. There is already a substantial body of knowledge in control theory that can and has been used in active vibration control. It is not proposed to make any more contribution to the already vast amount of literature pertaining to active vibration control

and especially to the body of control theory that can be applied. Instead focus shall be on two aspects of active vibration isolation from a control engineer's perspective. In the area of soft-mounts, to derive a multiple degree of freedom model for active force cancellation at the feet of machine in the presence of base flexibility and to demonstrate how active vibration isolation can be put into a framework of MIMO robust control design. The resulting model separates the base flexibility dynamics from the machine on rigid base dynamics, treating the former as a kind of modelling error or perturbation. The model fits very well into the robust control design and $\mathcal{H}_\infty$ optimal control theory framework providing a quantifiable error model. The other aspect is related to an area not intensively researched into, where active vibration isolation is proposed for a machine hard-mounted onto a base structure. Such a situation is most ideal for the implementation of active force cancellation at the feet of the machine. As a preliminary work, a method for determining the force transmitted from a machine hard-mounted to its base structure using another test structure with dissimilar characteristic is given. Next, the effectiveness and implementation of active force cancellation using control systems designed by $\mathcal{H}_\infty$ optimal control theory is investigated. The control system is robust only to modelling errors. This is compared with a Static Output Feedback (SOF) control system design. In the case studied, the SOF controller is robust to modelling errors and neglected dynamics.

In summary, from the perspective of vibration control, vibration control can be classified as passive, semi-active (where the system passive properties are actively modified) and active (where real-time actuation is provided). Active control can be divided into feedback, feedforward and combined feed-forward & feedback. Most of the feedforward control schemes reviewed are necessarily adaptive control. From another perspective, active feedback control can be further divided by whether sensors and actuators are collocated or not. Collocation has certain properties that can be exploited to simplify the design of the controllers. Examples of uses of non-collocation in adaptive vibration control and model based feedback control are also given in the review.

1.2 Active force cancellation for soft-mounted machine

Active vibration isolation is most appropriate for the case of machine mounted onto a base structure. If the machine disturbance is transmitted to the base structure, it may be

propagated to other part of the systems and possibly cause some damage or inconvenience. The idea of generating an opposing force to cancel the disturbance forces is much the same as that of using anti-noise to cancel the disturbing noise. Instead of applying cancellation at the machine body itself, active force cancellation can be applied at the point where the disturbance goes into the mounts and thence into the other parts of the systems. Instead of changing the characteristic of the transmission paths, those parts of the disturbance that will be transmitted into the base will be minimised via the isolators before they have the opportunity to be transmitted i.e. at the feet of the machine.

For a machine soft-mounted to a flexible structure it will be shown that a proper selection of k can result in a model with the base dynamics appearing as a decoupled term in the machine-isolator-base model. To a control engineer engaged to design a AVC system, it is most useful to have such "decoupled" model or better still to be able to design and test a control system that is robust to the modelling error introduced by the base flexibility.

In Chapter Three, an induced matrix norm condition for the base structure dynamics to be decoupled from the local measurements of the force transmitted for a machine soft-mounted at multiple points is introduced. The desired model is a force transmissibility matrix that is a product of a multiplicative error term and the force transmissibility matrix of the machine soft-mounted on a rigid ground. The matrix norm of the multiplicative error term gives the bound on the error against which a control system can be designed.

The multiplicative error model fits very well into a robust control design framework. Controllers can be designed to be robust to modelling errors. This means that a control engineer can design and test a controller with the machine soft-mounted onto a rigid test-bed that is not the actual base structure for the machine. The stability of the control system can be evaluated using the small gain theorem (Appendix D). A great benefit of this decoupling is that the actual base structure dynamics need not be known in detail.

1.3 Determining the force transmitted from a machine on hard-mounts

The problem of multi-point mountings for a machine that is hard mounted instead of using flexible isolators is considered next. Such is the case when machine alignment is critical or any machine motion has to be limited.

Unlike the case of active vibration suppression, machine disturbance is continuously generated. As there are no flexible elements to isolate or reduce the amount of disturbance transmitted, it is very important, from a control perspective, to have some knowledge of this disturbance. With no soft mounts to decouple the dynamics of the structure from the mounting, it is incorrect to use machine free vibration as a disturbance spectrum for the design of a controller. It is then necessary to determine the force that will be transmitted to the final mounting structure and use this as the disturbance spectrum. There will be instances when it is not possible or convenient to measure the force that will be transmitted by the machine on the final mounting structure. Mounting structures with dissimilar characteristic from that of the final mounting structure, on the other hand, may be available for used in estimating this force spectrum.

Hence in Chapter Four, the equations to determine the level of force that will be transmitted to a final base structure using measurements of the vibrating machine on another test-bed structure with dissimilar characteristics are derived. This analysis gives us an expression that requires data on the receptance or dynamic stiffness matrices of the machine on test-bed, machine on the final base structure (if possible to have) and the final base structure. No information is actually required of the test-bed. Experiments have been conducted to verify the usefulness of the derived expression. The results when compared with that obtained by other experimental methods are found to be more favourable.

From this experience it can be concluded that a machine disturbance spectrum under free vibration can be modified by the dynamics of the base structure. The installed force spectrum can be obtained from the force transmissibility matrix. A control engineer can then use this to specify the amount of attenuation in the frequency domain to be provided by the control system.

1.4 An experimental demonstration of active force cancellation using hard-mounts

The use of the force transmissibility matrix to define a disturbance rejection performance specification with the $\mathcal{H}_\infty$ optimal control method is demonstrated in Chapter Six. A rig comprising of a 5.5 kW AC industrial motor is hard-mounted on a structure. Four force actuators are located near its feet and four force sensors are located between the bottom of

each hard-mount and the base structure. Since the free vibration machine disturbance comprises of (typically time-invariant) spectral peaks, feedforward adaptive filtering as suggested in some literature could be used. However as the result of machine-structure dynamics interaction, the spectrum is modified, and feedback control is more appropriate. This situation provides a good test case to study active force cancellation using $\mathcal{H}_\infty$ optimal control method.

The (disturbance) force transmissibility matrix is estimated using a frequency domain identification method and compared with that obtained from modal analysis method. This is described in detail in Chapter Five. The identified model is expressed as a 4x4 matrix of transfer functions and subsequently converted to a suitable state space model. Model reduction technique is used to obtain a model that is compatible with the physical system and the results obtained from modal analysis. The reduced model is the force transmissibility matrix that is used in Chapter Six as definition for the disturbance rejection performance specification. To demonstrate the robustness of the control loop to modelling errors, the identified models of the actuators' dynamics are not used. Instead a diagonal matrix of 2^{nd} order transfer functions is used to represent all the four actuators. Various weighting functions are used as the performance specification and the results are compared. For comparison, the full order force transmissibility matrix is used in the design of a controller. The model of the controller is then reduced a smaller order.

All results and discussions on the implementation of the controllers in the experiment are given in Chapter Six. The controllers are found to be robust to modelling errors but not to unmodelled dynamics. This is the fault of the estimated model used in the design and not a flaw with the $\mathcal{H}_\infty$ optimal control method. If the unmodelled disturbances are modelled by some frequency dependent functions, the $\mathcal{H}_\infty$ optimal control method will design a controller that is robust to these higher frequency disturbances. For comparison, an alternative method, Static Output Feedback, for the design of MIMO controller using output feedback is given in the same chapter. A performance specification that is a function of the force transmissibility matrix is used to design a gain controller. The static gain controller has fewer parameters and is therefore easier to tune during. Hence it can be adjusted for modelling errors. In this study, it performs better than that designed using the $\mathcal{H}_\infty$ optimal control method. In general this may not always be true.

The conclusion that active force cancellation as an active vibration isolation method is feasible is given in Chapter Seven. The robust control design theory is a suitable method and could be used in active vibration isolation. It is suggested that the insertion of thermoplastic material between the hard-mounts and the machine may have the potential for greater benefits and could be investigated further. This material with a loss factor of about 0.9 at 24 Hz (1440 rpm) at a temperature of 30 °C can be used to provide damping.

CHAPTER TWO

A REVIEW OF SELECTED ACTIVE VIBRATION CONTROL TOPICS AND RESULTS OF PRELIMINARY EXPERIMENTS

2.1 Introduction

This review covers previous research work done in areas related to active vibration control of machines mounted onto flexible structures. It summarises the work into three categories basing on how the problem was modelled and studied. Except for the control of flexible space structures, which has been researched zealously, much of the examples of complex analysis and experiments to demonstrate the control of machine vibration transmission have been done using 1-degree of freedom (DoF) systems. In most of the work reviewed and described here, only a few examples using physical machines or engines as external disturbances in experiments are given (Watters *et al.*, 1988 and Jenkins *et al.*, 1990). More often than not, a controlled exciter e.g. an electro-magnetic shaker is used as the disturbance source, and the machine is assumed to be a rigid mass. To some degree this simplifies the modelling and the execution of the experiments.

A review of the types of actuators and sensors in active vibration control is also given in this review. The selection of the sensors and the actuators is influenced by the performance metrics and the dynamic range used for specifying the effectiveness of disturbance rejection. It also affects the transfer functions used in the design active vibration control. The different arrangements of active and semi-active dampers are also discussed. At the end of the chapter, in consideration of existing methods of control and availability of sensors and actuators, a set-up of actuators and sensors is proposed.

Finally examples of preliminary work done on active vibration control are also given. These are performed to get an understanding of the principles and the experimental methods for active damping and active vibration control.

For the purpose of discussion, the term soft-mount shall refer to the case where (flexible) isolators are used, and the term hard-mount shall refer to case where the machine is rigidly mounted to the structure without the use of flexible isolators.

2.2. Active vibration control (AVC)

The basic reasons for the need of active vibration control have been highlighted. There are many solutions that have been around and more are being sought after either in

specific areas or as improvements of existing solutions. Most solutions are primarily based on the basic understanding of the principle that vibratory responses in a machine or a structure can be reduced or amplified by controller driven actuators acting on responses to measurements made in the machine or the structure. Elements of active vibration control are similar to those found in any simple single loop control system, regardless of whether it is feedback or a feedforward loop: the barest requirements call for a sensor, an actuator and a controller or filter or an equaliser. The types of sensors and the actuators found in an AVC system will be discussed. The types of controllers used will also be included in the survey as control algorithms and controller design approaches as more and more implementations are done using a micro-processor (μ-p) or a Digital Signal Processor (DSP).

Firstly, a brief survey of the methods of AVC will be presented. The scope will be limited to different design approaches that have been taken to solve the problem of reducing vibratory responses of some pre-identified targets. To assist in the presentation of the survey, the general AVC problem is subdivided into categories following a scheme proposed by. McKinnell (1989). He identified three possible regions in which vibration can be controlled. These connected regions or subsystems are shown in the Figure 2.1.

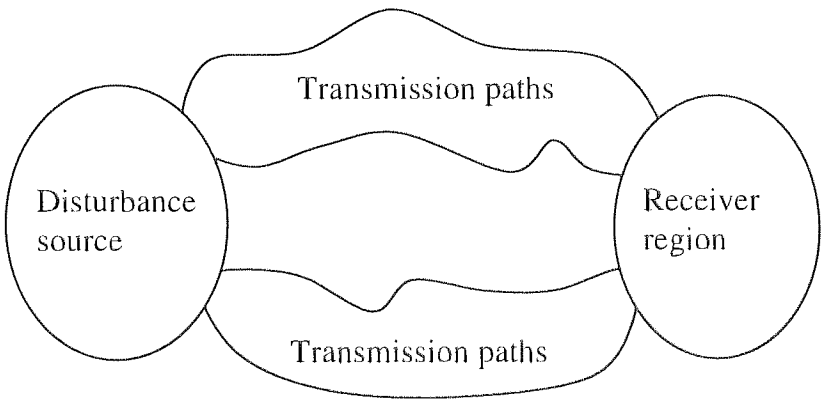

Figure 2.1 Region for which vibration control can be implemented

Region (a) is represented by disturbance sources. It can be a single piece of machinery that generates the vibration or it could be a combination of many machines and equipment. Transmission paths would form region (b). In the simplest case, it would be represented by isolators or mounting locations. These are discrete paths. In some cases, it could be a continuous path such as a flexible structure connecting one point of

disturbance to other areas where vibration sensitive equipment has to be protected, for example, laser interferometers. In more complicated systems such as in submarines or ships, transmission paths are more difficult to describe. The seawater would form short-circuit paths for vibration from part of the submarine to be transmitted to another. The last region, (c), the receiver region, could be any component or structure that vibration should not be allowed to propagate or persist, or a place or equipment where vibration is to be limited. It is sometimes also referred to as vibration sensitive region. In some cases, it may be hard to distinguish between the transmission paths and the vibration sensitive region. Controlling the vibration in region (c) may be the goal itself.

Any of these or all of these can be targets for active vibration control. The selection will depend, amongst many other factors, on the cost of design and implementation and the accessibility of the region for design, modification and location of sensors and actuators.

2.2.1 Active vibration control of the disturbance source

Although the thrust of the survey is focused more on the region (b) and region (c), it is worthwhile mentioning something about AVC of the region of disturbance source. Nelson (1991) and (Fuller *et al.*, 1996) used the term vibration control at source to mean cancellation of the primary vibration, $-f_p(\omega)$, by applying a control force $f_{cont}(\omega) = -f_p(\omega)$ on the body of the vibrating machine. It is very much the same concept as applying a *blocked* force Q_β (Lyon, 1987) to the machine to stop it from vibrating. Inertia mass actuators can be used, and the actuation can be externally or internally applied (if possible). With a more complex machine system, for example, a machine driving a generator or a propeller via a long (compared with the diameter) shaft, the term will mean something different. It will involve using active rotor-bearing control or active magnetic bearings to reduce the unbalanced forces that exist in the rotor or the shaft. State variable feedback control (Stanway and O'Reilly, 1984) and non-linear control (Smith and Weldon, 1994) are some of the methods used for magnetic bearing systems. In most of such systems, oil-filled bearings are often used to complement the active magnetic bearing systems.

To limit the scope of the survey, it is assumed that the disturbance source region has a well designed but not necessarily a perfect machine. For example, using a motor with a-

skewed armature that reduces the fluctuating forces. Undesirable forces can be generated and transmitted as the results of any imperfections and the interaction between a vibratory machine and the supporting structure. It has been shown that the dynamics of the supporting structure can in some cases caused a reduction in the attenuation of the force transmissibility ratio (Plunkett, 1958). One would therefore like to survey the work done in the area of vibration control of the receiver region and examine solutions that suppress vibration in this region.

2.2.2 Active vibration control of the receiver region

A conceptual model of the forces and moments generated and transmitted to the vibration sensitive region is proposed in Figure 2.2. Identifiable transmission path(s) may or may not necessarily exist. Only one arrow is drawn to typify this disturbance. AVC can be applied in this region to maintain some form of global response for example having a specified displacements field in a certain region of interest. It can also be used to control the behaviour at selected sensors' location (called controlled points) in response to transmitted forces and moments applied at some other locations.

The control of vibration in this area as represented by Figure 2.2 is characterised by the use of numerous sensors and displacement type actuators spread around or along the structure or distributed sensors and actuators. Another term that is commonly used to describe this situation is vibration suppression.

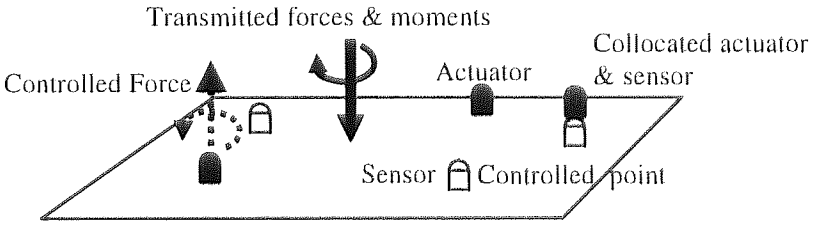

Figure 2.2 Vibration control at the receiver region

Many researchers in the area of control of vibration of flexible structures favour the use of such an arrangement. Perhaps some lessons could be learnt from the research in the field of vibration control of large space structures and also in the study of flexible robots. They do have certain characteristics in common. They are in general subjected to disturbances at one or more discrete points. These disturbances are typically treated as individual

events rather than continuous excitations. For example thrusters are fired intermittently to align the space structure or a robot is being slewed to a desired orientation. The nature of the disturbances could then be impulsive in nature, pulse-like or regarded in some cases as white Gaussian noise.

The model of the region is often described by Partial Differential equations or modelled using Finite Element models. FE models typically produce many modes but not all are used in practice. In the literature, the FE models typically have well-defined boundaries (e.g. clamped-free cantilever) and consist of trusses, beams and plates. Solutions to (Euler or Timoshenko) beam equation have been used in the study of control of flexible robot (Cannon and Schmitz, 1984) and space structure (Larson & Likins, 1977 and Martin & Bryson, 1980). Solutions to plate equations are used in the control of sound radiation (Junger & Feit, 1986 and Cremer *et al.*, 1988). The availability of closed form solutions for simple geometrical shapes is one of the reasons why they are used in the first place as models of physical systems. Nicholson and Bergman (1986a, 1986b) using the Green's functions obtained the characteristic equation for natural frequencies of free vibration of beam and plate coupled to harmonic oscillators or dampers attached to structure at discrete points. In effect Nicholson and Bergman have provided a solution for open loop control of plate vibration by proper selection of attachment locations. Simple geometrical shapes also provide for the basis of the understanding of the mechanics of active vibration control. For example, Gervater (1970) used a model of a beam to show how important the relative position of actuator and the sensor is in determining closed stability using velocity feedback. If the actuator and the sensor are collocated, the compliance transfer function of an undamped system has alternating poles and zeros along the imaginary axis. This becomes important in gain feedback - in terms of root locus feedback gain will cause the locus to move from the open loop pole to the zero in the left hand half plane thus ensuring closed loop stability. Wei and Bryson (1981) developed models of space structure using different boundary conditions for a beam and showed that model truncation of collocated systems creates no serious modelling errors, whereas model truncation of non-collocated sensors and actuators pairs create spillover problems. When the system gets more complex, some of these physical insights are lost, and the analytical approach to determine the model of the system loses its appeal. However the basic advantage of collocation over non-collocation still apply even to complex structures.

Different insights can be obtained when a general PDE is transformed into a modal equation or modal state equation. This transformation is also necessary for feedback control as no algorithm exists to determine suitable Linear Operators for the displacements and velocity feedback (Meirovitch, 1987) for use with the PDE. With modal equations, the concepts of eigenvalues and eigenfunctions are used to convey the response in terms of natural frequencies and displacements at the modal coordinates. When the displacement and velocity feedback gain operators satisfy the eigenvalue problem, an independent set of modal equations (decoupled equations of natural coordinates) is obtained. Hence the term Independent Modal-Space Control (Meirovitch & Baruh, 1982). In this set of equations, the eigenfunctions or mode shapes are not affected by the feedback. The control problem then becomes one of relocating the open loop eigenvalues using the pole allocation method or linear optimal control method (Meirovitch, 1987). The eigenvalues can be shifted without changing the eigenfrequency i.e. the algorithm seeks to increase damping, and increases the rate of convergence to stability. IMSC approach provides for a global control of the region and it needs the use of distributed actuators and sensors. However one very often has to work with finite number of actuators and sensors at discrete locations.

One can independently control a limited number of modes successfully. A careful selection must be made as to which modes are directly controlled. This means that modal truncation or selection of modal modes becomes necessary. Very often the lower modes or mode shapes is selected basing on the modal participation factor. Hughes (1982) advocates modal selection by some error criteria rather than modal truncation of higher modes. Sensors are to be placed at positions corresponding to the selected modes. However it is neither possible nor economical to measure all the modal states corresponding to all the selected modes. Then state observers, either the Luenberger (1971) observer or the Kalman-Bucy filter can be used to construct the missing states from the limited output measurements. With state feedback, poles allocation or pole assignments methods are known to work very well (Kailath, 1980). The point is that the resulting truncated modal equations are no longer decoupled, and for a large number of selected modes, a correspondingly large number of sensors will be needed. From Wei and Bryson (1981), it is known that modal truncation will result in model inaccuracy. For example, sensors located to measure the selected modes will also pick up displacements from those modes that are not selected for control. This gives rise to *observation*

spillover. The controller will respond to both selected and non-selected (residual) modes. Actuators under command of the controllers to suppress the controlled modes may end up exciting the residual modes as well. This gives rise to the *control* spillover problem. As control spillover does not affect the closed loop eigenvalues, it cannot destabilise the system (Meirovitch 1987). Observation spillover, on the other hand, can produce instability in the residual modes especially if actuators and the sensors are not collocated.

Observation spillover can be avoided using collocation of sensors and actuators and local feedback schemes or some filters to remove responses from unwanted modes. For example, using direct velocity feedback (Balas, 1979) and direct displacement feedback (Meirovitch, 1987), observation spillover can be avoided as there is no need to estimate any modal states. Meirovitch (1987) called this Static Output Feedback. The designed controller is a diagonal gain controller. There are however no equivalent pole allocation or optimal control algorithms to determine these gain values. When the modal coordinates are transformed to balanced coordinates, Gawronski (1996) showed that with collocation of sensors and actuators static gain matrix could be determined analytically. This controller is no longer diagonal. In fact the general use of the term Static Output Feedback does not necessarily imply that controller is restricted to being diagonal. As long as no modes need to be estimated in the design of the controller whether diagonal or otherwise, observation spillover can be avoided.

One of the way of minimising observation spillover is to filter the sensors' output for uncontrolled modes, but the filter usually distorts the signal thereby affecting closed loop eigenvalues. Chait and Radcliff (1989) developed a "modern modal control design" using an augmented observer to compensate for the distortion introduced by the filter. Other attempts to avoid the spillover problem take a circuitous route. Proper selection and using large number of sensors and actuators have been proposed. Auburn (1980) had tried to limit the gain of the controller so that the actuators are limited in output and hence do not excite uncontrolled residual modes. He called this "low authority" control. Raju and Sun (1989) used relatively large numbers of non-collocated actuators and sensors with respect to the number of modes to control, to limit the output and avoid exciting the uncontrolled residual modes. Similarly, Guigou *et al.* (1991) employed distributed sensors and actuators - effectively increasing the area of actuation and sensing - to provide active

vibration suppression of the base structure supporting a large simulated machine mounted via spring coils.

Collocation with local and direct feedback is still more appealing than central feedback as the latter is difficult and expensive. The control architecture is simple: measure, condition and output to actuator. Hence there is collocated positive position feedback by Goh and Caughey (1985). They showed that direct velocity feedback (Balas, 1979) for a model truncated to slow modes will result in an unstable system when the actuators' dynamics are neglected. Instead conditional global stability of large space structures can be achieved using positive position feedback (PPF) if actuators' dynamics are present. Agrawal and Band (1993) has also implemented PPF using piezoelectric sensors and actuators on a flexible spacecraft simulator, and more recently Sciulli and Inman (1997) used it in active vibration *isolation*. In 1990, Goh and Yan proposed the use of acceleration feedback to provide robustness in feedback vibration control. An experimental demonstration of this concept is given by Preumont and Loix (1994) using a B&K shaker and accelerometer in response to a disturbance on a beam. In summary, all of them use motion feedback - position, velocity and acceleration - to provide for closed loop damping or basically to move the open loop poles near the $j\omega$-axis to a location further away from it. The controllers used are typically filters - 2^{nd} order low pass or notch filters, and the plant is invariably a beam or a plate.

In more recent work conducted on the control of complex flexible structures, models are identified from experiments (Balas & Doyle 1990, Balas *et al.*, 1992 and Lublin & Athans, 1994). Balas & Doyle (1990) working on the Caltech Experimental Flexible Structure and Lublin & Athans (1994) on the M.I.T. Space Engineering Research Centre's Interferometer test bed started with FE models but eventually resorted to experimental identification to obtain more accurate multivariable descriptions of the structure for control design. These models are obtained first as transfer functions description and then converted into general state space forms. The identified models also include the actuators and sensors' dynamics. Typically the states are not necessarily associated with any modal or balanced coordinates. This mixed use of frequency domain identified model and converted state-space model quite fit into the framework of current control literature of robust control design and $\mathcal{H}_\infty$ optimal control method.

The survey of AVC for this region brings out some important aspects: (a) the nature of the region is typically modelled by PDE and model truncation is inevitable and (b) the proper location of sensors to avoid the more serious observation spillover is very necessary. To avoid spillover, collocation of sensors and actuators is often used, and in this case there are many control schemes, all which are designed to provide closed loop stability (and some in the presence of actuator dynamics) and improved damping. When models are experimentally identified, the internal states that are measurable and controllable are present in the measurements used to determine the model. In those works, the problem of spillover is seldom mentioned even if actuators and sensors are non-collocated. Robust control design can be robust to spillover. More importantly robust controllers can be designed for the spillovers if the error between the model and the "real" system are given as frequency domain uncertainty descriptions and incorporated into the model identified.

2.2.3 Active vibration control of transmission paths

When a discernible transmission path can be identified, a logical AVC scheme is to "block" or "annihilate" the disturbance along the paths before they reach the vibration sensitive region. Such discernible and discrete paths are "bottle-necks" of vibration transmission. Sensors can be positioned at the mounting locations as well as at other locations where it is necessary to minimise the vibration level e.g. at passengers' seats in a car.

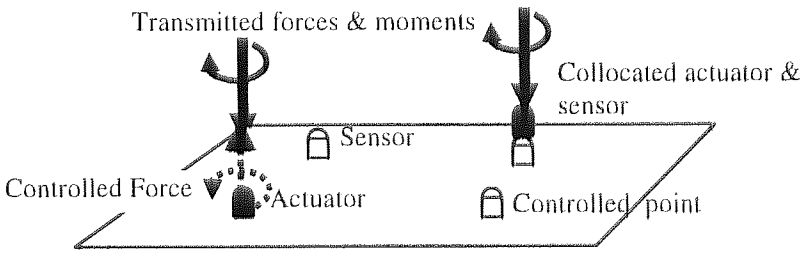

Figure 2.3 Vibration control along the transmission paths

Figure 2.3 is one possible conceptual model of AVC along the transmission paths. Another model is shown in Figure 2.5. In the case of machines mounted onto a structure, these paths are the isolators. Figure 2.3 and 2.5 are examples of active vibration isolation (McKinnell, 1989 and Nelson, 1991).

Feedforward control for active vibration isolation is one approach that uses the model shown in Figure 2.3. It employs many sensors on the receiver plate as well along the isolators. Some of these sensors, placed at appropriate positions on the receiver plate, are used to monitor the effectiveness of the control action. Actuators are very often placed in parallel to passive isolators i.e. placed between the disturbance source, e.g. a machine and the receiver-plate e.g. the supporting structure. This is characteristic of the works of Nelson *et al.*, (1987) and Jenkins *et al.*, (1990) at the Institute of Sound and Vibration Research (ISVR), University of Southampton, UK. Another arrangement has no sensors on the receiver plate. Instead it has a reference sensor at the disturbance source to provide a signature of the disturbance. The actuators are either in-line or attached to opposite end of the bottom of the mounts on the receiver plate side. Chaplin (1987) and Eghtesadi & Chaplin (1987) used this method to actively cancel the disturbances. It is similar in concept to that of active noise cancellation proposed by Ffowcs-Williams (cited in Sievers and von Flotow, 1988). An introduction to synchronisation vibration cancellation using inertia force is given by Swinbanks (1984).

The approach of Chaplin (1987) is simple and direct. It converts the time domain reference signal containing the machine speed and its harmonics into a spectrum, and anti-phase every spectra peak of the harmonics in the spectrum. This modified spectrum is then Inverse Fourier Transform back into a time domain signal and applied to the actuators. The actuators do not respond to any disturbance coming from other parts of the receiver region, and in essence, the method disregards the dynamics of the receiver region. The concept is the same as anti-noise cancellation. Control is local and the controller is basically a waveform synthesiser. There is no requirement for real-time signal processing if the signal is stationary and periodic. In such case, the time delay in computation is not important. This constraint on the signals containing only harmonically related components is limited by the state of microprocessor speed prevailing at that time. With current processor capability this is no longer a constraint.

On the other hand, the method of Nelson *et al.* (1987) is an attempt to produce a global reduction in the vibration in the receiver region. The disturbance signal of the machine is used as a reference signal to an array of filters. A multi-channel filtered-x LMS (Elliot and Nelson, 1986) algorithm is used to adaptively adjust the coefficients of these filters to

produce the outputs to drive the actuators. These coefficients are adjusted until the sum of the square of the signals from the accelerometers distributed on the receiver region reach some specified or desired level or some minimum value. The method does not need an explicit model of the transfer characteristics of the transmission path or the flexible base structure characteristics as the filter is adaptively tuned to match these characteristics. The method worked well at some positions of a plate especially at plate resonant frequencies, but did not quite achieve the global reduction for the range of frequencies as intended.

Feedforward control works relatively well when the disturbances are deterministic and especially well if the spectrum comprises narrow band resonance. With fast DSPs, the transfer characteristics of the path and the plant can also be time varying. This is of course a significant advantage. Such methods are also found in ANC (anti noise cancellation) literature (Kuo & Morgan, 1996 and Fuller *et al.*, 1996).

An application of such methods can be found in anti-vibration and noise in some car models. A schematic is shown in Figure 2.4.

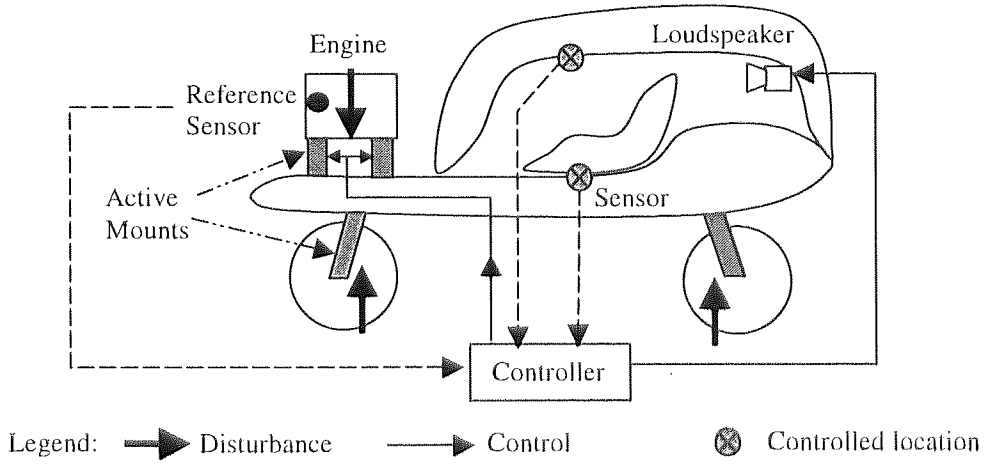

Figure 2.4 Active vibration control in a car model

In an experimental test-rig modelling a car body, Yang *et al.* (1996) used filtered-x LMS to achieve a very good reduction at a single point for the simulated engine speed of 33-Hz. Shoureshi and Knurek, (1996) demonstrated the effectiveness of noise control in the cabin of a passenger car. On the Volkswagen GTI (Fuller *et al.*, 1996), accelerometers placed on the chassis side of the (Freudenberg's) active engine mounts and on either side of the front sides provide the error signals for the multiple error LMS algorithm to

produce up to 20 dB attenuation at the driver's footwell. The attenuation is most significant at the engine speed.

The adaptive filters approach is similar to an on-line system identification of unknown plant. This normally works as long as the plant (and other electronics) is linear though not necessarily time-invariant. With disturbances that are periodic or predictable, anti-phase harmonic cancellation is possible. In fact with such schemes, the amplitude and phase characteristic of the controller is very important. However, when the disturbance is no longer deterministic or is hard to predict, such a feedforward control strategy is hard to implement. The phase between input and the output is likely to be random.

A variant of the model of Figure 2.3 is shown in Figure 2.5. Unlike the model shown in Figure 2.3 and that proposed by Chaplin (1987), this is completely a local control scheme. There is no reference sensor at the disturbance source and controlled points (sensor locations) are primarily at the feet of the isolators and not on the receiver (Figure 2.3). The actuators and sensors need not be collocated even though the figure appears to show that they are. For example, the sensor could be at the bottom of the isolator where the level of transmitted vibration is to be reduced and the actuator could be located at the top of the isolator.

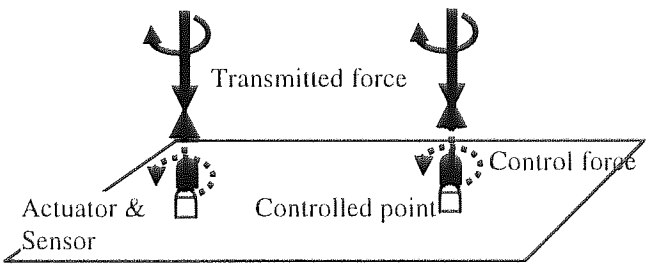

Figure 2.5 Active vibration isolation: local feedback

Pan *et al.* (1993a, 1993b) adopted another form of feedforward control using this arrangement. However models of the isolators and the receiver structure are needed with the additional assumption that the machine behaves as a single rigid mass. These models are used to determine the optimal control force needed to reduce the power flow from machine to the base of the isolators. The actuators are in parallel to the isolators and the power flow reduction has been demonstrated from a simulated machine (a shaker) to a beam (Pan *et al.*, 1993a) and via two isolators to a plate (Pan *et al*, 1993b). However the

method is dependent on the ability to get analytical model of structure and the assumption of rigid machine. It is unlikely to be robust to modelling inaccuracies.

Figure 2.5 is also very suitable for local feedback control. It is a classic 1-DoF example of active vibration isolation for machine on a rigid base using active and semi-active dampers, and active car suspension systems. And naturally a suitable model in the control of machine vibration to flexible structures (Watters *et al.*, 1988 and Scribner *et al.*, 1993) as well isolation of vibration-sensitive equipment (Schubert, 1991, Beard *et al.*, 1994, Preumont & Loix, 1994 and Anderson *et al.*, 1996) on a resonant base structure. The literature of such active vibration isolation model is plentiful especially for an actuator in parallel with passive isolator, and is still relatively current: for example in (Sciulli & Inman, 1997 and Su, 1997). It is not possible to provide an exhaustive survey of these in this brief review, and so attention will be focused on two groups of research effort.

These two groups of research are particularly relevant to us. One group using isolators with hard and soft-mounts is centred about von Flotow and his colleagues. The other group of Tanaka and Kikushima use only hard-mounts to solve the problem of active vibration isolation. It is not that other works are irrelevant. These works have a particularly strong bearing on the development of the design methodologies presented in the thesis.

Von Flotow in 1988 presented an expository overview of active control of machinery mounts. Some of what has been discussed above is briefly mentioned in this exposition but the introduction and survey of modern control techniques e.g. state-space methods in active vibration isolation are of special interest. Sievers and von Flotow (1988, 1989, and 1990) provided more reviews of state feedback approach e.g. Linear Quadratic Regulator (LQR) and Linear Quadratic Gaussian (LQG) in conjunction with disturbance modelling. The machine harmonic disturbance is modelled as states of 2^{nd} order mass-spring system. These are augmented with the plant model and the augmented system is solved by the LQR or the LQG method depending on the availability of states for measurements for disturbance rejection. In particular, a comparison of modern, classical and adaptive feedforward control methods is given in (Sievers and von Flotow, 1990). The discussions were mainly on SISO problems although suggestions of extension to MIMO were given.

The issue of resonant base structures affecting active vibration isolation was addressed later by Sievers *et al.*, (1989), Garcia *et al.*, (1990), Scribner *et al.*, (1990), and (Blackwood and von Flotow, 1992). Such resonant structures pose a problem in robust stability since not very accurate information can be obtained of real physical structures when designing the controller. At this time, the use of piezoelectric actuator unit has become popular and the fact that it can be controlled to be very stiff at low frequency and relatively more compliant at higher frequency makes it an ideal isolator. However, the stiffness of a piezoelectric is almost equivalent to a hard-mount, and Scribner *et al.* (1990) showed that a soft-mount in series with such a hard-mount is required for closed loop stability. Similarly von Flotow and Vos (1991) demonstrated that a necessary condition for robust stability of real structures, especially with non-collocation of actuators and sensors is the presence of sufficient passive damping. Without it, robust stability is not possible with linear time invariant controllers. Such a condition seems to be common sense, but the use of the term "control of lightly damped flexible structures" was so pervasive at that time that it appears that a simple practical solution is often forgotten.

Much discussion on robust control in the presence of uncertainty associated with flexible base structures is given using SISO control systems. Robust stability criteria and compensator designs are based on plant transfer functions and the Root-locus techniques. Robustness is given in these cases as suitable gain and phase margins assuming large modal overlaps. Effective control was demonstrated only for narrow band disturbances.

The developments presented above do not quite seem to fit into the more recent control methodologies of robust control design paradigm and the $\mathcal{H}_\infty$ optimal control framework developed specifically to handle model uncertainty. Part of the motivation for such developments and research is the lack of success in implementing LQR and LQG methodologies in the industries, other than in the space and aeronautical industries. In the early '90s the structural control community has begun to use the "newer" control methods for active isolation of structures against earthquakes. The standard model is a multiple-storey truss structure controlled at the base by a servo-hydraulic actuator linked to the structure by tendons or a servomotor linked to the structure. Examples of the use of $\mathcal{H}_2$ optimal control can be found in (Dyke *et al.*, 1995) and μ-synthesis control design in

(Nishimura and Kojima, 1997) for active vibration isolation of structure with uncertainties in its base.

In 1992, Blackwood and von Flotow used the machine mobility FRF with blocked force (Lyons, 1987)) as the machine model to determine the effect of base flexibility on active control. Both soft-mount and hard-mount 1-DoF system transfer functions (i.e. using one mounting location) of the active isolation system were derived, and the effect of base flexibility is given as a multiplicative perturbation of the rigid base model. With the soft-mount arrangement, a combination of active and passive isolator in parallel was shown to be effective for broadband disturbance. This is the beginning of an interesting development. The model formulation for soft-mount seems very appropriate for the robust control design paradigm and the $\mathcal{H}_\infty$ optimal control framework. It becomes the starting point of a MIMO model formulation in chapter three using soft-mounts but with active control at the base of the machine instead of on the opposite side of the receiver plate at the bottom of the soft-mount.

Another aspect of this thesis related to the subject of hard-mounts will be considered next. The advantages of active-passive isolation have, in a way, eclipsed the usefulness of hard mounting machines. However, there are situations that will need machine to be hard-mounted and the application of active vibration isolation techniques for these cases have attracted limited attention so far. Hence a review of the work of Tanaka and Kikushima on active vibration control of machine on hard mounts will be presented.

Tanaka and Kikushima's works (1985, 1988, and 1988) have being cited for example in (McKinnell, 1989) and (Fuller *et al.*, 1996), but very little is developed from where they have stopped. Briefly, the arrangement used can be represented as shown in Figure 2.6

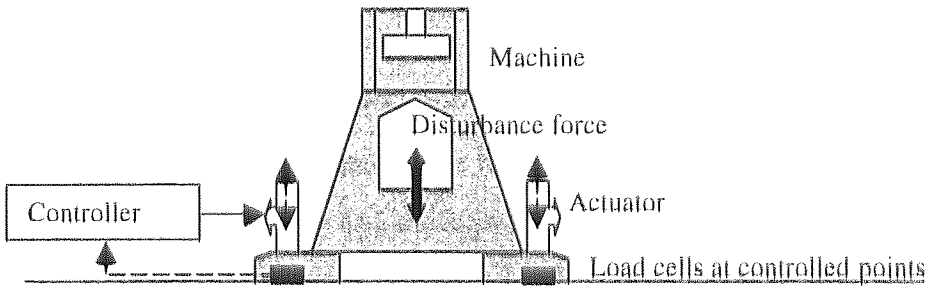

Figure 2.6 Principle of active force cancellation

A servo hydraulic actuator reacting against inertia mass is attached to the foot of a simulated machine representing a forge hammer. Only the dynamics of this actuator is used in the design of the compensator. The dynamics of the foundation are not modelled. The signal from the load cell is directly fed to the compensator that controls the "collocated" actuator. In addition the displacement of the inertia mass is used as an inner loop feedback signal to stabilise the actuator response. The difference in the works presented lies in the use of different compensators: Notch filters (1985), pole-zero compensators (1988) and Optimal design (1988). Once again this is very much a single local feedback loop approach. For MIMO, one can possibly adopt the method of closing one loop at a time. As each loop is closed, it is incorporated into the dynamics of the next loop to be closed (Sievers and von Flotow, 1990). Such an approach is rather an ad hoc way of implementing MIMO controller design using the method of classical control theory.

A similar arrangement of active force cancellation but using soft-mounts could be found in Lewis and Allaire's simulation study (1985). They had also used force actuation at the base of the machine to attenuate the force transmitted from an unbalanced machine rotor. The machine was soft-mounted and the measured variable was the relative motion between machine base and rotor, and not force. Classical controllers such as the PID controller and the Lead-Lag compensator were used in this simulation. One would have thought that since transmitted force is to the controlled variable, the measured variable should be the force measured at the bottom of the isolators. Active force cancellation using actuator in parallel with soft-mount had been realised on a diesel engine at one mounting location by Watters *et al.* (1988). In these cases, the actuator effectively adds to the stiffness of the isolators modifying the dynamic characteristic in response to some controlled signals. It is still possible that the active isolators may cause the machine to move under controlled actions.

An arrangement of the sort shown in Figure 2.6 may not need to have elastic supports or isolators. The disturbance forces that cause the ground vibration must pass through the contact parts between the machine and the supporting structure. It makes sense then that if the flow of the primary disturbances is blocked before it reaches the support, the support is no longer excited and so ground vibration should not exist. Furthermore the actuator forces are applied only in response to these measured disturbances. In order that the

actuators' forces are not attenuated by the compliance of the isolators during their operations in response to the primary disturbances, it would be better to have rigid connections between the actuators and the points of measurements. These will allow for the forces to be transmitted to cancel the primary disturbances. In this sense active force cancellation works better with hard-mounts than with soft-mounts. This is the case with the Freudenberg's active engine mount design for high performance engines (Fuller *et al.*, 1996). Below 25-Hz, the hydraulic fluid in the mount provides the necessary damping. Above 25-Hz, the fluid effectively provides the rigid link between the in-line electromagnetic actuator and the car body allowing the actuator force to cancel out the excitation caused by the engine.

This principle advocated by Tanaka and Kikushima appears to be sound. However, it is not possible to reduce the transmitted force to zero nor to perfectly cancel the primary disturbance. Some residual disturbance of magnitude less than the specified amount may persist. If the support structure were to be relatively stiff and well damped, then for this small magnitude, the dynamic stiffness of the structure would not allow for displacements of significant magnitude to occur. However if there exist parts on the supporting structure such as rails or panels that are relatively compliant, then no matter how small or bounded this residual may be, unacceptable motion may occur at these parts of the structure. A double mounting arrangement seems to be quite appealing to overcome such problem. The (upper) raft can be rigid and has machine-equipment on hard-mounts with active force cancellation. The rigid raft can then be soft mounted onto the superstructure.

2. 3 A review of sensors and control devices in active vibration control

In this section, an examination of the various types of sensors and actuators in use in active vibration control is given. The selection of these components will affect the model of the system and the performance index used to evaluate the effectiveness of AVC.

2.3.1 Dynamic Vibration Absorbers

Dampers or dynamic vibration absorbers (DVA) or tuned vibration absorbers (TVA) have been used to control vibration of mechanical systems. A simple classification of the various types of DVA given by Seto & Furuishi (1991) is reproduced as Figure 2.7.

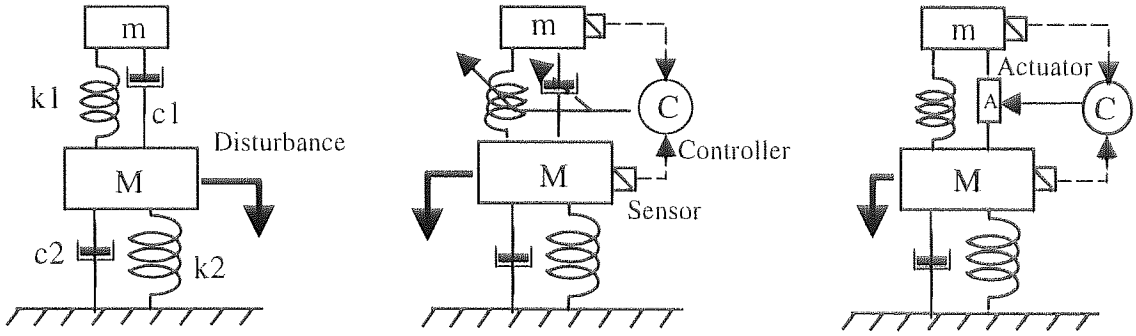

Figure 2.7 Types of dampers

A passive damper or DVA uses a pre-selected auxiliary mass and spring system to keep a vibrating system stationary at a designed frequency when the auxiliary inertia force or the spring force balances the disturbing force acting on the system. For time-invariant system, the use of passive dampers of DVA has proven to be quite satisfactory. Different designs of DVAs for translational or rotational vibration absorption are discussed in great details in Korenev and Reznikov (1993). Swinbanks (1984) gave a short history dating back to 1892 of TVAs used on board ships and a description of the Lancaster damper, a torsion type passive dampers used on marine diesel engines for many years. Semi-active dampers are shown in Figure 2.7b. They have the means to vary the auxiliary damper spring and damping elements to produce a reaction force to counter the disturbance force at more than one frequency. In an active damper, Figure 2.7c, a sensor senses either the effect of the disturbing force (Abu-Akeel, 1967) or the relative motion between the controlled and the auxiliary system (Seto & Furuishi 1991). An actuator is then activated to produce the reaction force. Typically, the sensors are built into the system. DVAs (passive and active) are typically actuators for vibration control for the model shown in Figure 2.2. For example Lords Corporation (Southward *et al.*, 1997) has installed and flight-tested active vibration absorbers on Cessna aeroplanes. Due to FAA certification requirements these 2-DoF active vibration isolators are installed on the fuselage and not as engine mounts. As they are attached via soft-mounts to the fuselage, they can be considered as TVAs.

2.3.2 Proof-mass actuators

For a more massive system like a flexible space structure, proof-mass actuators (Zimmerman *et al.*, 1988, 90) have been developed to control its vibration. Like active

DVA, they apply a force on the structure by reacting against a translating or rotating proof-mass. They typically do not have a mechanical spring to support the proof mass except for the presence of coil that provides support and damping. Electronic stiffness is provided to centre the mass. They are designed primarily to replace the heavy and difficult to mount electro-dynamic shaker for use in space structures. It is also limited in its displacement stroke. Zimmerman *et al.* (1990) actuators have built-in sensor and a microprocessor to act as stand-alone closed loop unit. For smaller system, a simple design of a proof-mass actuator uses an electro-magnetic shaker with an inertia mass e.g. a B&K 4810 with 500g weight as suggested by Preumont and Loix (1994). Such actuators are of course not optimal in terms of power to force generated but they are useful substitutes in the laboratory. The 1-DoF commercial inertia actuators built by Lords Corporation (Southward *et al.*, 1997) are tuned to resonate at or near engine cruise frequency in order to significantly improve the power efficiency of the actuators. These unlike the 2-DoF TVAs mentioned above are rigidly attached to the structure.

2.3.3 Actuators used in active vibration isolation

There is a difference between active mounts and the actuators used in AVC. An active mount has, in addition to conventional passive element, in-built actuator and sensor in a unit, e.g. Barry Controls STACIS 2000. The piezoelectric stack is both actuator and sensor and is another example of an active hard-mount. For majority of the cases, actuators and sensors are added to enhance the existing mounting systems. These are the subjects of review. An actuator used in active vibration control can be classified into:

a. Force generators
b. Displacement type actuators

An actuator behaves like a force generator when its internal mechanical impedance is much smaller than the mechanical impedance of the environment or the external structure against which it is acting. Conversely it behaves like a displacement type actuator when the external structure has relatively lower mechanical impedance.

Force generators used in active machine isolation are similar in design, and have similar response characteristics to the proof-mass actuators. The laboratory types proof-mass

actuators are close to ideal force generators. A typical frequency response of a 2nd order ideal force generator is shown in Figure 2.8. Only the first natural frequency due to the flexible spring support of the moving element of the shaker and the inertia mass is modelled. The specified resonant frequency of the shaker is typically higher, and between these two resonant frequencies the force generator has a constant magnitude, and very importantly almost a constant phase. Below the first inertia mass-spring frequency, the actuator has a positive phase that is phase stabilising for the system.

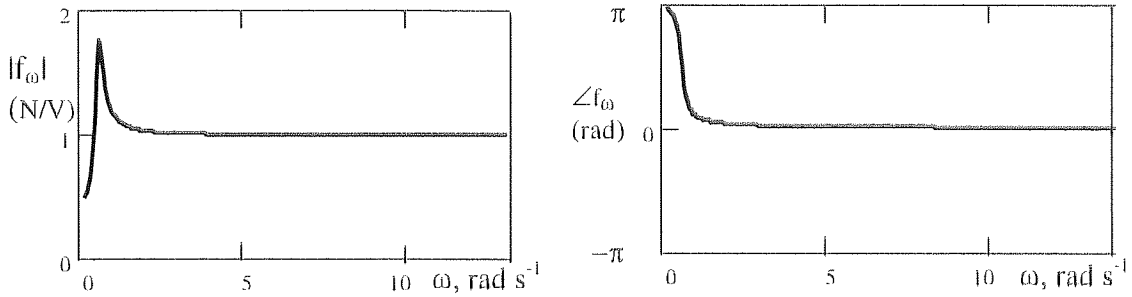

Figure 2.8. Dynamic response of an ideal proof mass actuator

A larger force generator can be realised using servo-hydraulic actuator (Tanaka & Kikushima 1985, 88, 89) acting on a rigid mount. Another type of force actuator is the active electromagnetic damper. They have a moving coil or a moving-armature. A modified loud speaker used by Shubert (1991) of Barry Controls has the moving coil of a speaker attached to the system. In order to generate a large dynamic force range, the coil is bonded to a heat sink, and the current is controlled to prevent overheating.

For higher frequencies, a lightweight piezoelectric inertia actuator (70 gm) is available from PCB Piezotronics, Inc. Its response shape is similar to Figure 2.8, but with a dynamic range of 200-5000 Hz. It has a peak force is 100 lbf and a constant force of 1 lbf. Sometimes these are used as TVA attached to the inside cabin of an aeroplane to suppress vibration arising from the engines.

The more conventional displacement actuators used servomotors or servo hydraulic actuators to move structures or the machine. For example, Miller of Lord Corporation (Miller *et al.*, 1992) has designed a fluid filled displacement actuator. Displacement type actuators of high bandwidth can be obtained from piezoelectric or rare earth permanent magnet actuators (Scribner *et al.*, 1990, and Blackwood & von Flotow, 1992). The piezoelectric stacks have relatively small amplitudes in the order of fraction of milli-inches and stiffness comparable to that of aluminium. They are capable of supporting

large machines with small static deflection. It can be controlled to respond to high frequency input and hence behaves like the ideal machine mount: very high stiffness at low frequency and low stiffness at high frequencies. For practical purpose, it is used with a soft-mount in series to provide system stability (Scribner *et al* 1990).

For both types of actuators, there are in general three ways to mount them as shown in Figure 2.9.

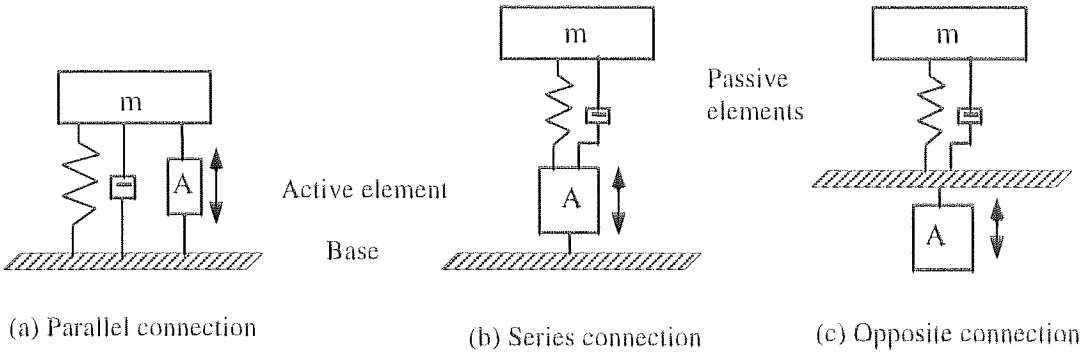

Figure 2.9 Actuators arrangements

An actuator that is placed in parallel to a soft-mount shares the static load with the passive element. It has to overcome the stiffness of the passive element before it can react against the mass of the machine or move the machine. In Figure 2.9b, an actuator in series with a passive element has to bear the entire load of the machine. It needs only to overcome its own stiffness. This is a suitable arrangement for a compact active mount design. Figure 2.9c shows the actuator mounted on the opposite on the receiver plate to the passive elements. Displacement type actuators are unlikely to be used in this configuration. They need a reference position to generate the required displacement. For force actuators the choice is between Figure 2.9a and 2.9c. Nelson *et al.* (1987) showed that the parallel arrangement of Figure 2.9a requires less force at mass-spring frequency to be effective compared with that of Figure 2.9c. The parallel arrangement may have some practical advantage, being compact in design. However the actuator dynamics is coupled into the system model equation, and may not be easily separated out.

2.4 Sensed variables and the plant model

Sensors are selected depending on whether motion - relative motion between machine and the base structure or absolute motion of the base structure - or net transmitted force to the base structure is chosen as a measured variable in the control scheme. The most often

used sensors are force transducers and accelerometers. Absolute velocity sensor or a geophone can also be used for the isolation of sensitive equipment from a vibrating base structure. The direct feedback of velocity measurements is equivalent to providing damping electronically.

A plant or system model can be determined by the measured transmitted force or base acceleration in response to a disturbance at the machine. For a free running or unloaded machine, the *disturbance* acceleration is actually the machine free vibration which is related to the *disturbance* force (blocked force) by the machine output mobility. The choice of sensor and actuator determines the plant model used in the design of a controller. For a 1-DoF case, the various inputs and outputs used are tabulated below in Table 2.1.

Authors	input variable	output variable (feedback)
Watters *et al.*, (1988)	*disturbance* force	transmitted force
Shubert (1991)	actuator force	equipment velocity
Scribner *et al.*, (1993)	(a) *disturbance* acceleration (b) *disturbance* force	transmitted force transmitted force
Blackwood and von Flotow (1992)	(a) actuator force (b) actuator force (c) actuator force (d) actuator displacement (e) actuator displacement	relative acceleration transmitted force structure acceleration transmitted force relative acceleration
Preumont and Loix (1994)	actuator force	structure acceleration

Table 2.1 Various combinations of input variables and output variables

Some of the combinations given in Table 2.1 can be represented by the various set ups of actuators, sensors and mounts shown in Figure 2.10. For example, Figure 2.10a shows a machine that is hard-mounted to a flexible base. The actuator force and the measured base motion are the input and output variable respectively. The force feedback is optional for the control of the actuator force. If the force sensor is at the foot of the machine mount, then disturbance force can be the input variable. Instead of an actuator, an active DVA can be used to absorb the energy causing the motion.

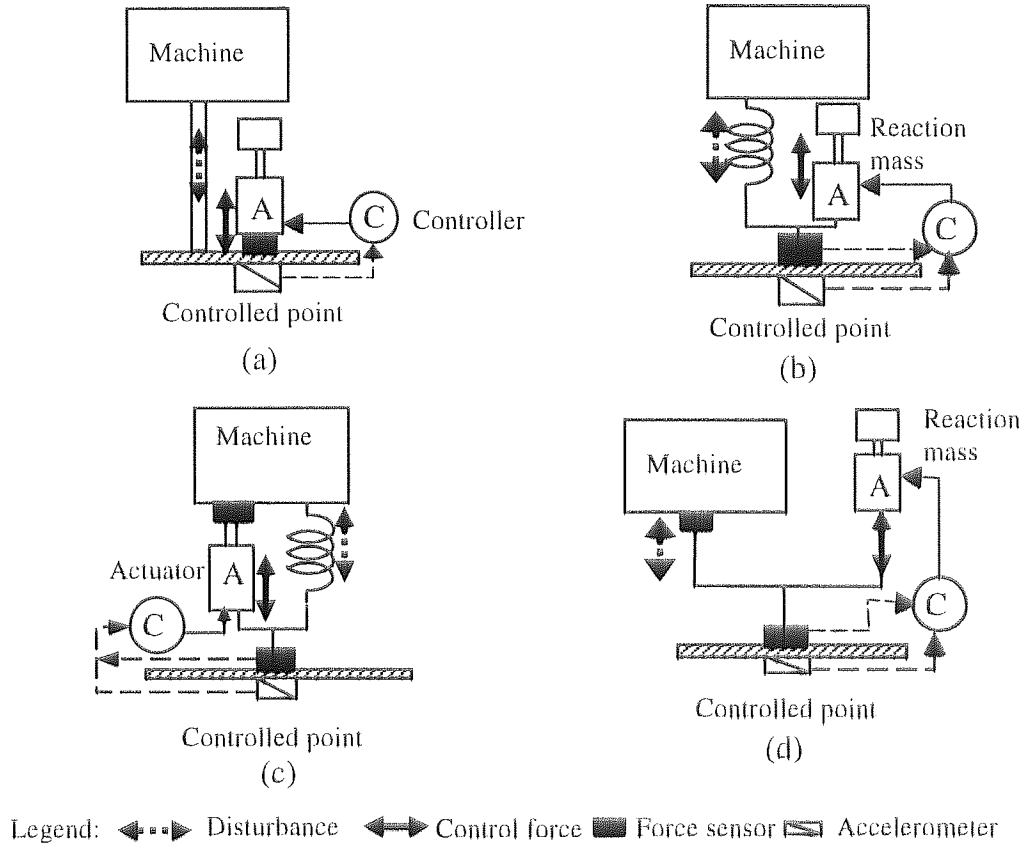

Figure 2.10 Arrangement of actuators, sensors and mounts

With the other arrangements, there is a choice between motion or force sensors for the output variable, but seldom both. With Figure 2.10b or Figure 2.10c the output variable is either the base acceleration or transmitted force and the input variable is the actuator force. The difference between Figure 2.10b and Figure 2.10c is that the former needs a reacting mass, but does not need to overcome the static stiffness of the passive mount. A variation of Figure 2.10c has no spring, and if a second force sensor is attached at the base of the machine, then the input variable can either be disturbance force or actuator force. This case is very similar to an active mount design. The actuator alone has to bear both the static and dynamic loading of the machine vibratory motion. Figure 2.10d has the same input and output variables as Figure 2.10c without spring. It has a machine and the actuator mounted on a common connection to the base. Machine alignment can be maintained even when the controlled force is applied to cancel the disturbance force. This arrangement to reduce the transmission of vibration is analogous to generating an anti-noise to cancel the noise.

Either transmitted force or base acceleration or relative acceleration between base and machine can be used as output variable. When the (open loop) transfer function matrix or

force transmissibility matrix (in the case of MIMO) is to be modified, it is less obvious which of these is more appropriate especially when the base is flexible. Watters *et al.* (1988) observed that resonant dynamics of a flexible supporting structure can couple into the system measured transfer function if measured base acceleration is used. On the other hand if measured net force transmitted is used, the transmissibility function using commanded actuation force to measured net transmitted force is not significantly influenced by the base structure dynamics. Models and simulation studies by (Burke & Abelhamid 1991) and (Blackwood & von Flotow 1992) also confirmed this observation.

Hence in this thesis it is decided to use net transmitted force measurement in response to commanded force actuation. Laboratory type electro-magnetic shakers can be used to provide actuation force. If the isolator paths are short, and machine disturbance not too large, the proposed arrangement is given in Figure 2.11. A 2-dimensional view is given to provide a clearer picture.

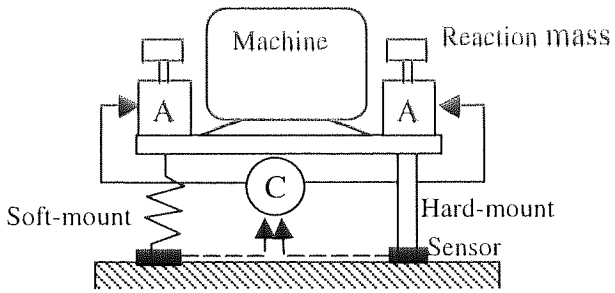

Figure 2.11 Active force cancellation at the feet of a machine

Both soft-mounts and hard-mounts model are detailed and analysed. The models are easier to obtain compared with the parallel connection arrangement shown in Figure 2.10c. The actuators' dynamics can be separated from the machine disturbance to net transmitted force and hence actuators' dynamics can be determined separately on a rigid ground. The open loop force transmissibility matrix can then be used as a disturbance rejection performance specification. Unlike the opposite arrangement of Figure 2.9c, the active force cancellation is provided nearer to the source of the disturbance. The configuration of Figure 2.11 works as long as there is relatively little phase change between the force at the top of the mount and that at the bottom of the mount. From the experience described below, the arrangement works better with hard-mounts. With soft-mounts the controlled forces when activated cause the machine to move. This would not be appropriate in situations where machine alignment is critical.

2.5 Preliminary works

Two examples of preliminary work on active damping and active vibration are given. They are used to show the concepts highlighted and provided some necessary experience. A simple active DVA was built to cancel the vibration due to unbalanced rotor in experimental rig shown in Figure 2.12. It is based on the simple pendulum damper.

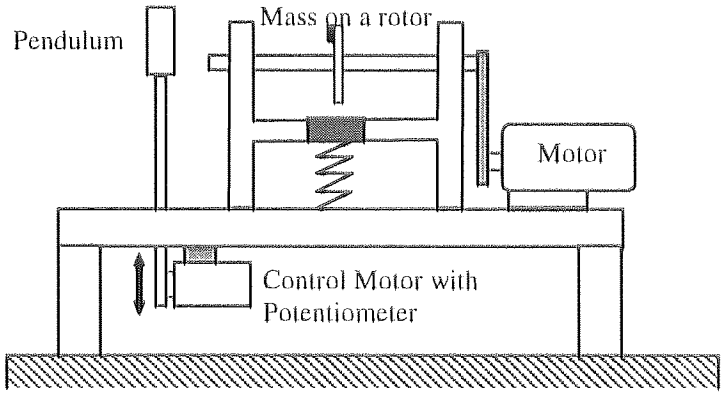

Figure 2.12 Active pendulum DVA for unbalanced rotor

The motor can be operated between 700 and 1140 rpm. A rotating imbalance mass creates a vibrating frequency corresponding to the motor speed. A control motor drives a pendulum up and down and this movement is measured by a potentiometer. The length of the pendulum, x_o, to absorb the vibration due to an unbalanced mass on the rotor is calibrated against a narrow range of disturbance frequency as shown in Figure 2.13.

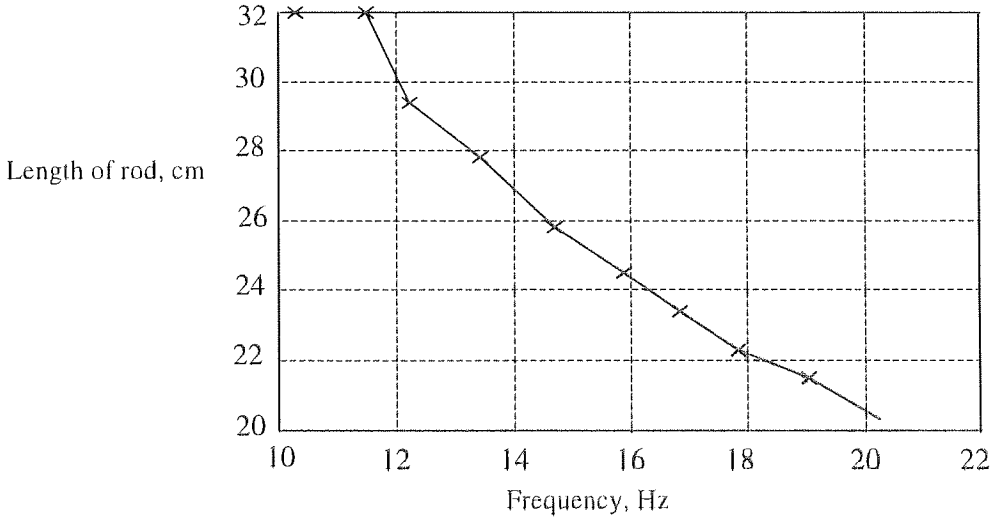

Figure 2.13 Calibration for rod length versus frequency

The calibrated curve of x_o is programmed as a look-up table. The control action is done in a repeated-loop comprising two steps: (a) course motions to drive the pendulum to a distance, x_o corresponding the detected resonant frequency and (b) fine adjustments of the

motion about x_o. In step (a) the controller performs a FFT on the accelerometer signal to determine the spectral peak corresponding to the disturbance frequency. The desired pendulum length is interpolated from values in the look-up table and the motor servoed the pendulum to this desired length. The controller then computes the RMS value of the accelerometer signal and micro-adjusts the length of the pendulum until the RMS reading is the smallest within a fixed period of time.

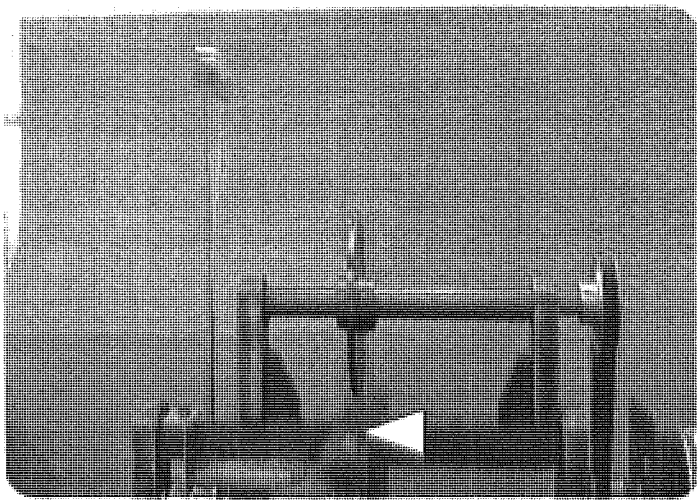

Photo 2.1 Machine vibrating at point indicated

When the pendulum control is inactive, Photo 2.1 shows the reference point (indicated by an arrow) vibrating rigorously. It is a blurred image. When the pendulum is adjusted to the right length, Photo 2.2 shows the same point to be stationary. The image is clearer.

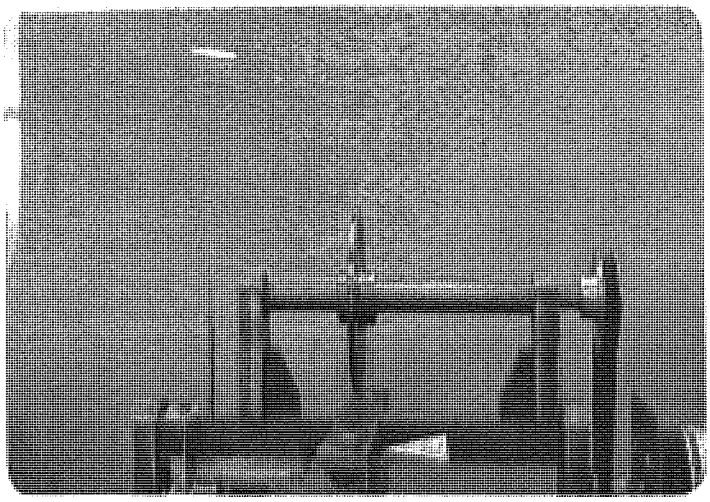

Photo 2.2 Effect of the active DVA on the vibrating machine

This active DVA is able to reduce the vibration for some frequencies within the calibrated range. The result of an experiment for the motor running at 1000 rpm is shown in Figure 2.14 below. A reduction of about 92% in RMS values has been achieved.

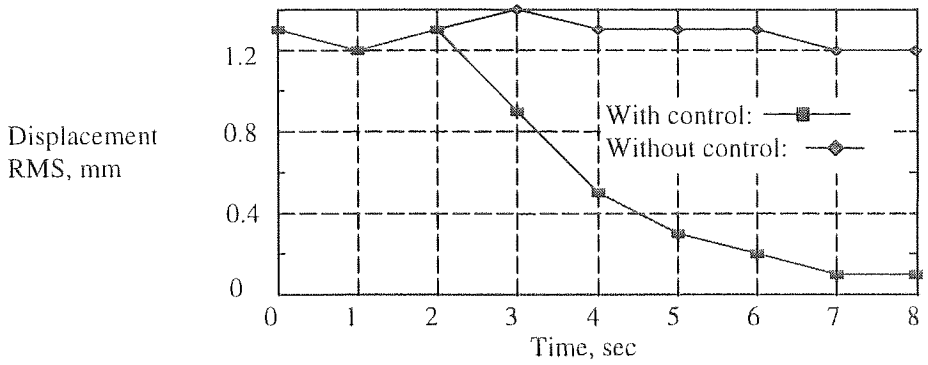

Figure 2.14 The effect of active DVA on measured RMS

A potential problem with this DVA design is that it can fail during operation. A pair of friction rollers is used to drive the pendulum up and down in a servo operation. With constant operation, the pendulum is cold worked over time and it becomes brittle. When the pendulum is at the desired length for effective absorption, it vibrates very vigorously. On one occasion, the pendulum sheared off at the rollers contact points.

A second piece of work relates to the use of force actuation in response to measured acceleration. The experimental rig is shown in Figure 2.15.

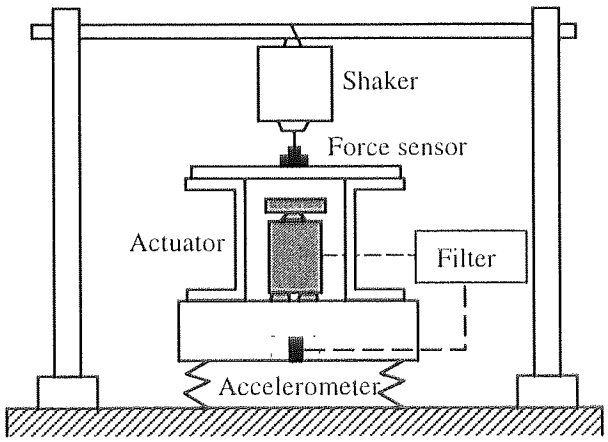

Figure 2.15 A rig for 1-DoF AVC using motion feedback and force actuation

Four coil springs are used to try to confine the motion to 1-DoF. The resonant frequency ω_0 is about 9.5 Hz. A low pass 2^{nd} order filter is tuned to have a natural frequency of ω_a=19 Hz and damping ζ=0.3. The machine is excited at its resonant frequency. The time record of the experiment shown in Figure 2.16 shows (1) when excitation is OFF, and then turned ON at (2), and the filter turned ON at (3). A sharp drop in the motion of the mass is recorded.

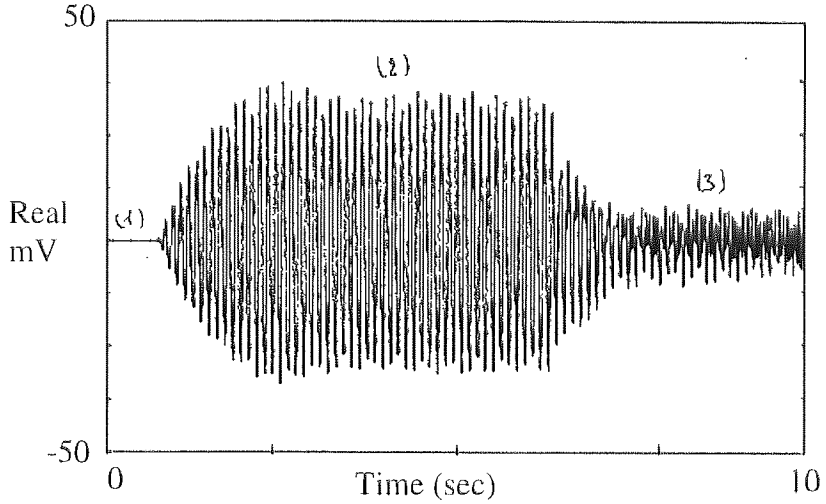

Figure 2.16 Time response of a 1-DoF active vibration experiment

Another experiment using two sets of collocated force actuators and accelerometers on a rigid block spring mounted onto a flexible beam at two points gave a reasonable reduction for vertical motion. A small rocking motion is also induced. This is not unexpected as the springs are not identical and the system c.g. is not symmetrically located with respect to the actuators. Equations of motion can be obtained for a rigid mass on a flexible beam and a LQ controller can be designed to de-couple the two motions (Chen and Batta, 1991).

The experiment on the active DVA confirms that if the disturbance is relatively predictable, the use of feedforward control is simple to use. FFT can be used to determine the disturbance frequency and the appropriate length of the pendulum can then controlled by the servo-system. However given the uncertainty in the estimation of the length of the pendulum using a potentiometer, a feedback loop is still necessary to ensure that the RMS displacement is reduced. Some form of robust control is required. With adaptive filtering, the controller is continuously monitoring and estimating and updating the model of the plant. This provides some robustness. So feedforward control must be used with complementary schemes to ensure some degree of robustness.

The experiments using force actuation show that local direct feedback requires a little more attention. Although a local controlled variable like vertical motion can be reduced there will some interaction between neighbouring actuators and sensors to produce rocking motion. Basing on this observation, using direct local feedback i.e. a diagonal controller for a machine mounted at four points may not necessarily reduce all vibratory motions. For the rocking motion, the use of hard-mounts may provide some degree of

constraint for this degree of motion. This makes the idea of active hard-mounting attractive especially for applications where the machine has to follow the vehicle in body manoeuvres at relatively low frequency but vibration must be prevented from exciting the vehicle body at machine operating frequencies.

2.6 Summary

The following points emerging from the vibration control literature review are relevant to active vibration isolation:

i. The control of vibration in the receiver region has been widely researched into. Vibratory responses to external disturbances may be reduced by the use of feedback and model based control methods. These models are mostly based on beams, plates and trusses. Much has been learnt from the control of flexible structures especially the relationship of the location of sensors and actuators to model based control. Direct local feedback using collocated sensors and actuators is one of the solutions examined. Such a problem is also known as vibration suppression.
ii. When the geometry of the problem provides for discrete and identifiable transmission paths, active vibration control of the disturbance along these paths can be used to cancel the disturbance before it reaches the vibration sensitive region. Problem of this nature is sometimes referred to as vibration isolation.
iii. In active vibration isolation, when more information is available about the disturbances, feedforward control can be applied to enhance disturbance rejection. Adaptive feedforward or feedback control methods can be used when disturbance is not easily predictable.
iv. In active vibration isolation, many arrangements of actuators and sensors are possible depending on the machine, the space availability and the dynamics of the receiver region. If the actuator is not in parallel with the isolator, the dynamics of the actuator may be excluded from the open loop transfer function. This provides some degree of simplification in model derivation.
v. Machine disturbances caused by inertia forces and synchronisation cancellation were demonstrated in 1892 (according to Swinbanks, 1984) by Sir Alfred Yarrow. So long as the disturbance can be identified and there is insignificant time delay between identifying the disturbance and generating an equal and opposite inertia

force, synchronisation cancellation using feedforward control is a good choice. When neither of the two requirements is satisfied, feedback control can be used.

vi. Active force cancellation is a viable solution and the use of current robust control theory and the $\mathcal{H}_\infty$ optimal control method have not been sufficiently explored in active vibration isolation. Indeed active vibration as a MIMO control problem is also not sufficiently examined, although as a m-DoF problem it is very well studied especially in the area of vibration suppression.

It is proposed to investigate the active vibration isolation problem from a MIMO control viewpoint. The use of $\mathcal{H}_\infty$ optimal control method and any other relevant MIMO methods will be explored. The objectives of these control design methods are

(a) to achieve a RMS reduction in the level of transmitted force to some acceptable level defined as a function of frequency;
(b) to be robust to some system uncertainties within some limits; and
(c) to use the minimum amount of control "effort" in attaining (a).

The final point is extremely important since solutions that require large amounts of control effort will involve physically large actuators or it may result in actuator saturation.

The principle of force cancellation basing on the measurements of the net transmitted force in response to actuator force will be used. It is the same principle as anti-noise cancellation. It is proposed that active force cancellation be placed as close to the disturbance as possible i.e. at the base of the machine. To achieve a short time delay between sensing, conditioning and actuation, the mounts must be short, and the controller-actuator pair must be have sufficient bandwidth. In view of these, the set-up of Figure 2.11 is proposed, and laboratory electro-magnetic shakers of sufficient force capability and bandwidth are available and can be used as force actuators. Load cells or quartz force sensors are possible force sensors but since the latter has higher bandwidth it is a better choice. Analogue controllers would not be capable of implementing MIMO controller designs and so a high-speed digital signal processor offering more flexibility and power will be used. The two types of mounts shown in Figure 2.11 will also be examined from a control design perspective. These are detailed in the later chapters.

CHAPTER THREE

MODELLING AND CONTROL OF ACTIVE VIBRATION ISOLATION OF A MACHINE SOFT-MOUNTED ON A FLEXIBLE BASE STRUCTURE AT MULTIPLE POINTS

3.1 Introduction

One of the most studied areas of active vibration control is the use of active control to enhance the performance of passive isolators. This approach is prudent. Most users are not only familiar with the successful use of resilient mounts but are also comfortable with the fact that in the event of a failure of the active isolation system, there is still a passive system to act as a back up.

Ideally the development of an active isolation stage should, as far as possible, be independent of the eventual supporting base or structure of the equipment or machinery. In the case where passive isolators are used, the machine and the isolation system should be tested as a sub-system, disconnected and independent of the final supporting structure. The selected measure of performance is transmissibility: either force or motion.

The main contribution of this chapter is the development of a mathematical model of a machine mounted on multiple isolators on a flexible base or structure. It is given as a force transmissibility matrix function in equation (3.26) as $(\mathbf{I}+\Delta_M)\cdot\mathbf{Go}$, a product of two terms that can be obtained independently. This model will enable the design and the testing of machine and the active isolation system on a base (e.g. machine vendor's site) that is not necessarily the same as the final base. The active vibration system is based on force cancellation applied at the machine feet-mounts interface. The derivation of the model is simpler compared with the case of actuators in parallel with passive isolators used for example in Watters *et al* (1989). The force transmissibility function matrix can also provide a force disturbance curve for the design of a local control system.

This chapter is organised to show the development of the model from 1-DoF to m-DoF and the implications on control of active vibration. It is arranged as follows:

i) 1-DoF analysis leading to a force transmissibility function for a machine on a rigid and a flexible base or structure.

ii) m-DoF analysis leading to a force transmissibility matrix function for a machine on rigid base, with forces and motions taken w.r.t. machine's centre of gravity.

iii)m-DoF analysis leading to a force transmissibility matrix function for a machine on a flexible base, with forces and motions taken at the machine-base interface.

iv)Discussions of the implications of the system model on control using the robust control framework.

In all the analyses, the main assumptions are that the machine is rigid, the mass of the isolators are negligible having only relative stiffness and the flexible base has potentially unknown dynamics.

Although symbols used in the thesis have already been defined, the subscripts relevant to the development of the model are re-stated here for clarity.

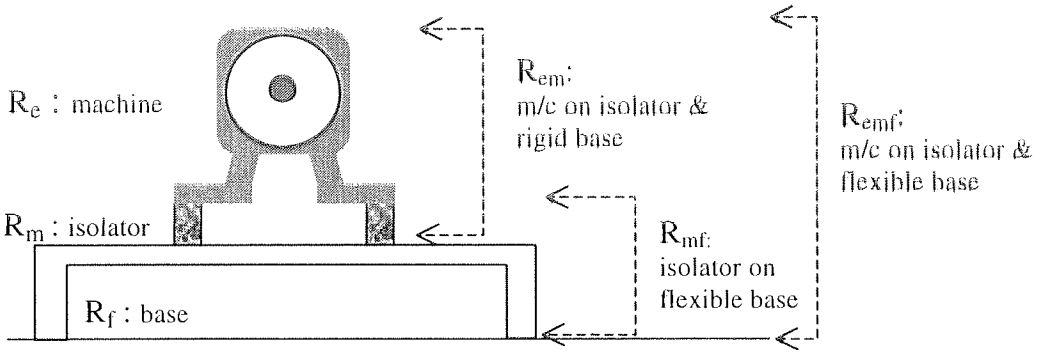

Figure 3.1 System definition and symbols

The letter "R" shall be used to represent receptance function and "D" its reciprocal, the dynamic stiffness function. In addition, the subscript "c", shall be used with "D" i.e. "D_c" to represent the combined or summation of stiffness of the machine-isolator on a rigid supporting structure for all forces and motions taken with respect to the c.g. of the rigid machine.

3.2 Motivation

There are many reasons why it is necessary to design active isolation system to improve upon the rejection of the disturbance into structures where machinery or equipment is installed. Firstly, it has to do with human comfort. Secondly, it is to protect the machinery and equipment. Thirdly, in some cases it is for survival as in avoiding detection of a submarine by its predators. And lastly, to overcome the limitations imposed by the use of

passive isolation alone, as a proper selection of flexible isolators may not be enough to prevent the transmission of vibration from a machine to its base. Soft or flexible isolators suffer from internal high frequency resonance (metal springs) and may have static deflections that are too large for sufficient positional control of a machine.

With active vibration isolation, active isolators are used in parallel or in series with the passive isolators to supplement the deficiencies of the passive isolators. This arrangement has many advantages. Many engineers are familiar with the design of passive isolators as the main vibration suppression system. And they act as a fail-safe device as well as a complementary device. Under certain conditions given here, they will effectively de-couple the flexible base modes from the measured force transmitted and hence permit the possible design of robust active vibration isolation.

Most active vibration isolation systems are designed typically using feedforward controllers with fixed reference signals and feedforward anti-noise cancellation technique for multiple mounting locations. They have been successfully demonstrated when the disturbance signals or the disturbance path characteristics are deterministic or relatively invariant in nature. For example, in the works of Chaplin (1983), Eghtesadi and Chaplin (1987), Jenkins, *et al.* (1990), and Pan *et al.* (1993a,1993b). In Fuller *et al.* (1996) there is a description of the Freudenberg active engine mount. Lotus Engineering successfully tested it on a Volkswagen Golf GTI. These methods do not need the model of the system as much as knowledge of the disturbance or the disturbance paths.

When disturbance signals are not known with a relatively high degree of accuracy, or when knowledge of some part of the system is uncertain, feedback controllers are required. This is the strength of feedback systems: protection against some degree of uncertainty. However they do need a model based on some predefined performance metric. Some successful simulation and experimental results of feedback active isolation have been reported. For example: using notch filters with actuators in parallel with isolators (Watters *et al.*, 1988), active damping (Chen and Batta, 1991) with actuators in series with isolators, and active vibration absorbers (Rider and Hodson, 1991). Yeong (1992) using a combination of digital notch and inverse filters for one axis has also successfully demonstrated active force control of narrow band rejection at Hughes Aircraft (the company's name in 1992).

The primary excitation of a machine on flexible isolators on a relatively rigid support will be one of well-separated narrow frequency lines and one could easily adopt the use of feedforward control. As shown by Plunkett (1958) amongst others, if the machine were to be mounted on a flexible base instead, there will be interaction between the vibrating machine and the dynamics of the flexible base. Such interactions will modify the primary excitation acting as a disturbance. So it would be desirable to determine what will be modified, and the kind of model that will be available to a control engineer to design an active vibration isolation system. This is the objective of this chapter:

To derive a suitable m-DoF model of a machine mounted via flexible isolators on a flexible base that can be used to determine the transmitted disturbance spectrum to the flexible base and the effect of the base flexibility on the machine disturbance spectrum measured on a rigid base.

Focus will be placed only on machine disturbance instead of the case where the disturbance comes from the supporting structure. To begin with, it is assumed that the disturbance acts at the machine centre of gravity (c.g.) and that the moments are taken about the c.g. By means of a transformation matrix, the location of forces and moments can be transferred to the mounting locations. The machine (a general term) can be regarded to be rigid in comparison with the supporting structure. Such structures include the hulls of ships and submarines, and the fuselages of helicopters and aeroplanes. They are relatively more flexible than the machinery and engines. The base structure considered here is arbitrary or has undefined geometry and hence is not confined to beams or plates. However for the purpose of illustration, an example using a beam will be shown. The assumption of rigid machine is quite appropriate when

i) the machine is massive and dense in comparison with the structure, which is light and flexible, e.g. diesel engine on ship's hull, jet engines mounted on wings of aeroplanes, internal combustion engines in land vehicles;

ii) in the frequency of interest, the first few modes of the base structure are below the first mode of the machine (Scribner *et al.*, 1993).

With these assumptions, the model will be derived starting from a 1-DoF model. This gives the motivation for the extension to the required m-DoF model.

What will eventually emerge is a model that will suit the framework of current control interest and methods of robust control theory and $\mathcal{H}_\infty$ optimal control. It will also permit the design and testing to be done using a test-bed totally dissimilar from the final base structure. This will be beneficial to control engineers engaged in the design of active vibration isolation. However, it still requires the proper selection of soft mounts' properties vis-à-vis the mounting locations and flexible base modal properties.

3.3 The classical 1-DoF model

A single mass, m, mounted via a spring and damper on either a rigid or a flexible base is the most commonly used model. These can be found for instance in Den Hartog (1965). The rigid and flexible base case studies are good examples of how an engineer can assess the suitability of an isolator for use with a machine on a flexible base but being tested on a rigid base. Without viscous damping, the force transmissibility of the two cases are given respectively as

$$\left[1+ms^2\left(\mathrm{R_m}\right)\right]^{-1} \text{ and } \left[1+ms^2\left(\mathrm{R_m}+\mathrm{R_f}\right)\right]^{-1} \tag{3.1}$$

In (3.1) the term $\mathrm{R_m} = 1/k$ is the reciprocal of the dynamic stiffness of the isolator. The second equation can be written as

$$\left(\frac{k}{k+m\,s^2}\right)\cdot\left[1+\frac{mk\,s^2\mathrm{R_f}}{k+m\,s^2}\right]^{-1} = \left(\frac{k}{k+m\,s^2}\right)\cdot\left[1-\mathrm{X}\right]^{-1} \tag{3.2}$$

If X in (3.2) is small (in a sense that will be defined in the later part of the chapter), then the force transmissibility due to base flexibility can be expressed approximately as

$$\left(\frac{k}{k+m\,s^2}\right)\cdot\left[1+\mathrm{X}\right] = \mathrm{G_0}\left[1+\mathrm{X}\right] \tag{3.3}$$

The term X in (3.3) is dependent on the mass m, isolator stiffness k and the base modal property given by R_f and G_o is the force transmissibility function of the rigid mass mounted on a rigid base. A detailed discussion for this 1-DoF case is given in (Blackwood and von Flotow, 1992). The advantage of the concept put forward by this expression is obvious: it shows that the effect of base flexibility is equivalent to a perturbation of G_o. By plotting (3.3) and comparing it with G_o, the peak magnitudes of $|R_f(j\omega_r)|$, at various flexible base resonant frequencies, ω_r, that are coupled onto G_o can be determined. The degree of coupling of G_o as shown by Blackwood and von Flotow (1992) is affected by $|X(j\omega)|$ and can be reduced by the judicious selection of k. The actual final base mounting affecting X is not physically needed as long as the design or engineering data (in the form of modal properties) is available. Similarly when active vibration control system is intended, one can choose those frequencies where the couplings are large and design suitable compensators to attenuate them e.g. notch filters or generalised filters (Wei and Byun, 1989).

The term X in (3.3) is like a perturbation term and a perturbed transmissibility function is similar to those expressions used in literature on robust controller design. In §3.8, it will be shown how the m-DoF model developed in this chapter fits naturally into the framework of robust controller design. In this framework, under certain conditions, optimal or sub-optimal controllers can be designed using the $\mathcal{H}_\infty$ control method. The complete information on $X(j\omega)$ (or a similar term Δ used in the later part of the chapter) is not normally needed as a general class of perturbation can be used and the actual base structure dynamics stiffness can be selected from this class.

Alternatively, when the full information is available, the use of (3.3) will provide the force transmissibility function as input disturbance spectrum. Suitable controllers for the active vibration control can then be designed. This is more desirable than using the machine free vibration as a disturbance spectrum (§4.4).

Although robust control is very important, the intention of developing the perturbed model can also be for the purpose of obtaining a disturbance spectrum. This will be the main issue that will be addressed in another chapter.

3.4 Extension to m-DoF

3.4.1 Machine model mounted on n-isolators on a rigid base

There is then a motivation to extend the concept to the general case of a rigid machine on *n* number of isolators. The derivation is quite straightforward but the extension of the perturbation model requires manipulation and refinement of some definitions. The perturbed model for multiple isolators can be simplified and compared with the 1-DoF model.

A rigid machine has 6-DoF and is mounted via resilient isolators on a rigid base. The machine properties are:

$$\mathbf{M} = \begin{bmatrix} m\mathbf{I} & \mathbf{0} \\ \mathbf{0} & \mathbf{J} \end{bmatrix}, \text{ where } m\mathbf{I} = \begin{bmatrix} m & 0 & 0 \\ 0 & m & 0 \\ 0 & 0 & m \end{bmatrix}, \text{ and } \mathbf{J} = \begin{bmatrix} J_{xx} & J_{xy} & J_{xz} \\ J_{yx} & J_{yy} & J_{yz} \\ J_{zx} & J_{yz} & J_{zz} \end{bmatrix} \tag{3.4}$$

I is a 3x3 identity matrix. Each isolator has 6 degrees of freedom. A model of a 6-DoF isolator can be represented by a 6x6 $\underline{\mathbf{k}}_i$ complex stiffness matrix (see Appendix A). The vector of displacements, $\mathbf{X}_c = \{x_c, y_c, z_c\}^T$ and rotations, $\Xi_c = \{\xi_c, \psi_c, \zeta_c\}^T$ of the machine c.g. can be given by $\mathbf{q}_c = \{\mathbf{X}_c^T, \Xi_c^T\}^T = \{x_c, y_c, z_c, \xi_c, \psi_c, \zeta_c\}^T$. Assume that the disturbance forces and moments $\mathbf{Q}_d$ act at the c.g. of the machine.

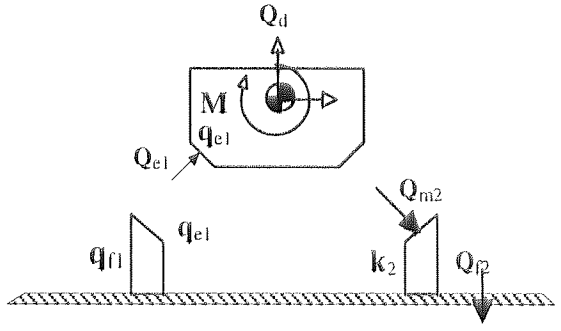

Figure 3.2 Forces and displacements on a rigid machine

The i^{th} isolator is located at a position $\mathbf{r}_i = \{r_{xi}, r_{yi}, r_{zi}\}^T$ from the c.g. At each isolator, there will be both displacements and rotations, and the displacement vector is:

$$\mathbf{X}_{ei} = \mathbf{X}_c + \Xi_c \times \mathbf{r}_i = \mathbf{X}_c - \mathbf{r}_i \times \Xi_c \tag{3.5}$$

Replacing the cross vector operation by a skew-symmetric matrix gives,

$$\underline{\mathbf{r}}_i = \begin{bmatrix} 0 & -r_{zi} & r_{yi} \\ r_{zi} & 0 & -r_{xi} \\ -r_{yi} & r_{xi} & 0 \end{bmatrix}$$

$$\mathbf{X}_{ei} = \mathbf{X}_c - \underline{\mathbf{r}}_i \cdot \Xi_c = [\mathbf{I} \; -\underline{\mathbf{r}}_i]_{3x6}\, \mathbf{q}_c = \mathbf{P}_i \cdot \mathbf{q}_c \tag{3.6}$$

The rotation at the i^{th} isolator, $\Xi_{ei} = \Xi_c$ and complete motion is given by $\mathbf{q}_{ei} = \{\mathbf{X}_{ei}^T, \Xi_{ei}^T\}^T$. In terms of the c.g. motion,

$$\mathbf{q}_{ei} = \begin{bmatrix} \mathbf{I} & -\underline{\mathbf{r}}_i \\ \mathbf{0} & \mathbf{I} \end{bmatrix} \cdot \mathbf{q}_c = \mathbf{P}_i \cdot \mathbf{q}_c \tag{3.7}$$

At the i^{th} isolator, there will be forces and moments acting on the system. This is given by

$$\mathbf{Q}_{ei} = -\underline{\mathbf{k}}_i . \mathbf{q}_{ei} = -\underline{\mathbf{k}}_i \cdot \mathbf{P}_i \cdot \mathbf{q}_c \tag{3.8}$$

The total restoring force at, and moment about the c.g. is given by,

$$\sum_{i=1}^{n} \mathbf{Q}_{ei} = -\sum_{i=1}^{n} \left(\mathbf{P}_i^T \cdot \underline{\mathbf{k}}_i \cdot \mathbf{P}_i \right) \cdot \mathbf{q}_c = -\mathbf{P}^T \cdot \underline{\mathbf{K}} \cdot \mathbf{P} \cdot \mathbf{q}_c \tag{3.9}$$

$$\mathbf{P}^T = \begin{bmatrix} \mathbf{I} & 0 & \cdots & \mathbf{I} & 0 \\ \underline{\mathbf{r}}_1 & \mathbf{I} & \cdots & \underline{\mathbf{r}}_n & \mathbf{I} \end{bmatrix} \text{ and } \underline{\mathbf{K}} = \text{diagonal } (\underline{\mathbf{k}}_1 \ldots \underline{\mathbf{k}}_n),$$

Each $\underline{\mathbf{k}}_i$ has been defined in Appendix A and it includes a loss factor term. For simplicity only resistive spring rates are considered and $\mathbf{K}$ = diagonal($\mathbf{k}_1 \ldots \mathbf{k}_n$) with a dimension of 6n x 6n. Assuming harmonic disturbance at the machine c.g., the equation of motion is given as,

$$\mathbf{M}\cdot\ddot{\mathbf{q}}_c + \mathbf{P}^T\cdot\mathbf{K}\cdot\mathbf{P}\cdot\mathbf{q}_c = \mathbf{Q}_d \tag{3.10}$$

$$\mathbf{q}_c = [-\omega^2\mathbf{M} + \mathbf{P}^T\cdot\mathbf{K}\cdot\mathbf{P}]^{-1}\cdot\mathbf{Q}_d = \mathbf{D}_c{}^{-1}\cdot\mathbf{Q}_d = \mathbf{R}_c\cdot\mathbf{Q}_d$$

Some literature (Rao, 1995) uses the term mechanical impedance for $[-\omega^2\mathbf{M}+\mathbf{P}^T\cdot\mathbf{K}\cdot\mathbf{P}]$. Here it is referred to as the dynamic stiffness, $\mathbf{D}_c$. For brevity $\mathbf{R}_c$ is used for its inverse. It relates the motion at the c.g. in response to applied forces at the machine c.g. Examples of rigid body motion would be the heaving in the vertical direction, rocking, and coupled lateral motions. Corresponding to each of the rigid body modes, there is a natural frequency associated with motion in that direction. If a viscous damping term is used then $\mathbf{C}$ = diagonal ($\mathbf{c}_1$,..., $\mathbf{c}_n$) and

$$\mathbf{M}\cdot\ddot{\mathbf{q}}_c + \mathbf{P}^T\cdot\mathbf{C}\cdot\mathbf{P}\cdot\dot{\mathbf{q}}_c + \mathbf{P}^T\cdot\mathbf{K}\cdot\mathbf{P}\cdot\mathbf{q}_c = \mathbf{Q}_d \tag{3.11}$$

$$\mathbf{q}_c = [-\omega^2\mathbf{M} + \mathbf{P}^T\cdot\mathbf{K}\cdot\mathbf{P} + j\omega\mathbf{P}^T\cdot\mathbf{C}\cdot\mathbf{P}]^{-1}\cdot\mathbf{Q}_d = \mathbf{R}_c\cdot\mathbf{Q}_d$$

Using equation (3.10) the vector of transmitted force to the rigid base is given by

$$\mathbf{Q}_{f\,(rigid)} = \mathbf{K}\cdot\mathbf{q}_e = \mathbf{K}\cdot\mathbf{P}\cdot\mathbf{q}_c = \mathbf{K}\cdot\mathbf{P}\cdot\mathbf{R}_c\cdot\mathbf{Q}_d \tag{3.12}$$

Hence the force transmissibility matrix function is given by

$$\mathbf{G}_o = \mathbf{K}\cdot\mathbf{P}\cdot\mathbf{R}_c \tag{3.13}$$

3.4.2. Effect of base flexibility when disturbance is applied at the machine c.g.

Let the base be flexible with receptance matrix, $\mathbf{R}_f$ or its inverse the dynamic stiffness matrix $\mathbf{D}_f$. At each isolator location

Relative motions : $\mathbf{q}_{ei}$-$\mathbf{q}_{fi}$.

Force/moment : $\mathbf{Q}_{fi} = \mathbf{k}_i\,\{\mathbf{q}_{ei}-\mathbf{q}_{fi}\} = -\mathbf{Q}_{ei}$

The restoring force at the feet of the machine is given by:

$$\mathbf{Q_c} = -\mathbf{P^T}\cdot\mathbf{K}\cdot(\mathbf{I} - [\mathbf{D_f} + \mathbf{K}]^{-1}\,\mathbf{K})\cdot\mathbf{P}\cdot\mathbf{q_c} = \mathbf{P^T}\cdot\mathbf{Q_f} = -\mathbf{P^T}\cdot\mathbf{Q_e} \tag{3.14}$$

The identity matrix, **I**, is of dimension 6x6. The equation of motion is therefore given by

$$\mathbf{M}\cdot\ddot{\mathbf{q}}_c + \mathbf{P}^T\cdot\mathbf{K}\cdot(\mathbf{I} - [\mathbf{D}_f + \mathbf{K}]^{-1}\mathbf{K})\cdot\mathbf{P}\cdot\mathbf{q}_c = \mathbf{Q}_d \tag{3.15}$$

$$\mathbf{q}_c = [\,(-\omega^2\mathbf{M} + \mathbf{P}^T\cdot\mathbf{K}\cdot\mathbf{P}) - \mathbf{P}^T\cdot\mathbf{K}\cdot[\mathbf{D}_f + \mathbf{K}]^{-1}\mathbf{K}\cdot\mathbf{P}\,]^{-1}\cdot\mathbf{Q}_d$$

$$= [\mathbf{D}_c - \Delta]^{-1}\cdot\mathbf{Q}_d$$

Where

$$\Delta = \mathbf{P}^T\cdot\mathbf{K}\cdot(\mathbf{D}_f + \mathbf{K})^{-1}\cdot\mathbf{K}\cdot\mathbf{P}$$

The term Δ represents the interaction between the base flexibility motions with the rigid machine motions. The transmitted force and the force transmissibility function are respectively:

$$\mathbf{Q_f} = [(\mathbf{I} - \mathbf{K}\cdot(\mathbf{D_f} + \mathbf{K})^{-1})\cdot\mathbf{K}\cdot\mathbf{P}\cdot(\mathbf{D_c} - \Delta)^{-1}]\cdot\mathbf{Q_d} \tag{3.16}$$

$$\mathbf{G_{f\,(flex)}} = [(\mathbf{I} - \mathbf{K}\cdot(\mathbf{D_f} + \mathbf{K})^{-1})\cdot\mathbf{K}\cdot\mathbf{P}\cdot(\mathbf{D_c} - \Delta)^{-1}]$$

The term $\mathbf{G_{f\,(flex)}}$ is the force transmissibility for a flexible base for the case where the disturbance is applied at the machine c.g. It is possible to simplify the force transmissibility $\mathbf{G_{f\,(flex)}}$. Using equation (3.14) and equation (3.15) to evaluate $\mathbf{P^T}\cdot\mathbf{Q_f}$ gives

$$\mathbf{Q_c} = -\mathbf{P^T}\cdot\mathbf{Q_f} = -\mathbf{P^T}\cdot[(\mathbf{I} - \mathbf{K}\cdot(\mathbf{D_f} + \mathbf{K})^{-1})\cdot\mathbf{K}\cdot\mathbf{P}\cdot(\mathbf{D_c} - \Delta)^{-1}]\cdot\mathbf{Q_d} \tag{3.17}$$

Let

$$\mathbf{G_c} = \mathbf{P^T}\cdot[(\mathbf{I} - \mathbf{K}\cdot(\mathbf{D_f} + \mathbf{K})^{-1})\cdot\mathbf{K}\cdot\mathbf{P}\cdot(\mathbf{D_c} - \Delta)^{-1}]$$

$$= \mathbf{P^T}\cdot[(\mathbf{I} - \mathbf{K}\cdot(\mathbf{D_f} + \mathbf{K})^{-1})\cdot\mathbf{K}\cdot\mathbf{P}\cdot\mathbf{R}\cdot(\mathbf{I} - \Delta\cdot\mathbf{R_c})^{-1}]$$

$$\mathbf{R_{mf}} = [\mathbf{D_f} + \mathbf{K}]^{-1},\ \mathbf{D_c}^{-1} = \mathbf{R_c} \text{ and } \mathbf{X} = \Delta\cdot\mathbf{R_c} = \mathbf{P^T}\cdot(\mathbf{K}\cdot\mathbf{R_{mf}}\cdot\mathbf{K})\cdot\mathbf{P}\cdot\mathbf{R_c};$$

Then (3.17) can be written as

$$\mathbf{Q}_c = \mathbf{G}_c \cdot \mathbf{Q}_d = \mathbf{P}^T \cdot [(\mathbf{I} - \mathbf{K} \cdot \mathbf{R}_{mf}) \cdot \mathbf{K} \cdot \mathbf{P} \cdot \mathbf{R}_c \cdot (\mathbf{I} - \mathbf{X})^{-1}] \cdot \mathbf{Q}_d \tag{3.17a}$$

From (Wilkinson, 1965)

$$[\mathbf{I} - \mathbf{X}]^{-1} = [\mathbf{I} + \mathbf{X} - \ldots . \mathbf{X}^k] \Leftrightarrow \lim_{k \to \infty} (\mathbf{X})^k \to 0 \quad \Leftrightarrow \rho(\mathbf{X}) = \rho(\Delta \cdot \mathbf{R}_c) < 1.$$

If $\rho(\mathbf{X}) << 1$, and neglecting terms $(\mathbf{X})^2$ and higher, then

$$\mathbf{G}_c \approx \mathbf{P}^T \cdot (\mathbf{I} - \mathbf{K} \cdot \mathbf{R}_{mf}) (\mathbf{K} \cdot \mathbf{P} \cdot \mathbf{R}_c + \mathbf{K} \cdot \mathbf{P} \cdot \mathbf{R}_c \cdot \mathbf{X})$$

$$= (\mathbf{P}^T \cdot \mathbf{K} \cdot \mathbf{P} \cdot \mathbf{R}_c + \mathbf{P}^T \cdot \mathbf{K} \cdot \mathbf{P} \cdot \mathbf{R}_c \cdot \mathbf{X} - \mathbf{P}^T \cdot \mathbf{K} \cdot \mathbf{R}_{mf} \cdot \mathbf{K} \cdot \mathbf{P} \cdot \mathbf{R}_c - \mathbf{P}^T \cdot \mathbf{K} \cdot \mathbf{R}_{mf} \cdot \mathbf{K} \cdot \mathbf{P} \cdot \mathbf{R}_c \cdot \mathbf{X})$$

$$= (\mathbf{P}^T \cdot \mathbf{K} \cdot \mathbf{P} \cdot \mathbf{R}_c + \mathbf{P}^T \cdot \mathbf{K} \cdot \mathbf{P} \cdot \mathbf{R}_c \cdot \mathbf{X} - \mathbf{X} - \mathbf{X}^2)$$

$$\approx (\mathbf{P}^T \cdot \mathbf{K} \cdot \mathbf{P} \cdot \mathbf{R}_c + \mathbf{P}^T \cdot \mathbf{K} \cdot \mathbf{P} \cdot \mathbf{R}_c \cdot \mathbf{X} - \mathbf{X})$$

and,

$$\mathbf{G}_c = \mathbf{P}^T \cdot (\mathbf{I} + \mathbf{K} \cdot \mathbf{P} \cdot \mathbf{R}_c \cdot \mathbf{P}^T \cdot \mathbf{K} \cdot \mathbf{R}_{mf} - \mathbf{K} \cdot \mathbf{R}_{mf}) \cdot (\mathbf{K} \cdot \mathbf{P} \cdot \mathbf{R}_c)$$

$$\mathbf{Q}_c = \mathbf{P}^T \cdot [\mathbf{I} + (\mathbf{K} \cdot \mathbf{P} \cdot \mathbf{R}_c \cdot \mathbf{P}^T - \mathbf{I}) \cdot \mathbf{K} \cdot \mathbf{R}_{mf}] \cdot (\mathbf{K} \cdot \mathbf{P} \cdot \mathbf{R}_c)\, \mathbf{Q}_d \tag{3.18}$$

The term Δ represents the equivalent coupled dynamic stiffness of the flexible base and isolator and $\mathbf{D}_c = \mathbf{R}_c^{-1}$ represents the dynamic stiffness of the machine and isolator on a rigid base. $(\Delta \cdot \mathbf{R}_c)$ can be regarded qualitatively as some "ratio" of stiffness. If the base is more rigid i.e. $\Delta \to 0$ then $(\mathbf{I} - \Delta \cdot \mathbf{R}_c)^{-1} \to \mathbf{I}$. The higher order terms $(\Delta \cdot \mathbf{R}_c)^2$ and above can be neglected under the condition that $\rho(\Delta \cdot \mathbf{R}_c) << 1$.

Comparing equation (3.16a) and (3.18) results in

$$\mathbf{Q}_f = [\mathbf{I} + (\mathbf{K} \cdot \mathbf{P} \cdot \mathbf{R}_c \cdot \mathbf{P}^T - \mathbf{I}) \cdot \mathbf{K} \cdot \mathbf{R}_{mf}] \cdot (\mathbf{K} \cdot \mathbf{P} \cdot \mathbf{R}_c) \cdot \mathbf{Q}_d \tag{3.19}$$

For forces applied and responses measured at the c.g. of the machine, the force transmissibility under the condition that $\rho(\Delta \cdot \mathbf{R}_c) << 1$, can be expressed as

$$\mathbf{G}_{f\,(flex)} = (\mathbf{I} + \Delta_M) \cdot (\mathbf{K} \cdot \mathbf{P} \cdot \mathbf{R}_c) = (\mathbf{I} + \Delta_M) \cdot \mathbf{G}_o \tag{3.20}$$

Where

$$\Delta_M = (\mathbf{K} \cdot \mathbf{P} \cdot \mathbf{R}_c \cdot \mathbf{P}^T - \mathbf{I}) \cdot \mathbf{K} \cdot (\mathbf{D}_f + \mathbf{K})^{-1} \tag{3.21}$$

It is now possible to determine the transmitted force from an operating machine to its base if the base flexibility and the force transmissibility of the machine on a rigid base are known. Typically this will allow machine testing on dissimilar bases to be carried out.

3.4.3. A more useful model

Equation (3.20) is rather limited in application as forces are usually not applied at the c.g., and measurements at the c.g. are not practical. Instead forces and measurements are usually applied and measured at the feet of a machine. When the machine is operating there would be a set of equivalent forces given by $\mathbf{Q}_e = [\mathbf{Q}_{e1} \ldots \mathbf{Q}_{ei} \ldots \mathbf{Q}_{en}]$ which appears at the feet of the machine. If $\mathbf{Q}_e$ is vectorised into a column order, then it will be a column vector of forces and moments. Similarly the same can be done for motion at the feet of the machine, $\mathbf{q}_e$. Hence

$$\mathbf{Q}_d = \mathbf{P}^T \cdot \mathbf{Q}_e \text{ and } \mathbf{q}_e = \mathbf{P} \cdot \mathbf{q}_c \tag{3.22}$$

$$\mathbf{q}_e = \mathbf{P} \cdot [-\omega^2 \mathbf{M} + \mathbf{P}^T \cdot \mathbf{K} \cdot \mathbf{P}]^{-1} \mathbf{P}^T \cdot \mathbf{Q}_e = \mathbf{P} \cdot \mathbf{R}_c \cdot \mathbf{P}^T \cdot \mathbf{Q}_e$$

Let $\mathbf{R}_{em} = [\mathbf{P} \cdot \mathbf{R}_c \cdot \mathbf{P}^T]$. This is the receptance matrix of a rigid machine mounted on a number of isolators onto a rigid base. It is an input-output transfer function relating force/moment to displacement/rotation at the feet of the machine. When control forces are applied at the feet of the machine, the forces transmitted to a rigid base are given by:

$$\mathbf{Q}_f = \mathbf{K} \cdot \mathbf{q}_e = \mathbf{K} \cdot \mathbf{R}_{em} \cdot \mathbf{Q}_{cont} = \mathbf{K} \cdot [\mathbf{P} \cdot \mathbf{R}_c \cdot \mathbf{P}^T] \cdot \mathbf{Q}_{cont}$$

The force transmissibility matrix function for machine on rigid base is given by

$$\mathbf{G}_o = \mathbf{K}\cdot\mathbf{R}_{em} = \mathbf{K}\cdot\mathbf{P}\cdot\mathbf{R}_c\cdot\mathbf{P}^T. \tag{3.23}$$

Using the example of $m\ddot{x} + kx = F + ky$, an equation of motion can be written as

$$\sum(\text{inertia terms}) + \sum(\text{spring force with } q_f = 0)$$
$$= \sum(\text{external forces}) + \sum(\text{spring force with } q_e = 0)$$

Hence the equation of motion for the flexible base can be given by

$$\mathbf{R}_{em}^{-1}\cdot\mathbf{q}_e = \mathbf{K}\cdot\mathbf{q}_f + \mathbf{Q}_{cont} = \mathbf{K}\cdot(\mathbf{D}_f+\mathbf{K})^{-1}\cdot\mathbf{K}\cdot\mathbf{q}_e + \mathbf{Q}_{cont}$$

Let δ represents the term $\mathbf{K}\cdot(\mathbf{D}_f+\mathbf{K})^{-1}\cdot\mathbf{K}$, then

$$\mathbf{R}_{em}^{-1}\cdot\mathbf{q}_e - \mathbf{K}\cdot(\mathbf{D}_f+\mathbf{K})^{-1}\cdot\mathbf{K}\cdot\mathbf{q}_e = (\mathbf{D}_{em} - \delta)\cdot\mathbf{q}_e = \mathbf{Q}_{cont}$$

The transmitted force in this case is given by

$$\begin{aligned}\mathbf{Q}_f &= \left(\mathbf{I} - \mathbf{K}\cdot(\mathbf{D}_f + \mathbf{K})^{-1}\right)\cdot\mathbf{K}\cdot(\mathbf{D}_{em} - \delta)^{-1}\,\mathbf{Q}_{cont} \\ &= \left(\mathbf{I} - \mathbf{K}\cdot(\mathbf{D}_f + \mathbf{K})^{-1}\right)\cdot\mathbf{K}\cdot\mathbf{R}_{em}\cdot(\mathbf{I} - \delta\cdot\mathbf{R}_{em})^{-1}\,\mathbf{Q}_{cont}\end{aligned} \tag{3.24}$$

Where

$$\delta\cdot\mathbf{R}_{em} = \mathbf{K}\cdot(\mathbf{D}_f+\mathbf{K})^{-1}\cdot\mathbf{K}\cdot\mathbf{P}\cdot\mathbf{R}_c\cdot\mathbf{P}^T = (\mathbf{K}\cdot\mathbf{R}_{mf})\cdot(\mathbf{K}\cdot\mathbf{P}\cdot\mathbf{R}_c\cdot\mathbf{P}^T) \tag{3.25}$$

Using the same argument as before: when $\rho(\delta\cdot\mathbf{R}_{em}) << 1$, the force transmissibility matrix for a machine on a flexible case can be given by

$$\mathbf{G}_{f\,(flex)} = (\mathbf{I} - \mathbf{K}\cdot(\mathbf{D}_f+\mathbf{K})^{-1})\cdot\mathbf{K}\cdot(\mathbf{D}_{em} - \delta)^{-1}$$

$$\approx (\mathbf{I} + \Delta_M)\cdot(\mathbf{K}\cdot\mathbf{P}\cdot\mathbf{R}_c\cdot\mathbf{P}^T) = (\mathbf{I}+\Delta_M)\cdot\mathbf{G}_o \tag{3.26}$$

where

$\Delta_M = (\mathbf{G}_o - \mathbf{I})\cdot\mathbf{K}\cdot\mathbf{R}_{mf}$, the same expression as given by equation (3.21).

Equation (3.26) together with (3.21) relates to force and motion at the feet of the machine. Compared with equation (3.20), the difference is in the additional term $\mathbf{P}^T$ in the expression $\mathbf{G}_o$. This is consistent as $\mathbf{G}_o$ in equation (3.20) is defined for disturbance acting on the machine c.g. and $\mathbf{Q}_d = \mathbf{P}^T\cdot\mathbf{Q}_{cont}$.

In summary, under the condition that $\rho(\delta\cdot\mathbf{R}_{em})<<1$, a simplified m-DoF model of a machine mounted via flexible isolators on a flexible base is obtained and it is given by (3.21) and (3.26). The equations can be used to determine the forces transmitted by a machine mounted onto a flexible base, using $\mathbf{G}_o$, the force transmissibility measured when the machine is mounted on rigid base, and knowledge of $\mathbf{R}_{mf}$. The coupled base flexibility receptance matrix $\mathbf{R}_{mf}$ $(=[\mathbf{D}_f+\mathbf{K}]^{-1})$ can be regarded as a perturbation to the force transmissibility function matrix, $\mathbf{G}_o$. The degree of perturbation is determined by the Δ_M. If Δ_M is small (see §3.5.3) then the interaction between $\mathbf{R}_{mf}$ and $\mathbf{G}_o$ is minimal.

The definitions of the magnitude of Δ_M and $\delta\cdot\mathbf{R}_{em}$ and the constraints imposed on them and the conditions for which $\rho(\delta\cdot\mathbf{R}_{em})<<1$ leading to the simplification of the force transmissibility will be discussed further below. These constraints and conditions will be given in terms of the physical properties of the system.

3.5 Discussion

3.5.1 The spectral norm as a measure of magnitude of force transmissibility matrix

In a 1-DoF model, the magnitude of the force transmissibility ratio is often used is to determine the maximum force transmitted from a vibrating machine to its base. Similarly, a suitable norm can be found as a measure of magnitude for the force transmissibility matrix for m-DoF cases. One candidate is the Hilbert or spectral norm $\|\mathbf{G}\|_s$ of a matrix defined in most literature as

$$\|\mathbf{G}\|_s = \bar{\sigma}(\mathbf{G}) = \text{the maximum singular value of } \mathbf{G}. \tag{3.27}$$

In this thesis, the symbol $\bar{\sigma}(\bullet)$ rather than $\|\bullet\|$ is used for the spectral norm. If $\mathbf{G}$ is not a constant matrix but is $\mathbf{G}(s=j\omega)$, then the spectral norm is a function of frequency ω. The spectral norm as a function of ω and the $\mathcal{H}_\infty$ (operator) norm $\|\bullet\|_\infty$ are particularly useful in the design of a control system. The $\mathcal{H}_\infty$ norm is related to the spectral norm by

$$\|\mathbf{G}(s)\|_\infty \triangleq \max_\omega \bar{\sigma}(\mathbf{G}(j\omega)) \tag{3.28}$$

For a stable scalar function $g(j\omega)$, it is simply the peak value of $|g(j\omega)|$ i.e.

$$\|g(j\omega)\|_\infty \triangleq \max_\omega |g(j\omega)|$$

If $\bar{\sigma}(\delta\cdot\mathbf{R}_{em})<<1$, then $\rho(\delta\cdot\mathbf{R}_{em})<<1$ (Wilkinson, 1965). Hence (3.26) and (3.20) are valid if and only if

$$\bar{\sigma}(\delta\cdot\mathbf{R}_{em})<<1 \text{ and } \bar{\sigma}(\Delta\cdot\mathbf{R}_c)<<1, \text{ respectively} \tag{3.29}$$

3.5.2 The effect of the coupled stiffness term $(\mathbf{D}_f+\mathbf{K})$ on Δ_M

The isolator stiffness matrix $\mathbf{K}$ as defined does not include its mass or inertia i.e. the isolators are massless. Since $(\mathbf{D}_f + \mathbf{K})^{-1} = \mathbf{D}_f^{-1}\cdot[\mathbf{I} + \mathbf{K}\cdot\mathbf{D}_f^{-1}]^{-1}$ and if $\rho(\mathbf{K}\cdot\mathbf{D}_f^{-1})<<1$, then

$$(\mathbf{D}_f + \mathbf{K})^{-1} = \mathbf{D}_f^{-1}\cdot[\mathbf{I} + \mathbf{K}\cdot\mathbf{D}_f^{-1}]^{-1} \approx \mathbf{D}_f^{-1}\cdot[\mathbf{I} - \mathbf{K}\cdot\mathbf{D}_f^{-1} + \ldots] \approx \mathbf{D}_f^{-1}$$

This would the case if the stiffness of each spring is much less than the respective local stiffness of the base structure. The perturbation term in (3.21) is simplified to

$$\Delta_M = [\mathbf{K}\cdot\mathbf{P}\cdot\mathbf{R}\cdot\mathbf{P}^T - \mathbf{I}]\cdot\mathbf{K}\cdot\mathbf{D}_f^{-1} \tag{3.21a}$$

This perturbed term comprises a number of identifiable sub-system response matrices. For example, in the 1-DoF case, the first term is equal to (1-transmissibility), and for transmissibility less than one it is a measure of isolator effectiveness for a machine on isolator on a rigid base. $\mathbf{K}$ is the isolator dynamic stiffness and $\mathbf{D}_f$ is the dynamic stiffness of the flexible base. The above expression is valid even if the base dynamic stiffness matrix contains mass or inertia elements. This is an advantage in using control force at the feet of the machine instead of between the machine and the base.

If the control force is applied between machine and the base, then the actuator becomes part of the isolator, and the effective mounts will have a mass or inertia term. In this case, the measured or derived coupled dynamic stiffness matrix $(\mathbf{D}_f + \mathbf{K})$ and the uncoupled base dynamic stiffness matrix $\mathbf{D}_f$ must include the mass of the actuators (Pan *et al.*, 1993).

3.5.3 The spectral norm of the perturbation term Δ_M

From (3.26), it can be observed that the interactions between the resonant peaks at the resonant frequencies, ω_r, of the flexible base modes and $\mathbf{G}_o(j\omega)$ depend on the magnitude of $\Delta_M(j\omega_r)$. Since $\Delta_M(j\omega_r)$ is a function of frequency, a suitable measure of the magnitude of (Δ_M) is the spectral norm $\bar{\sigma}(\Delta_M(j\omega))$. The smaller $\bar{\sigma}(\Delta_M(j\omega))$ is, the smaller is the effect of the flexible base modes being coupled to the rigid base $\mathbf{G}_o(j\omega)$ measurements. Then the dominant peaks in the force transmissibility will exist primarily at the rigid machine-spring frequencies, and not near the resonant frequencies of flexible base modes. Let $\{\underline{\omega}_o\}$ represents a set of rigid machine-spring frequencies. The resulting magnitude of $\mathbf{G}_{f\ (flex)}$ is a function of $\bar{\sigma}(\Delta_M(j\omega_r))$ and the relative closeness of ω_r to $\{\underline{\omega}_o\}$. The condition for how small $\bar{\sigma}(\Delta_M(j\omega))$ is and the terms affecting it will be discussed next.

Using the multiplicative property of matrix norm,

$$\bar{\sigma}(\Delta_M) \leq \bar{\sigma}(\mathbf{K}\cdot\mathbf{P}\cdot\mathbf{R}_c\cdot\mathbf{P}^T - \mathbf{I}) \cdot \bar{\sigma}(\mathbf{K}\cdot\mathbf{R}_{mf})$$

If $\bar{\sigma}(\Delta_M(j\omega)) < 1$ is required, $\forall\omega$, then the system must be designed to have

$$\bar{\sigma}(\mathbf{K}\cdot\mathbf{P}\cdot\mathbf{R}_c\cdot\mathbf{P}^T - \mathbf{I}) \cdot \bar{\sigma}(\mathbf{K}\cdot\mathbf{R}_{mf}) < 1, \ \forall\omega \qquad (3.30)$$

And since

$$\bar{\sigma}\,(\mathbf{K}\cdot\mathbf{P}\cdot\mathbf{R}_c\cdot\mathbf{P}^T - \mathbf{I}) \le \bar{\sigma}\,(\mathbf{K}\cdot\mathbf{P}\cdot\mathbf{R}_c\cdot\mathbf{P}^T) + \bar{\sigma}\,(\mathbf{I}) = \bar{\sigma}\,(\mathbf{K}\cdot\mathbf{P}\cdot\mathbf{R}_c\cdot\mathbf{P}^T) + 1.$$

If

$$\bar{\sigma}\,(\mathbf{K}\cdot\mathbf{P}\cdot\mathbf{R}_c\cdot\mathbf{P}^T) < 1 \text{ and } \bar{\sigma}\,(\mathbf{K}\cdot\mathbf{R}_{mf}) < 0.5, \text{ then} \qquad (3.31)$$

$$\bar{\sigma}\,(\Delta_M) \le \bar{\sigma}\,(\mathbf{K}\cdot\mathbf{P}\cdot\mathbf{R}_c\cdot\mathbf{P}^T - \mathbf{I})\,\bar{\sigma}\,(\mathbf{K}\cdot\mathbf{R}_{mf}) < 1 \quad \forall\omega \text{ or } \| \Delta_M \|_\infty < 1$$

The term $(\mathbf{K}\cdot\mathbf{P}\cdot\mathbf{R}_c\cdot\mathbf{P}^T)$ is the force transmissibility matrix for machine and isolators on a rigid base. The value of $\bar{\sigma}\,(\mathbf{K}\cdot\mathbf{P}\cdot\mathbf{R}_c\cdot\mathbf{P}^T)$ approaches the value of unity at low frequencies, and is possibly larger than unity for $\omega \in \aleph(\underline{\omega}_o)$, where $\aleph(\underline{\omega}_o)$ is the neighbourhoods of $\{\underline{\omega}_o\}$. It rolls off to below one after these frequencies. Hence $\bar{\sigma}\,(\mathbf{K}\cdot\mathbf{P}\cdot\mathbf{R}_c\cdot\mathbf{P}^T - \mathbf{I})$ will be less than unity for low frequencies and tends to unity at higher frequencies. It is possibly more than unity in for $\omega \in \{\underline{\omega}_o\}$. In most cases, for $\omega \in \{\underline{\omega}_o\}$, the behaviour of the system is very much determined by the parameters of the machine and the values of $\mathbf{K}$. If $\mathbf{K}$ contains some form of damping the magnitude of the force transmitted at these rigid body frequencies can be reduced. The proper selection of values of $\mathbf{K}$ has always been important.

The term $\mathbf{K}\cdot\mathbf{R}_{mf}$ represents the coupling of base flexibility modes with resonant frequencies ω_r, r =1...n., where $\bar{\sigma}\,(\mathbf{K}\cdot\mathbf{R}_{mf}(j\omega_r))$ becomes significant. Typically one would not design for ω_r anywhere near $\{\underline{\omega}_o\}$. When one has to, one should design a system such that $\bar{\sigma}\,(\mathbf{K}\cdot\mathbf{R}_{mf}(j\omega_r)) < 0.5$, for $\omega_r \in \aleph(\underline{\omega}_o)$. In this case, it is still possible to have $\bar{\sigma}\,(\Delta_M(j\omega)) < 1$. Such requirements may result in isolators being too soft and causing a large static deflection. If $\bar{\sigma}\,(\mathbf{K}\cdot\mathbf{R}_{mf}(j\omega_r))$ is large, then it must be at frequencies where $\mathbf{G}_o(j\omega)$ has high roll-off; for example in the case of a 2nd order system where $\mathbf{G}_o(j\omega)$ roll-off with a -40 dB/decade slope. At these frequencies, the magnitude of $\mathbf{G}_o(j\omega)$ is small for ω further away from $\{\underline{\omega}_o\}$. The multiplication of $1+\bar{\sigma}\,(\Delta_M(j\omega))$ into $\mathbf{G}_o(j\omega)$ will result in a small perturbed magnitude and a corresponding small measured transmitted force.

So whether $\overline{\sigma}(\Delta_M)<1$, $\forall\omega$ or not it should not be important for approximating the model measured response by (3.26). It is essential though that it be small for $\omega \in \aleph(\underline{\omega}_o)$. On the other hand, for a design of active vibration control system $\|\Delta_M\|_\infty$ being small is important. It will affect the stability of a feedback control system as discussed in §3.8.

Note that the requirement that $\overline{\sigma}(\Delta_M(j\omega))$ be small does not imply that $\overline{\sigma}(\delta\cdot\mathbf{R}_{em})<<1$ at all frequencies. Since

$$\Delta_M = (\mathbf{K}\cdot\mathbf{P}\cdot\mathbf{R}_c\cdot\mathbf{P}^T - \mathbf{I})\cdot\mathbf{K}\cdot\mathbf{R}_{mf} \text{ and } \delta\cdot\mathbf{R}_{em} = \mathbf{K}\cdot\mathbf{R}_{mf}\cdot\mathbf{K}\cdot\mathbf{P}\cdot\mathbf{R}_c\cdot\mathbf{P}^T$$

For $\omega < \min\{\underline{\omega}_o\}$, $\overline{\sigma}(\delta\cdot\mathbf{R}_{em}) > \overline{\sigma}(\Delta_M)$, and for $\omega > \min\{\underline{\omega}_o\}$, $\overline{\sigma}(\delta\cdot\mathbf{R}_{em}) < \overline{\sigma}(\Delta_M)$.

3.5.4 The implication of the term $\delta\cdot\mathbf{R}_{em}$

Recall that the primary condition for equation (3.20) and (3.25) to be valid is $\rho(\delta\cdot\mathbf{R}_{em})<<1$. It permits the simplification of the above expressions and the determination of the function from its parts. In Blackwood and von Flotow's (1992) example of control force between machine and base, since Δ_M is a scalar quantity, the magnitude $|\Delta_M|$ is used to determine the validity of the approximation of the force transmissibility by the expression $(1+\Delta_M)\cdot G_o$. In the case presented for control force at the source i.e. feet of the machine, it had been shown that $\overline{\sigma}(\delta\cdot\mathbf{R}_{em}(j\omega))$ must be very much less than 1. In §3.7 this difference in the requirement for the validity of (3.26) will be discussed in greater detail using the 1-DoF model example. For both cases $\|\Delta_M\|_\infty$ determines the magnitude of the peaks of the flexible base modes that are coupled to $\mathbf{G}_o$. In particular, when $\overline{\sigma}(\Delta_M(j\omega_r))$ are small then the coupled peaks of the flexible base to $\mathbf{G}_o$ will be small. Since

$$\overline{\sigma}(\delta\cdot\mathbf{R}_{em}) \le \overline{\sigma}(\mathbf{K}\cdot\mathbf{R}_{mf})\cdot\overline{\sigma}(\mathbf{K}\cdot\mathbf{P}\cdot\mathbf{R}_c\cdot\mathbf{P}^T)$$

If (3.31) is satisfied, then

$$\rho(\delta\cdot\mathbf{R}_{em}) \le \overline{\sigma}(\delta\cdot\mathbf{R}_{em})<<1, \ \forall\omega \text{ or } \|\delta\cdot\mathbf{R}_{em}\|_\infty<<1.$$

As $\omega \rightarrow 0$, the term $\overline{\sigma}(\mathbf{K}\cdot\mathbf{P}\cdot\mathbf{R}_c\cdot\mathbf{P}^T) \rightarrow 1$ and $\overline{\sigma}(\delta\cdot\mathbf{R}_{em}(j\omega)) \rightarrow \overline{\sigma}(\mathbf{K}\cdot\mathbf{R}_{mf}(j\omega))$.

At each frequency, as both $\overline{\sigma}(\delta\cdot\mathbf{R}_{em})$ and $\overline{\sigma}(\Delta_M)$ are partly determined by $\overline{\sigma}(\mathbf{K}\cdot\mathbf{R}_{mf})$, it will useful to have $\|\mathbf{K}\cdot\mathbf{R}_{mf}\|_\infty << 1$ for all frequencies. This can also imply that $\overline{\sigma}(\mathbf{K}\cdot\mathbf{R}_{mf}) < 0.5$ especially if the "much less than means" an order of one-tenth and smaller.

All the conditions discussed above are rather conservative, for example, equation (3.31) is. They imposed an upper bound on the magnitudes of $\overline{\sigma}(\mathbf{K}\cdot\mathbf{P}\cdot\mathbf{R}_c\cdot\mathbf{P}^T)$ and $\overline{\sigma}(\mathbf{K}\cdot\mathbf{R}_{mf})$. The highest resonant peak of the coupled base structure should be very small. Particularly these peaks should not coincide with those of $\mathbf{K}\cdot\mathbf{P}\cdot\mathbf{R}_c\cdot\mathbf{P}^T$. It would be helpful if the structure has adequate damping as discussed in (von Flotow and Vos, 1991). The spectral norm of each function indicates only the largest magnitude amongst its different modes at each frequency. For example, the peak of $\overline{\sigma}(\mathbf{K}\cdot\mathbf{R}_{mf})$ at a frequency ω_p corresponds to a peak of one of the modes of $\mathbf{K}\cdot\mathbf{R}_{mf}(j\omega_p)$. Hence the multiplication of the spectral norms of two functions ignores the interaction amongst the various individual mode shapes of each of the function. It may be such that even though $\overline{\sigma}(\mathbf{K}\cdot\mathbf{P}\cdot\mathbf{R}_c\cdot\mathbf{P}^T)$ and $\overline{\sigma}(\mathbf{K}\cdot\mathbf{R}_{mf})$ are large at a frequency ω, there may be some mode shapes mis-matched, and the resulting coupling small.

In practice, one can avoid being too conservative. For (3.26) to be an acceptable representation of the actual force transmissibility, $\|\delta\cdot\mathbf{R}_{em}\|_\infty << 1$ is not really needed. It is possible to have $\|\delta\cdot\mathbf{R}_{em}\|_\infty < 1$ and $\overline{\sigma}(\mathbf{K}\cdot\mathbf{R}_{mf}(j\omega_r)) << 1$ for any $\omega_r \in \aleph(\underline{\omega}_o)$.

If one were to examine $\mathbf{K}\cdot\mathbf{R}_{mf}$ and $\mathbf{K}\cdot\mathbf{P}\cdot\mathbf{R}_c\cdot\mathbf{P}^T$, something similar to a "ratio" of stiffness can be observed: the isolator stiffness, $\mathbf{K}$, to coupled base receptance, $\mathbf{R}_{mf}$, and isolator stiffness, $\mathbf{K}$, to machine mounted on rigid base receptance $\mathbf{R}_{em}$ respectively. *They are therefore dimensionless.* The terms $\mathbf{R}_{em}=\mathbf{P}\cdot\mathbf{R}_c\cdot\mathbf{P}^T$ and $\mathbf{R}_{mf}$ suggest how they can be determined. Figure 3.3 shows the machine being tested on isolators on rigid ground (Figure 3.3a), and (if physically possible) the base structure being tested on isolators against a rigid ground (Figure 3.3b). The magnitudes of the flexible base modes that will be coupled to $\mathbf{G}_o$ can be minimised by proper selection of the isolators' stiffness and damping properties i.e. $\mathbf{K}$ vis-à-vis the base structure property $\mathbf{R}_{mf}$.

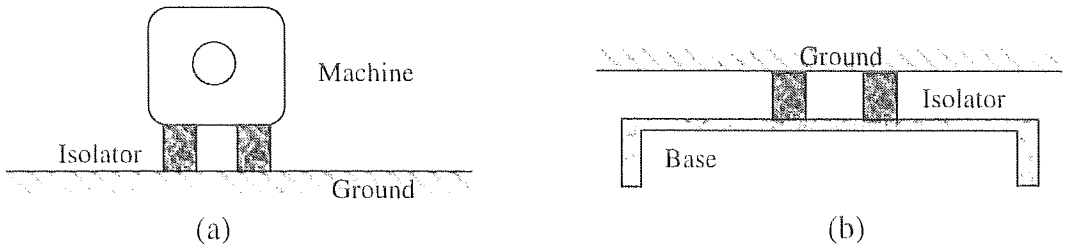

Figure 3.3 Interpretations of $\mathbf{R}_{em}$ and $\mathbf{R}_{mf}$

3.6 Example of a machine on a flexible beam

A model of a 3.7 kg machine mounted via two flexible isolators on a 1.5 m flexible mild steel beam (details in Appendix B) is used an example to illustrate some of the points discussed. The system actual model is given by the force transmissibility function matrix:

$$(\mathbf{I} - \mathbf{K}\cdot(\mathbf{D}_f+\mathbf{K})^{-1})\cdot\mathbf{K}\cdot\mathbf{R}_{em}\cdot(\mathbf{I}-\delta\cdot\mathbf{R}_{em})^{-1} \quad (N/N)$$

Figure 3.4 and 3.5 show the effect of $\mathbf{K}$ ($k_z=k_{zo}\cdot(1+jn_z)$), where k_{zo} is the spring stiffness or the stiffness coefficient and n_z is the isolator loss factor, on the perturbed model given in (3.26), i.e.

$$(\mathbf{I} + \Delta_M)\cdot(\mathbf{K}\cdot\mathbf{P}\cdot\mathbf{R}_c\cdot\mathbf{P}^T) \quad (N/N)$$

In this example, the loss factor for damping is used instead of viscous damping and it implies that the results are valid only for steady state or cyclic operations. When $k_{zo}=1000$ ($N\ m^{-1}$) and $n_z=0.07$, Figure 3.4a shows that $\|\delta\cdot\mathbf{R}_{em}\|_\infty<1$ for the given frequency range, and Figure 3.4b shows the comparison between the actual model and the perturbed model.

The match is almost perfect. The perturbed model plots are shifted slightly for clarity. As ω increases, $\bar{\sigma}(\Delta_M(j\omega_r))<<1$. At the flexible base mode resonant frequency, $\omega_r \approx 68$ Hz, $\bar{\sigma}(\Delta_M(j\omega_r)) \approx 1$ but coupled with the magnitude of the rigid base transmissibility function at that frequency, the discrepancy between the magnitude of the actual and perturbed model is quite small. Hence even if $\bar{\sigma}(\Delta_M(j\omega_r)$ is not small, if ω_r are far into the roll-off portion of $\mathbf{G}_o$, the magnitude of the perturbation is still small.

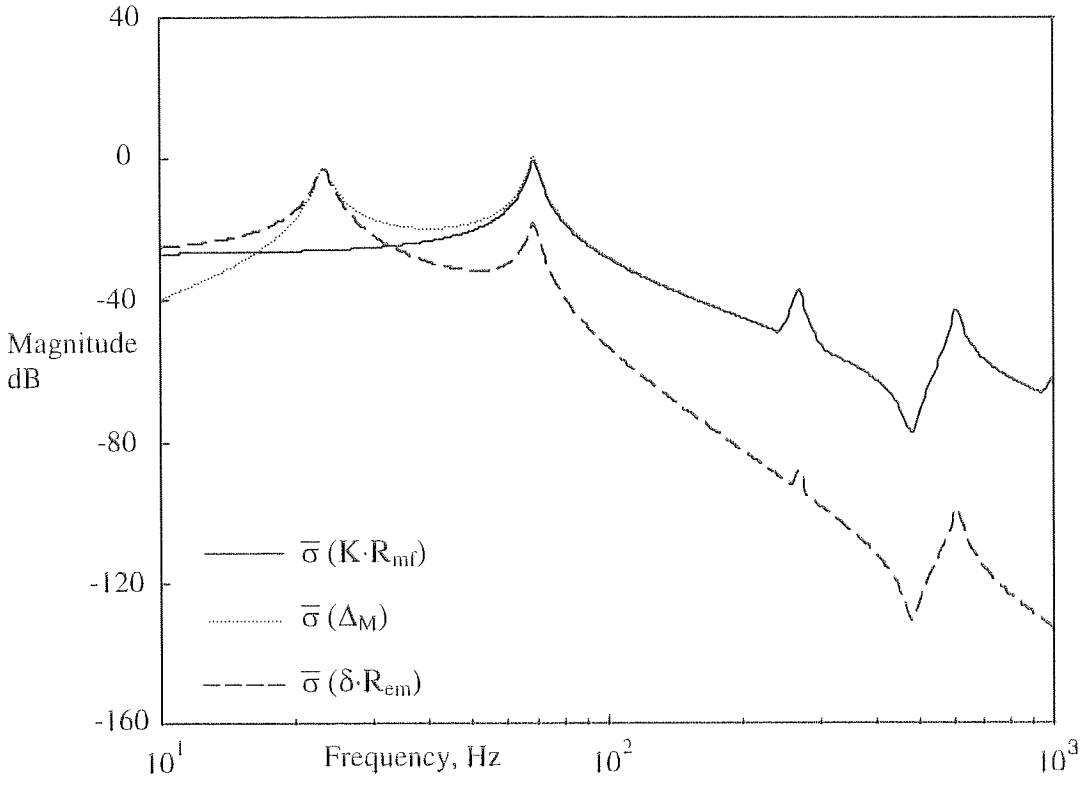

Figure 3.4a Plots of $\overline{\sigma}$ (δ·R$_{em}$), $\overline{\sigma}$ (Δ_M) & $\overline{\sigma}$ (K·R$_{mf}$) for soft isolators

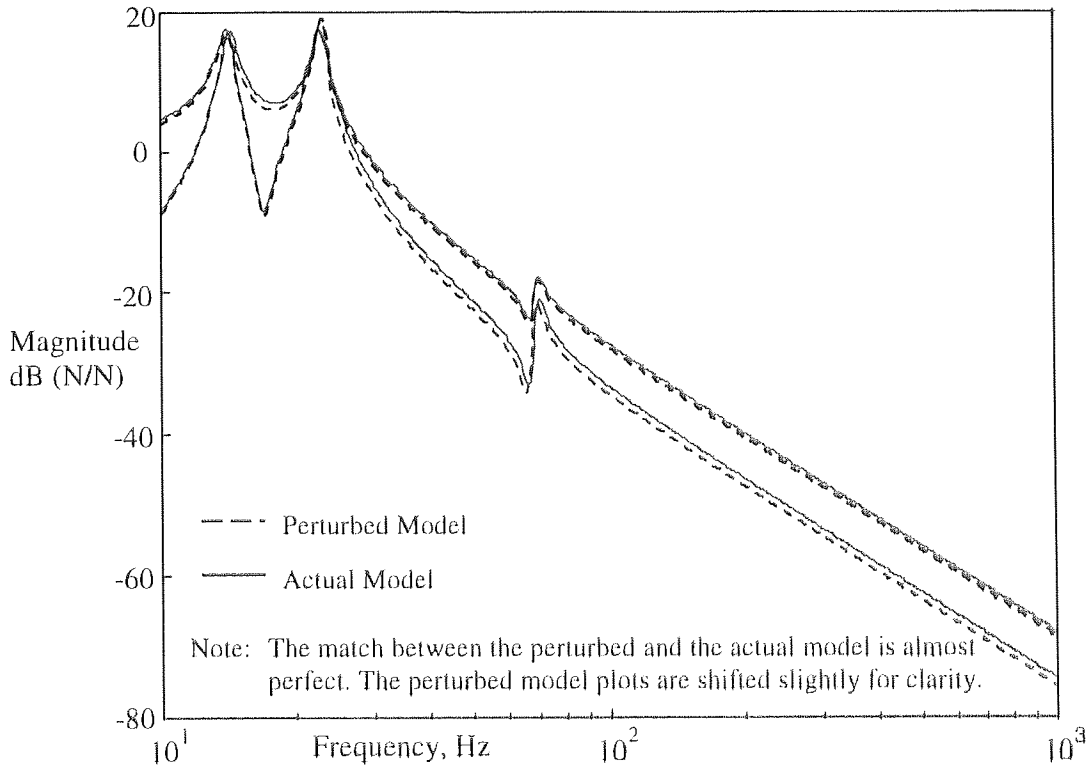

Figure 3.4b Perturbed model versus the actual plant model for soft isolators

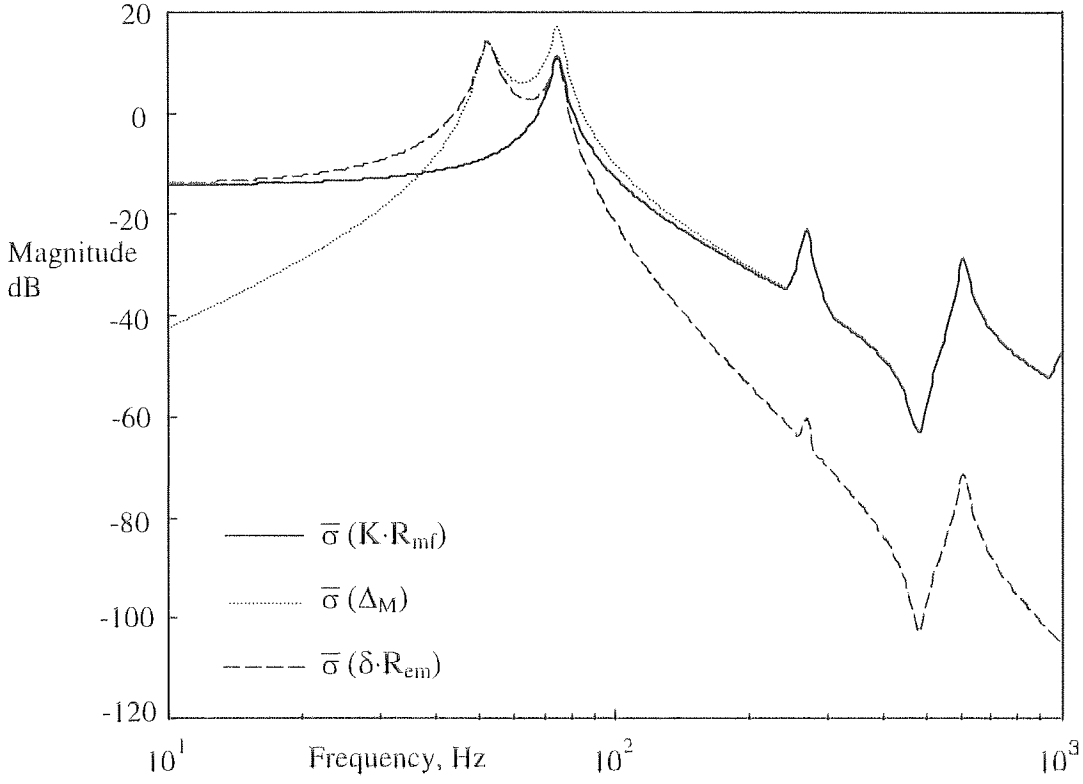

Figure 3.5a Plots of $\overline{\sigma}$ ($\delta \cdot R_{em}$), $\overline{\sigma}$ (Δ_M) & $\overline{\sigma}$ ($K \cdot R_{mf}$) for stiffer isolators

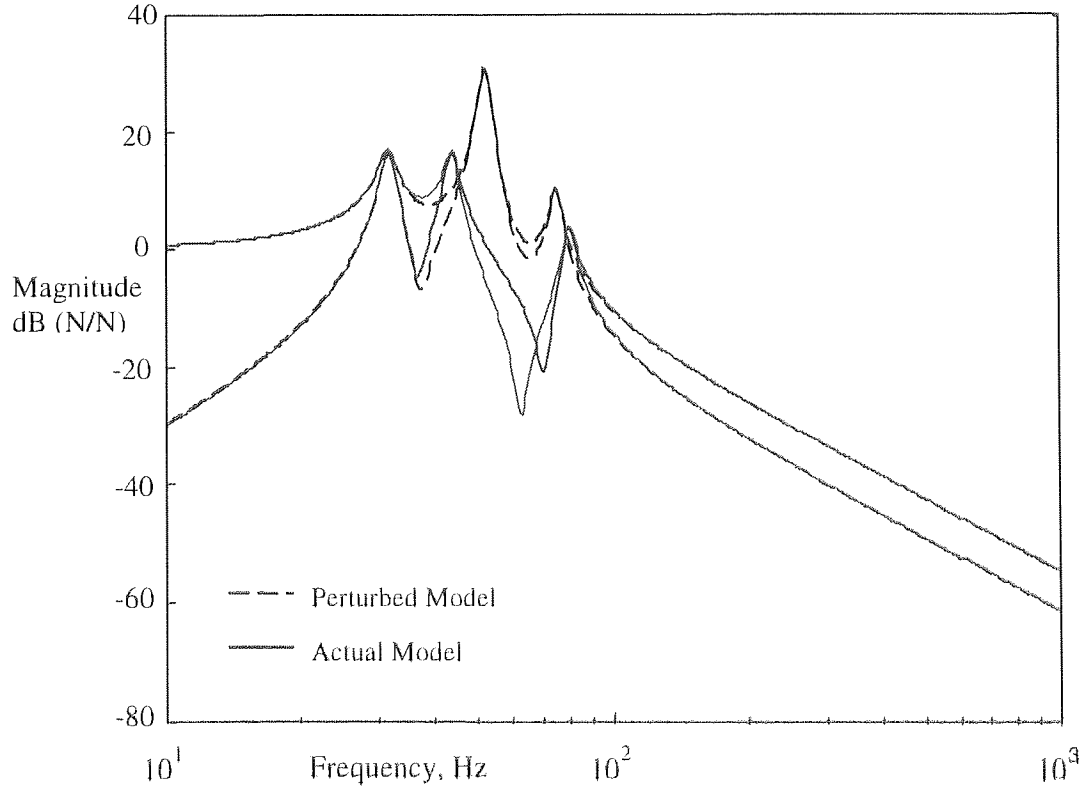

Figure 3.5b Perturbed model versus the actual plant model for stiffer isolators

When the stiffness coefficient, k_{zo}, is increased 5 times, it can be seen from Figure 3.5a $\overline{\sigma}(\delta\cdot\mathbf{R}_{em})>1$ between 40 ~ 80 Hz. From Figure 3.5b, it is observed that the two equations are very different in the same range. With $\overline{\sigma}(\Delta_M(j\omega_r))>1$ at ω_r close to the maximum $\underline{\omega}_o$, the magnitude of the perturbation is higher than that of the actual response.

This simple model reiterates the importance of $\overline{\sigma}(\delta\cdot\mathbf{R}_{em}(j\omega))$ as a condition for the validity of (3.26), and $\overline{\sigma}(\Delta_M(j\omega_r))$ in determining the magnitude of the perturbation. It should be small for $\omega_r \in \aleph(\underline{\omega}_o)$.

3.7 Reduction to 1-DoF and comparison with Blackwood and von Flotow's work

The work of Blackwood and von Flotow (1992) will be briefly presented. A force $-Q_\beta$ will cause machine vibration at the machine-isolator interface, and using the combined receptance (Garvey, 1996) approach, the transmitted force to the base is given by

$$Q_f = \frac{R_e}{R_e + R_m + R_f} Q_\beta = \left(1 + \frac{R_f}{R_e + R_m}\right)^{-1} \frac{R_e}{R_e + R_m} Q_\beta \tag{3.32}$$

The second term on the right hand side of the equation is the case when $R_f=0$. It is the force transmissibility of the case of a machine on flexible isolator on a rigid base. Immediately one could see the terms relating to $k\cdot R_{em}$ being separated out from the flexible base receptance matrix.

To be consistent with the approach used to develop the m-DoF model, the combined stiffness of each component (see Chapter 4) should be used and form

$$\begin{aligned} Q_f = &\left[R_f^{-1}\cdot\left(R_f^{-1}+R_m^{-1}\right)^{-1}\right]\cdot\left[R_m^{-1}\cdot\left(R_e^{-1}+R_m^{-1}\right)^{-1}\right] \\ &\times\left\{1-\left[R_m^{-1}\cdot\left(R_f^{-1}+R_m^{-1}\right)^{-1}\right]\cdot\left[R_m^{-1}\cdot\left(R_e^{-1}+R_m^{-1}\right)^{-1}\right]\right\}^{-1}\cdot Q_\beta \end{aligned} \tag{3.33}$$

Equation (3.33) appears more complex but it is consistent with the use of the inverse of combined dynamic stiffness matrix. When $R_f \rightarrow 0$, the term $k \cdot R_{em}$ is again the term remaining on the right hand side.

One would like to see how much of the base flexible modes affect the control loop. In the case where the control force is located at the feet of the machine, the transmitted force has the same expression as that given above except that term Q_{cont} replaces Q_β. Although this differs from that of Blackwood and von Flotow's, (where the control force is between machine and base) a comparison is still appropriate. Hence for the 1-DoF models the definitions are as follows:

$$R_e = \frac{1}{ms^2};\ R_m = \frac{1}{k};\ P^T = P = 1;\ k \cdot R_{em} = \frac{k}{ms^2 + k}$$

With m as the mass of the rigid machine and k the spring stiffness. For a flexible base with low modal overlap, the dynamic stiffness can be approximated as

$$\frac{1}{D_f} \approx \sum_{r=1}^{N} \frac{\phi_r^2}{\left(s^2 + 2\zeta_r \omega_r s + \omega_r^2\right)}$$

with ζ_r, and ω_r representing the damping and the resonant frequency of the r^{th} mode and ϕ_r is the mass normalised r^{th} mode shape at the mounting point. Blackwood and von Flotow (1992), assumed that $R_f << (R_e + R_m)$, and (3.32) becomes

$$Q_f \approx \left(1 - \frac{R_f}{R_e + R_m}\right) \frac{R_e}{R_e + R_m} Q_{cont} \tag{3.34}$$

$$Q_f \approx \left[1 + k \cdot D_f^{-1}\left(k \cdot R_{em} - 1\right)\right] k \cdot R_{em}\, Q_{cont} \tag{3.35}$$

Garcia *et al.* (1990) showed that, $m\phi_r^2$, the ratio of machine mass to effective modal mass is important in determining the degree of interaction of flexible modes with a control loop. Blackwood and von Flotow (1992) showed that if

$$m\phi_r^2 << 2\zeta_r \tag{3.36}$$

Then

$R_f << (R_e + R_m)$, and

$$Q_f = (1+\Delta)\cdot k \cdot R_{em} \cdot Q_{cont} \tag{3.37}$$

Where $\Delta = k \cdot D_f^{-1} \cdot (k \cdot R_{em} - 1)$, and $\Delta(j\omega_r)$ appears as resonant peaks along the curve of $k \cdot R_{em}(j\omega)$, the force transmissibility of machine on rigid seating. The value of $\Delta(j\omega_r)$ at each frequency, ω, governs the size of the peak and these can be used to design suitable lead-lag compensators to minimise the peaks of Q_f. Blackwood and von Flotow (1992) provided only 1-DoF examples.

When the relevant substitutions are made in (3.21) and (3.26) or (3.33) and assuming that $R_m >> R_f$, an equation same as (3.37) is obtained. Furthermore (3.21) and (3.25) become

$$\delta \cdot R_{em} = \left(\sum_{r=1}^{N} \frac{k\phi_r^2}{\left(s^2 + 2\zeta_r \omega_r s + \omega_r^2\right)} \right) \frac{k}{ms^2 + k}$$

$$\Delta_M = \left(k \cdot R_{em} - 1\right) \cdot k \cdot R_f$$

With ω_o as the spring-mass natural frequency, and at $\omega = \omega_r$, base eigenfrequencies

$$\delta \cdot R_{em}(j\omega_r) = \frac{\omega_o^2}{\left(-\omega_r^2 + \omega_o^2\right)} \frac{m\phi_r^2}{(j2\zeta_r)} \left(\frac{\omega_o^2}{\omega_r^2} \right)$$

$$\Delta_M(j\omega_r) = \left(\frac{-\omega_o^2}{-\omega_r^2 + \omega_o^2} \right) \left(\frac{m\phi_r^2}{j2\zeta_r} \right)$$

The term $\Delta_M(j\omega_r)$ is identical to $\Delta(j\omega_r)$ derived by Blackwood and von Flotow (1992) for force sensors. In addition, Δ_M can be compared with $\delta \cdot R_{em}$ and $k \cdot R_f$ and these are tabulated in Table 3.1.

Frequency range	$\delta \cdot R_{em}(j\omega_r)$	$\Delta_M(j\omega_r)$	$k \cdot R_f(j\omega_r)$
$\omega_r << \omega_o$	$-\frac{jm\phi_r^2}{(2\zeta_r)}\left(\frac{\omega_o}{\omega_r}\right)^2$	$-\frac{jm\phi_r^2}{(2\zeta_r)}$	$-\frac{jm\phi_r^2}{(2\zeta_r)}\left(\frac{\omega_o}{\omega_r}\right)^2$
$\omega_r >> \omega_o$	$\frac{jm\phi_r^2}{(2\zeta_r)}\left(\frac{\omega_o}{\omega_r}\right)^4$	$\frac{jm\phi_r^2}{(2\zeta_r)}\left(\frac{\omega_o}{\omega_r}\right)^2$	$\frac{jm\phi_r^2}{(2\zeta_r)}\left(\frac{\omega_o}{\omega_r}\right)^2$

Table 3.1 Comparison of $\delta \cdot R_{em}$, Δ_M and $k \cdot R_f$

The condition $\rho(\delta \cdot R_{em})<<1$ arises only when the stiffness of individual components are combined to form the receptance matrix for a machine on isolator on a base and to derive (3.21) and (3.26). Blackwood and von Flotow (1992) used combined receptance (mobility) to derive (3.32). Hence for the 1-DoF it is shown that both (3.32) and (3.33) represent the same model. The simplification of these two equations takes different paths, and results in two different conditions, Δ_M and δR_{em}. In both cases, Δ_M determines the magnitude of the coupling.

When $m\phi_r^2<<2\zeta r$, then $\Delta_M << 1$ or $R_f<<(R_e+R_m)$. However for the approach used here to develop the model it is required that

$$(\delta \cdot R_{em})(j\omega_r) = \frac{m\phi_r^2}{j\zeta_r}\left(\frac{\omega_o}{\omega_r}\right)^2 << 1$$

And this gives

$$\left|\Delta_M(j\omega_r)\right| << \left|\frac{\omega_r^2}{\omega_o^2}\right| \qquad (3.38)$$

This reduces the requirement on $(m\phi_r^2 \div 2\zeta_r) << 1$ for $\omega_r >> \omega_o$ since the least upper bound can be greater than 1. However, it tightens the requirement for $\omega_r << \omega_o$ since the least upper bound must be less than 1. On examining Table 3.1 again, it is observed that

i) For $\omega_r << \omega_O$, $k \cdot R_f = \delta \cdot R_{em}$ and $|\Delta_M| < |\delta \cdot R_{em}|$. Hence $|\delta \cdot R_{em}| << 1 \Rightarrow |\Delta_M| << 1$.

ii) For $\omega_r >> \omega_O$, $k \cdot R_f = |\Delta_M|$ and $|\Delta_M| > |\delta \cdot R_{em}|$. Hence $|\Delta_M| < 1 \Rightarrow |\delta \cdot R_{em}| << 1$.

From this it appears that if $|k \cdot R_f| << 1$, then the desired condition and a small perturbation can be realised. It may appear strange but since $R_f < R_m \Rightarrow R_f < (R_e + R_m)$, it is not an unreasonable choice. More often than not in practice engineers will choose a suitable spring rate that is smaller than the local stiffness of a support with sufficient damping.

The difference in the condition for the approximation of (3.26) to be valid therefore stems from the use of combined mobility function by Blackwood and von Flotow instead of combined dynamic stiffness function. From a simple example (3.7) and the consistency applied in the derivation for 1-DoF and m-DoF, it is to be concluded that the primary condition is $\delta \cdot R_{em}$.

3.8 Implication on control design

It may be possible in Blackwood and von Flotow's formulation to replace mobility function with mobility response matrix to get a multiple-input-multiple-output (MIMO) model. To extend their concept of designing compensators basing on $\|\Delta(j\omega_r)\|$ (undefined norm) may be difficult. One of the problems associated with using classical frequency response (to design compensators) for mxm MIMO systems is the m(m-1) interactions amongst the various input-output channels. This makes designing controller using closing one loop at a time difficult. Nevertheless there have been attempts by MacFarlane (1970) and Rosenbrook (1974) amongst others to extend frequency response methods to MIMO problems. For 2x2 plant, these methods are quite applicable. Unfortunately, the gain and phase margin obtained from the characteristics (eigenvalues) loci are only valid for simultaneous changes in all the loops. They would not be useful indicators for robust stability.

The extension of Blackwood and von Flotow's 1-DoF model to an m-DoF model using combined dynamic stiffness given here is original. It results in a MIMO model that fits nicely into the framework of robust control design or the $\mathcal{H}_\infty$ control method. Two aspects that will be useful for this problem will be presented. These are used subsequently in the design of active control of vibration when the mount is rigid.

Firstly, for the proposed method of active force control at the feet of the machine the disturbance, $-Q_\beta$ and the control force, Q_{cont} are taken as inputs to the system. This is on the assumption that the controlled forces of the actuators are applied at the machine feet-mount interface, the same locations where Q_β forces are measured. This will result in a standard block diagram of a system with output plant uncertainty. More importantly, Figure 3.6 is also suitable for active control at the source when flexible isolators are not used whether $\Delta_M=0$ or not. This is pursued in chapter 5.

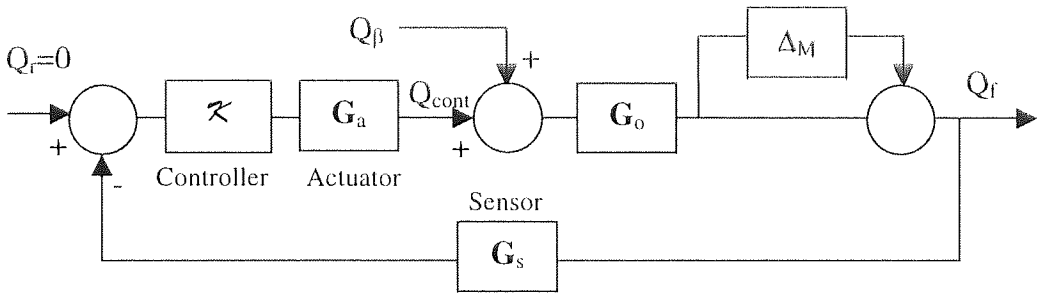

Figure 3.6 A control block diagram for a system given by equation (3.26)

Secondly, ignoring the dynamics of the actuator and the sensor for the present, and defining a weighting function $\mathbf{W}_2$ (chapter 6) the diagram can be redrawn into the standard Linear Fractional Transformation form as shown in Figure 3.7 below.

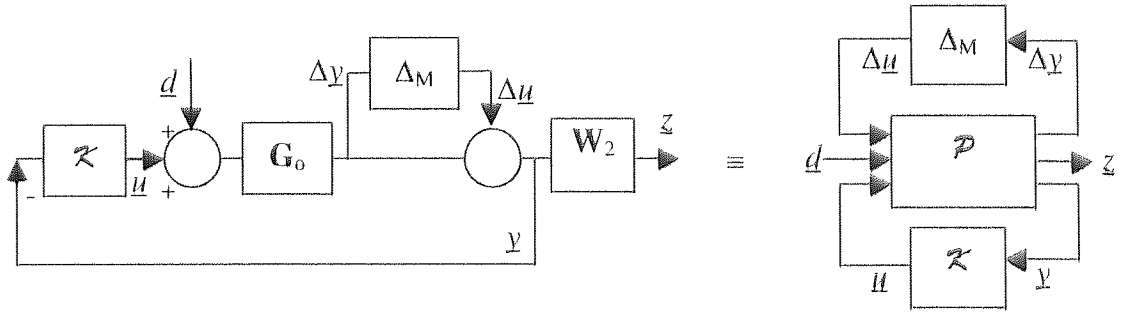

Figure 3.7 Equivalent LFT block diagram for Figure 3.6

Standard symbols used in control literature are used e.g. $-\mathbf{Q}_\beta$ being replaced by $\underline{d}$, and $\mathbf{Q}_f$ is replaced by some desired results $\underline{z}$. This is in recognition that although it is desired to have $\mathbf{Q}_f = 0$, it is unrealistic in general. Acceptable force transmitted levels are usually set vis-à-vis the cost of achieving them.

$\mathcal{P}$ is the so-called generalised system representation defined as:

$$\mathcal{P} = \begin{bmatrix} \mathbf{0} & \mathbf{G}_o & | & \mathbf{G}_o \\ \mathbf{W}_2 & \mathbf{W}_2\mathbf{G}_o & | & \mathbf{W}_2\mathbf{G}_o \\ -- & -- & -- & -- \\ \mathbf{I} & \mathbf{G}_o & | & \mathbf{G}_o \end{bmatrix} = \begin{bmatrix} \mathcal{P}_{11} & \mathcal{P}_{12} \\ \mathcal{P}_{21} & \mathcal{P}_{22} \end{bmatrix} \tag{3.39}$$

It is a generalised model that incorporates a performance function into the model of the machine on flexible isolators on rigid base. It is a mapping defined as:

$$\begin{Bmatrix} \Delta\underline{y} \\ \underline{z} \\ \underline{y} \end{Bmatrix} = \mathcal{P} \cdot \begin{Bmatrix} \Delta\underline{u} \\ \underline{d} \\ \underline{u} \end{Bmatrix} \tag{3.40}$$

When $\Delta_M=0$, the diagram on the right side of Figure 3.7 defines a standard $\mathcal{H}_\infty$ optimal control problem of finding a $\mathcal{K}$ that stabilises the system and meeting the requirements of set on $\underline{z}$ through $\mathbf{W}_2$. When $\underline{d}=0$, it defines the standard robust stability analysis problem. If Δ_M is a single-block unstructured uncertainty the two problems are equivalent by small gain theorem. In practice, details of Δ_M need not be known except that $\|(\Delta_M)\|_\infty < 1$, and is a full complex block. The Δ_M given by (3.21) can be chosen to satisfy these requirements.

For the model derived here using flexible isolators, it is quite meaningless to discuss the case for $\Delta_M=0$. This will leave us with a problem of a machine on flexible isolators mounted onto a rigid base. The appeal for the model developed then is the use of robust control theory to design $\mathcal{K}$ that meets the desired level of transmitted force to a final mounting in the presence of Δ_M. In brief, it means finding a $\mathcal{K}$ through an iterative process that satisfies the requirements of robust performance.

Applying Linear Fractional Transformation to the blocks on the right side of Figure 3.7 gives:

$$\mathbf{N} = F_l(\mathcal{P}, \mathcal{K}) = \mathcal{P}_{11} + \mathcal{P}_{12} \cdot \mathcal{K} (\mathbf{I} - \mathcal{P}_{22} \cdot \mathcal{K})^{-1} \cdot \mathcal{P}_{21} = \begin{bmatrix} N_{11} & N_{12} \\ N_{21} & N_{22} \end{bmatrix}$$

$$\mathbf{M} = N_{22}$$

$$\mathbf{T} = F_u(\mathbf{N}, \Delta_M) = N_{11} + N_{12} \cdot \Delta_M (\mathbf{I} - N_{22} \cdot \Delta_M)^{-1} \cdot N_{21}$$

The right side of Figure 3.7 reduces to Figure 3.8. The problem becomes that of designing $\mathcal{K}$ that internally stabilises $\mathbf{N}$ and checking that $\|\mathbf{T}\|_\infty < 1$ $\forall$ admissible Δ_M, $\|(\Delta_M)\|_\infty < 1$, for robust performance.

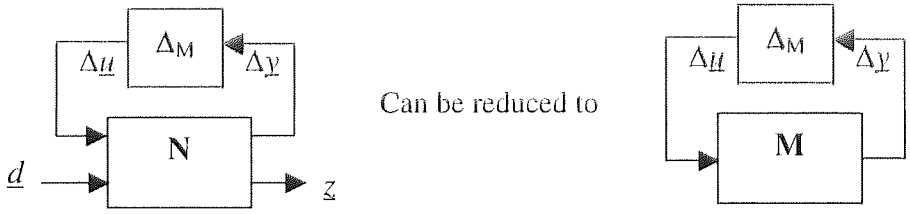

Figure 3.8 The M-Δ block problem

This is very involved, requiring the use of structured singular value approach (Stein & Doyle, 1991) and (Packard & Doyle, 1993). For a possible set of Δ_M with $\bar{\sigma}(\Delta_M(j\omega)) < 1$ it is quite sufficient to find a $\mathcal{K}$ that internally stabilises $\mathbf{N}$ and satisfying $\rho(\mathbf{M} \cdot \Delta_M(j\omega)) < 1$ $\forall \Delta_M$ in the set, $\forall\omega$ of interest. This ensures that the closed loop system is (robust) stable to this given set but with no definite knowledge in advance as to whether the desired performance is achieved for all the Δ_M.

Ultimately, it depends on the selection of the passive isolators with respect to the supporting structure and the definition of suitable weighting functions that is of relevant to a given problem. In fact, for a given problem, it is not essential that Δ_M be known exactly but the values of $\bar{\sigma}(\Delta_M(j\omega))$ for a range of ω must be given. If the design of an active control for vibration for a given set of design parameters is all that is required, then

a design with nominal stability and performance with the same framework can be achieved.

For the problem of machine on hard mounts, the design effort to include Δ_M can be quite significant even to check for robust stability. The order of the controller, $\mathcal{K}$ is at least as high as the system, not counting the actuators dynamics currently ignored in the discussion above. An alternative solution has been found which will be discussed.

3.9 Summary

In this chapter, a m-DoF model for a machine mounted via flexible isolators on to a flexible supporting base structure that fits neatly into the robust stability framework or a standard $\mathcal{H}_\infty$ optimal control problem has been developed. The resulting model is based on the selection of transmitted force as a performance metric and the application of control force at the feet of the machine instead of between the machine and the base. Hence the resulting model is the force transmissibility matrix of the form (3.26):

$$\mathbf{G}_{f\,(flex)} = (\mathbf{I}+\Delta_M)\cdot\mathbf{G}_0.$$

Where $\mathbf{G}_0$ is force transmissibility matrix of a machine mounted via isolators on a rigid base. Δ_M is the associated perturbation or uncertainty due to the use of a flexible base instead of a rigid base.

The model is derived using combined dynamic stiffness matrix of a machine on rigid base, and the inverse of the combined dynamic stiffness matrix of the coupled isolator and flexible base structure. It is an original extension of the 1-DoF models presented by Blackwood and von Flotow in 1992 who used combined receptance function instead.

The difference and the similarity of the m-DoF model have been discussed. Principally, the condition for the above equation to be valid is shown to be dependent on the product of two force transmissibility matrices: $\mathbf{K}\cdot\mathbf{R}_{mf}$ and $\mathbf{K}\cdot\mathbf{R}_{em}$ and not on Δ_M. In both cases, the magnitude of the base flexible modes coupled into $\mathbf{G}_0$ is dependent on $\bar{\sigma}(\Delta_M)$. The spectral norm and the related $\mathcal{H}_\infty$ norm are used as measures of magnitude because of (a)

they are induced norms and hence possess the sub-multiplicative property and (b) they are also principal gains relating input magnitude and directions to output magnitude and directions as used in $\mathcal{H}_\infty$ control problem.

The advantage of having such a model and the standard $\mathcal{H}_\infty$ control method is that it is possible to design a suitable feedback control system without having to know in detail the flexible base dynamics. This lack of knowledge or uncertainty can be formulated as suitable frequency weighting (performance specification) function. One can then analyse if the controller provides a stable closed loop system and whether it is able to meet the desired performance requirements set for the level of transmitted force or not. Such an approach has been actively applied in flexible space structures hosting sensitive equipment and machines. In later chapters it is shown how (3.26) in its original form can be used as a design performance specification in the standard $\mathcal{H}_\infty$ framework. This will be applied to the case where the machine is directly rigidly mounted to the supporting base structure.

CHAPTER FOUR

THE DETERMINATION OF TRANSMITTED FORCE OF A MACHINE HARD-MOUNTED ONTO A FINAL STRUCTURE USING A DISSIMILAR TEST STRUCTURE

4.1 Introduction

Much study has been done on machine mounting via flexible mounts (previous chapters) and the interaction between the foundation and a vibratory machine (Plunkett, 1958, and Dejong, 1983). These early works were concerned with the how the dynamics of the foundation or the supporting structure and the mounted machine interact. To some extent, depending on **k**, the use of flexible isolators de-couples the two components. However, there are situations where flexible isolators cannot be used and mounting structures are not rigid. In such cases, it would useful to a control engineer to know in advance how this will affect transmission of vibration so that he can design a suitable active vibration control. To a manufacturer of machines, the answers to such problems would be useful too in providing solutions to their customers.

In this chapter, answers to some of these problems would be investigated. The theoretical and practical aspects of testing machines to determine the level of force transmitted from the machines to the final foundations using test-beds whose dynamic characteristics are different to those of the final foundations would be examined. Such a scenario will be useful to a machine manufacturer as a form of acceptance test at the manufacturer's test-bed, and as a performance specification for the control engineer if there is a requirement to build an active vibration control system for the contracted machine. In both situations, it is often the case that the test-bed is not necessarily the same as the actual final mounting. The summary of this work is given in Lau *et al.* (1997).

The testing method developed in the chapter will be called Method 1. It involves the determination of the relevant receptance matrices and requires the measurements of acceleration at the feet of the machine. Two other methods will also be presented: Method 2 is based on the work of Dejong (1983) using free vibration measurements, and Method 3, a modification of Method 2, is based on the measurement of blocked force responses (Lyon, 1987).

With regards to notations used in the chapter, as there will be no flexible isolators, subscript "f" replaces "mf" and subscript "ef"" replaces "emf". Subscripts will be used only when necessary and for clarity. Any additional symbols will be defined in the text. In addition, the numeral subscripts "1", and "2" shall refer to locations e.g.

$\mathbf{R}_{f1}$: Receptance matrix of the mounting at manufacturer's works.

$\mathbf{R}_{ef2}$: Receptance matrix of machine on the mounting at final site.

4.2 The need for machine to be hard-mounted

It is not always practical to mount machines flexibly, particularly when the rigidity of the mounting is needed to maintain shaft alignment. When low vibration is a consideration, the system engineer will frequently wish to specify the maximum level of force a machine would transmit to its supporting structure, referred in this chapter as the mounting. It is in the interests of both the system engineer and the machine manufacturer

i. If vibration acceptance tests can be performed in the manufacturer's own works so that any problems can be detected and addressed at an early stage.

ii. The actual (transmitted) machine disturbance is available for the design at the early stage of any active control vibration system if needed.

There are two difficulties associated with these propositions. Firstly, the transmitted vibration characteristics of the machine are dependent on the characteristics of its mounting. And so the transmitted forces determined at the manufacturer's works might be quite different to those transmitted when the machine is commissioned, unless the two mountings have similar dynamic characteristics as stipulated in BS 4675 Pt1 (1976). Secondly, it is significantly easier and cheaper for the machine manufacturer to measure acceleration; velocity or displacement at the machine feet than it is for him to measure the force transmitted by the feet to the mounting.

To the control engineer, engaged in the design of active vibration isolation or control, knowledge of the disturbance spectrum and the structural dynamics of the supporting structure (Scribner *et al.*, 1993) is very important. The work described here shows that the transmitted machine disturbance spectrum is modified by the machine-structure interaction and shows how this resultant force transmissibility can be determined.

This would not be the case if a machine were to be mounted on (flexible) isolator. The manufacturer can test the machine on flexible isolators on the works floor and he

confident that the machine will behave in a similar way on the same flexible isolators on a floor elsewhere. It has been shown (in the previous chapter) that such flexible mounts isolate the dynamics of the supporting structure from the machine disturbance. Also, the characteristics of the isolators are normally sufficiently simple to be represented as a spring-damper combination and so forces can be calculated by hand from displacement values.

4.3 The Set of equivalent forces at the feet

Suppose that a very detailed Finite-Element model of the machine has been created and the m DoFs (degrees of freedom) of this model have been ordered in such a way that the first n DoFs relate to the points where the feet will be in contact with the mounting. The displacements vector of the machine is $\mathbf{q}$ and this can be partitioned into two components $\mathbf{q}_e$ and $\mathbf{q}_i$ as below where $\mathbf{q}_e$ is the vector of displacements at the feet extremities and $\mathbf{q}_i$ is the vector of other (internal) displacements.

$$\mathbf{q} = \begin{Bmatrix} \mathbf{q}_e \\ \mathbf{q}_i \end{Bmatrix} \tag{4.1}$$

Here it is assumed that the connection between the machine and the mounting are point contacts, and that rotational stiffness in each of the three directions is negligible. The assumption is subjective but is quite valid at low frequencies where transmission by vertical translation is the most significant. Transmissions via bending moments become relatively important only at higher frequencies (Moorhouse and Gibbs, 1993).

There are potentially 3 DoF at each point of a machine and one might consider that movements at each foot of a machine can be defined by the movements of several points on that foot. Usually, it is legitimate to consider only one point for each foot of a machine and hence 3 DoF per foot. Sometimes, it is clear that the stiffness of the test-bed and final mounting is much less than that of the machine itself in one or two directions. This will obviously have very little impact on vibration levels in the two flexible directions. In this case, only 1 DoF would be assigned at each foot corresponding to the vertical movement.

Let the vector of forces acting on the machine as a result of its operation be $\mathbf{Q}$ and this can be partitioned into $\mathbf{Q}_e$ and $\mathbf{Q}_i$ as in (4.2). There is some suitably partitioned dynamic stiffness matrix $\mathbf{D}$ which is determined from the stiffness, damping and mass matrices ($\mathbf{K}$, $\mathbf{C}$ and $\mathbf{M}$ respectively) and the angular frequency ω according to (4.3). This matrix relates $\mathbf{Q}$ to $\mathbf{q}$ according to (4.4).

$$\mathbf{Q} = \begin{Bmatrix} \mathbf{Q}_e \\ \mathbf{Q}_i \end{Bmatrix} \tag{4.2}$$

$$\begin{aligned} \mathbf{D} &= \begin{bmatrix} \mathbf{D}_{ee} & \mathbf{D}_{ei} \\ \mathbf{D}_{ie} & \mathbf{D}_{ii} \end{bmatrix} \\ &= \left(\begin{bmatrix} \mathbf{K}_{ee} & \mathbf{K}_{ei} \\ \mathbf{K}_{ie} & \mathbf{K}_{ii} \end{bmatrix} + j.\omega. \begin{bmatrix} \mathbf{C}_{ee} & \mathbf{C}_{ei} \\ \mathbf{C}_{ie} & \mathbf{C}_{ii} \end{bmatrix} - \omega^2 . \begin{bmatrix} \mathbf{M}_{ee} & \mathbf{M}_{ei} \\ \mathbf{M}_{ie} & \mathbf{M}_{ii} \end{bmatrix} \right) \end{aligned} \tag{4.3}$$

$$\mathbf{Q} = \begin{Bmatrix} \mathbf{Q}_e \\ \mathbf{Q}_i \end{Bmatrix} = \begin{bmatrix} \mathbf{D}_{ee} & \mathbf{D}_{ei} \\ \mathbf{D}_{ie} & \mathbf{D}_{ii} \end{bmatrix} \cdot \begin{Bmatrix} \mathbf{q}_e \\ \mathbf{q}_i \end{Bmatrix} = \mathbf{D} \cdot \mathbf{q} \tag{4.4}$$

The receptance of the machine denoted by $\mathbf{R}$ is simply the inverse of the dynamic stiffness matrix as in (4.5). Matrix $\mathbf{R}$ is defined and partitioned as in equation (4.6) below.

$$\mathbf{R} = \begin{bmatrix} \mathbf{R}_{ee} & \mathbf{R}_{ei} \\ \mathbf{R}_{ie} & \mathbf{R}_{ii} \end{bmatrix} = \begin{bmatrix} \mathbf{D}_{ee} & \mathbf{D}_{ei} \\ \mathbf{D}_{ie} & \mathbf{D}_{ii} \end{bmatrix}^{-1} = \mathbf{D}^{-1} \tag{4.5}$$

$$\mathbf{q} = \begin{Bmatrix} \mathbf{q}_e \\ \mathbf{q}_i \end{Bmatrix} = \begin{bmatrix} \mathbf{R}_{ee} & \mathbf{R}_{ei} \\ \mathbf{R}_{ie} & \mathbf{R}_{ii} \end{bmatrix} \cdot \begin{Bmatrix} \mathbf{Q}_e \\ \mathbf{Q}_i \end{Bmatrix} = \mathbf{R} \cdot \mathbf{Q} \tag{4.6}$$

The set $\mathbf{q}_i$ of displacements is never of any interest in this context and can be ignored. Expanding in terms of $\mathbf{q}_e$ and pre-multiplying by $\mathbf{R}_{ee}^{-1}$ produces equation (4.7) for $\mathbf{Q}_e$ in terms of $\mathbf{Q}_i$ and $\mathbf{q}_e$.

$$\mathbf{Q}_e = \mathbf{R}_{ee}^{-1} \cdot \mathbf{q}_e - \mathbf{R}_{ee}^{-1} \cdot \mathbf{R}_{ei} \cdot \mathbf{Q}_i \tag{4.7}$$

The vector of forces, $\mathbf{Q}_e$, acting at the feet of the machine is the algebraic sum of two components. The first of these components is a matrix multiplied by the vector of displacements at the machine feet. The second is a matrix multiplied by the vector of internal forces in the machine when it is operating.

As long as the machine is operating, the same internal forces, $\mathbf{Q}_i$, would be expected to exist whatever the machine mounting. So the rightmost term $[\mathbf{R}_{ee}^{-1} \cdot \mathbf{R}_{ei} \cdot \mathbf{Q}_i]$ of (4.7) can be regarded as a constant vector for any given frequency. To stop the machine from vibrating an external force given by (4.8) has to be applied to balance this internal force causing vibration. In the absence of any other forces, this would give $\mathbf{q}_e$=0, and from (4.7),

$$\mathbf{Q}_\beta = -\mathbf{R}_{ee}^{-1} \cdot \mathbf{R}_{ei} \cdot \mathbf{Q}_i \tag{4.8}$$

This set of forces is also known as the blocked force (Lyon, 1987). The force $\mathbf{Q}_\beta$ is numerically the same as $\mathbf{Q}_{e0}$ which is the set of forces applied by the machine feet to a mounting that is infinitely stiff i.e. with displacement at the feet, $\mathbf{q}_e = 0$. In this extreme case, the force equal in value to the blocked force would be transmitted to the mounting.

Alternatively in (4.7), if $\mathbf{Q}_e$=0, then

$$\mathbf{q}_e^{\,0} = \mathbf{R}_{ei} \cdot \mathbf{Q}_i \tag{4.9}$$

The vector, $\mathbf{q}_e^{\,0}$, of displacements is called the free vibration (Dejong, 1983) and is caused by a set of internal forces of the machine in operation. This vector could be obtained from a set of measurements taken at the feet of the machine freely suspended or suspended by very flexible cord. From (4.8) and (4.9), it is shown that the blocked force and the free vibration are related by (4.10)

$$-\mathbf{Q}_\beta = \mathbf{R}_{ee}^{-1} \cdot \mathbf{q}_e^{\,0} \tag{4.10}$$

$\mathbf{Q}_\beta$ and $\mathbf{q}_e^0$, are ideal quantities. The word ideal is used in the same sense as the electrical circuit concepts of short-circuit current (Norton's equivalent) and open-circuit voltage (Thevenin's equivalent).

The term $\mathbf{R}_{ee}$ is therefore analogous to the source impedance (electrical, not mechanical impedance which is the reciprocal of mobility) of the equivalent circuit. In the event that the machine is not attached to any mounting and is not operating, $\mathbf{R}_{ee}$ would represent the machine (external) point receptance matrix relating displacement at the machine feet to external force applied at these points. As the internal receptance is of no more interest in the later part, $\mathbf{R}_{ee}$ shall be abbreviated to $\mathbf{R}_e$. Equation (4.7) can be written as (4.7a), with the subscript 'e' referring to the machine element. Hence

$$\mathbf{Q}_e = \mathbf{R}_e^{-1} \cdot \mathbf{q}_e + \mathbf{Q}_\beta. \qquad (4.7a)$$

In theory it is possible to measure $\mathbf{Q}_\beta$ or $\mathbf{q}_e^0$ and use either one of them to determine the force that will be transmitted from a machine to the mounting. This is shown below using (4.12). In practice it is quite difficult to measure $\mathbf{Q}_\beta$ or $\mathbf{q}_e^0$. For $\mathbf{Q}_\beta$ a mounting with theoretically infinite stiffness will be needed, and for $\mathbf{q}_e^0$ the machine has to vibrate naturally in air as if freely suspended on a wire.

Using the above set of equations, a method of determining the force transmitted to the final mounting without using $\mathbf{Q}_\beta$ or $\mathbf{q}_e^0$ is proposed. This will use instead a set of measurements obtained for the machine mounted on the manufacturer's test bed and whose dynamic characteristics is not the same as that of the final mounting. The proposed method will be compared with that using $\mathbf{q}_e^0$ as proposed by Dejong (1983) and another method based on the block force measurement.

4.4 The force transmitted to the mounting

The case where the machine is rigidly attached to the mounting will be considered. In this case, the displacements at the machine feet are equal to those of the mounting at the points of connection. The connection forces acting on the machine feet are the opposite of the forces acting on the mounting. The mounting has some measurable dynamic stiffness

$\mathbf{D}_f$ and relates $\mathbf{Q}_e$ to $\mathbf{q}_e$ directly by (4.11). Since it much easier to apply a force and to measure the displacement, rather than the reverse, it is preferred to use the mount receptance matrix $\mathbf{R}_f$ in the equations.

$$\mathbf{Q}_e = - \mathbf{D}_f \cdot \mathbf{q}_e = - \mathbf{R}_f^{-1} \cdot \mathbf{q}_e. \tag{4.11}$$

Combining (4.7a) and (4.11) gives a closed expression for the forces between machine and mounting as in (4.12).

$$\mathbf{Q}_e = \mathbf{R}_f^{-1} \cdot [\mathbf{R}_f^{-1} + \mathbf{R}_e^{-1}]^{-1} \cdot \mathbf{Q}_\beta. \tag{4.12}$$

The formula is most easily understood for a single-point mounting in which case all of the quantities in (4.12) are simply scalars. If $\mathbf{R}_e^{-1}$ becomes very large compared with $\mathbf{R}_f^{-1}$ then $\mathbf{Q}_e$ approaches zero. If $\mathbf{R}_e^{-1}$ becomes very small compared with $\mathbf{R}_f^{-1}$ then $\mathbf{Q}_e$ approaches $\mathbf{Q}_\beta$. Both of these limiting cases are consistent with our expectation.

Equation (4.12) can be used to deduce expression (4.13) that relates the vector $\mathbf{Q}_{e2}$ of forces transmitted by the machine feet to the final mounting to the vector $\mathbf{Q}_{e1}$ of forces transmitted by the feet to the test-bed mounting.

$$\mathbf{Q}_{e2} = \mathbf{R}_{f2}^{-1} \cdot [\mathbf{R}_{f2}^{-1} + \mathbf{R}_e^{-1}]^{-1} \cdot [\mathbf{R}_{f1}^{-1} + \mathbf{R}_e^{-1}] \cdot \mathbf{R}_{f1} \cdot \mathbf{Q}_{e1} \tag{4.13}$$

In this case $\mathbf{R}_{f1}$ represents the receptance matrix of the manufacturer's test-bed mounting and $\mathbf{R}_{f2}$ represents the receptance matrix of the final mounting. Equation (4.13) would not normally be used in the form given since the vector of forces $\mathbf{Q}_{e1}$ is not measured directly in the method proposed here but is deduced from the vector of displacements $\mathbf{q}_{e1}$ using (4.11). Equation (4.14) is the most concise expression for the predicted vector of forces which will be exerted on the final mounting by the machine feet in terms of the displacements (accelerations) measured at the machine feet when the machine is on the test-bed mounting,

$$\mathbf{Q}_{e2} = - \mathbf{D}_{f2} \cdot \mathbf{R}_{ef2} \cdot \mathbf{D}_{ef1} \cdot \mathbf{q}_{e1} \tag{4.14}$$

Where

$\mathbf{D}_{f2}$ = Dynamic stiffness matrix of final mounting (without machine).

$\mathbf{R}_{ef2} = [\mathbf{R}_{f2}^{-1} + \mathbf{R}_e^{-1}]^{-1}$ = Receptance matrix of machine on final mounting.

$\mathbf{D}_{ef1}=[\mathbf{R}_{f1}^{-1}+ \mathbf{R}_e^{-1}]$=Combined Dynamic stiffness matrix of machine on test-bed mounting.

The method being proposed can now be stated clearly as follows: To discover the set of forces which will be transmitted by the machine to the final mounting, the quantities $\mathbf{D}_{f2}$, $\mathbf{R}_{ef2}$ and $\mathbf{D}_{ef1}$ must first be established for all frequencies of interest. Then the machine is run on the test-bed and the vector of displacements at the machine feet is measured. Equation (4.14) is applied for each frequency component being examined. This method does not use $\mathbf{Q}_\beta$ or $\mathbf{q}_e^0$. For the purpose of comparative study, this method will be explicitly called Method 1. Note that with this approach, the characteristics of the test-bed mounting alone are never actually required. There is no necessity to ensure that the test-bed is very stiff.

Two other methods involving the use of $\mathbf{Q}_\beta$ or $\mathbf{q}_e^0$ will also be presented and discussed to provide additional motivation for the development of the proposed method. These will be called Method 2 and Method 3.

Method 2 is given by (Dejong, 1983). The machine is freely suspended and a set of measurements at the feet of the machine (possibly taken at the manufacturer's location). This corresponds to $\mathbf{q}_e^0$. With the same notation, the force transmitted to the final mounting is given by (4.15).

$$\mathbf{Q}_{e2} = [\mathbf{R}_e + \mathbf{R}_{f2}]^{-1}\, \mathbf{q}_e^0 \tag{4.15}$$

Method 3 uses (4.12), which can be rewritten as (4.16).

$$\begin{aligned}\mathbf{Q}_{e2} &= \mathbf{R}_{f2}^{-1} \cdot [\mathbf{R}_{f2}^{-1} + \mathbf{R}_e^{-1}]^{-1} \cdot \mathbf{Q}_\beta \\ &= \mathbf{R}_{f2}^{-1} \cdot \mathbf{D}_{ef2}^{-1} \cdot \mathbf{Q}_\beta\end{aligned} \tag{4.16}$$

The blocked force can be measured at the manufacturer's works using a very stiff base or mounting.

4.5 The combined dynamic stiffness and the combined receptance matrices

In (4.14) and (4.16), the term $\mathbf{D}_{ef2} = [\mathbf{R}_{f2}^{-1} + \mathbf{R}_e^{-1}]$ is referred to here as a combined dynamic stiffness to indicate that the individual components are dynamic stiffness quantities. The measurements or the determination of $\mathbf{D}_{ef2}$ as a matrix is done with the machine rigidly attached onto the mounting. Such an arrangement and derivation of the equations result from using a force source, $\mathbf{Q}_\beta$ as input to the equation.

Equation (4.15) on the other hand involves the term $[\mathbf{R}_e + \mathbf{R}_{f2}]$, which is the combined receptance matrix. It is derived from the using a displacement source $\mathbf{q}_e^0$ as input. Note that this term is not the inverse of the combined dynamics stiffness matrix.

The two quantities $\mathbf{Q}_\beta$ or $\mathbf{q}_e^0$ are sources of disturbances. As to which equation or model to use to determine the transmitted force will depend on whether the disturbance is best modelled by a force source, $\mathbf{Q}_\beta$ or a displacement source $\mathbf{q}_e^0$. If the structural (driving point) impedance is significant compared to that of the machine, then a force source and hence the combined dynamics stiffness matrix $[\mathbf{R}_f^{-1} + \mathbf{R}_e^{-1}]$ and its inverse $[\mathbf{R}_f^{-1} + \mathbf{R}_e^{-1}]^{-1}$ should be used. It will result in a model that resembles physical reality. The fact that the plant dynamics is non-trivial implies that structural driving point impedance (at the mount locations) is significant and that force source should be used.

In this case it is expected that (4.14) and (4.16) would give a better estimation of the transmitted force. The reservation with using (4.16) lies in how accurate $\mathbf{Q}_\beta$ can be measured. Equation (4.14) does not need the use of a theoretically infinitely stiff mounting at the manufacturer works.

Furthermore in relation to our stated intention of using force feedback and force actuation, the use of combined dynamic stiffness and its inverse is more appropriate. When displacement actuation is used or actuation amplitude is important - for example, piezo-actuators between base and machine (Scribner *et al.*, 1993) and hydraulic actuators (Dyke *et al.*, 1994) in active damping using position, velocity or acceleration feedback - then combined receptance or mobility (Blackwood and von Flotow, 1992) is used.

4.6 An Example: A single DoF mounting using (4.14)

The proposed method will be applied to a case example. It has a "machine" that comprises three masses and two spring-damper connections as shown in Figure 4.1. When the machine "operates", a 1N force is applied to the top mass at all frequencies. The test-bed mount (Figure 4.1) is a single mass connected to ground by a spring-damper connection and with another spring-damper connection to which the "machine" will be fixed. The final mounting (Figure 4.2) arrangement is to be similar to the test-bed mount except that the both the spring and the damper in the connection to ground are doubled and another mass is to be fixed to the existing one via a spring and damper.

The $\mathbf{D}_{ef1}$ and $\mathbf{D}_{ef2}$ can be found using (4.17) and (4.18) respectively, as suggested by Liao and Tse (1993). These transformations will result in the addition of the required elements of the component dynamic stiffness matrices.

$$\mathbf{D}_{ef1} = \mathbf{U}_1^T \cdot \mathbf{D}_{mt} \cdot \mathbf{U}_1 \tag{4.17}$$

$$\mathbf{D}_{ef2} = \mathbf{U}_2^T \cdot \mathbf{D}_{mf} \cdot \mathbf{U}_2 \tag{4.18}$$

Where

$$\mathbf{D}_{mt} = \begin{bmatrix} \mathbf{D}_e & 0 \\ 0 & \mathbf{D}_{f1} \end{bmatrix} \tag{4.19}$$

$$\mathbf{D}_{mf} = \begin{bmatrix} \mathbf{D}_e & 0 \\ 0 & \mathbf{D}_{f2} \end{bmatrix} \tag{4.20}$$

And $\mathbf{U}_i$ (i=1,2) is a non-square matrix transforming the independent co-ordinates of the composite system (for example, machine-test mount) to that of the co-ordinates of the components (i.e. machine and test mount subsystems). It consists of rows that are zeros everywhere except for locations corresponding to the independent co-ordinates. At these locations it is a one. In this example, q_{e1} is a scalar corresponding to the displacement of mass3. The terms of equation (4.14) are also scalar, obtained from the respective matrices in (4.17) and (4.18) and the final mount receptance matrix.

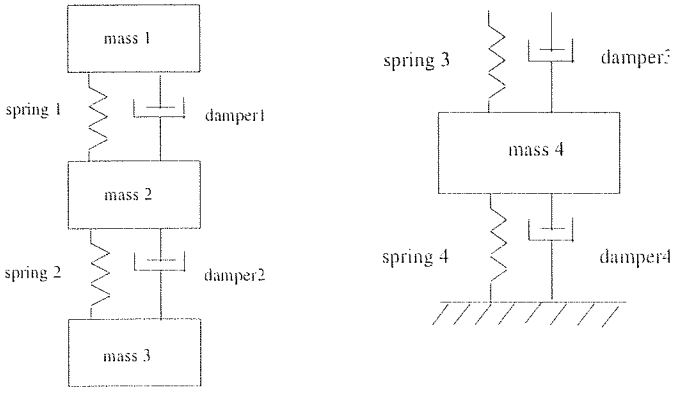

Figure 4.1. Model of the machine and the test-bed mount

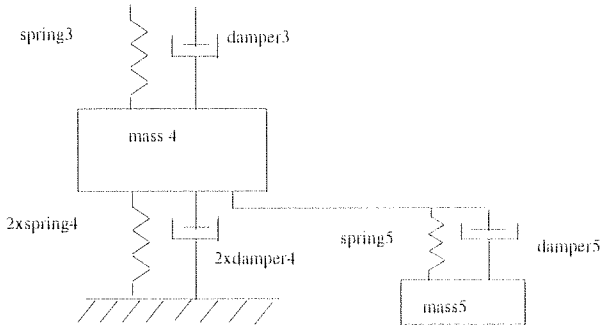

Figure 4.2. Model of the final mounting

$N\ m^{-1}$	$N\ m^{-1}\ s$	kg
Spring1 =1.0e6	Damper1 =1.0e2	Mass1 =5.0
Spring2 =3.0e6	Damper2 = 1.0e2	Mass2 =2.0
		Mass3 =3.0

Table 4.1. Machine parameters

$N\ m^{-1}$	$N\ m^{-1}\ s$	kg
Spring3 =4.0e6	Damper3 =1.0e2	Mass4 =5.0
Spring4 =5.0e6	Damper4 =2.0e2	
Spring5 =2.0e6	Damper5 =1.0e2	Mass5 =4.0

Table 4.2. Test-bed and final mount parameters

The forces Q_{e1} and Q_{e2}, and displacements q_{e1} and q_{e2} at the machine foot on both mounting arrangements are computed for 1000 frequency steps for angular frequency ω between 0 and 5000 rads/sec. These are plotted in Figure 4.3 and Figure 4.4 respectively. They show differences in the vibration level on two different mounts up to about 2500 rads/sec. At higher frequencies, the two mounts have the same vibration levels. By examining (4.13), it will be clear that this will indeed be the case whenever $|R_e|$ becomes much greater than $|R_{f1}|$ and $|R_{f2}|$ as the frequency of the disturbance increases.

The "measurements" in this example were computed values and so no measurement errors could be present. Hence in Figure 4.5, the amplitude of the ratio between Q_{e2} and q_{e1} is identical to the ratio of the dynamic stiffness of the left-hand side of equation (4.14) - the two lines coincide. However, the potential for errors exists when an accelerometer is used for measurements of q_{e1}. In Figure 4.5, the amplitude of the receptance of the test-bed mount R_{f1} at the machine-mount interface is also plotted since this will affect the measurements of q_{e1}. At about 1670 rad s^{-1}, R_{f1} has an anti-resonance (i.e. R_{f1}^{-1} is large), and the displacement q_{e1} at the machine foot attached to the test-bed mount reaches a substantial local minimum. From (4.14), if R_{f1}^{-1} is large, any noise in the measurements may be "amplified" by the use of (4.14) to give an impression of large Q_{e2}. On the other hand, at about 1410 rad s^{-1}, R_{f1} has a peak (R_{f1}^{-1} is small) and the force transmitted approaches a local minimum value.

4.7 Experimental Set-up to determine the force transmitted

While it might be possible to use a Finite Element Analysis package to determine some of the dynamic stiffness and receptance matrices, it is almost certain that direct measurements would be required if only for confirmation. Hence an experiment is set up to mimic the procedures and measurements a manufacturer and customer will have to make. This will include measurements of $\mathbf{D}_{ef1}$ and $\mathbf{R}_e$ at the works whilst a customer would have the data representing $\mathbf{D}_{f2}$ over the specified range of frequencies. Measurements must also be made for $\mathbf{q}_e^0$, $\mathbf{q}_{e1}$, and $\mathbf{Q}_\beta$. Only the experiment pertaining to the use of (4.14) will be discussed in detail but results will compared with that obtained using Method 2 and Method 3.

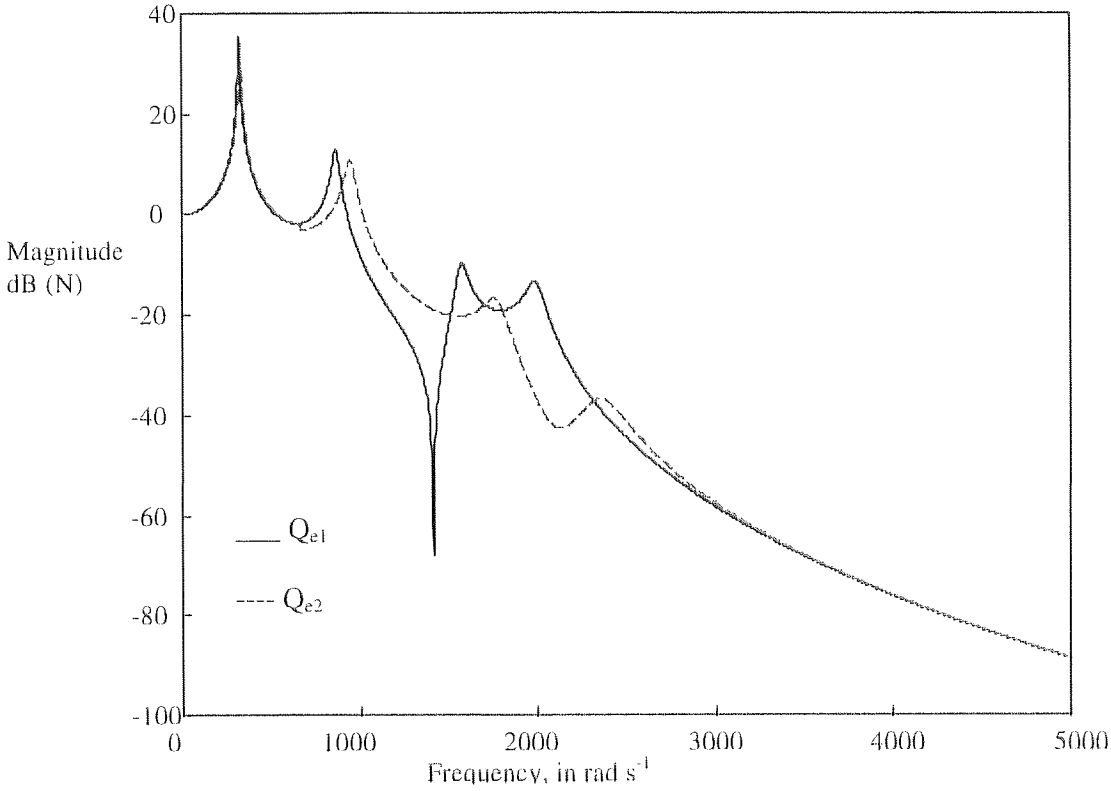

Figure 4.3 Forces, Q_{e1} on test-bed and Q_{e2} at final mounting.

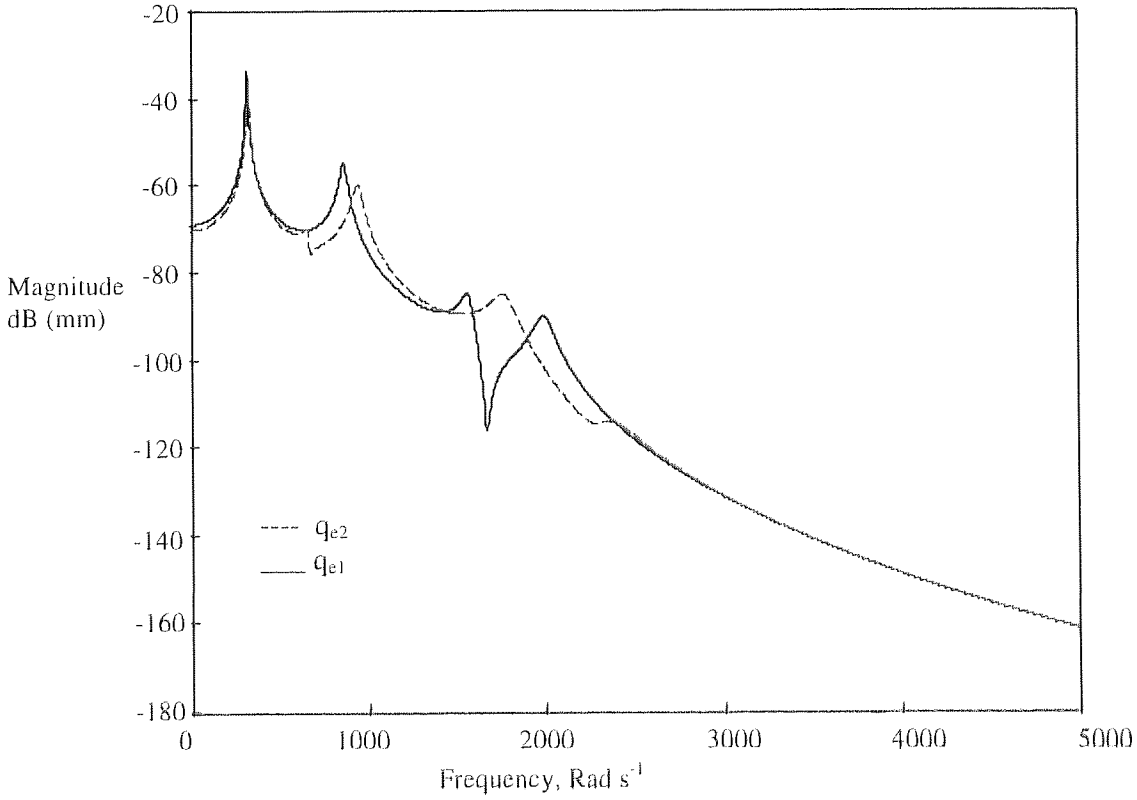

Figure 4.4 Displacements q_{e1} at test-bed and q_{e2} at final mounting

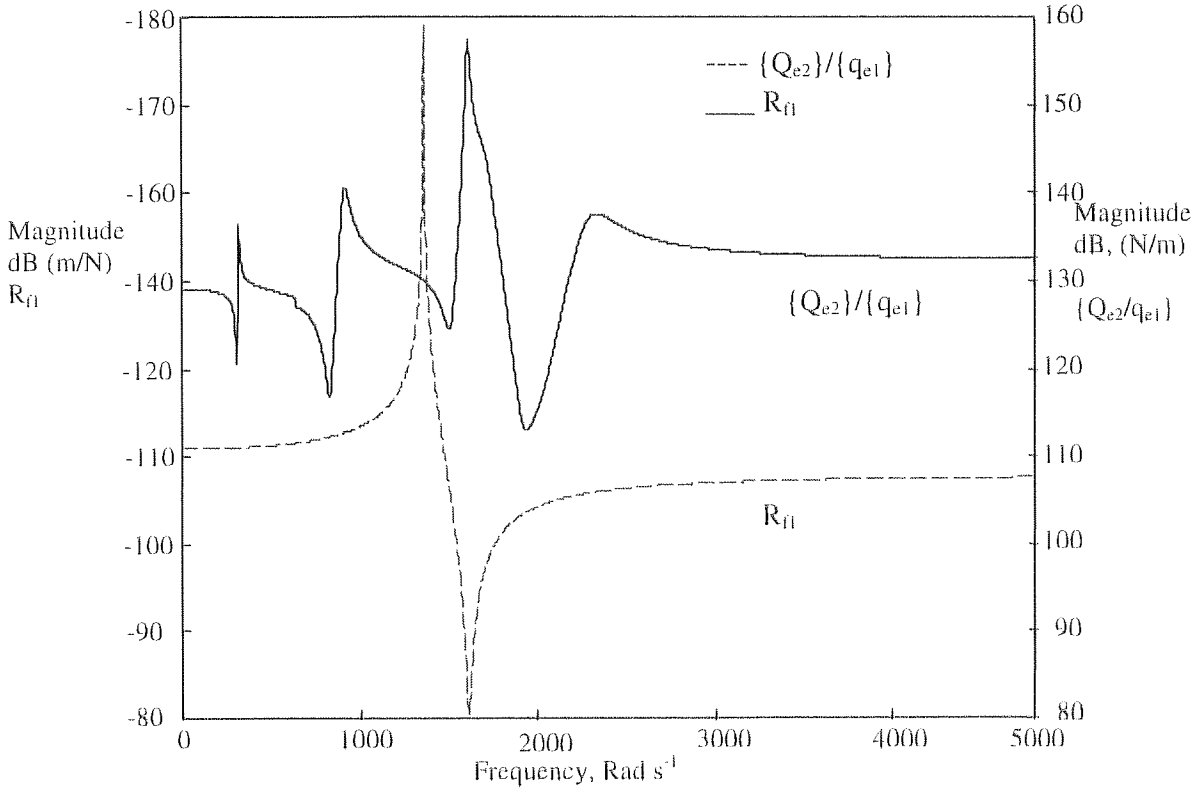

Figure 4.5 Ratio of $\{Q_{e2}\}/\{q_{e1}\}$ and R_{fl}

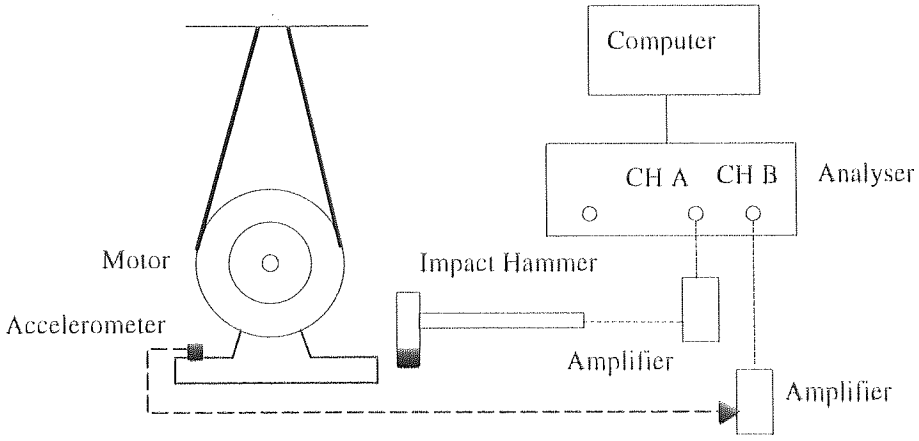

Figure 4.6 Set up for the measurement of $\mathbb{R}_e$ and q_e^0

The equipment, which a machine manufacturer is most likely to have and be conversant with, is used in an experiment to determine how well equation (4.14) will predict the magnitude of the transmitted force to the final mounting. Some tests conducted in the experiment would however not be feasible or necessary in machine acceptance tests. For example, in the experiment a pair of strain gauge load cells (a block of aluminium with "dumb-bell" shape machined out) is used as part of both the final and the test-bed mounting. This acts as the rigid attachment, and is used to measure $\mathbf{Q}_{e2}$ the (vertical) force transmitted. The load cells circuit has a dynamic range (-3dB) of 10-1000Hz and an internal resonant frequency at about 800Hz. The measurements will enable us to compare the values computed using equation (4.14) and that physically measured by the load cells.

In most cases, the manufacturer and the customer will be concerned with the total force transmitted, and would like to limit such the magnitude of the transmitted force. It will be the responsibility of the manufacturer to perform the necessary trouble shooting if the machine fails the test. Hence in this part of the discussion, the verification process is limited to comparing the total force measured and the total force that will be predicted by the proposed method using (4.14).

The procedures are as follows:

i. Measurements at the works: To mimic factory measurements, a set up similar to Figure 4.6 and 4.7 can be used. To measure $\mathbf{R}_e$ and $\mathbf{q}_e^0$ the machine has to be suspended flexibly so that the natural frequencies of the six "rigid-body-modes" are well below the lowest frequency at which dynamic flexibility will be measured. The test-bed mounting consists of a solid stainless steel modular (pallet) fixture block and the pair of load cells. The set-up shown in Figure 4.7 is used for the measurement of $\mathbf{R}_{ef1}$, the combination of the machine on the test-bed mounting, and the displacement $\mathbf{q}_{e1}$ at four feet of the machine. The load cell output gives the value of $\mathbf{Q}_\beta$ provided the flexibility of the load cells and the test-bed mounting are both negligible.

ii. Measurements at the site: To mimic 'site' measurements, a mild steel frame structure and the load cell described above are used as a final mounting. Figure 4.8 can be used for the measurement of $\mathbf{R}_{f2}$, receptance matrix of the final mounting and $\mathbf{R}_{ef2}$

the receptance of the machine on the final mounting. Where the machine cannot be mounted onto the final mounting, $\mathbf{R}_{ef2}$ can be estimated from $\mathbf{R}_{ef2}=[\mathbf{R}_{f2}^{-1}+\mathbf{R}_{e}^{-1}]^{-1}$.

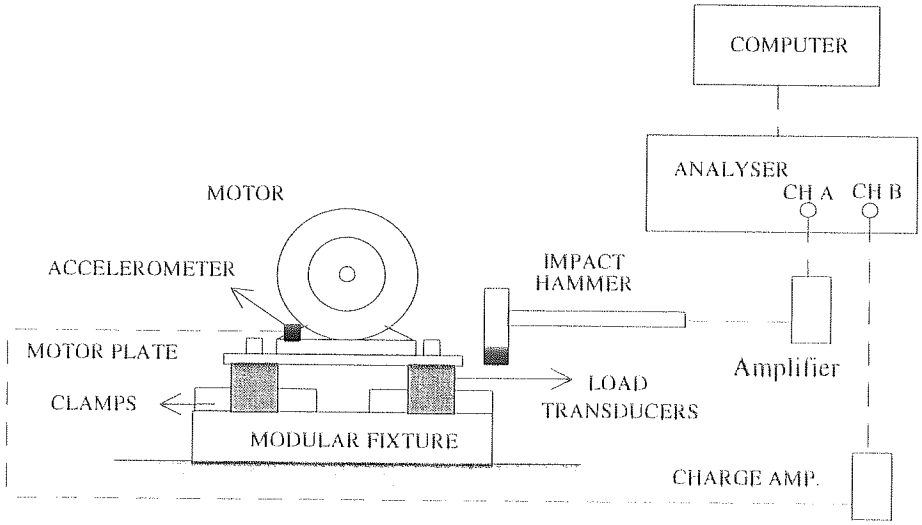

Figure 4.7 Set up for measurement of $\mathbf{R}_{ef1}$ and $\mathbf{q}_{e1}$

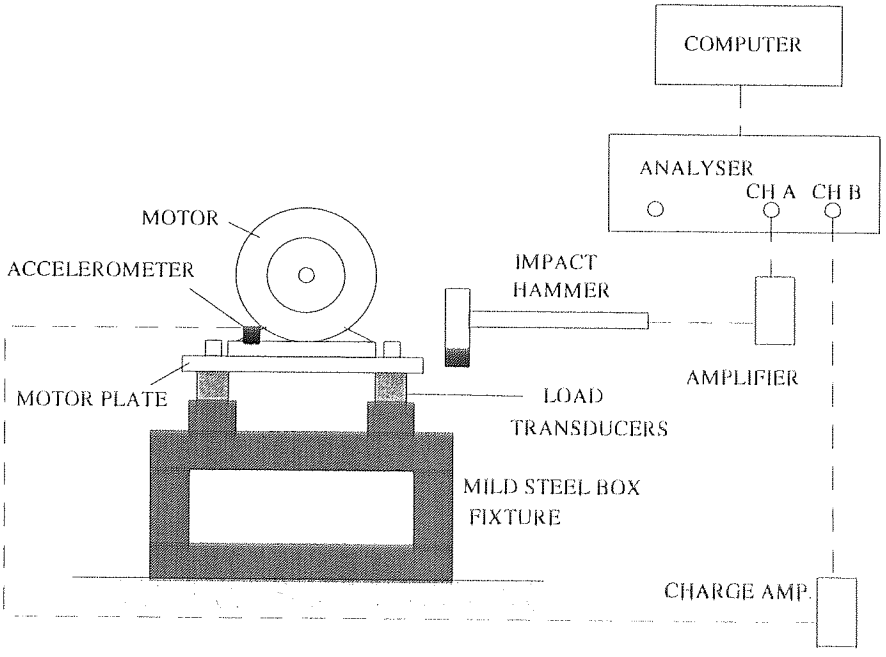

Figure 4.8 Set up for measurement of $\mathbf{R}_{f2}$ and $\mathbf{R}_{ef2}$

iii. Testing: Impact hammer testing method (BS 6897 Pt 5 1995) can be used to obtain the receptance matrices. The resulting vibration of the structure should be sufficient to generate measurable signals (greater than the 'floor' signal level of the accelerometer and the impact hammer under free running conditions). The resolution and frequency range has to be properly selected and it is important to maintain the same resolution (discrete frequency points) for all the tests. This allows for subsequent mathematical operation on the data points.

iv. Verification: The motor was operated at its rated speed of 1440 rpm (24 Hz). For the site measurements, the strain gauges on the load cells were connected to a D.C. Wheatstone bridge circuit that was connected to a strain meter with high pass cut-off frequency at 10 Hz. The experimental measurements are therefore restricted to 10-400 Hz, and only data between 10-200 Hz were used (a quarter of the dynamic range). If the specified range of frequencies extends to 4 kHz and the machine or the mounting was expected to have damping as low as 2% of critical, then using a spectrum analyser with 801 frequency "lines" would be inadequate. It would be necessary to examine the range 10 Hz - 400 Hz separately from the range 400 Hz - 4.0 kHz in order to reduce the effect of amplitude ambiguity.

Each receptance matrix in (4.14) is computed and stored as stacks of 4x4 complex matrices. Each stack of 4x4 matrix contains values of the elements of the matrix at a discrete frequency in Hz, and each value of the element in the stack is an average of ten "acceptable" recordings. The computed $\mathbf{Q}_{e2}$ of (4.14) is a stacked matrix of 4x1 vectors of 801 points. In this experiment, for comparison with the load cells measurements of overall vertical force transmitted, the absolute values of the elements of $\mathbf{Q}_{e2}$ are algebraically summed together at each discrete frequency point.

4.8 Results of an experiment using the proposed Method One

The vector $\mathbf{q}_{e1}$ of displacements at the feet of the machine mounted on the test-bed is given in Figure 4.9a and Figure 4.9b. The points marked "X" indicate the component of the disturbance spectrum corresponding to the speed of 1440 rpm or 24 Hz. The points marked "Y" indicate the component with frequency of 33 Hz, which appear to be of some significance since they are of comparable magnitude to those of the 24 Hz.

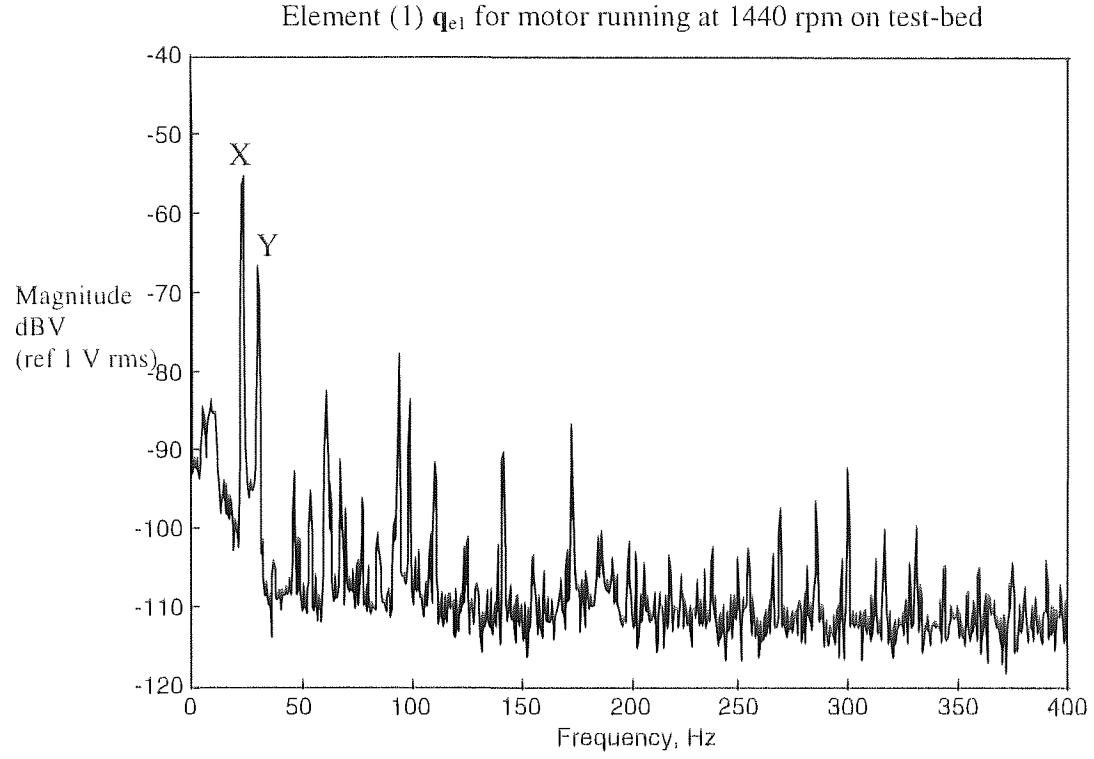

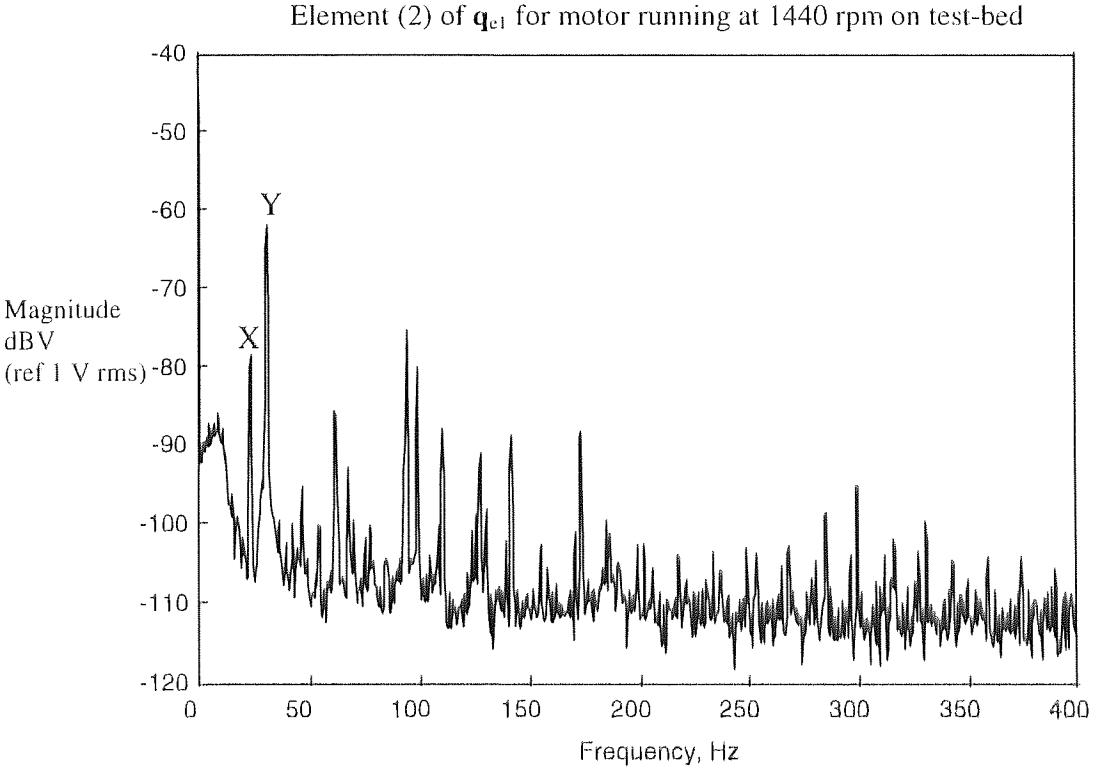

Figure 4.9a Measurements of element (1) and (2) of vector $\mathbf{q}_{e1}$ of displacements at the works for motor running at 1440 rpm

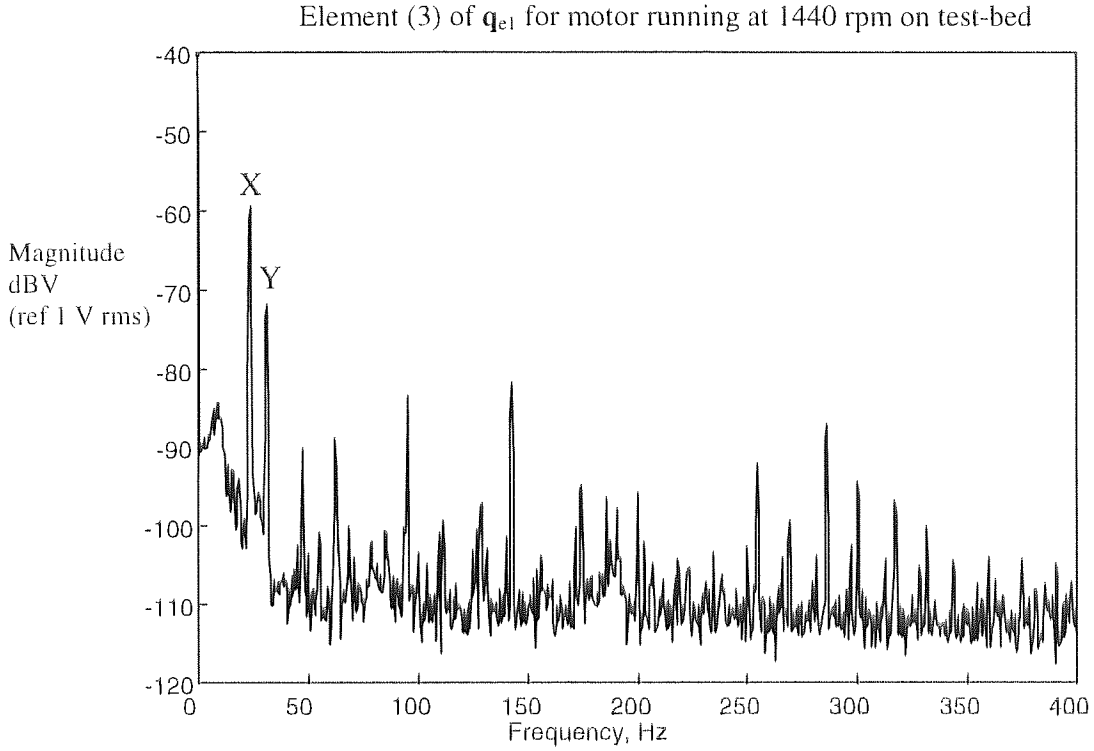

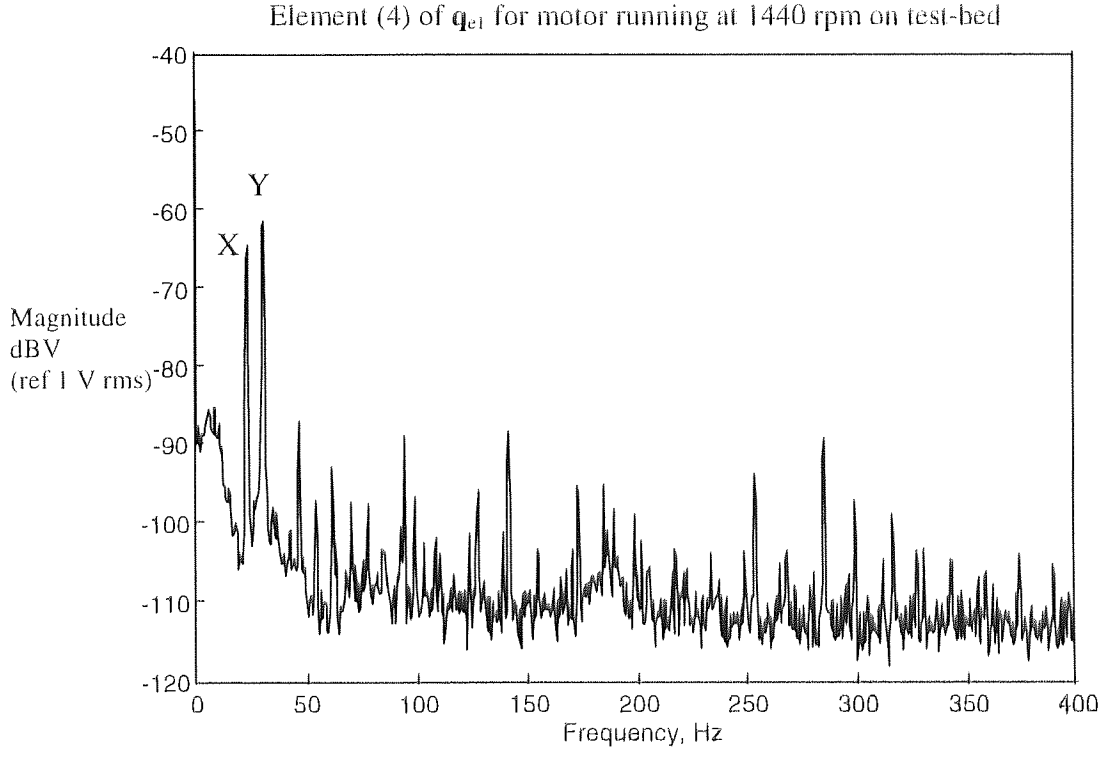

Figure 4.9b Measurements of element (3) and (4) of vector $\mathbf{q}_{el}$ of displacements at the works for motor running at 1440 rpm

The load cell measures the force transmitted to the final mounting. This is shown in Figure 4.10. The two components corresponding to 24 and 33 Hz are observed in this spectrum and are more dominant than the others. The plot of the calculated $\mathbf{Q}_{e2}$ using (4.14) with the measured inverse of the combined dynamic stiffness $\mathbf{R}_{ef2}$ for the machine on the final mounting is shown in Figure 4.11. The same peaks at 24 and 33 Hz are predicted although very slightly higher in magnitude than that measured. Their values are given below.

	24 Hz	33 Hz
Measured	25 dB	20 dB
Predicted	25 dB	22 dB

Table 4.3 Comparison between measured and calculated $\mathbf{Q}_{e2}$ at selected peaks

It is observed that (4.14) does indeed provides a means to determine at the least the dominant components of the transmitted force. The additional component so close to 24 Hz is a characteristic peculiar to this AC motor. In later discussion on active control, this transmitted force spectrum will become the disturbance spectrum for design. The effectiveness of the control system to attenuate a band-limited disturbance with two dominant frequencies will be demonstrated.

When the spectrum plots are normalised by their respective peak magnitude at the operating speed of 24 Hz, it is observed that in both cases, the transmitted 33 Hz component is about 0.55~0.7 times that of the 24 Hz component. These are shown in Figure 4.12 and Figure 4.13. They represent the relative magnitude distribution of the measured and calculated transmitted force respectively. These two plots distinctly show the presence of the higher harmonics. However the relative magnitudes of the higher harmonics for Method 1 tend to be slightly higher in comparison with that measured.

If the individual measurements of $\mathbf{R}_{f2}^{-1}$ and $\mathbf{R}_{e}^{-1}$ in $[\mathbf{R}_{f2}^{-1} + \mathbf{R}_{e}^{-1}]^{-1}$ to estimate the receptance matrix of machine on final mounting were used instead, then the calculated $\mathbf{Q}_{e2}$ shown in Figure 4.14 tends to "over-predict" the two dominant peaks at 24 and 33 Hz. They also "under-predict" above 70-200 Hz.

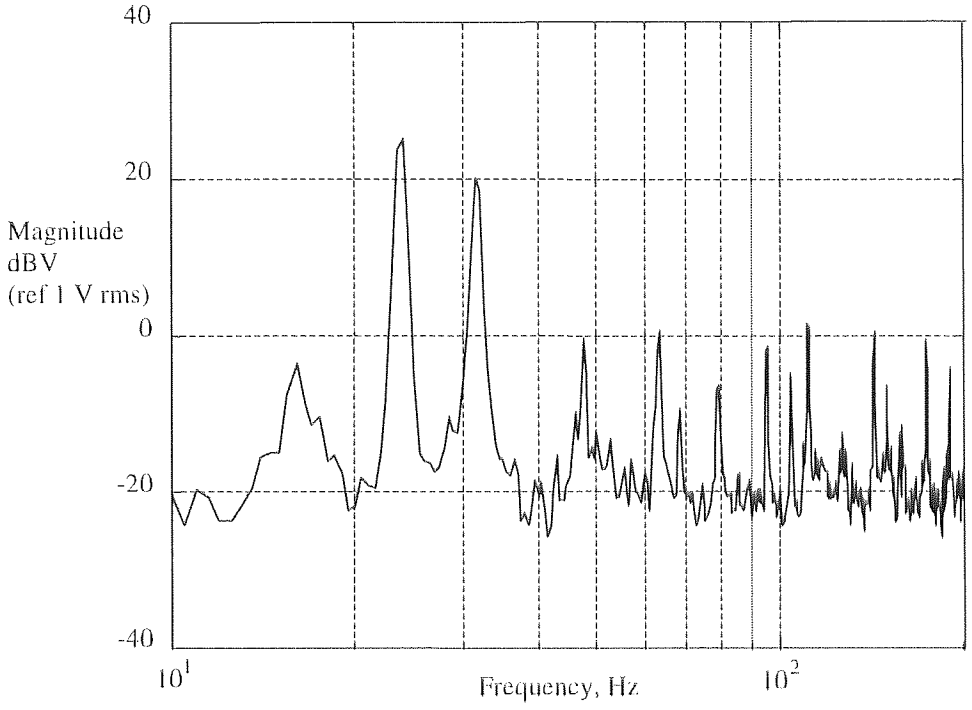

Figure 4.10 Load cell measurement of Q_{e2} for motor running at 1440 rpm

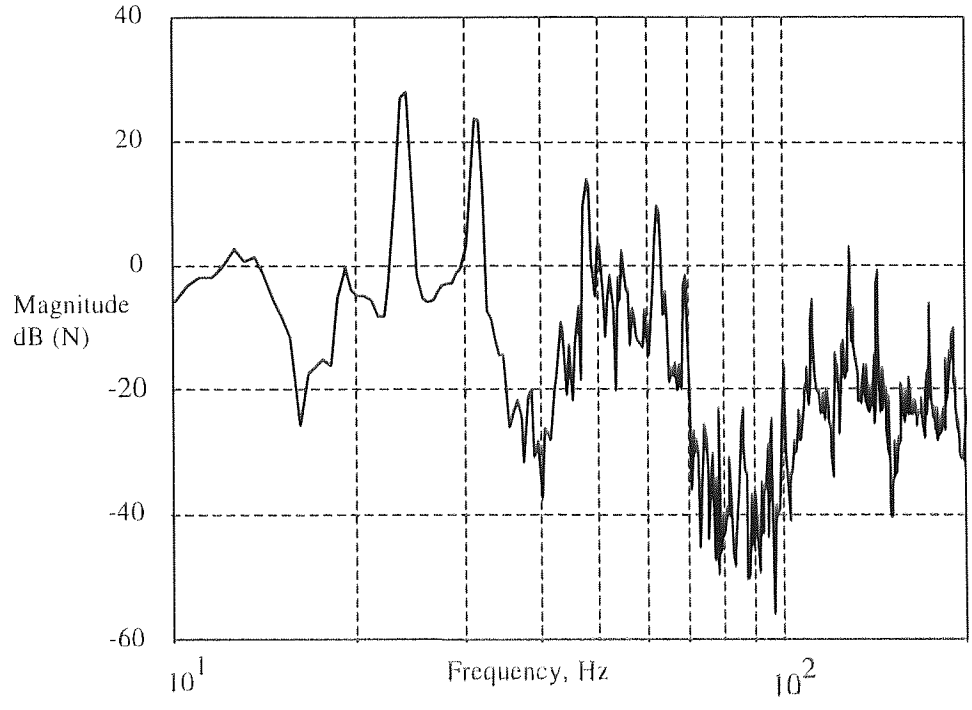

Figure 4.11 Calculated Q_{e2} using Method 1 for motor running at 1440 rpm

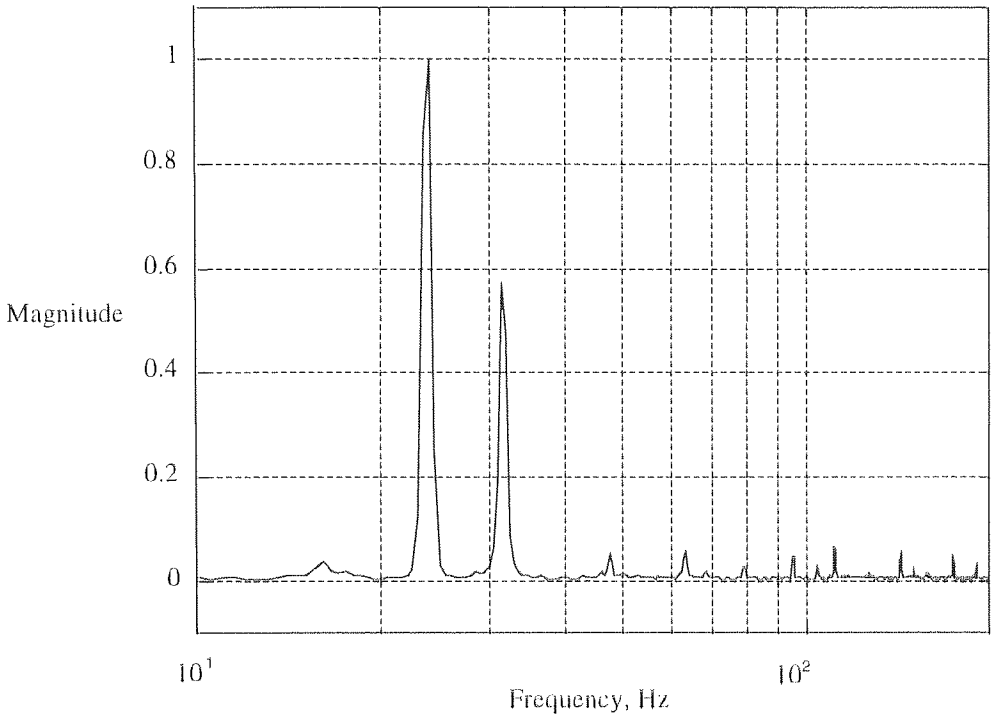

Figure 4.12 Normalised measured Q_{e2} for motor running at 1440 rpm

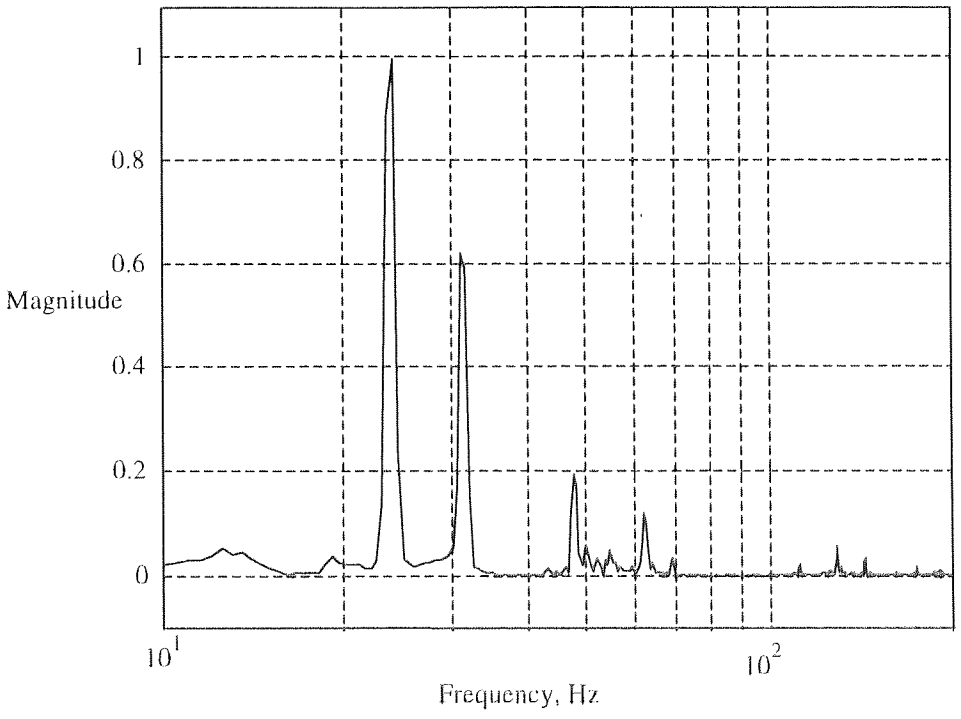

Figure 4.13 Normalised calculated Q_{e2} using Method 1 for motor running at 1440 rpm

The relative magnitude distribution of the calculated transmitted force is shown in Figure 4.15. The second peak at 33 Hz is much smaller than that of the peak at 24 Hz in comparison with that measured plot shown in Figure 4.12. Only a few peaks are recognisable in as that of the measured transmitted force.

In both cases discussed above, it is shown that the proposed method provides indication of the presence of the major components of the transmitted force. If the final mounting is accessible, then using the inverse of the combined dynamic stiffness $\mathbf{R}_{ef2}$ in (4.14) gives a reasonable estimate of $\mathbf{Q}_{e2}$ for the 24 Hz and 33 Hz components. This is not the case though if the individual measurements of $\mathbf{R}_{f2}^{-1}$ and $\mathbf{R}_{e}^{-1}$ in $[\mathbf{R}_{f2}^{-1} + \mathbf{R}_{e}^{-1}]^{-1}$ were used. The estimates tend to be higher than that measured. So more conservative values are obtained in the event that it is not possible to use $\mathbf{R}_{ef2}$.

4.9 Results using Method 2 and Method 3

The vector $\mathbf{q}_{e}^{0}$ of free vibration displacements at the feet of the machine is given in Figure 4.16(a) and Figure 4.16(b). The calculated $\mathbf{Q}_{e2}$ using Method 2 and 3 are shown in Figures 4.17 and 4.18 respectively. In comparison with the measured $\mathbf{Q}_{e2}$, it is observed that both methods under-estimated the 24 Hz component, especially Method 3, which is off by a large margin. The 33 Hz component is quite well estimated by the two methods. These two methods could only estimate the 24 and the 33 Hz components. Higher components, for example, the ones close to 50 and 60 Hz are not estimated well enough. In contrast, Method 1 is able to compute and display these two spikes.

In terms of relative magnitudes, Method 1 gives the closest match for 33 Hz with respect to 24 Hz component. In conclusion, the proposed method is more accurate than these other two methods. In addition, the proposed method does not require additional test rig other than the usual test-beds for motors. In fact the individual receptance matrix of the motor and the test-bed is not required. Only the receptance matrix of the motor on the test-bed and the accelerometers' measurements at the feet of the machine are needed. The greatest difficulty associated with Methods 2 and 3 are the measurements of free vibration and blocked force response. These are hard to obtain accurately.

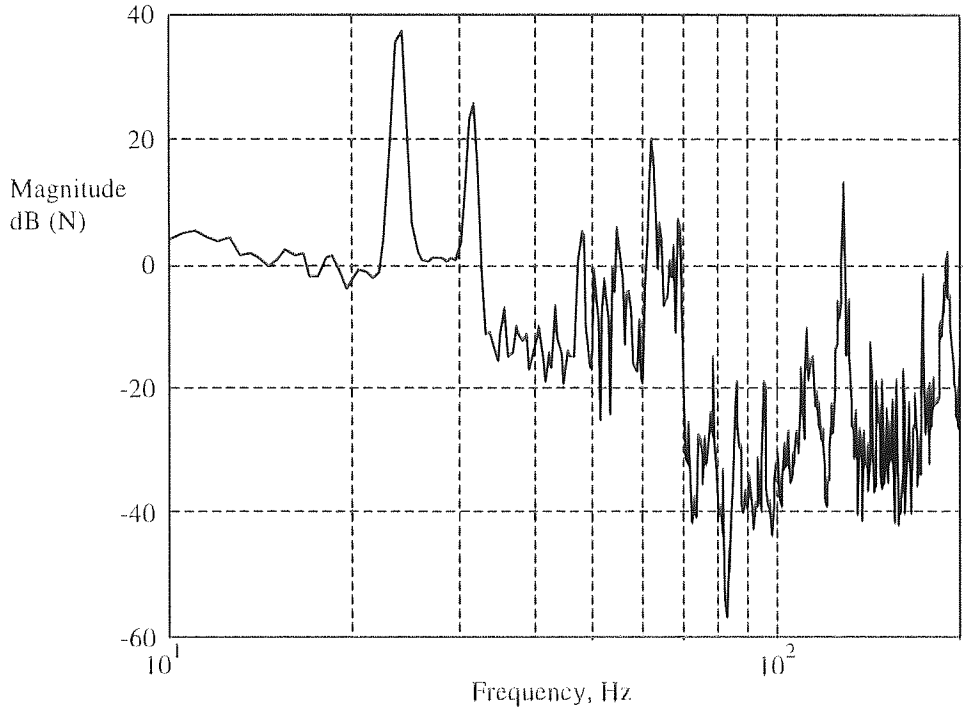

Figure 4.14 Calculated $\mathbf{Q}_{e2}$ using $[(\mathbf{R}_{f2})^{-1}+(\mathbf{R}_e)^{-1}]^{-1}$ for motor running at 1440 rpm

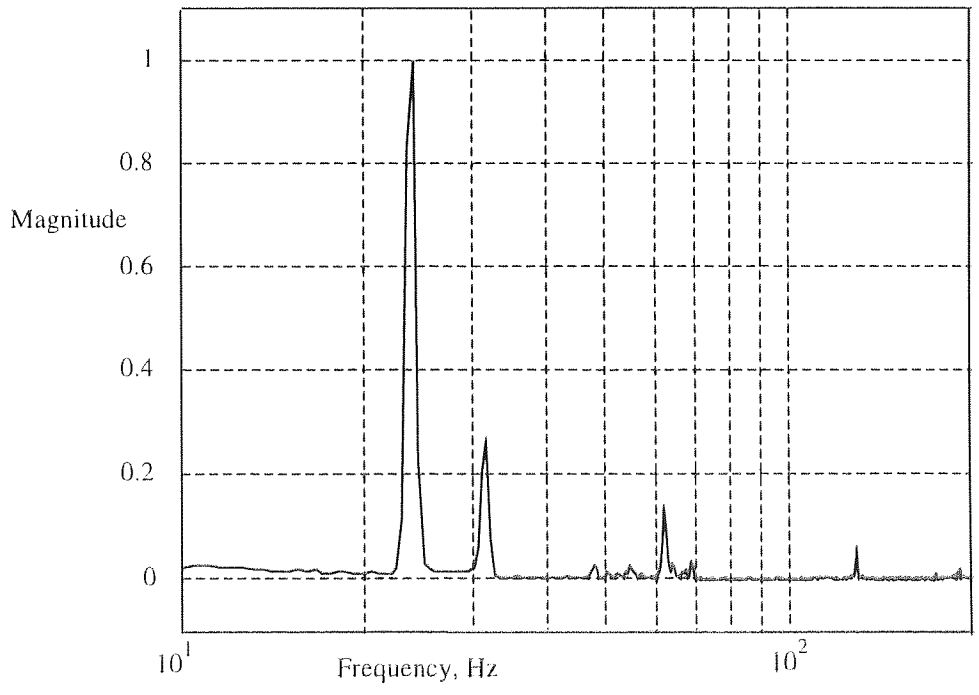

Figure 4.15 Normalised calculated $\mathbf{Q}_{e2}$ using $[(\mathbf{R}_{f2})^{-1}+(\mathbf{R}_e)^{-1}]^{-1}$ for motor running at 1440 rpm

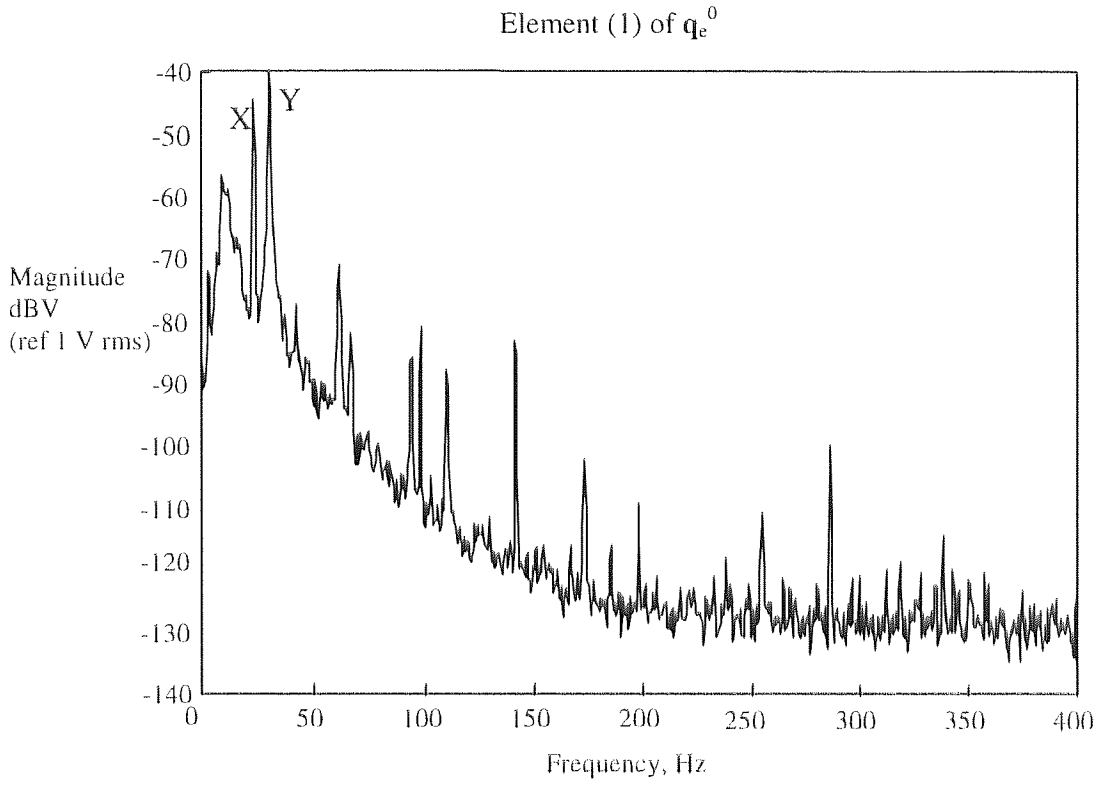

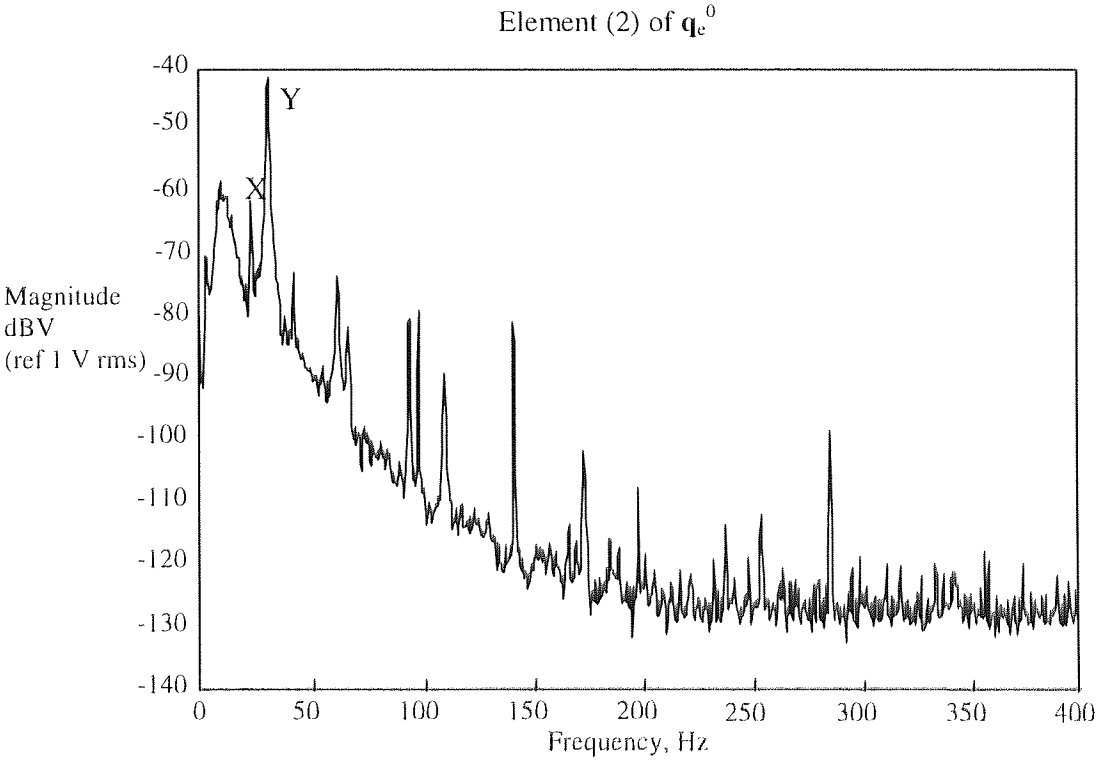

Figure 4.16a Elements (1) and (2) of vector $\mathbf{q}_e^0$ of displacements measured at the four feet of the machine operating at 1440 rpm

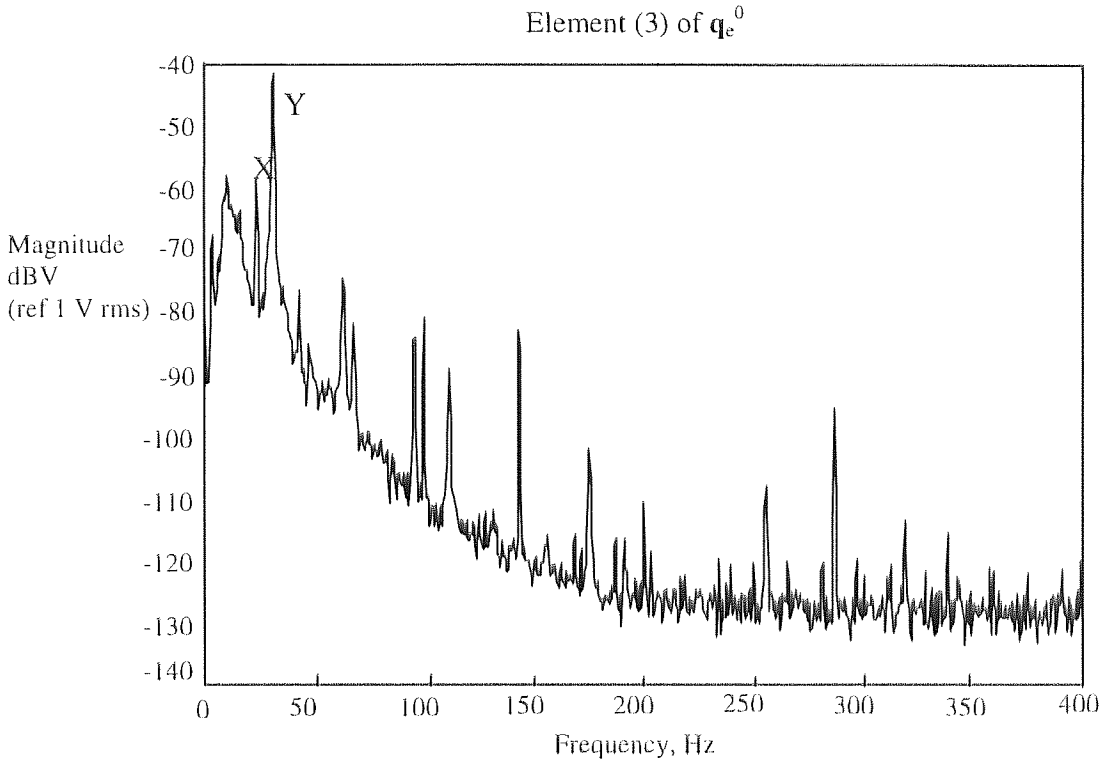

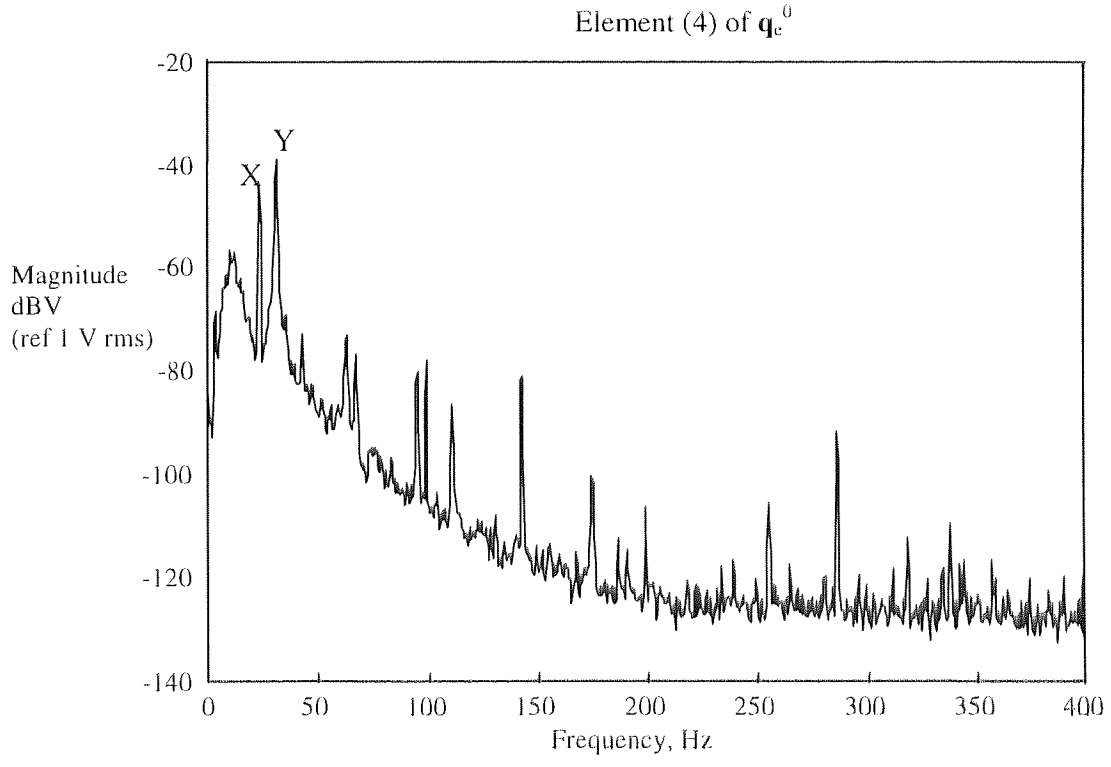

Figure 4.16b Elements (3) and (4) of vector $\mathbf{q}_e^0$ of displacements measured at the four feet of the machine operating at 1440 rpm

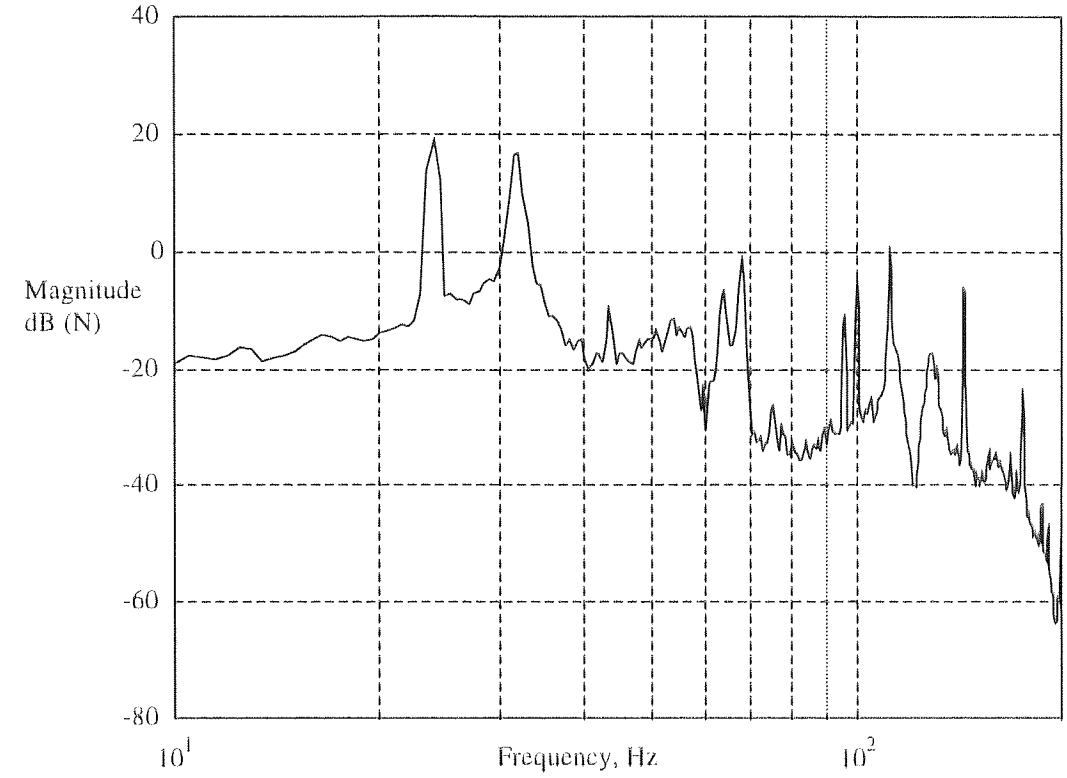

Figure 4.17 Calculated Q_{e2} using Method 2 for motor running at 1440 rpm

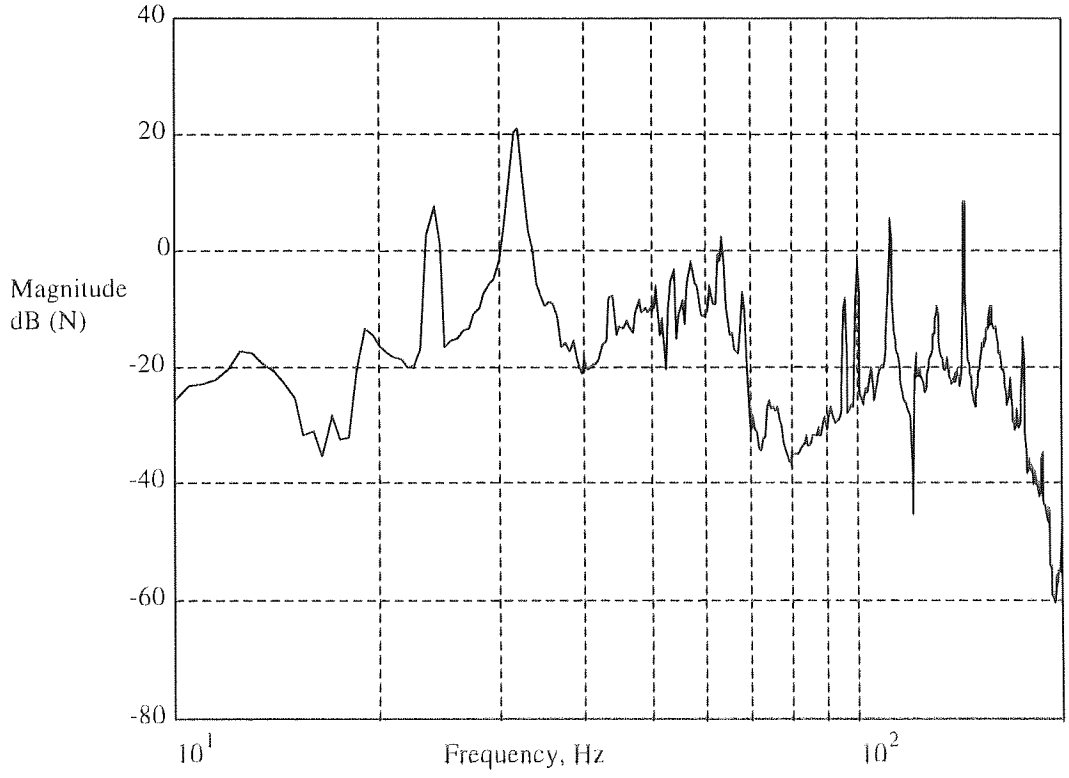

Figure 4.18 Calculated Q_{e2} using Method 3 for motor running at 1440 rpm

In fact if they are easy to obtain, then Method 2 is preferred. It requires the least amount of measurements. $\mathbf{R}_e$ and $\mathbf{q}_e^0$ can be measured using the same rig for free vibration, and $\mathbf{R}_{f2}$ is needed anyway. Addition of $\mathbf{R}_e$ and $\mathbf{R}_{f2}$ is frequency point-wise. This of course is itself a source of potential errors. In comparison Method 1 requires more measurements of the machine on the mountings, and hence is able to provide more accurate estimates.

4.10 General comments on the proposed method (Method 1)

There are three facts that need to be stated with regards to the proposed method.

a. When the effect of rotations at each mounting location was ignored, the matrices of (4.14) should in general be a 12x12 matrix and not a 4x4 matrix. In using a 4x4 matrix it is assumed that the horizontal DoFs are not at all constrained by the load cells. This may not be strictly true.

b. Method 1 including the other two methods would depend on linearity. Some non-linear effects may occur.

c. For method 3, the measurements of blocked force assume that the mounting structure at the manufacturer's works is much stiffer than the machine feet. They may not be. It would be incumbent upon the manufacturer to ensure that such a stiff test-bed is available.

Even if the above three points are taken into consideration, there are at least three main difficulties with the whole proposition presented here.

a. Firstly, the acquisition of complete sets of data representing the receptance of the machine and the combination of machine-on-test-bed-mounting requires a relatively large number of tests.

b. Secondly, the use of conversion formulae (4.11) and (4.14) to deduce reaction forces from accelerations and to predict reaction forces on the final mounting from data obtained on the test-bed mounting can augment errors as shown in the experiment.

c. Finally, even if the manufacturer does spend the time and money to acquire accurate information for the receptance matrices for the machine feet and the test-bed mounting, it is possible that measurements of final mounting $\mathbf{R}_{f2}$ will not be available at the time the machine is being tested.

Addressing the last issue first. The data for $\mathbf{R}_{f2}$ is very likely to come from some finite element design. Experimentally obtained $\mathbf{R}_{f2}$ will be useful to have at least for confirmation. Computing $\mathbf{R}_{ef2}$ from $\mathbf{R}_{f2}$ and $\mathbf{R}_{e}$ and using them in equation (4.14) would require some correction to give reasonable estimation of $\mathbf{Q}_{e2}$. If a combination of machine-on-final-mounting is available, some improvement in the results is achieved. Though this may seem to be no longer a factory acceptance test situation, (4.14) nevertheless offers an advantage of not using in-line force transducers at the site to ascertain acceptable force transmission to the supporting structure. The machine can be installed as specified, and measurements easily albeit tediously obtained.

With regards to the first concern, the number of measurements can be reduced if all of the DoFs at the machine feet are independent or if there are weak coupling between them. Then the off-diagonal terms of the receptance matrix can be neglected. Normally, a strong coupling between the three directions at any one of the machine feet at all frequencies is expected, but at higher frequencies, only a weak coupling between them - assuming that the feet are some distance apart - is expected. At the higher frequencies most of the energy is concentrated in the higher modes for which the phase and amplitude relationship between two degrees of freedom at some distance becomes quite random. For the mounting, the relative weakness of the coupling between degrees of freedom at different foot seating is even more pronounced by virtue of its geometry. It would be prudent to first verify if off-diagonal elements are indeed negligible, which take only a small number of measurements. More importantly, it is prudent to check that there is dynamic reciprocity, so that the number of measurements (lower or upper part of the matrix) can be halved even if the matrix is not nearly diagonal. This is the case especially for $\mathbf{R}_{ef2}$ and the $\mathbf{R}_{ef1}$, the inverse of $\mathbf{D}_{ef1}$ where the reciprocity can be applied.

Since the terms $\mathbf{R}_{f2}$, $\mathbf{D}_{ef2}$, and $\mathbf{R}_{ef1}$ of (4.14) involves the inversions of the matrices, a check on their respective condition numbers $\kappa(\mathbf{R}_{f2})$, $\kappa(\mathbf{D}_{ef2})$, and $\kappa(\mathbf{R}_{ef1})$ is needed. These

matrices become ill conditioned with respect to inversion in some frequency ranges. For a given $\mathbf{q}_{e1}(\omega)$, using the algorithms provided for by Matlab to compute $\mathbf{Q}_{e2}(\omega)$, there is a loss of accuracy in the last (log10(8.4*105)) = 6 digits using the IEEE double precision format with 16 decimal digits of accuracy in the region of 60-70 Hz. The difference in accuracy in using $\mathbf{D}_{ef2}$, and $\mathbf{R}_{f2}^{-1}$ and $\mathbf{R}_{e}^{-1}$ in $[\mathbf{R}_{f2}^{-1} + \mathbf{R}_{e}^{-1}]^{-1}$ is a factor of 1000 in the same region (in favour of $\mathbf{D}_{ef2}$). However, in both cases, the loss of accuracy due to inversion in the more critical region between 20-40 Hz, is smaller than 0.01% for both cases.

The use of (4.14) with accelerometers has its own set of problems. At those frequencies where the norm of $\mathbf{D}_{ef1}$ is low, very little force is needed to produce large displacements. These are near the resonant frequencies. Near the anti-resonant frequencies the norm of $\mathbf{D}_{ef1}$ is high, and a very large force is necessary to produce a small displacement. Consequently, if a small displacement is measured at one of these anti-resonant frequencies, it suggests that a large force is present. Unfortunately, accelerometers are typically "noisy", giving some finite signal at every frequency though the actual accelerations involved are infinitesimal. At such anti-resonant frequencies, as the calculation of $\mathbf{Q}_{e2}$ in (4.14) depends on the norm of $\mathbf{D}_{ef1}$, the noise in an accelerator signal can suggest that much larger forces are present than actually exist. One way round this problem is to artificially reduce the norm of $\mathbf{D}_{ef1}$ at anti-resonant frequencies so that the potential for amplifying noise to unacceptable levels is removed.

Another issue relating to the use of accelerometers is the effect of the dynamics of the mounting coupled with the measurements of $\mathbf{q}_{e1}$ to give the predicted transmitted force $\mathbf{Q}_{e2}$. The spectral-norm of equation (4.14) is given by (4.21),

$$|\mathbf{Q}_{e2}| \leq \|\mathbf{D}_{f2}\| \cdot \|\mathbf{R}_{ef2}\| \cdot \|\mathbf{D}_{ef1}\| \cdot |\mathbf{q}_{e1}| \tag{4.21}$$

The product of the individual norms is shown in Figure 4.19. The magnitudes are large because the condition numbers of the matrices are used and multiplied together. These have no particular meaning. The left-hand side of equation (4.21) which is the computed norm of $\mathbf{Q}_{e2}$ is shown in Figure 4.20. The regions of the "valleys" and the "peaks" of the calculated $\mathbf{Q}_{e2}$ closely followed that of the product of the norms of receptance and dynamic stiffness matrices of the right hand side of (4.21).

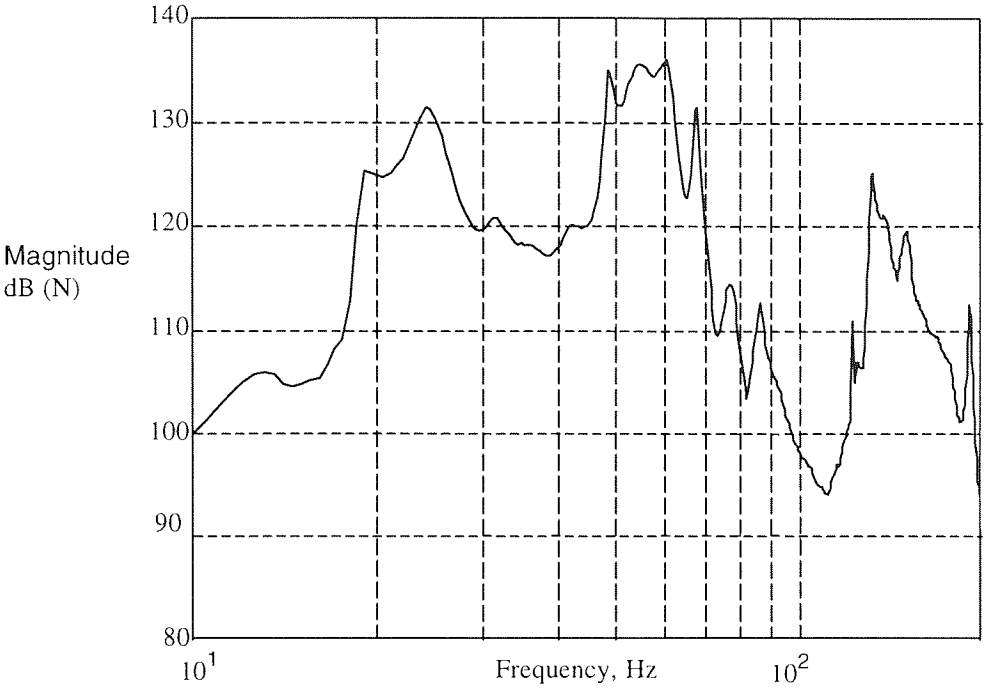

Figure 4.19 Product of norms of matrices of right side of (4.14)

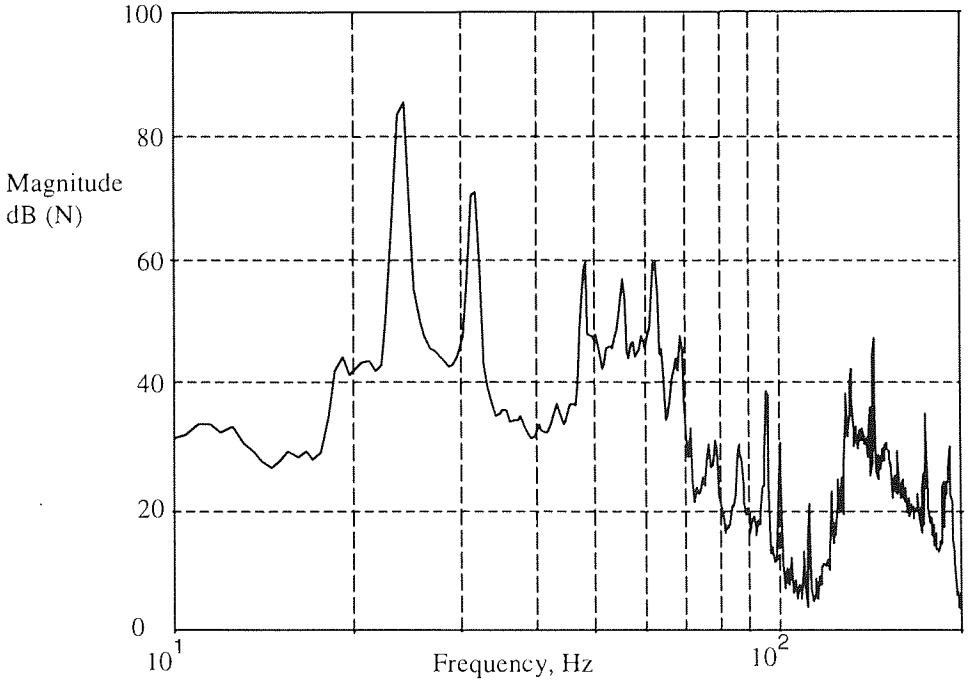

Figure 4.20 Norm of $\mathbf{Q}_{e2}$ of (4.14)

In comparison, the measured $\mathbf{Q}_{e2}$ does not show this coupled effect. This difference is in shown Figure 4.10 and Figure 4.11 where there is backbone profile for the calculated $\mathbf{Q}_{e2}$.

The effects of structure flexibility coupled onto acceleration measurements have been observed by (Watters *et al.*, 1988) and subsequently discussed in (Blackwood and v. Flotow, 1992). If one is primarily interested in predicting transmitted force on a dissimilar mounting from that of the test-bed, the proposed method is all right. However if the primarily intention is active control, then one would like as little of this coupling as possible in the control loop. Hence in the next chapter the use of force sensors rather than accelerometers in determining the transmitted force will be discussed.

The alternative to what is proposed here is to ensure that the test-bed mounting has similar dynamic characteristics as the final mounting as specified in BS 4675 Pt 1 (1976). This option can be rather costly if implemented for every application.

4.11 Summary

In this chapter, the case of a machine that is to be rigidly attached to a mounting has been examined. In particular investigated the case where the level of force that can be transmitted by a machine to its final mounting is being determined on another mounting with dissimilar dynamic characteristics has been investigated. This will be of interest to a machine manufacturer especially if the testing can be done at the factory or if necessary at the site using accelerometers rather than force sensors. A method has been proposed that will enable a manufacturer to perform such a test.

The theoretical and practical aspects of the proposed method have been discussed. A simulated model and an experiment are described to demonstrate the workability of the proposed method that could be implemented on a microcomputer system and a spectrum analyser. The principal difficulties in using the proposed method are the cost of collecting the data and performing the calculations, and the accuracy of the proposed method. If there were small coupling between the various degree of freedoms, the test effort can be minimised. Otherwise, the principle of dynamic reciprocity can help to reduce the number of measurements needed. Adjustments for differences in the test-bed and final mount

dynamics may be necessary and artificial "clipping" of the characteristics at certain frequencies to ensure that false large values of $\mathbf{Q}_{e2}$ are not computed.

The level of force calculated is higher than that measured. In comparison with the use of the blocked force or the free vibration, the proposed method gives a more accurate prediction. Furthermore, it is more difficult to set up the test rig to measure either the blocked force or the free vibration accurately. Nevertheless attempts had been made to obtain these measurements.

In addition, the proposed method allows a control engineer to determine in advance the likely disturbance that can be transmitted from machine to the final mounting. The machine free vibration $\mathbf{q}_e^0$ spectrum by itself is not suitable for use as a disturbance performance specification for the design of active vibration cancellation. For unlike the case of the use of flexible isolators, the dynamics of the final mounting cannot be de-coupled, and the interaction with the machine disturbance spectrum will inevitably modify it. In the case presented it is observed that only the two critical spectral lines are dominant in the force transmitted spectrum. For such situations, the use of feedforward control loop may be sufficient for active force cancellation. Hence the knowledge of the resulting modified disturbance spectrum will enable the control engineer (a) to specify a performance requirement and (b) and decide the type of control loop for the design of an active control system to attenuate the transmission of the force disturbance to the final mounting.

In the method proposed, once all the relevant receptance matrices are available, only accelerometers are required to measure the motions at the feet of the machine in order to determine the force that will be transmitted in the final mounting. These are easier to use by comparison with in-line force sensors. However the coupling of the accelerometers' signals with the dynamics of the structure is not an ideal combination for the performance of the control loop. In this respect, the use of force sensors may be inevitable. The objective will be to obtain the force transmissibility function or matrix in form similar to (4.12) rather than (4.14).

CHAPTER FIVE

IDENTIFICATION OF THE FORCE TRANSMISSIBILITY MATRIX OF A MACHINE HARD-MOUNTED ONTO THE STRUCTURE

5.1 Introduction

The model for a force transmissibility matrix of two cases of a machine mounted onto a flexible support base structure: (a) using isolators ("soft-mount") and (b) direct rigid mounting ("hard-mount") have been presented in the previous chapters. For both cases, the methods of determination of the force transmissibility function matrix using a test-bed that is not necessarily the same as the final base support structure have been given. In chapter three, it was demonstrated how in principle, the force transmissibility function matrix can be used for the design of active vibration isolation system. In chapter six, it will be shown how in practice this can be done but only for the case of a hard-mounted machine. In this chapter, an experimental case study is presented. The reasons for such a study will be given followed by discussions on the determination of the force transmissibility matrix for a machine hard-mounted onto a flexible structure.

Unlike a majority of the literature cited in the thesis, the case studied involves a 5.5 kW variable speed industrial AC motor rather than a simulated disturbance using a shaker. The motor is hard mounted onto a flexible structure. Four Electro-magnetic actuators mounted at the machine feet are used to provide the active force to cancel the disturbance. They are mounted on top of, rather than being in parallel with, the mounts. A force sensor is installed at the bottom of each of the four mounts to measure the transmitted force, and the outputs of these sensors are used as controlled variables.

A frequency domain identification method is used to determine the force transmissibility or transfer function matrix. As a hard mount separates each actuator and sensor, the transfer function matrix obtained is non-minimum phase, modally dense and proper. Each transfer function element in the 4x4 matrix has an order between six to ten. To enable an efficient design of a controller, the transfer function matrix is transformed to a state space model. This is done using zero-pole to state space transformation to avoid the problem of ill-condition matrix. The resulting state space model has 154 states. The order of the model is reduced by a method of balanced residualisation to 12 states.

The original and the reduced order force transmissibility matrix will be used as a performance objective for the design of controller to provide active force cancellation.

5.2. Active control of machine hard-mounted onto a foundation

There are some issues that have to be highlighted. Firstly, the reasons for a case study for machine hard mounted; secondly, the use of feedback rather than feedforward active vibration control and lastly, the reasons why force measurement and actuation are used. In discussions, the rationale behind the design of the experiment presented here will made be clearer.

There are a number of situations where soft mounting is neither a preferred nor a suitable solution. For example when accurate alignment of equipment or when limited machine motion is required. In the Freudenberg's active engine mount (Fuller *et al.*, 1996) a rigid connection between the actuator and the car body is needed to provide effective force cancellation of the primary excitation caused by the engine vibration. This last example shows that when active force cancellation is used in vibration isolation, hard mounting of the machine is desirable. Another arrangement that is possible or effective with hard mounts is when a set of equipment is to be rigidly mounted onto a raft to meet some alignment requirement and the raft is in turn mounted via isolators onto a foundation. Such a configuration is quite common for diesel engine driven pumps that come mounted on a skid made of C-channels. The skid is normally rubber mounted onto the superstructure such as an off shore structure. This is like the double mounting arrangement discussed in (Sommerfelt and Tichy, 1988) and (Ross, 1988). There is a difference though in that the method suggested here have only one spring-mass frequency. The objective remains the same: reduce the force transmitted to the raft or the final base structure.

Without the presence of soft mounts, the dynamics of the structure will be coupled to the disturbance measurements. With hard mounts and if the structure is relatively stiff, the transmitted vibration spectrum arising from the machine operation may still have well-separated narrow spectral peaks as shown in the previous chapter. A feedforward control strategy may be applied. When the structure is less stiff, the spectrum gets adulterated, and the transmitted force spectrum may have fewer resonant peaks due to the machine disturbance and may include some coupled base flexible modes. In this case, feedback control is preferred. For this reason Watters *et al.* (1988) used a feedback control in the

experiment on a single active isolation mount of a 590 kg (1300 lb), 140 BHP diesel engine mounted on a grillage of 2.4 m x 2.4 m I-beam.

The specific measure of performance for disturbance rejection or the performance metric can either be a reduction in the force transmissibility or the transfer function relating applied force to measured motion (Scribner *et al.*, 1993) or applied motion to motion. Power flow as a measure of disturbance rejection had also been used in vibration control. Goyder and White (1980) had argued that reducing vibration in a structure by reducing either the motion (displacement, velocity or acceleration) or force amplitude without considering the relative phase angle may not always be successful. Furthermore, the use of power in vibration control is valuable in that it combines both force and velocity into a single concept. Pan *et al.* (1992) and Pan and Hansen (1993) had demonstrated the use of active feed forward control of power flow for multiple isolators. In their case, the number of sensors used is increased e.g. a impedance head to measure input power, and a pair of force sensor and accelerometer to measure output power at each mounting location.

If the base effective modal mass is significant in comparison with the machine mass, then the machine disturbance can be viewed as a force source. Otherwise it is viewed as motion source. If the base is relatively stiff then a reduction in transmitted force in response to a force disturbance source is a meaningful specification, for if it is more compliant, a reduction in the transmitted force may well cause an increase in acceleration measured at some parts in the structure. As observed by Watters *et al.*, (1988), if acceleration measurements at the machine mounts are to be used as feedback signals, much of the effect of the base flexibility gets coupled into the signals in spite of the use of flexible isolators. This coupling was not observed in the transmitted force signals measured. With the system shown in Figure 5.1, a force disturbance model is appropriate and under the certain conditions stipulated, and to avoid "corruption" of the feedback signal the force transmissibility function is adopted as a performance metric.

Also from a control perspective, such a function can be used as a design specification in shaping the loop transfer function for disturbance rejection. The resulting closed loop transmissibility function can then be compared with the open loop transmissibility function to provide a measure of the effectiveness of active isolation.

Force actuation is used in closed loop control to provide the force transmissibility function. If motion actuation is used, the resulting closed loop system may result in the machine disturbance appearing as a motion source to the system (Scribner *et al.*, 1990).

Watters *et al.* (1998) located the force actuator between the machine and the base. In the case of hard mounting, this actuator will double up as a rigid mount (Chaplin, 1983). Compact actuators capable of supporting the mass of the machine will be needed. Control signals must inevitably be superimposed on a DC signal and a variation in the total signal strength in response to the controller will cause the machine to move. This will affect equipment alignment. Furthermore the actuators must be supplied continuously energised to keep the actuators rigid and stiff if machine alignment is essential. It may be possible that the net power supplied is zero.

To provide for force actuation and to maintain machine alignment, the proposed location of the force actuators is at the feet of the machine. This is in part motivated by Tanaka and Kikushima (1985, 1988, 1988). They have designed active force cancellation of an impulsive force generated from a simulated forge hammer rigidly mounted to the ground. Two servo-hydraulic actuators mounted at the feet of the machine provide the force actuation to actively cancel the impulse measured at the feet of the machine. In this configuration, each actuator has to react against its own inertia mass and no DC signal is needed, as there is no need for static force actuation. Different types of SISO controllers were tried out with (a) a lead-lag compensator (1985, 1988), (b) a pole-zero controller or notch-filter (1988) and (c) an Optimal Linear Quadratic Regulator design (1988). In all these cases, only the dynamics of the servo-hydraulics actuator was considered and the dynamics of the ground was ignored. Apparently it is the only work done of this sort reported (Fuller *et al.* 1996). The exception is in the control of flexible space structures where they have been successfully deployed on space structures but they may appear hazardous in vehicles and ships. With a proper housing design, the real constraint is space and the inertia force that can be generated.

From our discussion presented, it appears that there is currently a vast amount of literature on active vibration isolation with soft mounts, and a relatively sparse amount of work done using hard mounted machines. It is our intention to contribute to the latter part using MIMO controller design for four inputs and four outputs. The rig and the investigation

that will be presented in this chapter may not necessary be an end by itself but may well be useful for a double mounting arrangement with rigid mounting on a raft and soft mounting onto the foundation. Instead of using (4.12) to determine the force transmissibility matrix, a frequency domain identification method will be used to obtain this matrix.

5.3. Experimental Model

5.3.1 The Hardware description

The system comprises an industrial 5.5 kW 50 Hz AC machine rigidly mounted to an aluminium plate via four force aluminium mounts. The plate is in turn mounted onto a mild steel base structure. This plate is added to artificially provide some perturbation for the controller design e.g. to mess up the machine force disturbance spectrum. In practice, the support must be stiffer and well damped. The side and front view of the rig are given in Photo 5.1 and Photo 5.2. Figure 5.1 gives the location number of the hard-mounts.

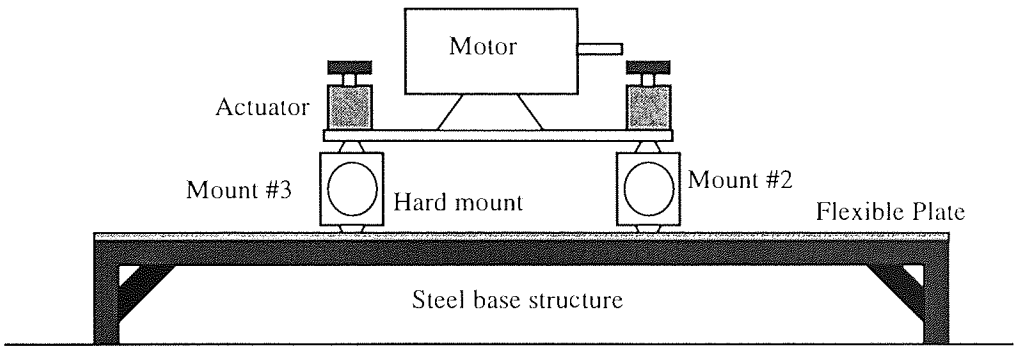

Figure 5.1 Side View of the plant or system used in the experiment

When the machine is operating, there will be horizontal and vertical forces and moments of forces acting at the points of support. In most cases, the primary concern in active isolation has always been the vertical component. The horizontal plane forces can be reduced using additional shear damping material. To restrict the system responses to vertical forces, an 'ideal' mount design should be stiff in the vertical direction and more mobile in the other directions. One suitable design is shown Figure 5.2a

Strain gauges could be attached to the mid-section of each mount, and the mounts could then be used as force sensors for measuring the vertical forces transmitted.

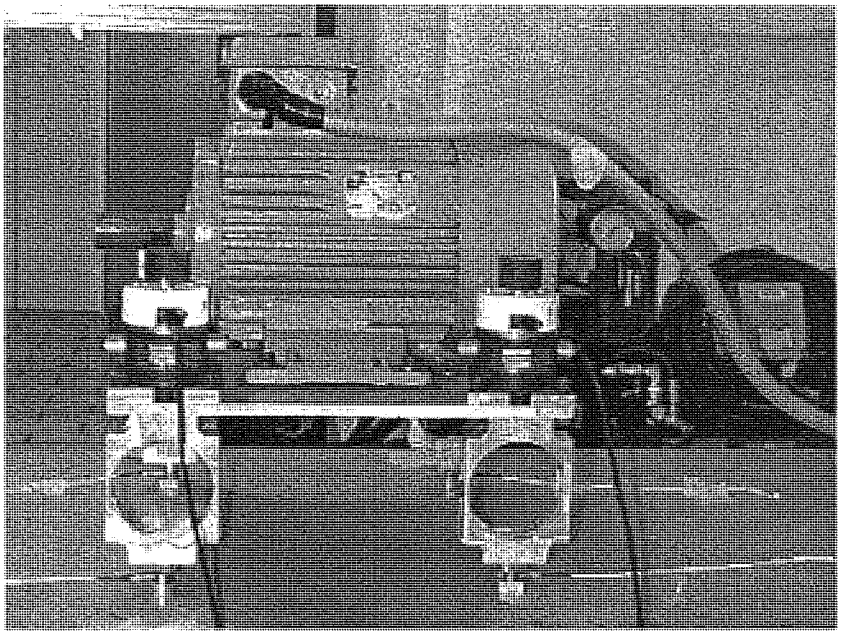

Photo 5.1 Side view of the motor on the plate

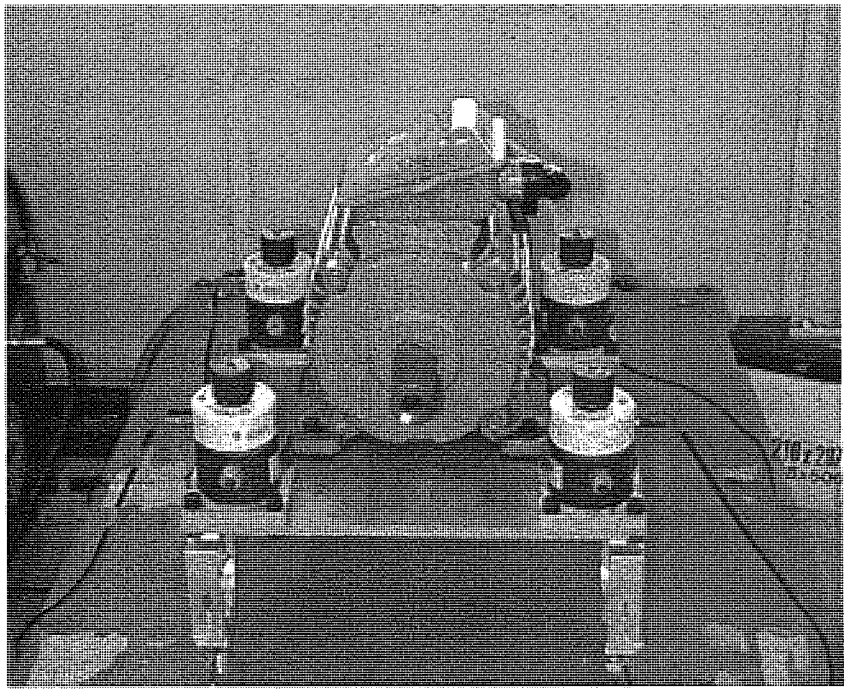

Photo 5.2 Front view of the motor on the plate

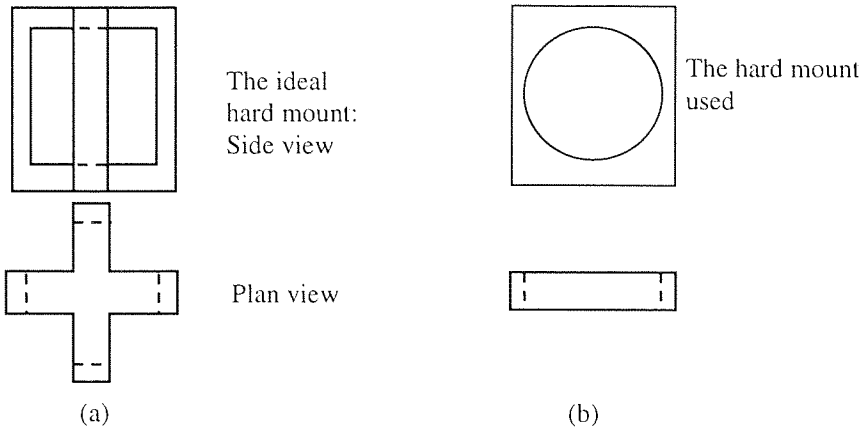

Figure 5.2 Hard mount design

As a compromise between design and manufacturing, a simple ring type load cell design is used for the mount design as shown in Figure 5.2b. Each piece is machined from a block of aluminium. It is relatively rigid in the vertical direction, and flexible in the other. It was tested as a force transducer using strain gauges measuring direct strain at four points at the mid-section of the mount. The gauges are connected for full bridge configuration. With one side bolted down to a rigid base and other side to a shaker via a stinger, the frequency response is shown Figure 5.3.

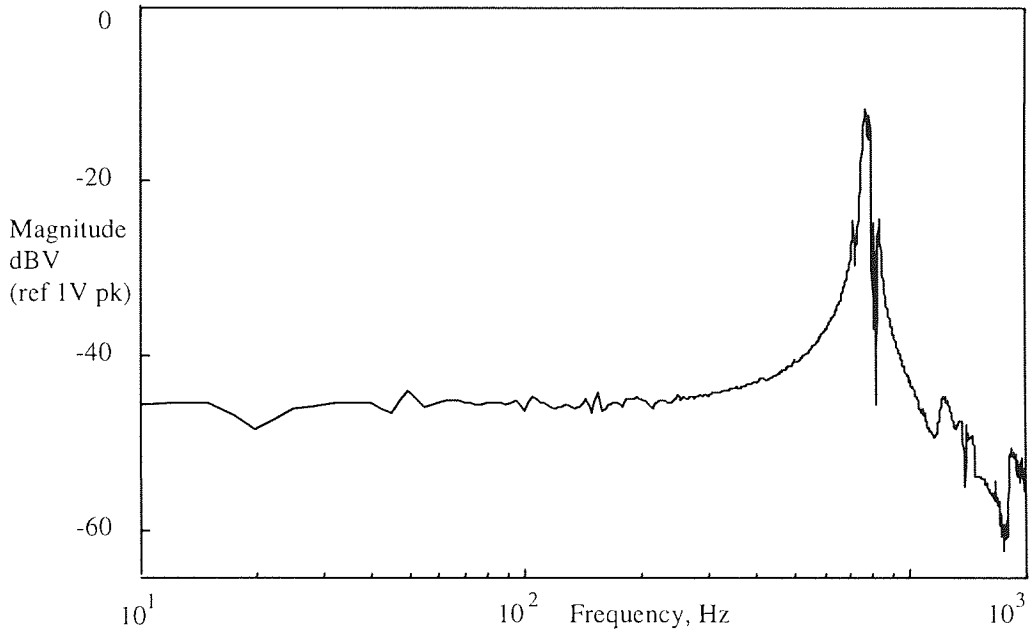

Figure 5.3 Frequency response of rigid mount, measured at its centre

The internal resonant frequency is between 700 and 800 Hz, with a relatively flat response down to 3 Hz. It would be quite appropriate for the system operating at 1440

rpm (24 Hz). However when all four load-cells-cum-mounts were used, the measurements were swamped by noise induced by ground loops. Another configuration using a quartz force ring sensor (PCB 201A02) at the foot of each aluminium mount was adopted. It has a sensitivity of 89 NV^{-1} and a dynamic range up to about 400 N. The bandwidth of this measurement system is higher and the signals are less noisy. Fewer lead wires are needed. These quartz sensors need pre-tensioning to sense both compressive and tensile forces. Such adjustments have to be made during the set-up. They are used in preference to quartz force link sensors, as they are relatively shorter. Link type sensors are factory set with a specified pre-compressive force and hence are easier to set up.

5.3.2 Plant identification

With active force cancellation through the transmission path, the resultant transmitted force is the algebraic sum of the control force and the disturbance. If this sum is small enough, then the transmitted force is reduced. This situation can be represented by Figure 5.4a. The symbol $\mathbf{G}_p$ is used to represent the force transmissibility matrix relating an input force vector at the top of the hard mounts to the vector of forces transmitted to the base structure at the bottom of the mounts. The symbol $\mathbf{G}$ represents the transfer function matrix between the input command vector, $\underline{\boldsymbol{u}}$, to the actuators and the output force vector transmitted into the structure at the same point as the transmitted force from the disturbance. $\mathbf{Q}_f$ is the net transmitted force vector.

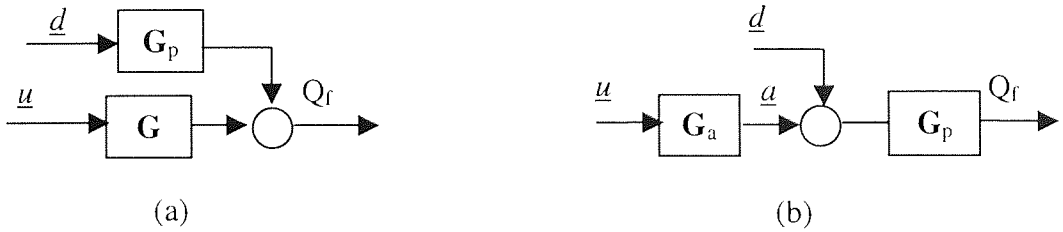

Figure 5.4 Block diagram of the target system.

Each actuator is rigidly attached to the top of a hard-mount. Let the actuators' dynamics relating the command input $\underline{\boldsymbol{u}}$ to an output force, $\underline{\boldsymbol{a}}$, be given by $\mathbf{G}_a$. Assuming that the effect of impedance loading is small, the matrix $\mathbf{G} \approx \mathbf{G}_p \cdot \mathbf{G}_a$. Figure 5.4a can be represented by the block diagram in Figure 5.4b, and adopt the latter as an approximate model of the set-up in Figure 5.1.

From a control system perspective, the desired closed loop objective is to design a controller that will provide the signals to a set of actuators to cancel or reduce the disturbance produced by the machine. Similar to the case presented in §3.8, the desired closed loop system model can be represented by Figure 5.5.

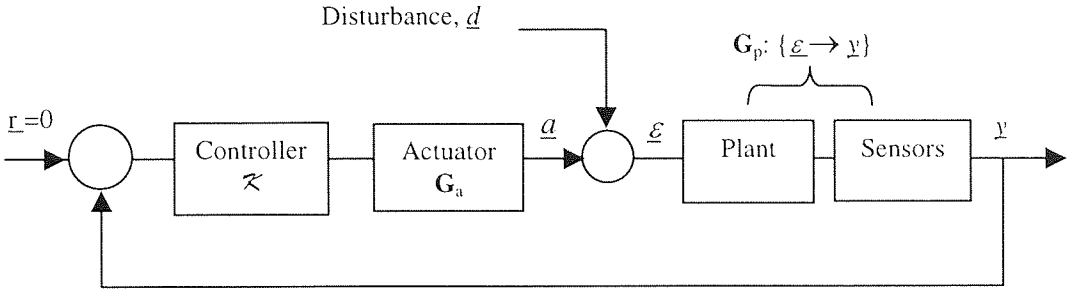

Figure 5.5 A system model for the control of the rig shown in Figure 5.1

The dynamics of the sensors and any effect of noise measurements can be incorporated into $\mathbf{G}_p$. The output disturbance problem then becomes an input disturbance problem. Hence

$$\mathbf{G}_p : \underline{\varepsilon} \rightarrow \underline{y} \tag{5.1}$$

The elements $\mathbf{G}$ and $\mathbf{G}_p$ or $\mathbf{G}_a$ and $\mathbf{G}_p$ in Figure 5.4 will have to be determined and used in Figure 5.5. It is recommended that $\mathbf{G}_a$ and $\mathbf{G}_p$ be chosen because the disturbance matrix $\mathbf{G}_p$ can be determined separately from $\mathbf{G}_a$, which can be based on a transfer function of a typical actuator. This is saves time and effort. In this case only 16 transfer functions for $\mathbf{G}_p$ and 1 for $\mathbf{G}_a$ have to be determined. In anticipation of experimental model identification each transfer function element may need many tests runs to achieve reasonable resolutions and accuracy. However estimating $\mathbf{G}_a$ and $\mathbf{G}_p$ will incur some errors. The $\mathcal{H}_\infty$ controller provides some degree of robustness to errors so long as the disturbance is within the frequency range for which the model is valid.

There are several ways in which the model of the system can be obtained. One way is to analytically derive the system input/output characteristics by physically modelling the structure, the motor, the mountings and the connections. Often this method can result in models with a set of complex partial differential equations that may not necessarily correlate well with the observed response of the physical system. The Finite Element

modelling technique could also be used, especially if modal parameters are of interest. In most cases, the supporting structure of the machine is inevitably coupled to some other super-structure, and these connections are a source of uncertainty (Dejong and Quartaroaro, 1987) in the boundary conditions. Hence experimental measurements or model updating are inevitable. Lastly, the model can be constructed by measuring the input-output relationship of the actual physical system in situ. This approach is adopted because (a) it has been used to determine the force transmissibility of hard-mounted machine using dissimilar base structures and (b) the main interest is in the input-output relationship rather than the modal parameters. Moreover the choice of locations of sensors and actuators for the machine to affect certain modes of the system is limited. Recall that what is needed is information relating to the external rather than the internal behaviour of the system.

The purpose of model identification is to obtain the force transmissibility matrix that can be used as a performance specification for the design of active vibration isolation using the technique of active force cancellation. The choice now is the method of model identification.

5.3.3. The Maximum Likelihood Estimator (MLE)

There are basically two approaches to system identification: time domain and frequency domain techniques. Time domain techniques are based mainly on discrete time equations, which may not be a good approximation of a continuous time system (e.g. a system with mode shapes). As there is no intention to design on-line adaptive algorithms for the real-time control, a time domain technique is not necessary. Since experiments performed for the hard mount case were done in the frequency domain, in the sense that swept-sine testing was performed, it is natural to continue the system identification in the frequency domain. Furthermore, a continuous time system can be Laplace transformed into the s-domain. If the system is stable (in the sense that it has no right half plane poles), its transfer function defined over the s-plane can be determined from the measured frequency response (s=jω). A frequency domain identification technique is selected to determine the system poles and zeros such that the transfer function evaluated at s=jω matches the measured response within certain confidence level.

The basic concept in frequency domain identification is to minimise the error between the measured transfer function and an assumed model structure with unknown parameters i.e.

$$\varepsilon = \sum W(j\omega_k)\left|G_m(j\omega_k) - \frac{N(j\omega_k)}{D(j\omega_k)}\right|^2 \qquad (5.2)$$

There are a variety of least square algorithms or weighted least square methods – (Sanathanan and Koerner, 1963) and (Whithead and Williams, 1988). The curve-fitting algorithm in the Hewlett Packard (HP) Dynamic Signal Analyser uses a combination of frequency dependent weighting function and coherence function (Adcock and Potter, 1985). Such methods are quite useful when additive noise is assumed only at the output measurements.

When sensors are used in the input (to the system) and output measurements, contamination by noise at both channels and cross channels is inevitable. A suitable candidate to handle this is an algorithm developed by Schoukens, Pintelon and Renneboog (1988) that is based on the Maximum Likelihood Estimator (MLE). For the brevity, the algorithm is called the MLE (for linear systems). The measurements are first recorded in the time domain, and Fourier transformed into the frequency domain. The poles and zeros of the transfer functions are then estimated in the frequency domain. Most estimation algorithms require *a priori* noise analysis of the measurement system to obtain the probability distribution function (PDF) of the noise measurements. Also the PDF of the (time domain) noise measurements has to be white and Gaussian. Since the DFT of noise measurement leads to approximately Gaussian frequency domain noise (Schoukens and Renneboog, 1986), the frequency domain MLE is robust with respect to noise PDF (time domain) that is not exactly white and Gaussian (Pintelon and Schoukens, 1990). To improve upon the estimates, a few periods or time records are needed by the MLE algorithm to perform a noise analysis and estimation can be done on the averaged data.

5.3.4. Input signal for excitation

For frequency domain technique where the Discrete Fourier Transformation (DFT) is used, the choice of excitation signals should be restricted to those signals whose DFT

spectra do not suffer from leakage errors. Suitable excitation signals include (a) stepped-sine i.e. using a single frequency at a time, (b) periodic chirp, and (c) multi-sine or harmonic summation of sine waves. Present day Frequency Response Analyser and Spectrum Analyser are quite capable of generating excitation signals of types (a) and (b). The stepped sine is quite time consuming, and FFT algorithm is quite efficient to generate frequency response using the broad band signals of (b) and (c). Both of these allowed us to design a frequency band limited signal of interest.

There is an advantage of using the multi-sine over the periodic chirp. The former can be designed to give a desired band width and amplitude distribution in the frequency domain. The signal is given by:

$$x(t) = \sum_{k=1}^{N} A_k \cos(2\pi f_k t + \phi_k); f_k = \frac{n_k}{T_r} \text{ ; } T_r \text{ is measurement period} \qquad (5.3)$$

An example of the spectra of a multi-sine excitation is shown in Figure 5.6 for comparison with that of the periodic-chirp excitation.

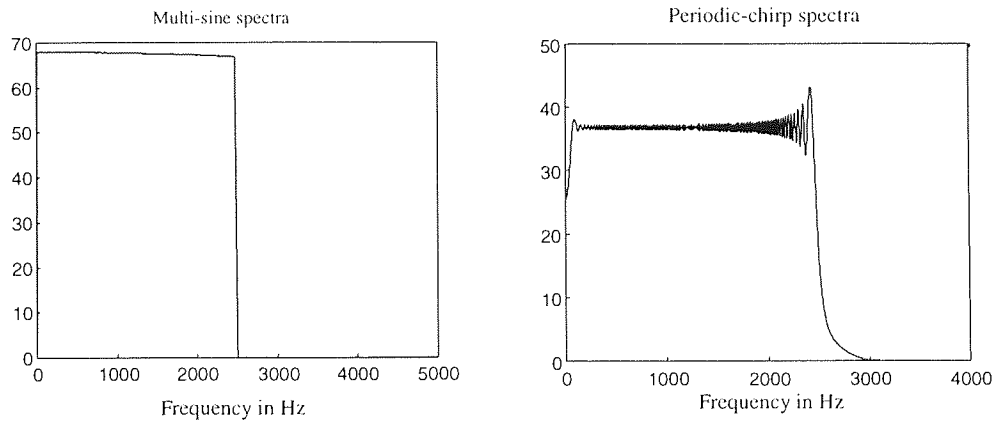

Figure 5.6 Spectrum of the multi-sine and periodic chirp

Although continuous spectra are shown, they actually are discrete in frequency. Each discrete frequency is a harmonic of the fundamental frequency, f_1. The number of harmonics, N, can be selected to give f_{span}=N x f_1. Both signals have a span of 2500 Hz. The multi-sine excitation signal has an almost flat spectrum because the amplitudes distribution has been intentionally designed that way. The design can be done by setting A_k to be the same and using the Schroeder formula (Schroeder, 1970) to calculate the

phase of each component in the signal x(t). The phase affects the shape of a single time record signal of period, T_r, and "limits" the energy injected into the system. If this single time record signal contains integer number of cycles of every periodic component in the excitation, there will be no leakage during conversion from time to frequency domain. This is assured by the formula generating the multi-sine signal and by selecting the Analyser frequency resolution to be equal f_1 divided by an integer.

With multi-sine excitation and the use of MLE for linear systems, the number of harmonics (and hence the frequency resolution) and frequency span needed to define the model accurately can be controlled. Multi-sine signals can easily be generated using an arbitrary waveform generator. The recorded responses can be then analysed with the coded version of the MLE for linear system algorithm (Kollár, 1994).

A choice of f_{span}=50 Hz for the span is made after conducting a series of preliminary tests. Firstly, although the motor disturbance spectrum is much higher than 50 Hz, the order of the system model estimated for the range of this spectrum turns out to be exceedingly high for any single input-output transfer function. As discussed below, even at f_{span}=50 Hz, the model has 154 states. The average order of each transfer function is about 8, and that is after some adjustments in the model obtained. Secondly, from a test on a structure described in the previous chapter, at the rated speed of 1440 rpm or 24 Hz, the measured principle components of the transmitted force are found at 24 Hz and 33 Hz. A span of 50 Hz should be sufficient. This will place the operating frequency at mid-range of the band-limited signal.

The fundamental frequency of the excitation signal used is f_1 = 0.125 Hz and N=400 so that f_{span} = 50 Hz. The machine operating speed of 1440 rpm corresponds to 24 Hz or the 192^{nd} harmonic. The power amplifier of the shaker is adjusted to give a measured excitation signal of about 100 mV (100 N) peak to peak or ±50 N force amplitude at each mount. Hence a constant input for each set of measurements is maintained. The excitation signal amplitude corresponds to about 50% of the average transmitted force when the machine is operating. Each record or period is 8 seconds and a sample of one period of the waveform is shown in Figure 5.7. A total of ten periods of the excitation signal and the corresponding response signals are captured. Sampling of all signals is synchronised to the excitation signal.

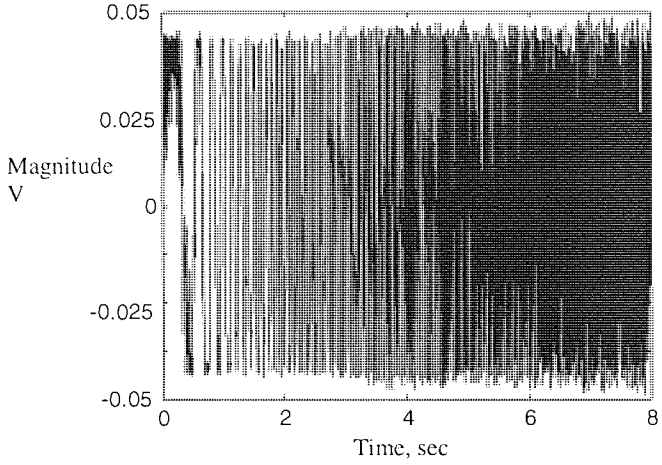

Figure 5.7. One period of the mutli-sine excitation signal

5.3.5 Estimation of the System disturbance transfer function matrix

The system disturbance transfer function matrix, $\mathbf{G}_p$, is the map of input excitation by forces at the feet of the machine to forces measured by the sensors at the bottom of the mount. A multi-sine excitation at each actuator location represents the harmonics of the machine disturbing the system at each foot. Each time measurement at each of the four sensors' locations comprises ten (10) periods of the response. Every measurement period is synchronised with a period of the multi-sine excitation.

A shaker via a stinger to is attached to the top of a mount, j=1, as shown in Figure 5.8 and excitation force is applied. The responses, $g_{ij=1}$, are measured at the bottom of each of the four mounts i=1,2,3, and 4. This is repeated for the other three mount locations j=2,3, and 4. With four inputs and four outputs, a total of sixteen transfer functions, g_{ij}, have to be obtained. The subscripts i and j are used to refer only to the mounting locations and g_{ij} is to be read as response at mount #i due to input at mount #j. Unlike modal analysis, the subscripts i=j here does not mean that excitation and response are at the same point. Hence $g_{ij} \neq g_{ji}$, and the resulting transfer function matrix of responses is not symmetric.

For the actuators, as they are rigidly bolted to the mount, their transfer function matrix is a 4x4 diagonal matrix, $\mathbf{G}_a$. The goal of control is to reduce the disturbance transmitted to the base support using the actuators.

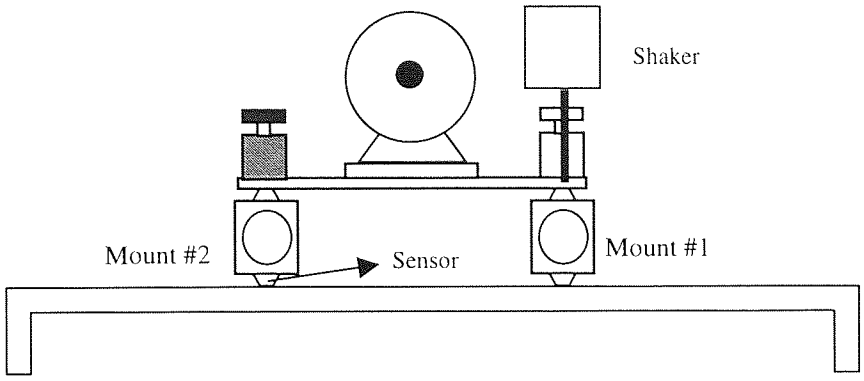

Figure 5.8 System Identification Set-up

There are a few methods of obtaining the system matrix transfer function $\mathbf{G}_p$. For example,

(a) Modal analysis method.

(b) Identifying, for each input j, a SIMO model using the Chebyshev curve fitting method, and then combining the resulting four SIMO models into a single MIMO system transfer function matrix.

(c) Identifying each g_{ij} and then combining them into a single 4x4 transfer function matrix.

A modal analysis using global or multi-curve fitting method could be used on the four columns of $\mathbf{G}_p(j\omega)$. Such an approach takes into account of the fact that the properties of the individual $g_{ij}(j\omega)$ are related. They are after all representing the system as seen from different locations. There is a difference however in the case presented here from that of a typical modal analysis method. The latter automatically assumes symmetry in the system matrix since it is typical to excite and measure at least at one common point, but as mentioned earlier, there is no symmetry in the resulting transfer function matrix. For this reason, the global curve fitting is applied to all four columns instead of any single column or row. The results of a typical column (input at mount #2) frequency response using the Imperial College Analysis, Testing and Software, (ICATS) are shown in Figure 5.9a and Figure 5.9b.

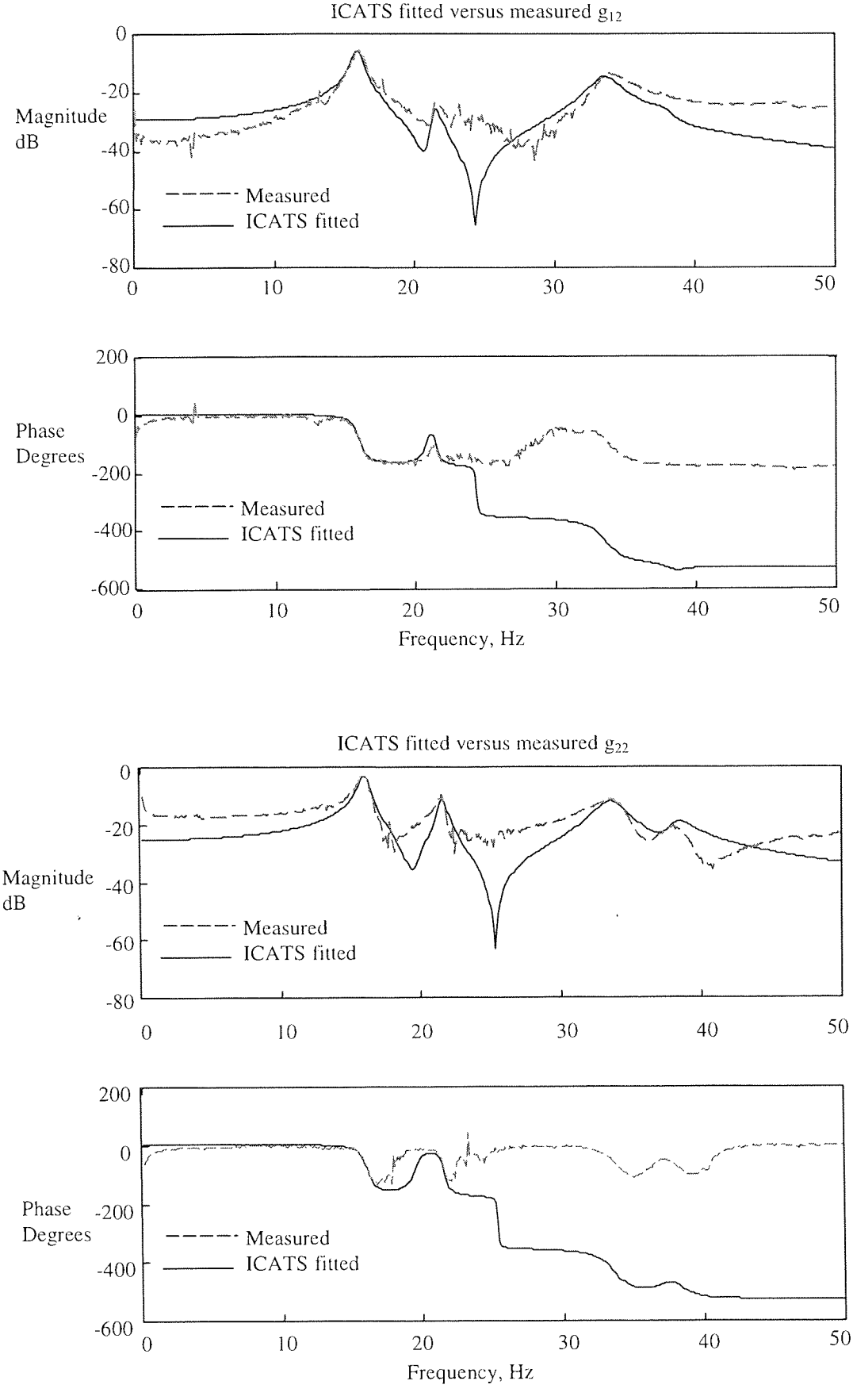

Figure 5.9a Bode plots of ICATS fitted curves with measured g_{i2} curves

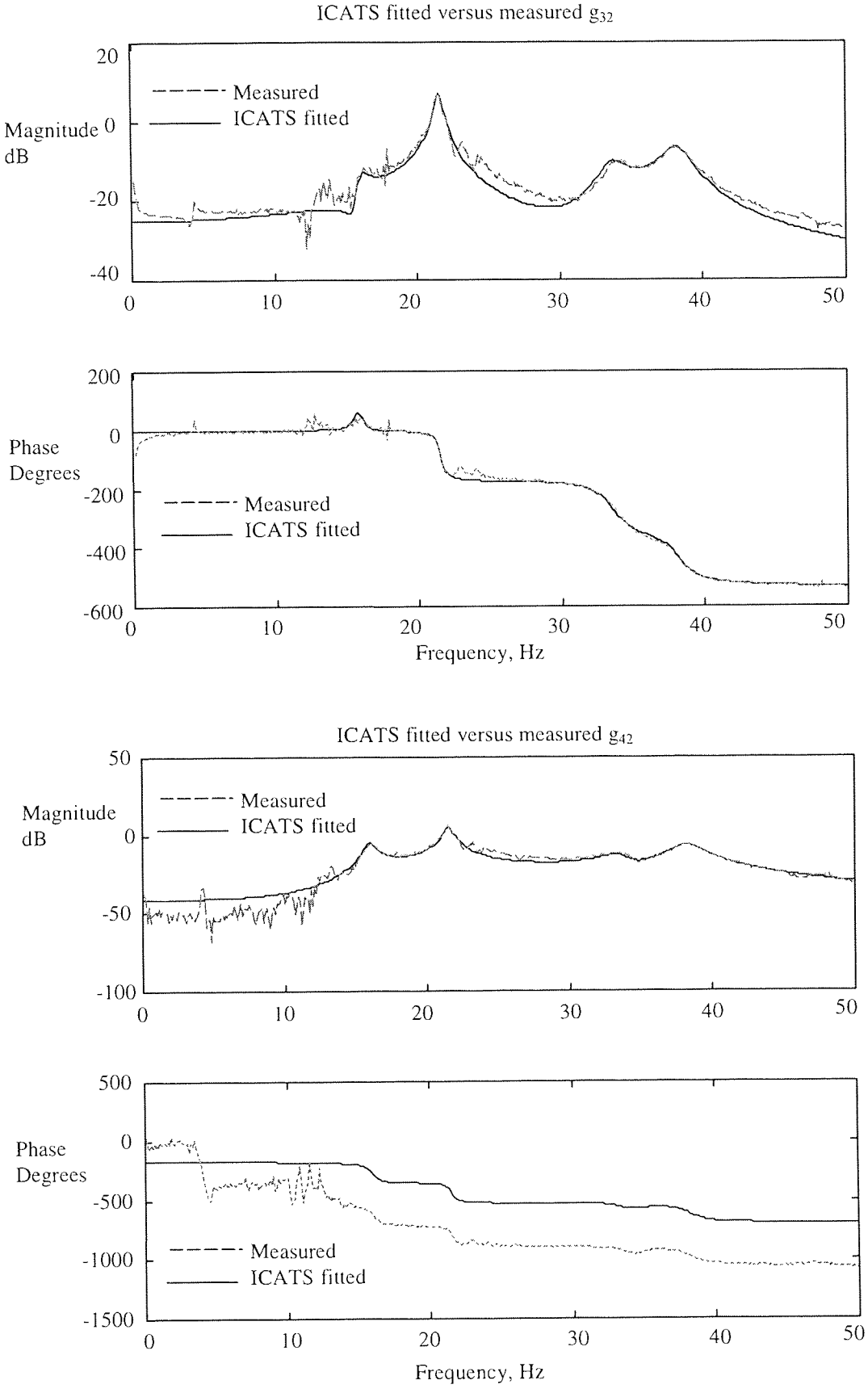

Figure 5.9b Bode plots of ICATS fitted curves with measured g_{i2} curves

There are four sets of natural frequencies from analysis of each of the column. Taking the greatest common factor gives the set of (averaged) natural frequencies as:

[12.9, 15.9, 21.5, 21.6, 24.3, 33.8, 38, 46.7] Hz

The curve fitting of responses at mount location #1 and mount location #2 (Figure 5.9a) are typically not as good as that for mount #3 and mount #4 (Figure 5.9b). This is also the case for all the other inputs j=1,3 and 4. It is likely that mount locations #1 and #2 are not ideal for identifying the modal parameters of the system. If this were to be the objective, then the sensors at such locations have to be relocated. However the primary interest here is to identify the transfer functions of the response matrix for the force transmitted from machine to a fixed mounting locations.

The Chebyshev polynomial curve fitting method (Balas and Doyle, 1989) can be extended on each column of the desired $\mathbf{G}_p$ to obtain four SIMO models. It is based on the Chebyshev polynomial curve-fitting algorithm of Adcock and Potter (1985) for SISO systems and is available on some signal analysers. One problem with this is that the method does not guarantee that a stable transfer function will be fit to the raw data. Like the method adopted below, putting four SIMO model together to form the MIMO model will result in an excess number of states or poles, and model reduction is needed.

Instead of a two-step approach of finding SIMO models and then an MIMO model, each g_{ij} can be identified as a SISO model and then assembled into a MIMO model. This is also necessary because the responses of the mounts due to an excitation are not measured simultaneously but sequentially. With either approach, due to measurement errors, a system pole may take different values in some of the SISO (or SIMO) models and in combining them, it may result in more poles than there really are. Hence model reduction is needed get the right number of poles that represent the physical system.

Each transfer function, g_{ij}, is estimated using the input excitation and the MLE for Linear Systems approach discussed previously. The algorithm (Kollár, 1994) typically results in high order numerator and denominator polynomial (and sometimes additional poles and zeros are intentionally added to achieve a good fit). Some adjustments can be done to get suitable order for g_{ij} that matches the measured data. These are as follows:

i. As g_{ij} represents the dynamic force transmissibility for input j to output i, matching pair of poles and zeros at the origin are removed.

ii. For any given amount of data corruption, it is easier to make accurate estimates of poles and zeros closer to the imaginary axis. Hence cluster of poles and zeros far away from the imaginary axis can be dropped as long the gain constant of the transfer function is appropriately adjusted.

iii. Similarly for pairs of pole and zero very close to each other, it is hard to resolve their effects on the system. They too can be eliminated so long as a good fit is obtained. It does not matter even if they are on the right half plane.

The results of the estimation and fitting exercise are shown in Appendix C. The estimated transfer functions are given by solid lines whilst the measured ones are in dashed lines. The plots are in general reasonably good with a couple of exceptions. For example, the first estimated plot for the transfer function g_{23}, is shown in Figure 5.10. The transfer function needs term of order s^{16}. The equation is given as

$$g_{23}(s) = \frac{s^{16} + 5.9s^{15} + 1.1e5s^{14} - 6.5e6s^{13} - 1.8e10s^{12} - \ldots + 1.4e32s^{2} - 2.4e32\,s - 1.0e35}{s^{16} + 59.37s^{15} + 3.2e5s^{14} + 1.6e7s^{13} + 3.9e10s^{12} + \ldots + 3.1e31s^{2} + 7.1e31s + 1.8e34}$$

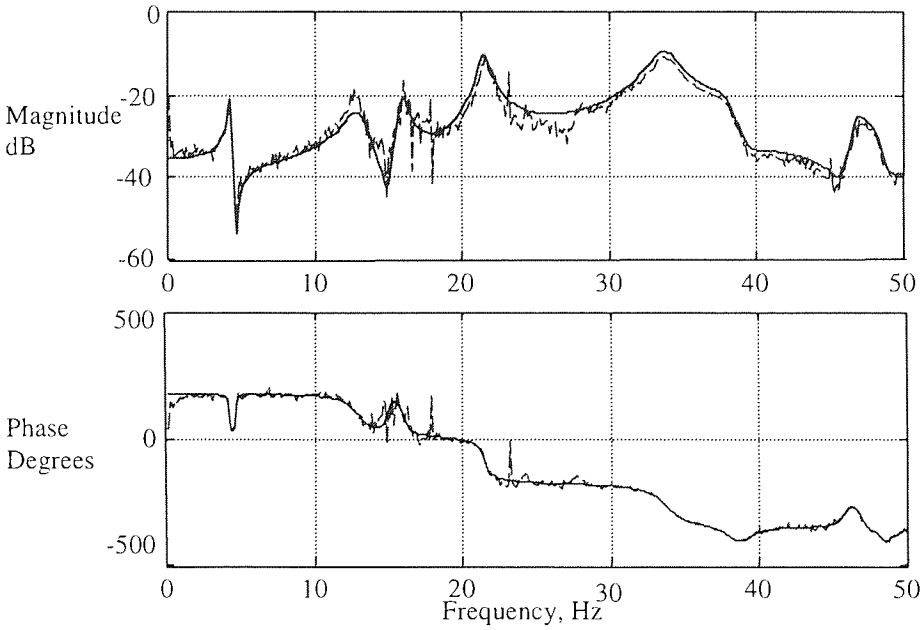

Figure 5.10 Bode plot of element g_{23} before reduction to lower order

This Bode plot shows that relatively good fit is possible. To keep the order of the model small, complex poles and zeros that are closed to each other have been removed, and it is fitted up to about 40 Hz instead of 50 Hz. The highest order of g_{23} is s^{10} in both numerator and denominator, and this reduced plot is shown in Appendix C.

From modal analysis, the system should not have more than 8~9 modes. When the transfer functions are combined into a MIMO model, due to measurement errors, there will be more than 8 or 9 system poles. An ad-hoc approach of identifying a set of common poles and the greatest common denominator for $[g_{ij}]$ has been done. The number of such poles and frequencies match those obtained from ICATS reasonable well. Instead of this ad-hoc approach of trying to get a Smith-McMillan form, a state-space model reduction method is preferred and is more efficient.

5.3.6. Conversion to State-space model {**A**,**B**,**C**,**D**}

A typical estimated transfer function, g_{ij}, is given by a set of zeros and poles and the corresponding expanded numerator and denominator polynomials. The average order of the polynomial is about eight and coefficients of these polynomials are very small but the variation in the polynomial coefficients is very large. As the roots of the polynomials are sensitive to the coefficients, any the perturbations in these coefficients will affect different roots differently. Hence representing g_{ij} as a transfer function will give rise to an ill-conditioned state space model representation with a condition number for **A** matrix, $\kappa(\mathbf{A})=10^{34}$. Analysis and design using such ill-conditioned matrix can be problematic.

Each g_{ij} is subsequently represented as a zero-pole (roots of the polynomials) model and $[g_{ij}]$ is converted to {**A**,**B**,**C**,**D**} using zero-pole to state space representation resulting in a condition number $\kappa(\mathbf{A})=53$. The dimension of **A** is 154x154, and **D** has full rank of four. This model is labelled as $\mathbf{G}_{154}$, and has very large number of excess states. It does not represent the physical system that has at about 8 to 9 modes according to ICATS analysis.

5.4 Model Reduction

There are a variety of ways to reduce the model and two principal routes can be identified (a) using modal analysis and model updating and (b) using state space model reduction

method. A brief discussion on the differences between these two approaches can be found in (Mottershead and Friswell, 1993). If the ICATS modal model were to be used, then modal truncation can be applied to reduce the number of modes. Since identifying structural parameters is not the principal objective, the modal model is not used. The state space method adopted here eventually gives a better fit with measured responses. The $\mathbf{G}_{154}$ state space model is transformed into a balanced realisation and Hankel singular values are used to determine the most important states affecting input-output responses.

The motivation in state space domain is very simple. Any system $\mathbf{G}=\{\mathbf{A},\mathbf{B},\mathbf{C},\mathbf{D}\}$ with state vector $\mathbf{x}$ can be transformed by $\underline{\mathbf{x}} = \mathbf{T}\cdot\mathbf{x}$ to give a Kalman Canonical Decomposition of the form given in (5.4):

$$\begin{bmatrix} \dot{\underline{x}}_{co} \\ \dot{\underline{x}}_{c\bar{o}} \\ \dot{\underline{x}}_{\bar{c}o} \\ \dot{\underline{x}}_{\bar{c}\bar{o}} \end{bmatrix} = \begin{bmatrix} \underline{\mathbf{A}}_{co} & 0 & \underline{\mathbf{A}}_{13} & 0 \\ \underline{\mathbf{A}}_{21} & \underline{\mathbf{A}}_{c\bar{o}} & \underline{\mathbf{A}}_{23} & \underline{\mathbf{A}}_{24} \\ 0 & 0 & \underline{\mathbf{A}}_{\bar{c}o} & 0 \\ 0 & 0 & 0 & \underline{\mathbf{A}}_{\bar{c}\bar{o}} \end{bmatrix} \begin{bmatrix} \underline{x}_{co} \\ \underline{x}_{c\bar{o}} \\ \underline{x}_{\bar{c}o} \\ \underline{x}_{\bar{c}\bar{o}} \end{bmatrix} + \begin{bmatrix} \underline{\mathbf{B}}_{co} \\ \underline{\mathbf{B}}_{c\bar{o}} \\ 0 \\ 0 \end{bmatrix} \underline{\mathbf{u}} \tag{5.4}$$

$$\underline{\mathbf{y}} = \begin{bmatrix} \underline{\mathbf{C}}_{co} & 0 & \underline{\mathbf{C}}_{\bar{c}o} & 0 \end{bmatrix} \begin{bmatrix} \underline{\mathbf{x}}_{co} \\ \underline{\mathbf{x}}_{c\bar{o}} \\ \underline{\mathbf{x}}_{\bar{c}o} \\ \underline{\mathbf{x}}_{\bar{c}\bar{o}} \end{bmatrix} + \mathbf{D}\underline{\mathbf{u}}$$

The vector $\underline{\mathbf{x}}_{co}$ is controllable and observable, $\underline{\mathbf{x}}_{c\bar{o}}$ is controllable but not observable, $\underline{\mathbf{x}}_{\bar{c}o}$ is observable but not controllable, and $\underline{\mathbf{x}}_{\bar{c}\bar{o}}$ is uncontrollable and unobservable. In terms of input-output behaviour, the original system $\{\mathbf{A},\mathbf{B},\mathbf{C},\mathbf{D}\}$ and the reduced order system given by $\{\underline{\mathbf{A}}_{co},\underline{\mathbf{B}}_{co},\underline{\mathbf{C}}_{co},\mathbf{D}_p\}$ are the same although their internal behaviour are not. Hence if the system can be partitioned into the above form, a reduced model that is both controllable and observable can be obtained and which is similar in response to the transfer function matrix $\mathbf{G}$. The dimension of $\underline{\mathbf{x}}_{co}$ is the minimal realisation order of the system. In practice it is neither computationally efficient nor useful to transform into the Kalman Canonical Decomposition form and determine the vector $\underline{\mathbf{x}}_{co}$ and the associated matrices. Due to computation errors, states which are weakly controllable or observable may end up otherwise.

The practical goal is to find a low approximation $\mathbf{G}$ of $\underline{\mathbf{G}}$ such that

$$\| \underline{\mathbf{G}} - \mathbf{G} \|_\infty \text{ is small} \tag{5.5}$$

In principle, there are three ways to reduce the model of the system or the controller: truncation, residualisation and Hankel norm approximation. When the state-space model is transformed to the Jordan form, truncation basically means removing the higher frequency modes. An appropriate alternative is to transform to balanced realisation (Moore 1981) instead of using the Jordan form.

Any $\mathbf{G} = \{\mathbf{A},\mathbf{B},\mathbf{C},\mathbf{D}\}$ which has a minimal realisation can be transformed by $\mathbf{x}_b = \mathbf{T}\cdot\mathbf{x}$, ($\mathbf{T}$ non-singular) to give a $\mathbf{G}_b=\{\mathbf{A}_b,\mathbf{B}_b,\mathbf{C}_b,\mathbf{D}_b\}$ representation such that the controllability Grammian, $\mathbf{P}_b = \mathbf{Q}_b$, the observability Grammian = Σ, where

$$\Sigma = \text{diagonal } (\sigma_1\mathbf{I}_{s1}, \sigma_2\mathbf{I}_{s2},\ldots \sigma_n\mathbf{I}_{sn}) \tag{5.6}$$

and $\sigma_1 \geq \sigma_2 \geq \ldots, \geq \sigma_n$. The $\mathbf{I}_{si}$ are identity matrices of appropriate dimension and the decreasingly ordered σ_i are called the Hankel singular values of the system defined by

$$\sigma_i = \sqrt{\lambda_i(\mathbf{P}_b \cdot \mathbf{Q}_b)}\ , \ i = 1,2,\ldots, n \tag{5.7}$$

The respective Grammians of $\mathbf{G}$ satisfy the following Lyapunov equations:

$$\mathbf{A}\cdot\mathbf{P} + \mathbf{P}\cdot\mathbf{A}^T + \mathbf{B}\cdot\mathbf{B}^T = \mathbf{0} \text{ and } \mathbf{A}^T\cdot\mathbf{Q}+\mathbf{Q}\cdot\mathbf{A} + \mathbf{C}^T\cdot\mathbf{C} = \mathbf{0} \tag{5.8}$$

and

$$\mathbf{P}_b=\mathbf{T}\cdot\mathbf{P}\cdot\mathbf{T}^* \text{ and } \mathbf{Q}_b=(\mathbf{T}^{-1})^*\cdot\mathbf{Q}\cdot\mathbf{T}^{-1}$$

If $\mathbf{G}$ is not of minimal realisation, it is still possible to find a $\mathbf{T}$ such that

$$\mathbf{P}_b \cdot \mathbf{Q}_b = \begin{bmatrix} \Sigma^2 & \mathbf{0} \\ \mathbf{0} & \mathbf{0} \end{bmatrix} \tag{5.9}$$

Such a representation $\mathbf{G}_b=\{\mathbf{A}_b,\mathbf{B}_b,\mathbf{C}_b,\mathbf{D}_b\}$ is called a balanced realisation of $\mathbf{G}$. After the process of balancing, each state x_i is just as controllable as it is observable. The measure of a state's joint controllability and observability is given by its associated Hankel singular value σ_i i.e. with balanced realisation, the size of σ_i is a relative measure of the contribution that x_i makes to the input-output behaviour of the system. Hence the objective of model reduction can now be rephrased as finding a model, $\mathbf{G}_p$, with fewer states such that input-output behaviour is almost similar to $\mathbf{G}$ by removing those states that contribute little to the input-output behaviour of the system. This can be done using the equivalent balanced realisation system $\mathbf{G}_b$.

Let $\{\mathbf{A}_b,\mathbf{B}_b,\mathbf{C}_b,\mathbf{D}_b\}$ and the corresponding Σ be partitioned compatibly as

$$\mathbf{A}_b=\begin{bmatrix}\mathbf{A}_{11} & \mathbf{A}_{12}\\ \mathbf{A}_{21} & \mathbf{A}_{22}\end{bmatrix},\quad \mathbf{B}_b=\begin{bmatrix}\mathbf{B}_1\\ \mathbf{B}_2\end{bmatrix},\quad \mathbf{C}_b=[\mathbf{C}_1 \quad \mathbf{C}_2];\ \mathbf{x}_b=\begin{bmatrix}\mathbf{x}_1\\ \mathbf{x}_2\end{bmatrix} \tag{5.10}$$

$$\Sigma=\begin{bmatrix}\Sigma_1 & 0\\ 0 & \Sigma_2\end{bmatrix}$$

Where

$$\Sigma_1=\text{diagonal}((\sigma_1,\sigma_2,\ldots\sigma_k) \text{ and } \Sigma_2=\text{diagonal}(\sigma_{k+1},\sigma_{k+2},\ldots\sigma_n)$$

In balanced truncation (Moore, 1981), k is determined by selecting those Hankel singular values σ_i which are small. The reduced model is then obtained by removing the least observable and controllable state $\mathbf{x}_2$ associated with Σ_2. This leaves $\mathbf{D}$ matrix unchanged. Since $\mathbf{G}(\infty)=\mathbf{G}_b(\infty)=\mathbf{D}$, the reduced order system matches the original system at infinite frequency.

In balanced residualisation (Fernando & Nicholson, 1982), the same principle is used to select k. However, instead of removing the state $\mathbf{x}_2$, set $\dot{\mathbf{x}}_2=0$ and solve for $\mathbf{x}_2$ in terms of $\mathbf{x}_1$ and $\mathbf{u}$ and back substitute into the original equation. If $\mathbf{A}_{22}$ is non-singular, then

$$\dot{\mathbf{x}}_2 = 0 \Rightarrow \mathbf{x}_2 = -\mathbf{A}_{22}^{-1}[\mathbf{A}_{21}\mathbf{x}_1 - \mathbf{B}_2\mathbf{u}]$$

$$\dot{\mathbf{x}}_1 = [\mathbf{A}_{11} - \mathbf{A}_{12}\mathbf{A}_{22}^{-1}\mathbf{A}_{21}]\mathbf{x}_1 + [\mathbf{B}_1 - \mathbf{A}_{12}\mathbf{A}_{22}^{-1}\mathbf{B}_2]\mathbf{u}$$

$$\mathbf{y} = [\mathbf{C}_1 - \mathbf{C}_2\mathbf{A}_{22}^{-1}\mathbf{A}_{21}]\mathbf{x}_1 + [\mathbf{D} - \mathbf{C}_2\mathbf{A}_{22}^{-1}\mathbf{B}_2]\mathbf{u} \qquad (5.11)$$

By setting $\dot{\mathbf{x}}_2 = 0$, the process of balanced residualisation retains the same steady state gain of the original system, since $\dot{\mathbf{x}}_1 = 0$ and $\dot{\mathbf{x}}_2 = 0$ in the steady state. Liu and Anderson (1989) showed that the balanced truncation and residualisation have the same error bound that is given by:

$$\| \mathbf{G} - \mathbf{G}_p \|_\infty \leq 2(\sigma_{k+1} + \sigma_{k+2} + \ldots + \sigma_n) \qquad (5.12)$$

Balanced residualisation is selected here because the behaviour of the system at infinite frequency using a band limited excitation signal is not known. It is more meaningful to try to retain the model accuracy at low frequency. Once the model is expressed as a balanced realisation, a bar chart of its Hankel singular values in descending order can be plotted. The plot of the balanced realisation equivalent of $\mathbf{G}_{154}$ is shown in Figure 5.11.

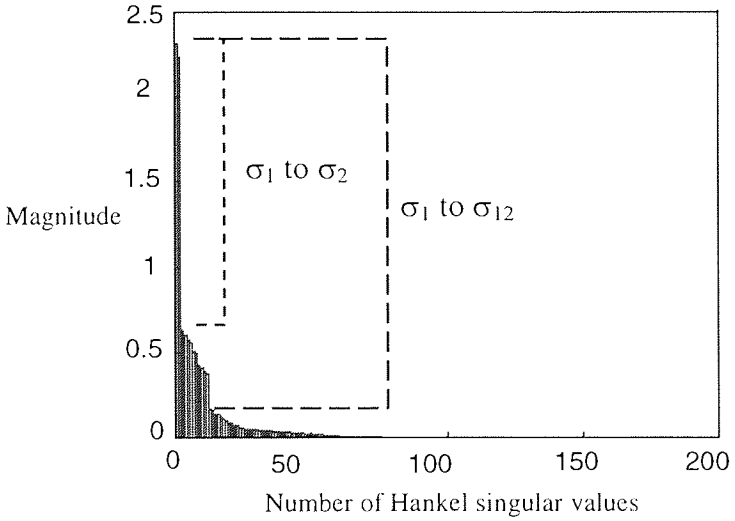

Figure 5.11 Bar graph of the Hankel singular values in descending order

By examining the bar chart, one can choose k= 2 since the 1st and the 2nd Hankel singular values are much larger than the others are. One can also choose k=8 or k=12 where there is a drastic change in the values of σ_i. The selection of k can be based on the residual errors given by (5.12), by comparing the maximum singular values of the resulting

reduced model with that of $\mathbf{G}_{154}$ and also with the sum of magnitudes of the 16 measured frequency responses, and comparing the frequency response with g_{ij}.

Matching $\overline{\sigma}(\mathbf{G}_{12})$ with (magnitude scaled) cumulative magnitude plot of the measured FRF and $\overline{\sigma}(\mathbf{G}_{154})$ is a useful indicator for selecting k. These are shown in Figure 5.12.

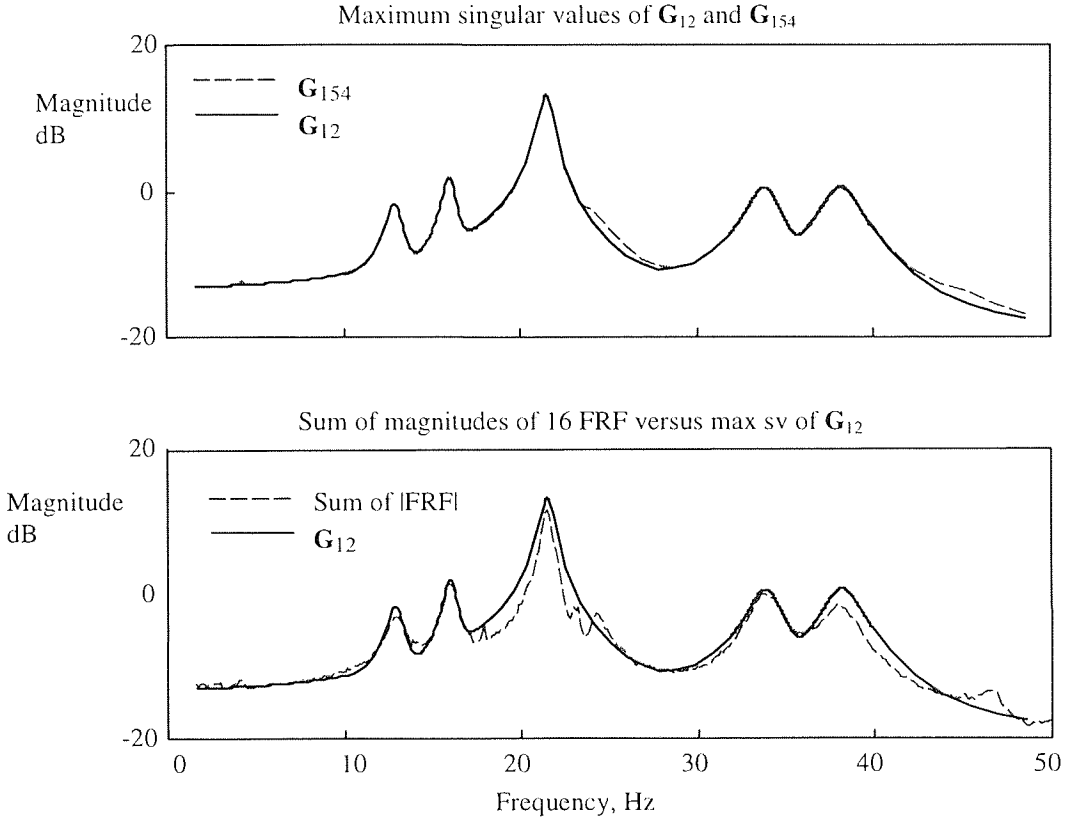

Figure 5.12 Plots of $\overline{\sigma}(\mathbf{G}_{12})$, $\overline{\sigma}(\mathbf{G}_{154})$ and (factor· $\sum_{i,j=1}^{4}\left|\text{measured } g_{ij}\right|$)

With k=2, $\overline{\sigma}(\mathbf{G}_2)$ matches only one peak of $\overline{\sigma}(\mathbf{G}_{154})$ at 21.5 Hz. With k=12, as seen in Figure 5.12, $\overline{\sigma}(\mathbf{G}_{12})$ matches most of the peaks of the measured Σ|FRF| and $\overline{\sigma}(\mathbf{G}_{154})$ well. The higher mode at about 46.5 Hz is missing in $\mathbf{G}_{154}$, although it is found as a relatively (to other modes) small peak in the cumulative amplitude plot of the measured FRF. Hence it would also be absent in $\mathbf{G}_{12}$ model.

The frequency response of the state space model $\mathbf{G}_{12}$ is also compared with each of the measured frequency response functions (FRF). Figure 5.13 to Figure 5.16 show the magnitude plots of g_{ij} of $\mathbf{G}_{12}$ and the measured g_{ij}. The complete set of Bode plots is given in Appendix C.

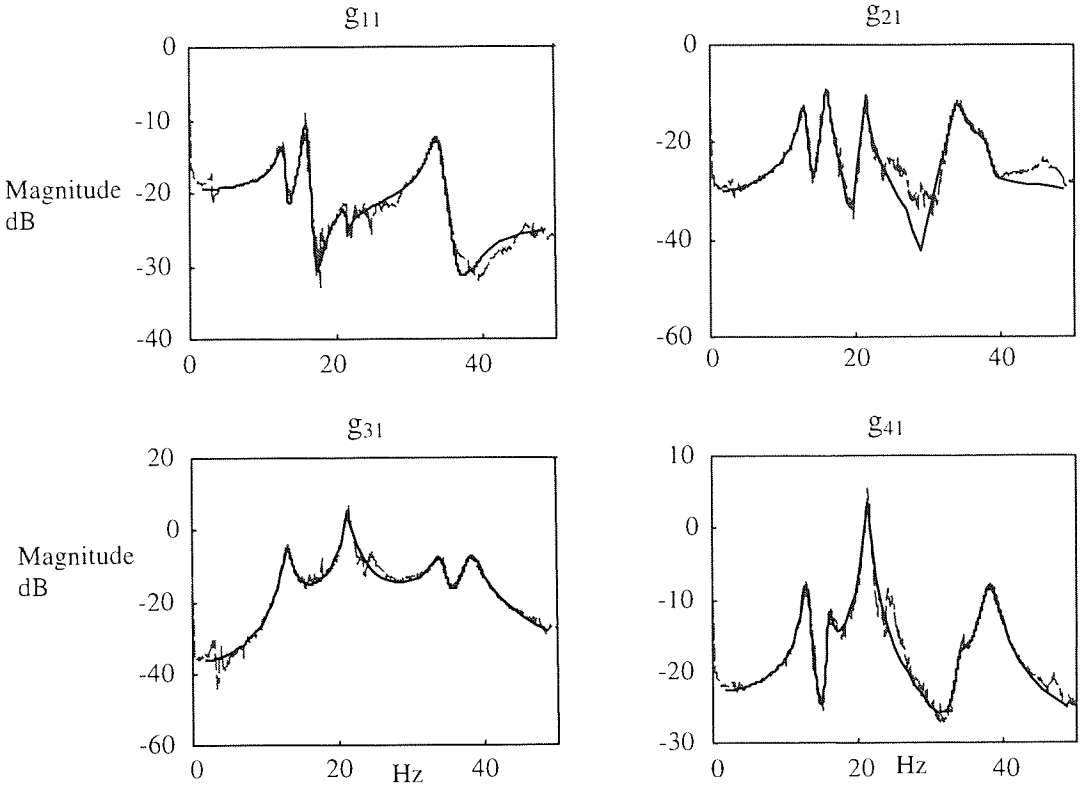

Figure 5.13 Magnitude plots of measured g_{i1} (---) and g_{i1} of $\mathbf{G}_{12}$ (—).

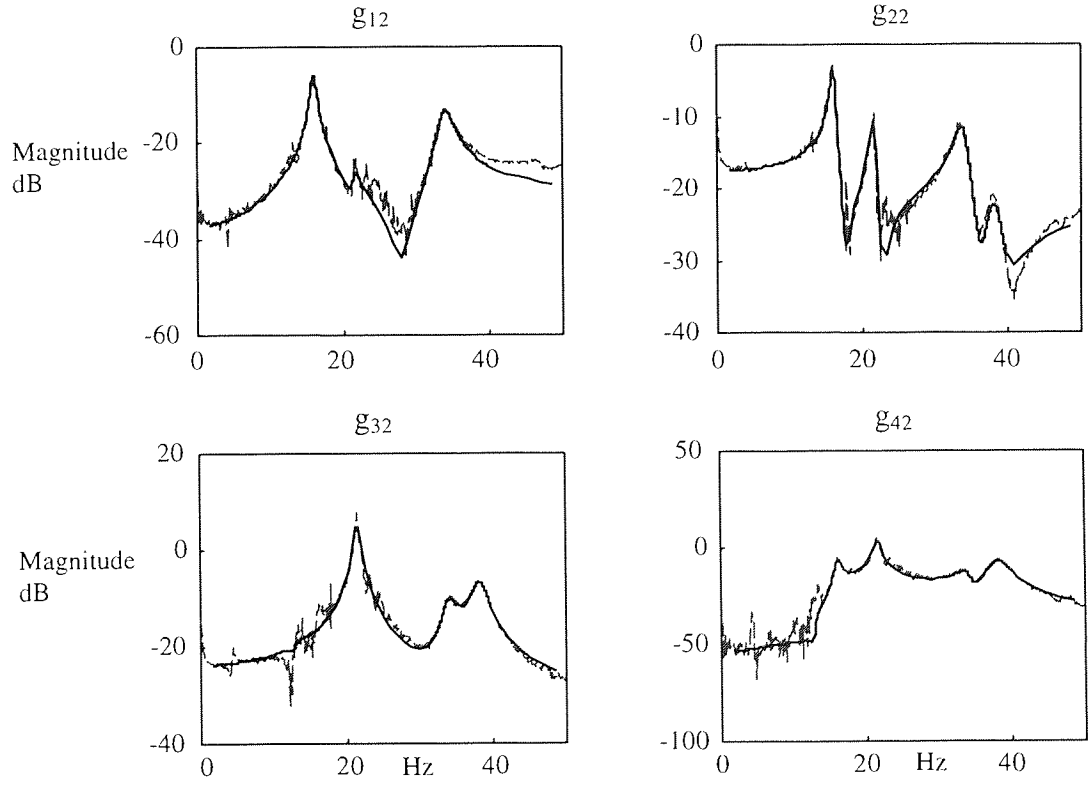

Figure 5.14 Magnitude plots of measured g_{i2} (---) and g_{i2} of $\mathbf{G}_{12}$ (—).

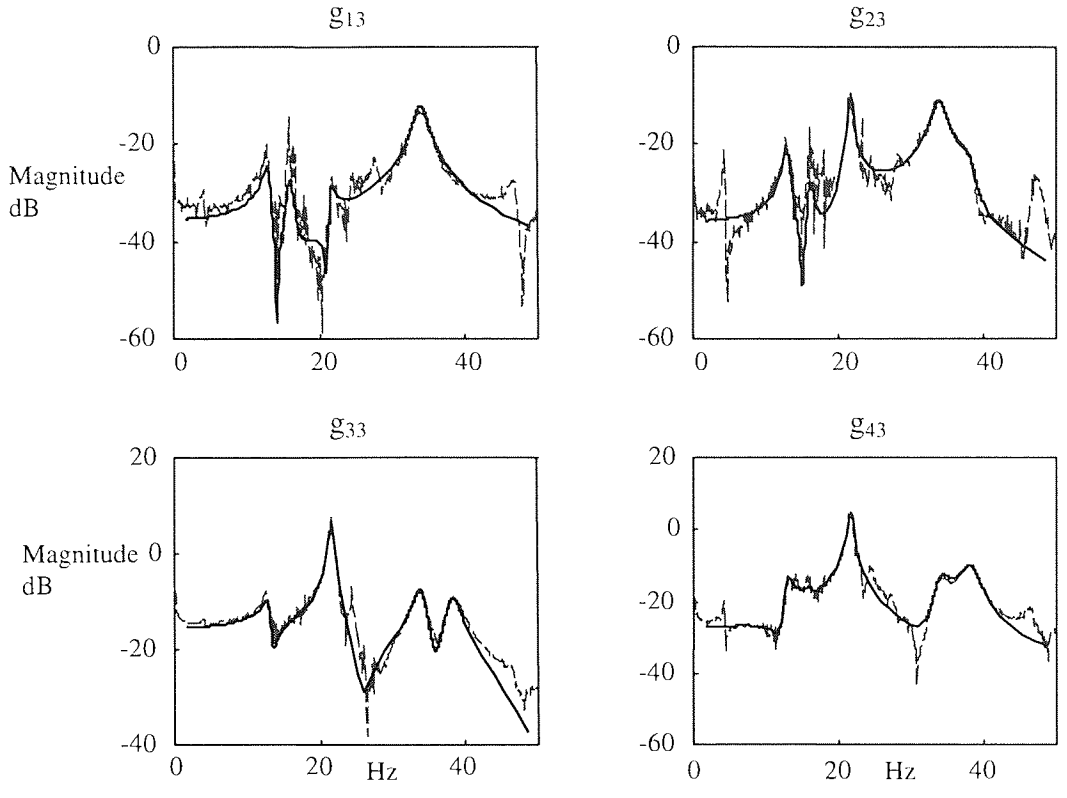

Figure 5.15 Magnitude plots of measured g_{i3} (---) and g_{i3} of $\mathbf{G}_{12}$ (—).

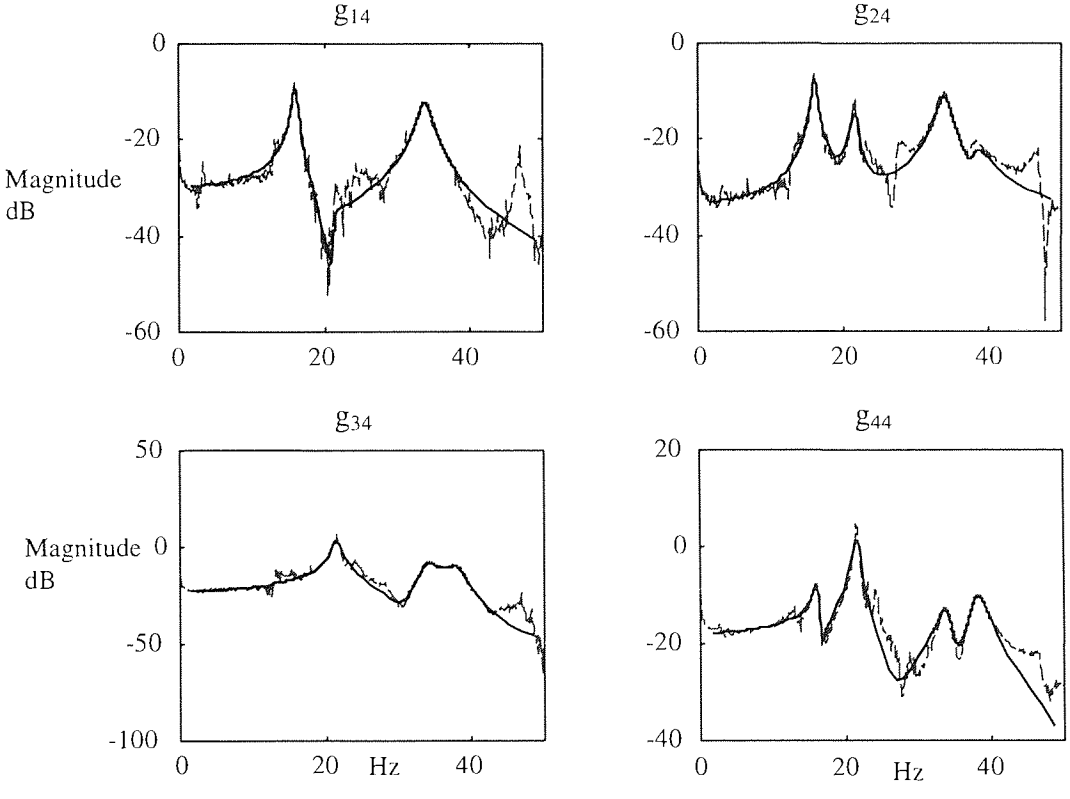

Figure 5.16 Magnitude plots of measured g_{i4} (---) and g_{i4} of $\mathbf{G}_{12}$ (—).

The mode corresponding to the 46.5 Hz, prominent amongst measured g_{i4} and g_{i3}, i=1,2, plots is not given by the corresponding g_{i4} and g_{i3} of $\mathbf{G}_{12}$. A reason for this poor fit is that in an attempt to reduce the order of the estimated transfer functions for g_{24}, g_{44}, g_{31}, g_{23} in $\mathbf{G}_{154}$ the pole at about 46 Hz was neglected. Hence it is unlikely that $\mathbf{G}_{12}$ would have it in those g_{ij}. The model from ICATS also fails to show this peak in all the g_{i4}, but fitted it for g_{i3}, i=1,2. As the primary excitations of the motor is at 24 Hz and 32 Hz (Chapter 4), the error at this frequency is tolerable. One can conclude that the fit is quite acceptable up till 40 Hz.

The resulting system matrices {**A**,**B**,**C**,**D**} for $\mathbf{G}_{12}$ is given by:

A =

-2.67	**-135.03**	-1.50	0.23	-2.16	-0.19	2.13	1.39	0.09	-3.18	0.39	0.71
134.97	**-2.16**	-0.66	0.52	-2.14	-0.08	1.71	1.01	0.08	-3.02	-0.02	0.48
1.22	-0.97	**-3.94**	**93.95**	-28.35	2.07	5.11	38.14	-4.31	-8.19	-3.58	-0.79
0.58	-0.96	**-94.01**	**-1.45**	1.31	39.04	-17.40	-0.42	-1.54	-0.10	-2.05	-0.27
-0.24	0.66	28.64	0.70	**-7.25**	**204.94**	91.50	-24.63	6.16	-33.81	7.22	-11.54
-0.26	-0.38	-7.49	-39.64	**-203.69**	**-4.01**	-3.72	77.07	-15.14	-7.07	-12.38	1.84
-1.02	-0.22	-0.53	16.91	-91.87	1.84	**-4.93**	**-201.53**	-15.15	9.96	-11.21	-0.09
-0.92	-0.15	-38.41	-4.67	24.92	-76.37	**203.16**	**-6.82**	5.01	-11.17	4.40	-9.64
0.12	0.16	5.06	2.39	-2.19	14.89	14.47	-1.42	**-1.32**	**107.29**	-8.44	17.89
0.64	1.23	8.66	2.00	33.18	12.82	-1.95	13.94	**-108.05**	**-6.27**	67.79	24.93
-1.04	1.20	4.92	3.06	-2.67	12.10	9.85	-0.74	6.02	-68.63	**-1.92**	**87.59**
-0.55	0.66	1.86	1.05	12.03	2.04	3.48	8.44	-17.70	-28.53	**-87.56**	**-1.82**

B =

1.44	1.83	2.05	1.66
-1.84	-1.64	-1.34	-1.34
-1.06	-1.57	0.33	1.12
-0.66	-0.96	0.10	0.61
-1.54	1.72	1.31	-1.10
-1.40	-0.58	1.32	0.65
-1.00	1.54	0.76	-1.01
-0.63	-1.49	1.11	1.71
0.89	-0.16	-0.23	-0.51
1.80	-0.09	-1.39	0.15
0.96	0.59	-0.34	0.31
1.06	-0.06	-0.41	0.26

C =

0.00	0.06	-1.16	0.73	-0.88	-0.17	0.98	0.67	0.11	-0.27	0.15	-0.32
0.31	0.41	-1.38	0.97	-0.82	-0.37	1.10	1.01	0.18	-0.22	0.31	-0.48
2.70	2.40	0.08	-0.03	2.53	-1.16	-1.67	0.67	-0.73	2.17	-0.87	0.31
2.23	1.93	1.31	-0.50	-0.65	1.72	-0.12	-2.20	0.74	0.59	0.78	-0.96

D =

0.07	-0.02	0.00	-0.01
-0.02	0.08	0.00	0.01
0.00	-0.01	0.06	0.01
-0.01	0.00	0.02	0.04

The **A** matrix is almost block diagonal dominant and has the form that looks like:

$$\mathbf{A}_i = \begin{bmatrix} -\zeta_i\omega_i & \omega_i \\ -\omega_i & -\zeta_i\omega_i \end{bmatrix};\ \mathbf{A} \approx \text{diagonal}\ (\mathbf{A}_i).$$

However, the block diagonal ω_i value and ζ_i value are not the modal frequency and damping factor respectively. These are given by the eigenvalues of **A** in Table 5.1

Mode i	1	2	3	4	5	6
Modal frequency, ω_i (Hz)	12.95	16.02	21.47	21.59	33.91	38.20
Modal damping, ζ_i	0.037	0.024	0.020	0.011	0.027	0.028

Table 5.1 Modal frequencies and damping factors of $\mathbf{G}_{12}$.

Only some "ω_i" of $\mathbf{A}_i$ match the eigenvalues of **A** e.g. the first block diagonal has ω_1=135 rad s^{-1} or 21.48 Hz and ζ_1=0.02. This is because **A** is not truly block diagonal matrix and in general the states of a state space model has no physical meaning.

The set of modal frequencies given in Table 5.1 almost matches six (underlined) of the eight ICATS model given by {12.9, 15.9, 21.5, 21.6, 24.3, 33.8, 38, 46.7} Hz. However, the damping values obtained from both methods are different. ICATS give values of

structural damping factor, η, whereas those of $\mathbf{G}_{12}$ are viscous damping factor, ζ. A typical set of values is given for illustration.

	ICATS	MLE model, $\mathbf{G}_{12}$
Modal frequency, Hz	21.5	21.47
Modal Damping	η=0.025	ζ = 0.02

Table 5.2 Comparison of a damping value of the ICATS and MLE model

The transfer function $\mathbf{G}_{12}(j\omega) = \mathbf{C}(j\omega\mathbf{I}-\mathbf{A})^{-1}\mathbf{B}$, would almost be of the same form that obtained using ICATS, with $\mathbf{G}_{ICATS}=\mathbf{U}^*\cdot\mathbf{D}_m(j\omega)\cdot\mathbf{U}$, where $\mathbf{D}_m(j\omega)$ is the modal matrix and $\mathbf{U}$ is the modal participation vector.

From the evidence provided above, it is observed that the balanced system $\mathbf{G}_{12}(j\omega)$ is a reasonable model of the system under investigation because:

a. Its transfer functions g_{ij} matched quite closely the measured g_{ij} at least up to 40 Hz.
b. The error using (5.12) in choosing k=12 is reasonably small and it is given by:

$$0.16 < \| \mathbf{G}_{154} - \mathbf{G}_{12} \|_\infty = 0.1635 < 5.294 = 2 \sum_{13}^{154} \sigma_i$$

c. The $\bar{\sigma}(\mathbf{G}_{12}(j\omega))$ plot matches the measured $\Sigma|FRF|$ and $\bar{\sigma}(\mathbf{G}_{154}(j\omega))$ at various modal frequencies except at 24.1 and 27.9 Hz.

5.5. Comparing $\mathbf{G}_{12}$ model time responses with measured time responses.

Referring to Figure 5.1, mount #1 (right side as view from the shaft end) and mount #2 (left side) are at the front (shaft end) of the motor, and mount #4 (behind mount #1) and mount #3 are to the rear of the motor.

The sinusoidal response of the $\mathbf{G}_{12}$ model to a 24 Hz is shown in Figure 5.17. The input is scaled to give an output of about 0.5-mV peak to peak for the response at mount location #3. This corresponds to the measured signal at the same location.

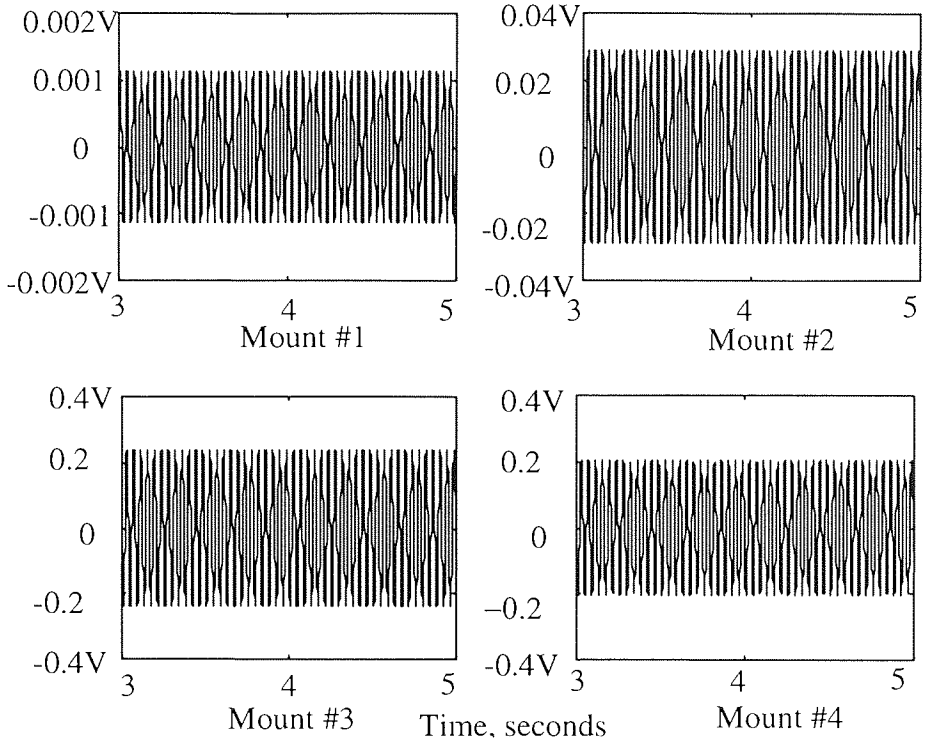

Figure 5.17 Time response $\mathbf{G}_{12}$ to sine input of 1440 rpm

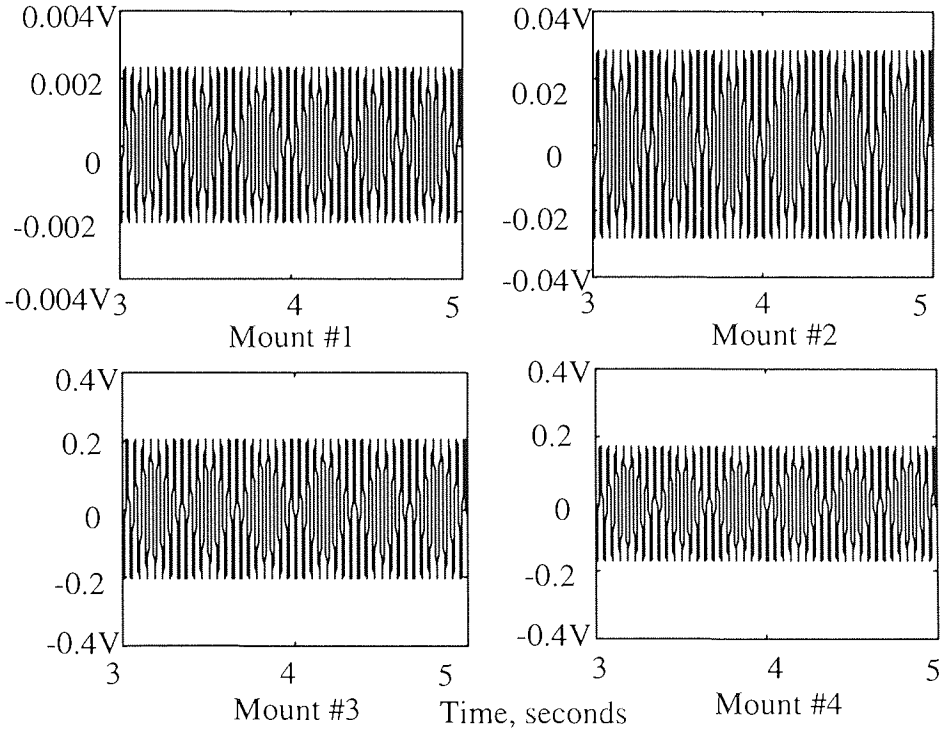

Figure 5.18 Time response of $\mathbf{G}_{12}$ to sine input of 1320 rpm

The sinusoidal responses at all mount locations to 22.33 Hz (1340 rpm) are shown in Figure 5.18. As seen in these figures, the responses are quite periodic. They do not quite match with the observed waveform shown in Figure 5.20 and Figure 5.22 respectively. The amplitude of the response at mount location #1 is definitely too small. It is about 0.05 that of mount location #2. And mount location #2 is itself slightly smaller than that measured.

From the magnitude plots of Figure 5.13-Figure 5.16, it is observed that g_{1j} in the region of the operating speeds between 22 and 24 Hz are not so well estimated. This is particularly so for g_{13} and g_{14}. There are many small peaks and troughs and the estimated transfer function is an average value. The responses of mount location #2 given by g_{2j} are just as difficult to estimate. In general g_{3j} and g_{4j} have better estimation in the region of interest.

There are three other main issues that can contribute to the anomalies identified above:

a. The presence of noise in the measurements

b. The spatial distribution of the disturbance existing at the feet of the machine

c. The spectral distribution of the disturbance at each mount location.

Band limited white noise can be added to the sine excitation representing the noisy measurement and operation. Figure 5.19 and Figure 5.21 show the model responses when random noise is uniformly added to the excitations corresponding to 1440 and 1340 rpm respectively. For 1440 rpm, the effect of the noise on the model mount #1 is the most pronounced. The peak is increased by an order of about 100 times, but it is still 50% smaller than the measured amplitude of the response at mount location as shown in Figure 5.20. Amplitude wise, model responses for mount location #3 and #4 are quite compatible with the measured response.

Measured responses for 1340 rpm shown in Figure 5.22 for comparison with the model response to sine plus band limited noise shown in Figure 5.21. The measurements showed that mounts #3 and #4 have a stronger harmonic content than mount #1 and mount #2.

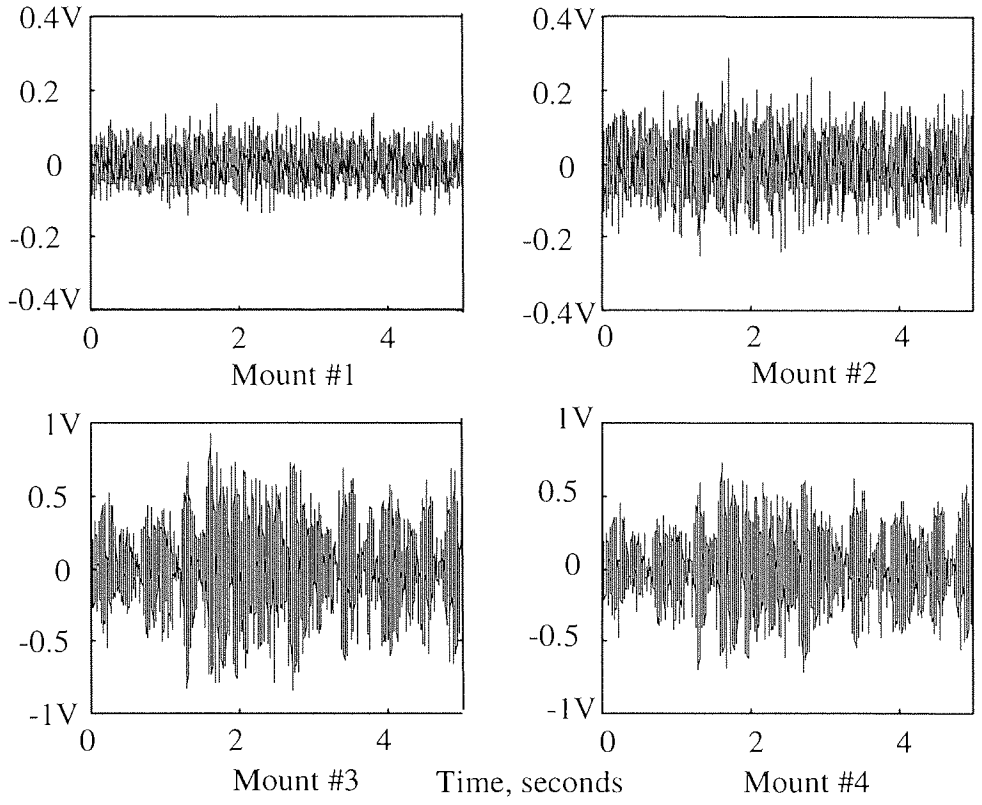

Figure 5.19 Time response of $\mathbf{G}_{12}$ to a 1440 rpm sine wave with band limited noise

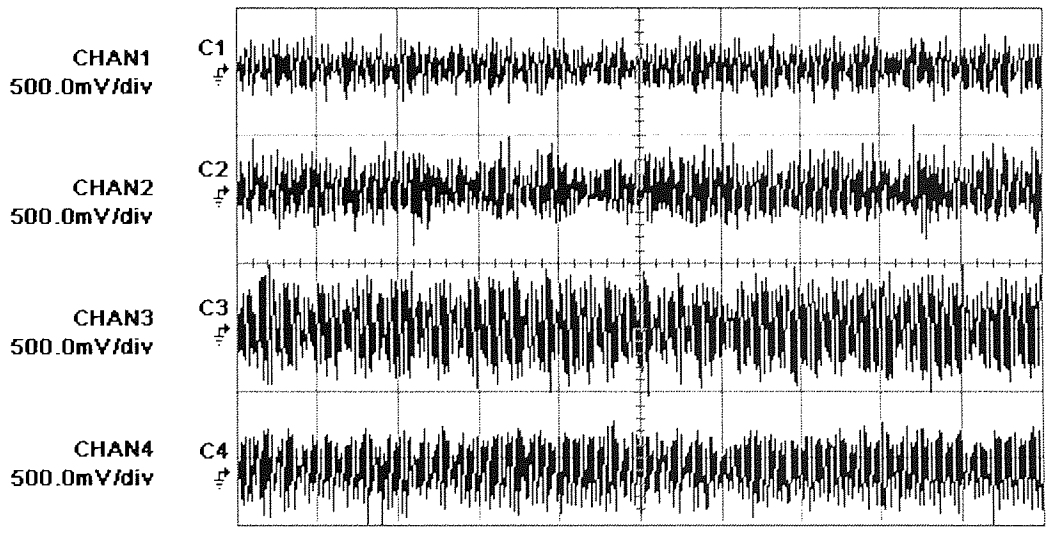

Figure 5.20 Measured response of the system at 1440 rpm. Time base is 500 ms/div

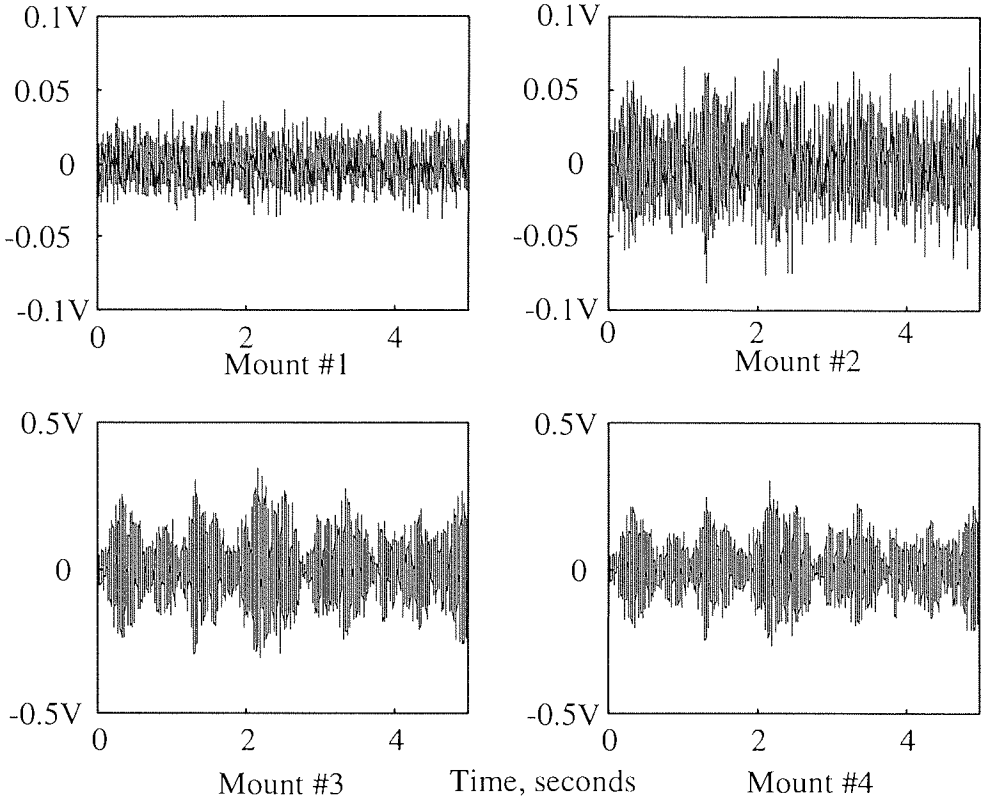

Figure 5.21 Time response of $\mathbf{G}_{12}$ to a 1340 rpm sine wave with band limited noise

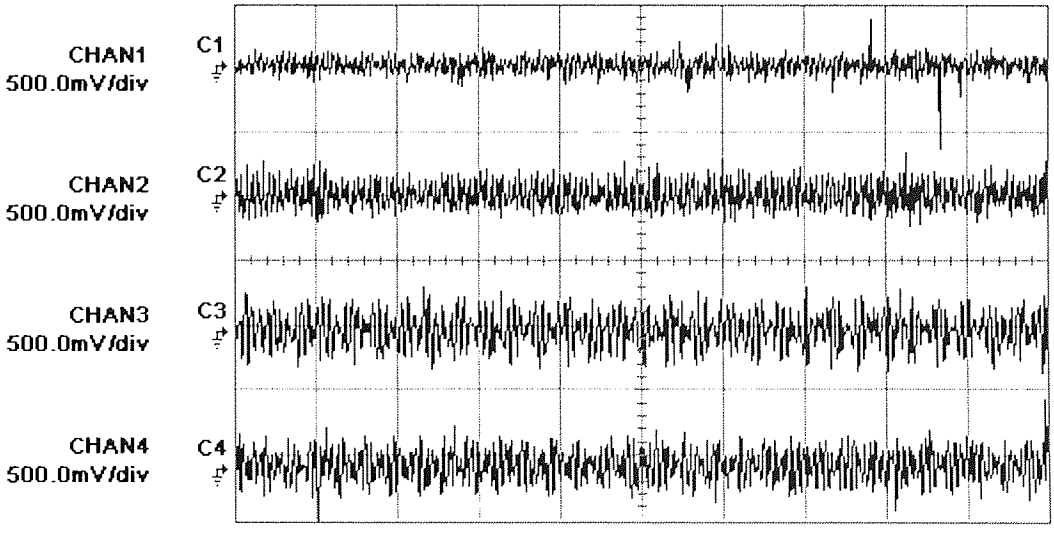

Figure 5.22 Measured responses of system at 1340 rpm. Time base is 500 ms/div

This observation is used to adjust the noise level for the input to the system model. As seen in the figures, the adjusted model response correspondingly shows a stronger harmonic content for mount #3 and mount #4. Also the relative amplitude amongst the various mounts are quite similar to that measured. Mount #3 and #4 are less influenced by the presence of band limited white noise.

For both excitations, the predicted magnitudes at mount #1 and to some extent mount #2 are consistently smaller than that measured. In fact both of these mount locations are also relatively difficult to control compared with mount #3 and mount #4 when model based control is applied.

The second issue relates to spatial amplitude distribution of the disturbance amongst the four mounts. In simulating the model responses, the input excitations for all the four mount locations are given the same amplitude. The motor centre of gravity is not exactly at the geometrical centre of the mounting plate (between the motor and the four mounts). In fact it is located closer to mount location #3 and mount #4. When the motor is operating, the force will not be evenly distributed among the four mount locations. The actual excitations at the mount locations are not replicated due to the lack of information about the spatial distribution of the disturbance existing at the feet of the machine.

The third issue relates to the spectral content at each mount locations. When the motor is running, the spectral distribution at each mount location needs not be the same, and even if they are the same, the magnitudes are not necessarily the same at all the four feet.

An example of a free vibration acceleration spectrum is shown in chapter four. Typically, its harmonics content is higher than the band limited multi-sine excitation used to determine the model. For the case of the more rigid structure discussed in chapter four the transmitted spectrum is dominated only by two spectral lines. For example when the motor is running at 1320 rpm and 1440 rpm the measured transmitted force has a 22 Hz and 33, and 24 and 33 Hz spectral lines respectively. These are also observed at all four mounts' locations when the flexible plate is added, but higher spectral frequency at about 80 and 90 Hz respectively are also present. At 1460 rpm, these higher spectral lines become more pronounced especially at mount #1 and mount #2. A spectral plot of the force measurement at mount #2 for motor running at 1460 rpm is given in Figure 5.23.

Since the model determined here is band-limited to 50 Hz, such spectral lines will create some problem in the model based controller design discussed in the next chapter.

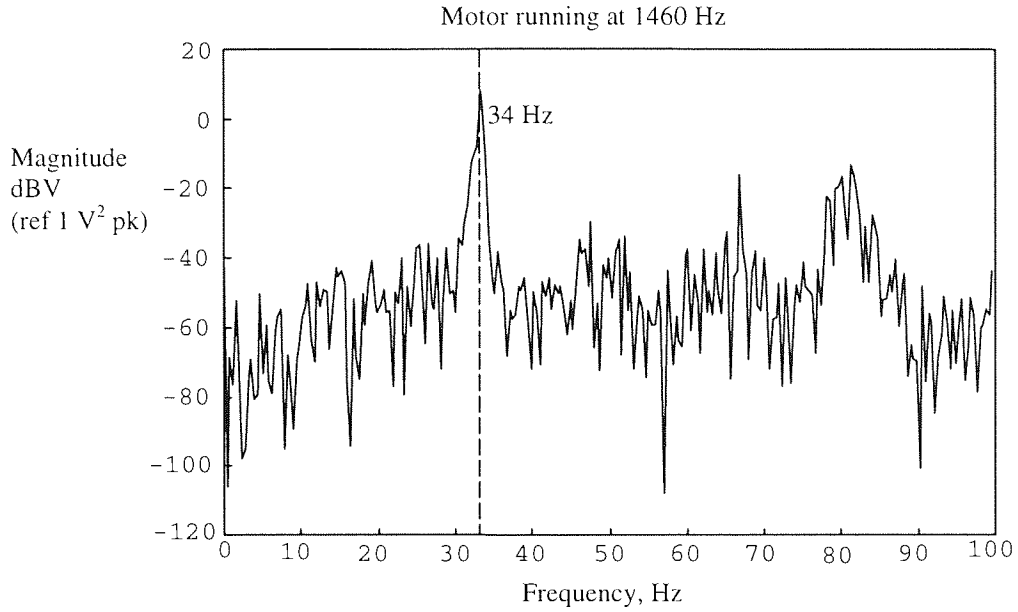

Figure 5.23 Spectral plot of mount #2 sensor at 1460 rpm.

To get a better simulation results, another set of four sensors will be needed. They should to be located at the top of the hard-mounts to determine $\underline{d}_i(j\omega)$ for i=1,2,3,4. These will give information on the relative magnitude of the forces transmitted and the spectral content at each foot to the system at each rated speed of 1440 rpm or any other operating speed. These $\underline{d}_i(j\omega)$ can then be used as inputs to the estimated model. The model outputs can then be compared with the measured $\underline{y}_i(j\omega)$ at the bottom of each of the four mounts. Hence the use of single input/multiple output measurements with a shaker at each location at a time is a good representation only if the excitations are independent. If the system is sufficiently linear, then the responses will be a super-position of the responses to the various sinusoids found in the disturbance, $\underline{d}$. The problem is that the spatial distribution is not exactly known and four additional sensors at the top of the mounts may be needed.

The effects of these uncertainties can be made worse by the presence of non-linearity. The use of low amplitude excitation signals is to minimise the non-linear effects. Notwithstanding these problems, the use of this model in the design of a controller is not disastrous as the model based designed controller did perform relatively well in some range of machine operation. Any machine disturbance larger than 50 Hz that will excite the plate significantly will create problems for the model based controller designed since

the model was not defined beyond 50 Hz. It is therefore more a problem of lack of robustness in the model being formulated than the failure of the model to represent the system response in the range of frequency of interest.

5.6 Actuator model

A Gearing and Watson GWV4 electro-dynamic shaker is used as the actuator. It has a sinusoidal peak force of 17.8 N or a peak acceleration of 892 m s^{-2}. A frequency response test is done with a mass of 0.25 kg attached to the actuator that is mounted onto a rigid base via a force sensor and excited by a power amplifier. Two mounting configurations were tried: (a) via a trunion and (b) direct mounting to the system. The directly mounted actuator has a larger bandwidth, although a smaller magnitude.

For this thesis, the direct mounting arrangement is used. The input voltage used for Figure 5.24 is 1 V peak. Since the gain near the 1st peak frequency of 20 Hz is 0.008, the sensor output is about 8 mV. With the measurement system sensitivity of 1 N $(mV)^{-1}$, the corresponding force is about 8 N. The actuator force magnitude tapered off to about 5 N until the frequency approaches a resonance at about 2000 Hz.

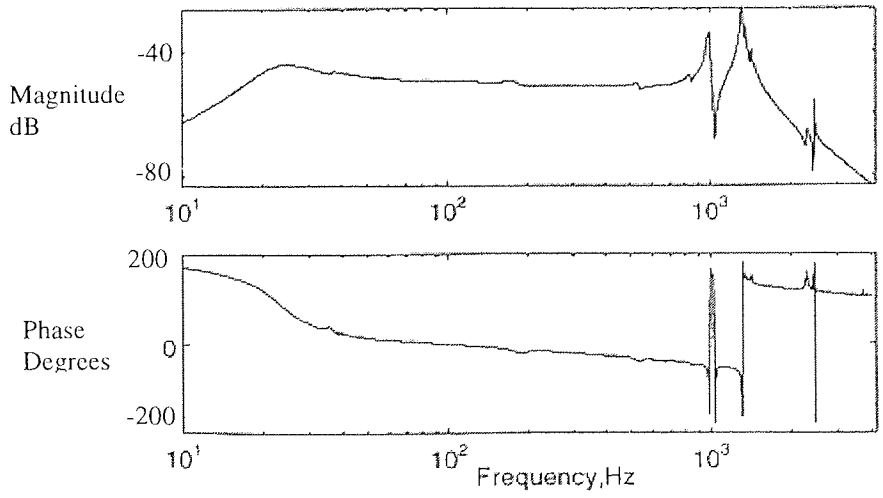

Figure 5.24 Frequency response plot of the GWV4 shaker with 0.25 kg mass

The resonance close to 20 Hz is due to the 0.25 kg mass and the moving table of the shaker. The suspension axial stiffness is 0.45 kgf mm^{-1} or 4414.5 N m^{-1}, and the moving mass is 0.02 kg. Together with the attached inertia mass of 0.25 kg, the actuator first resonant frequency is calculated to be

$$f_a = \frac{1}{2\pi}\sqrt{\frac{4414.5}{0.27}} = 20.35\text{Hz} \tag{5.13}$$

The actuator (and its power amplifier) transfer function is given by the measured voltage from the force sensor to the input voltage to the power amplifier. A model for the measured Bode plot using either a multi-sine or a chirp is given as

$$G_a(s) = k\frac{s^{14} - 1400s^{13} + 2.8e8s^{12} + 2.9e12s^{11} - 5.1e16s^{10} ... + 9.3e47s + 7.9e49}{s^{14} + 1515s^{13} + 3.4e8s^{12} + 3.7e12s^{11} + 4.5e16s^{10} ... + 1.1e47s + 1.2e49}$$

This fits every kink, peak and trough, but is too cumbersome to use. Instead of identifying such a transfer function for each actuator, it was decided for simplicity to approximate the transfer function with a simple 2nd order transfer function of the form

$$G_a(s) = \frac{kV_f}{V_{in}} = k\frac{s^2}{s^2 + 2(0.7)(\omega_a)s + \omega_a^2} \tag{5.14}$$

The k is variable of the amplifier. This is similar to the ideal force generator. Similar form of transfer function was obtained using a B & K 4810 mini-shaker. Although (5.14) does not quite match exactly the measured Bode plot, it is appropriate enough for the actuator in operating range. The positive phases of the actuators in this range provide the necessary phase stabilisation (Wei and Byun, 1989). It is robust enough to tolerate the difference between the actual actuator dynamics and the approximation given by (5.14). This is demonstrated by the ability to provide stable feedback and force attenuation using a model based designed controller for frequencies below 1320 rpm, and the Static Output Feedback designed controller for 1440 rpm.

5.7 Summary

In this chapter the physical system to be investigated has been presented. The rig is chosen to provide a platform to study the use of active force cancellation to limit the transmitted force for machine that is to be hard-mounted onto a base structure. If the

structure is relatively rigid, the reduction in the transmitted force that can be achieved will be quite a meaningful measure of effectiveness. A hard mount is quite ideal also for force actuators attached to the top or bottom of the mount. The dynamics of the actuators can then be separately identified from the transfer function matrix relating the input to the top of the mount and the force transmitted into the base structure. To provide some degree of uncertainty and base structure dynamics, a flexible plate is added between the hard mounts and the supporting structure. This would not be done usually in practice.

The model of the physical system to be investigated is determined using a frequency domain technique. A frequency range and resolution have been identified after some trial tests. The resulting model is also the force transmissibility matrix. Two methods of estimating the model have been presented: modal extraction method using ICATS and the Maximum Likelihood Estimator for linear systems. The former gives a model that is physically meaningful with a set of modal frequencies, (structural) damping and eigenvectors or the modal participation factors. Modal truncation would have been used to reduce the model order had the modal model been selected. The latter method gives a set of poles-zeros model that when converted to a state space representation contains more poles than the physical system would have. It has 154 states! Most of the poles are in fact approximately close to each other and differ as a result of measurement errors. Taking this into account, a set of system poles is obtained. These poles have the same modal frequencies as that obtained from modal extraction method. Instead of an ad-hoc manner of adjusting the state space model to give a model that has the same number of poles as that obtained from ICATS, the approach of residualising the system that is internally balanced has been adopted. Using a combination of selecting appropriate Hankel singular values, error criterion and matching the maximum singular values of the reduced model with the sum of magnitudes of measured FRF, a 12^{th} order model, $\mathbf{G}_{12}$ has been obtained.

Comparing the two methods of model matching, it is found that the state space, $\mathbf{G}_{12}$ model gives a reasonably good fit with the most of the measured frequency response up till 40 Hz.

Time responses simulation results of the $\mathbf{G}_{12}$ model however do not exactly match the corresponding measured responses especially at mount location #1 and to some extent

mount location #2. The match is more acceptable for the other two mount locations. The causes for this imperfect match have been discussed. In part it is because it is hard to emulate the input disturbance spatial and spectral distribution that exists at the time of machine operation. The use of a shaker at each location to excite the responses at all locations for measurements will only provide measurements for the determination of a model. However, without the knowledge of the disturbance spectrum at the machine feet when the machine is operating, it would be difficult for the simulated mounts' responses to match the actual measured responses accurately.

The identified model is a force transmissibility matrix. It will be used as a performance specification for the design of an active vibration isolation system in the next chapter.

CHAPTER SIX

ACTIVE VIBRATION CONTROL OF A MACHINE HARD-MOUNTED TO THE STRUCTURE USING FORCE CANCELLATION AND FORCE TRANSMISSIBILITY MATRIX AS A PERFORMANCE SPECIFICATION

6.1 Introduction

The objectives of controller designs and the reasons for the choice of control strategy using the $\mathcal{H}_\infty$ approach and the static output feedback (SOF) method will be presented. Of the two, the $\mathcal{H}_\infty$ controller has a relatively high order than the SOF controller, which is essentially a static gain controller. Both types of controllers did not destabilise the system. All controllers are implemented on a PC. The use of force transmissibility matrix function as a (disturbance) performance specification in the design of these controllers in active force cancellation will be shown. The results of simulations and experiments using these controllers are given. For the machine running at 1340 rpm and below, simultaneous reduction of force transmission at all four feet of the mount has been achieved using controllers designed by both methods. Reduction in RMS values ranges from 30% to 80%. When the machine is operating at 1440 rpm, the $\mathcal{H}_\infty$ controller is not effective in attenuating disturbance at two locations, and a little effective at the other two. The poor performance at 1440 compared with that at 1340 rpm of the $\mathcal{H}_\infty$ controller is expected from simulation results. The SOF controller on the other hand is able to attenuate disturbance for the machine operating up to 1700 rpm. The results obtained from simulation and implementation are better. RMS reduction varies from 30% to 54%. However in general a SOF controller will not always result in a stable system. The summary of the work is given in Lau *et al.* (1998).

There are some differences between the work presented here and those discussed in the Literature. Active force cancellation is applied at the feet of the machine that is hard mounted to a flexible base structure. Nelson (1991) referred to this as active vibration control to the source (the term "source" was used to mean the machine), and actuation is applied to the machine. The control strategy studied here is considered as control of disturbance through the transmission path. This is also different from Watters' *et al.* (1988) work where the actuator is placed between machine and base. The advantages and disadvantages of these arrangements had been addressed in chapter two.

6.2 Controller Design Objectives

A practical objective for the design of the controllers in the case studied is the rejection of disturbances entering the support structure. This can be achieved by two design goals:

i. To minimise the RMS of measured transmitted forces at all mount locations
ii. To maintain stability in the presence of neglected high frequency dynamics of the structure and the actuator.

It would be desirable to specify independently the amount for RMS reduction in transmitted force at each location. However, this would be difficult especially if interaction exists between the actuator action at one location with another location preventing the independent control of attenuation at each mount location. Attempts to cancel the force at one location may result in the actuator exciting the other mounts via the structure. The overall reduction in the RMS values of the transmitted force is more practical and realisable. A suitable design goal can then be a reduction in the system RMS gain, defined as

$$\|\mathbf{G}\|_{\text{RMS\_gain}} = \sup_{|u|\neq 0} \frac{\|\mathbf{G}\cdot\mathbf{u}\|_{\text{RMS}}}{\|\mathbf{u}\|_{\text{RMS}}} \tag{6.1a}$$

For a given magnitude of vector of input disturbances, reduction in the RMS gain means reduction in the magnitude of vector of transmitted disturbances at all mount locations. This design goal is appropriate when the interaction discussed above exists, and when the disturbance is not known exactly except that it is bounded. By transforming the signals into the frequency domain, it can be shown that the RMS gain is also the $\mathcal{H}_\infty$ norm i.e.

$$\|\mathbf{G}\|_\infty = \sup_{|u|\neq 0} \frac{\|\mathbf{G}\cdot\mathbf{u}\|_{\text{RMS}}}{\|\mathbf{u}\|_{\text{RMS}}} = \overline{\sigma}(\mathbf{G}(j\omega)) \tag{6.1b}$$

Minimising this norm also means minimising $\overline{\sigma}(\mathbf{G}(j\omega))$ or the "worst case" overall "amplification" of the disturbances.

6.3 Force transmissibility function as a performance objective

Since the disturbance transfer function or the force transmissibility matrix from machine to the supporting structure, given by $\mathbf{G}_p$ identified in chapter five, is also the system itself,

design goal #1 can be attained by reducing $\|\mathbf{G}_p(s)\|_\infty$ by means of passive design or active control system. The proposed approach of this thesis is to use active force cancellation with force feedback signals from the force sensors at the interface of the hard-mounts and a controller, $\mathcal{K}$, in series with the actuators, modelled as $\mathbf{G}_a(s)$. It uses the system model $\mathbf{G}_p(s)$ and indirectly $\|\mathbf{G}_p(s)\|_\infty$ as a cost function or performance specification to design various types of controllers, $\mathcal{K}$.

The configuration is represented in Figure 6.1, which is similar to Figure 3.6 with $\Delta_M=0$, and $\mathbf{G}_p=\mathbf{G}_o$.

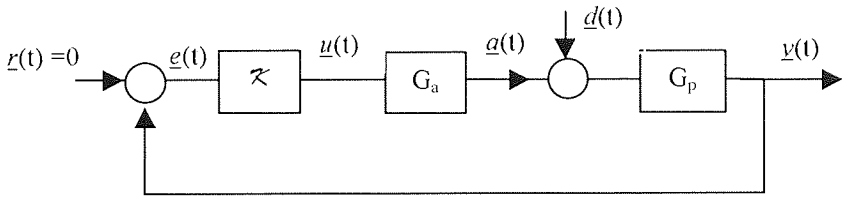

Figure 6.1 Block diagram of the target system

Let

$$\mathbf{T}_{yd} = \mathbf{S}\,\mathbf{G}_p = (\mathbf{I} + \mathbf{L})^{-1}\,\mathbf{G}_p;\ \text{with}\ \underline{r}(t) = 0$$

And

$$\mathbf{L}\ \text{is the Loop gain matrix} = \mathbf{G}_p\,\mathbf{G}_a\,\mathcal{K} \tag{6.2}$$

$$\mathbf{S}\ \text{is the (input) sensitivity matrix;}\ \bar{\sigma}(\mathbf{S}) = \frac{1}{\underline{\sigma}(\mathbf{I} + \mathbf{L})} \tag{6.3}$$

In the classical loop shaping approach, the controller $\mathcal{K}$ is designed such that magnitude plot of $\underline{\sigma}$ ($[\mathbf{I} + \mathbf{L}(j\omega)]$) is larger than the disturbance spectrum over some frequency range. Unfortunately, the free vibration machine spectrum is not an appropriate choice for a disturbance spectrum because the resulting installed disturbance spectrum will include the coupled effect of the dynamics of the supporting structure.

As $\mathbf{G}_p$: $\underline{d} \rightarrow \underline{y}$; $\underline{a} = 0$ represents the disturbance spectrum, a (internal) stabilising controller $\mathcal{K}$ can be designed such that

$$\bar{\sigma}(\mathbf{S}) \cdot \bar{\sigma}(\mathbf{G}_p) < 1;\ \text{or}$$

$$\underline{\sigma}(\mathbf{I}+\mathbf{L}) > \bar{\sigma}(\mathbf{G}_p) \;\; \forall\, \omega \in [0, \omega_c]\text{; } \omega_c = \text{closed loop bandwidth} \tag{6.4}$$

Hence $\mathbf{G}_p$, the force transmissibility matrix, is a suitable (disturbance) performance specification for $\mathcal{K}$. A more intuitive requirement is to design a $\mathcal{K}$ such that

$$\bar{\sigma}(\mathbf{T}_{yd}(j\omega)) < \bar{\sigma}((\mathbf{G}_p(j\omega)) \text{ for } \omega < \omega_c \tag{6.5}$$

Where ω_c is some specified closed loop bandwidth, and $\mathbf{T}_{yd}$ is a function of $\mathcal{K}$.

Equation (6.5) provides two points for discussion. Firstly, it is not necessary to design a $\mathcal{K}$ such that $\mathbf{T}_{yd}$ is smaller than $\mathbf{G}_p$ for the entire given frequency range. For instance, there will be frequencies in the range that the machine will not likely to be operating, and at other frequencies, the disturbance transmitted may be small. In the latter case, if the supporting structure is sufficiently stiff, the transmitted force may not cause any motion vibration in the support. Secondly and more importantly, $\bar{\sigma}((\mathbf{G}_p(j\omega))$ can be a rather complicated function. It may be easier to select some simple frequency-weighted function $\mathbf{W}_2$ or more precisely, $\mathbf{W}_2^{-1}$ as a performance weighting function. Such a function can be selected basing on the spectral norm of $\mathbf{G}_p$.

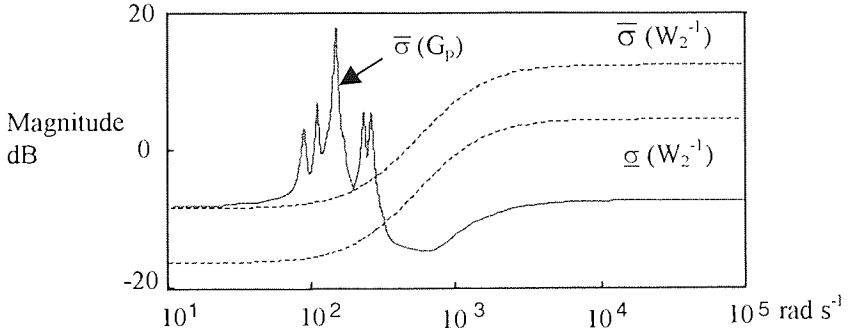

Figure 6.2 $\mathbf{W}_2$ as a disturbance rejection performance specification

For example, Figure 6.2 shows the (magnitude) Bode plot of the maximum singular values of $\mathbf{G}_p(j\omega)$. It has many resonance peaks in a narrow band. Basing on this plot, one can a select a $\mathbf{W}_2^{-1}$ comprising 2nd order lead compensator transfer functions with gain smaller than $\bar{\sigma}((\mathbf{G}_p(j\omega))$ in the range of 10 to 300 rad s^{-1}. Then admissible controllers $\mathcal{K}$ are to be designed such that $\mathbf{T}_{yd}$ is smaller than $\mathbf{W}_2^{-1}$ in a sense of (6.6), i.e.

$$\bar{\sigma}(\mathbf{T}_{yd}(j\omega)) \le \gamma \cdot \underline{\sigma}((\mathbf{W}_2^{-1}(j\omega)),\ \forall\omega \in [\omega_1,\omega_2] \tag{6.6}$$

Where γ is ideally equal to 1. If (6.6) is satisfied in the range shown in Figure 6.2, then (6.5) will be satisfied for $\omega < 300$ rad s^{-1}. Beyond 300 rad s^{-1}, the open loop transmitted force is sufficiently small. The controller frequency response can roll off to some small values after this frequency so that the open and closed loop response could be the same.

Using (6.6) it can be shown that the controller design problem can be treated as an optimisation problem. Furthermore, the condition given in (6.6) can be further refined. For each ω in the interval, with $\underline{\sigma}(\mathbf{W}_2^{-1})=1/\bar{\sigma}(\mathbf{W}_2)$,

$$\frac{\bar{\sigma}(\mathbf{T}_{yd}(j\omega))}{\underline{\sigma}(\mathbf{W}_2^{-1}(j\omega))} \le \gamma \quad \Rightarrow \bar{\sigma}(\mathbf{W}_2(j\omega))\bar{\sigma}(\mathbf{T}_{yd}(j\omega)) \le \gamma \tag{6.7}$$

$$\Rightarrow \bar{\sigma}(\mathbf{W}_2(j\omega)\cdot\mathbf{T}_{yd}(j\omega)) \le \gamma$$

Hence the problem is to find all admissible controllers $\mathcal{K}$ and a bound γ such that $\sup_{\omega}(\bar{\sigma}(\mathbf{W}_2(j\omega)\cdot\mathbf{T}_{yd}(j\omega)) = \left\|\mathbf{W}_2\cdot\mathbf{T}_{yd}\right\|_\infty$ is bounded by γ or having $\|\mathbf{W}_2\cdot\mathbf{T}_{yd}\|_\infty=\gamma_{min}\le\gamma$, $\gamma_{min}>0$. This is then the minimisation problem related to minimising $\|\mathbf{G}_p\|_\infty$.

On the other hand, assuming that a set of admissible controllers $\mathcal{K}_{opt}$ can be found that gives $\|\mathbf{W}_2\cdot\mathbf{T}_{yd}\|_\infty=\gamma_{min}\le\gamma$, then using the property that $\underline{\sigma}(\mathbf{W}_2)\cdot\bar{\sigma}(\mathbf{T}_{yd}) \le \bar{\sigma}(\mathbf{W}_2\cdot\mathbf{T}_{yd})$ would give

$$\underline{\sigma}(\mathbf{W}_2(j\omega))\bar{\sigma}(\mathbf{T}_{yd}(j\omega)) \le \gamma_{min} \Rightarrow \frac{\bar{\sigma}(\mathbf{T}_{yd}(j\omega))}{\bar{\sigma}(\mathbf{W}_2^{-1}(j\omega))} \le \gamma_{min}$$

$$\Rightarrow \bar{\sigma}(\mathbf{T}_{yd}(j\omega)) \le \gamma_{min}\bar{\sigma}(\mathbf{W}_2^{-1}(j\omega)) \tag{6.8}$$

For the special case where $\mathbf{W}_2 = w \cdot \mathbf{I}$, $\underline{\sigma}(\mathbf{W}_2^{-1}) = \bar{\sigma}(\mathbf{W}_2^{-1})$, the specification given by (6.6) and consequently (6.5) can be met provided the optimal controllers, $\mathcal{K}_{opt}$, exist. Otherwise γ or w has to be defined.

Where $\mathbf{W}_2 \neq w \cdot \mathbf{I}$, it is often sufficient to define it as a diagonal matrix (w_{ii}), i=1,2,3,4 especially if the g_{ii} of the $\mathbf{G}_p$ are more dominant than the other off-diagonal elements g_{ij}. Although this is not case here (the g_{ij} as shown in Appendix C are not necessarily much smaller than the g_{ii}), defining $\mathbf{W}_2$ as a full matrix will increase the order of the controller. As a compromise between using $\mathbf{W}_2 = w \cdot \mathbf{I}$ and $\mathbf{W}_2 = [w_{ij}]$, $\mathbf{W}_2$= diagonal (w_{ii}), i=1,2,3 and 4 is chosen, with $\bar{\sigma}(\mathbf{W}_2^{-1}) > \underline{\sigma}(\mathbf{W}_2^{-1})$. Both plots are shown in Figure 6.2.

For the general case, (6.8) suggests that if a set of admissible optimal controllers $\mathcal{K}$ can be found then

$$\bar{\sigma}(\mathbf{T}_{yd}(j\omega)) \leq \gamma \bar{\sigma}(\mathbf{W}_2^{-1}(j\omega)) \qquad (6.6a)$$

This means that (6.6a) could be used instead of (6.6) i.e. specify $\bar{\sigma}(\mathbf{T}_{yd}(j\omega))$ in terms of $\bar{\sigma}(\mathbf{W}_2^{-1})$ instead of $\underline{\sigma}(\mathbf{W}_2^{-1})$. This is less demanding and places less effort on the requirement on the design of admissible controllers. Furthermore, there are computational methods to find $\mathcal{K}$ that minimises $\|\mathbf{W}_2 \cdot \mathbf{T}_{yd}\|_\infty$, the $\mathcal{H}_\infty$ norm of the weighted function.

6.4 The H-infinity ($\mathcal{H}_\infty$) Design approach

The $\mathcal{H}_\infty$ optimal controller design paradigm is one method to solve the above minimisation problem. A weighted closed loop function is used as a cost function in the design. The suitability of the $\mathcal{H}_\infty$ control framework for MIMO systems was also shown in chapter three. There, it was mentioned that certain amount of robust stability could be achieved in the presence of uncertainty either as neglected or unmodelled dynamics. Indeed in chapter five, the high frequency dynamics of the actuator and the plate in the structure was neglected and not modelled. These two features meet the two design goals. Consequently the $\mathcal{H}_\infty$ control paradigm is used to design a controller to minimise the system RMS gain.

To use the $\mathcal{H}_\infty$ method, the block diagram is redrawn as Figure 6.3. The effect of sensor noise will not be shown explicitly as this has already been taken that into consideration.

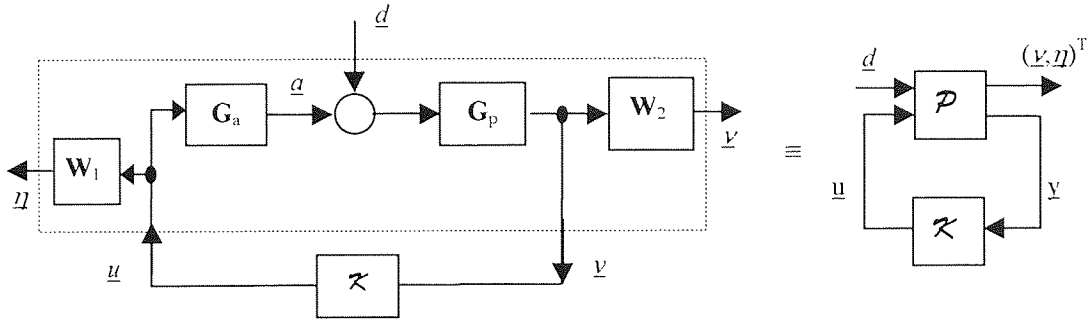

Figure 6.3 Block diagram of the weighted system model

The desired level of force that can be transmitted is defined by the weighting function $\mathbf{W}_2$. Considering that $\underline{d} \rightarrow \underline{v}$, then

$$\underline{v} = (\mathbf{W}_2 \cdot \mathbf{S} \cdot \mathbf{G}_p) \cdot \underline{d} = (\mathbf{W}_2 \cdot \mathbf{T}_{yd}) \cdot \underline{d} = \mathbf{T}_{zd} \cdot \underline{d}$$

This is exactly the minimisation problem discussed above. A weighting function $\mathbf{W}_1$ to limit the controller output by limiting inputs to the actuators can be added. This will prevent the actuators' outputs from saturating.

These specification and constraint functions can be incorporated into system that is now represented by the components within the dotted line shown in Figure 6.3. Let $\mathcal{P}$ represents this generalised system model. Here $\mathcal{P}$: $\underline{w} \rightarrow \underline{v}$ where

$$\underline{w} = \begin{Bmatrix} \underline{d} \\ \underline{u} \end{Bmatrix}; \underline{v} = \begin{Bmatrix} \underline{z} \\ \underline{y} \end{Bmatrix}, \text{ and } \underline{z} = \begin{Bmatrix} \underline{\upsilon} \\ \underline{\eta} \end{Bmatrix}. \tag{6.9}$$

The closed loop system transfer function relating the input (disturbance) $\underline{d}$ to the output $\underline{z}$ is given by

$$\underline{z} = \begin{bmatrix} \mathbf{W}_2 \cdot \mathbf{S} \cdot \mathbf{G}_p \\ \mathbf{W}_1 \cdot \mathcal{K} \cdot \mathbf{S} \cdot \mathbf{G}_p \end{bmatrix} \underline{d} = \mathbf{T}_{zd}\, \underline{d} \tag{6.10}$$

The transfer function $\mathbf{T}_{zd}$ is also given by the lower linear fractional transformation of $\mathcal{P}$ and $\mathcal{K}$ defined as

$$\mathbf{T}_{zd} = F_l(\mathcal{P}, \mathcal{K}) = \mathcal{P}_{11} + \mathcal{P}_{12}\mathcal{K}(\mathbf{I} + \mathcal{P}_{22}\mathcal{K})^{-1}\mathcal{P}_{21}$$

$$\mathcal{P} = \begin{bmatrix} \mathcal{P}_{11} & \mathcal{P}_{12} \\ \mathcal{P}_{21} & \mathcal{P}_{22} \end{bmatrix} = \begin{bmatrix} \mathbf{W}_2\mathbf{G}_p & \mathbf{W}_2\mathbf{G}_p\mathbf{G}_a \\ \mathbf{0} & \mathbf{W}_1 \\ \mathbf{G}_p & \mathbf{G}_p\mathbf{G}_a \end{bmatrix} \tag{6.11}$$

$$\mathcal{P}_{11} = \begin{bmatrix} \mathbf{W}_2\mathbf{G}_p \\ \mathbf{0} \end{bmatrix}; \mathcal{P}_{12} = \begin{bmatrix} \mathbf{W}_2\mathbf{G}_p\mathbf{G}_a \\ \mathbf{W}_1 \end{bmatrix}; \mathcal{P}_{21} = \mathbf{G}_p; \mathcal{P}_{22} = \mathbf{G}_p\mathbf{G}_a$$

Defining $\mathbf{T}_{zd}$ in terms of $F_l(\mathcal{P}, \mathcal{K})$ helps to emphasise the dependence of $\mathbf{T}_{zd}$ on $\mathcal{K}$ as it is obtained by using $\mathcal{K}$ to close a lower feedback loop around $\mathcal{P}$. In state space form, $\mathcal{P}$ can be defined as:

$$\begin{Bmatrix} \dot{x} \\ \underline{z} \\ \underline{y} \end{Bmatrix} = \begin{bmatrix} \mathbf{A} & \mathbf{B}_1 & \mathbf{B}_2 \\ \mathbf{C}_1 & \mathbf{D}_{11} & \mathbf{D}_{12} \\ \mathbf{C}_2 & \mathbf{D}_{21} & \mathbf{D}_{22} \end{bmatrix} \begin{Bmatrix} x \\ \underline{d} \\ \underline{u} \end{Bmatrix} \tag{6.12}$$

Where the state vector x includes the states of $\mathbf{G}_p$, $\mathbf{G}_a$ and $\mathbf{W}_2$ (since $\mathbf{W}_1$ is a diagonal matrix of real numbers, it contributes no additional states to $\mathcal{P}$). For the system under investigation, considering only diagonal $\mathbf{G}_a$ and $\mathbf{W}_2$, x has a dimension of 170x1. The model given by (6.11) can be also to be used to test whether $\mathcal{K}$ provides robust stability and performance for a prescribed set of uncertainty, Δ with $\|\Delta\|_\infty \leq 1$. The tests given in terms of the upper linear fractional transformation of (6.11), $\mathbf{T} = F_u(F_l(\mathcal{P}, \mathcal{K}), \Delta)$ can be found in (Skogestad and Postlethwaite, 1996) for example. Designing $\mathcal{K}$ to meet robust performance will result in the higher order of $\mathcal{K}$ compared with that obtained for (6.11).

For the present, Δ is ignored, and the objective is limited to finding all admissible controllers, $\mathcal{K}$, such that

$$\|F_l(\mathcal{P},\mathcal{K})\|_\infty = \|\mathbf{T}_{zd}\|_\infty = \left\| \begin{matrix} \mathbf{W}_2\mathbf{S}\mathbf{G}_p \\ \mathbf{W}_1\mathbf{K}\mathbf{S}\mathbf{G}_p \end{matrix} \right\|_\infty \leq \gamma \qquad (6.13)$$

Where ideally γ=1. In control literature, (6.13) with γ=1 is considered as a standard $\mathcal{H}_\infty$ control problem or an $\mathcal{H}_\infty$ small gain problem (Chiang and Safonov, 1992). In a more general case, the $\mathcal{H}_\infty$ (optimal) control approach allows us to find all admissible controllers $\mathcal{K}$ that minimises $\|\mathbf{T}_{zd}\|_\infty$, where "admissible" means that $F_l(\mathcal{P},\mathcal{K})$ is to be internally stable, and the minimum of $\|\mathbf{T}_{zd}\|_\infty$ is not necessarily 1. Such controllers if they exist are in general not unique for MIMO systems. In addition, the optimisation problem is theoretically and numerically complicated. In practice, sub-optimal controllers can be equally desirable and very likely to be sufficient in most applications.

Given a $\gamma > \gamma_{min} > 0$, the sub-optimal $\mathcal{H}_\infty$ control strategy is to find all admissible controllers, $\mathcal{K}$, if there are any, such that $\|\mathbf{T}_{zd}\|_\infty < \gamma$. Such problems can be solved efficiently by the bisection algorithm developed by Doyle *et al* (1989) and implemented by function labelled here as *hinfsyn* (Balas *et al*, 1991). In practice, the desired γ is not specified but is calculated by the function. Instead an interval $[\gamma_1, \gamma_2]$ is specified for the function to search for a $\gamma \in [\gamma_1, \gamma_2]$ for which admissible controllers $\mathcal{K}$ may exist. The conditions or assumptions that have to be satisfied for the existence of a sub-optimal solution can be found in (Doyle *et al.*, 1989) or in (Skogestad and Postlethwaite, 1996).

Chang and Safonov developed an alternative γ-iteration, which will be called the function *hinfopt* (Robust Control Toolbox, 1992). In this case, the problem is formulated as

$$\| \gamma' \mathbf{T}_{zd} \|_\infty < 1 \qquad (6.14)$$

The function finds a γ' and a set of $\mathcal{K}$ that solve this $\mathcal{H}_\infty$ small gain control problem (see Appendix D). Typically γ' is almost the reciprocal of γ. What γ and γ' tell us is that if a $\mathcal{K}$ can be found then

$$\bar{\sigma}(\mathbf{T}_{yd}(j\omega)) \leq \gamma \cdot \bar{\sigma}(\mathbf{W}_2^{-1}(j\omega)) \;\forall\; \omega \in [\omega_1,\omega_2]$$

As long as $\gamma \cdot \bar{\sigma}(\mathbf{W}_2^{-1}(j\omega))$ is sufficiently smaller than $\bar{\sigma}(\mathbf{G}_p(j\omega))$, for $\omega \in [60,300]$ rad s^{-1}, the desired goal is achieved. Hence with $\gamma \cdot \bar{\sigma}(\mathbf{W}_2^{-1}(j\omega))$ and Figure 6.2, the largest value of γ for which the corresponding admissible controller is acceptable or not can be found. If not, $\mathbf{W}_2(j\omega)$ has to be redefined again.

The disturbance rejection specification, $\mathbf{W}_2$ can be simply defined in a form discussed in §6.2 and given by (6.15):

$$\mathbf{W}_2 = \begin{bmatrix} w_{11} & 0 & 0 & 0 \\ 0 & w_{22} & 0 & 0 \\ 0 & 0 & w_{33} & 0 \\ 0 & 0 & 0 & w_{44} \end{bmatrix}; w_{ii} = \frac{(s\tau_{i2}+1)^2}{\alpha_i^2(s\tau_{i1}+1)^2}; i = 1,2,3,4 \tag{6.15}$$

$\tau_{i1} > \tau_{i2}$.

Each w_{ii} is a low pass filter such that its inverse (elements of $\mathbf{W}_2^{-1}$) is a high pass filter. As shown in Figure 6.2, the high pass filter attempts to limit the maximum singular value of the force transmissibility in the desired operating frequency range of the motor. At those frequencies where the model has small maximum singular value, $\mathbf{W}_2^{-1}$ can have a higher value. To keep the design process simple, all w_{ii} is designed to be equal, and different w_{ii} values can obtained by varying α_i, τ_{i1} and τ_{i2}. Alternatively, one can also specify the weighting functions, w_{ij} for every element in $\mathbf{W}_2$, but this is not used eventually as it will increase the dimension of $\boldsymbol{x}$ without a considerable return in benefit.

For a properly scaled system, $\mathbf{W}_1$ can be defined as a 4x4 identity matrix: $\mathbf{W}_1 = \mathbf{I}_{4x4}$. The scale factors are chosen to represent the maximum outputs of the actuators in response to the full-scale voltages of the controller. Such values can be obtained from the actuators' and the controller data sheets.

6.5 The design of a $\mathcal{K}_{28}$ controller using the $\mathbf{G}_{12}$ model

Two ways to find $\mathcal{K}$ using the $\mathcal{H}_\infty$ approach will be demonstrated and their implementation will be discussed. This design method will result in a set of controllers with at least the

same dimension as the generalised plant $\mathcal{P}$. The first set of $\mathcal{K}$ is designed using the $\mathbf{G}_{12}$ model in $\mathcal{P}$, and the second set of $\mathcal{K}$ is designed using $\mathbf{G}_{154}$ model in $\mathcal{P}$ but the order of the model of this set of controllers is subsequently reduced.

With $\mathbf{G}_p = \mathbf{G}_{12}$ as the plant model, a set of controllers that will be easier to implement can be designed. The *hinfsyn* and *hinfopt* algorithms are used for this purpose. The first set of disturbance specification used is given by $\mathbf{W}_2 = w \cdot \mathbf{I}$. In this case, each actuator is in a local feedback loop and directly attenuate the disturbance measured at its own sensor location. After some trial and error, $\alpha = \sqrt{0.3}$ is selected to give the desired attenuation and the "best" w is given as:

$$w = \frac{\left(\frac{s}{1000} + 1\right)^2}{0.3\left(\frac{s}{400} + 1\right)^2} \tag{6.16}$$

The state vector x of $\mathcal{P}$ corresponding to $\mathbf{G}_{12}$ is of dimension 28x1. Hence the resulting controller is labelled as $\mathcal{K}_{28}$. Since this controller is to be implemented on the actual system, it must be tested for closed loop stability on the original plant model $\mathbf{G}_{154}$, which though contains excess poles nevertheless, has some relevant poles neglected in $\mathbf{G}_{12}$.

In brief, the design procedure involves:

a) Finding a suitable $\mathbf{W}_2$ to give a stable $\mathcal{K}_{28}$
b) Checking that the $\mathcal{K}_{28}$ must stabilised the closed loop system using $\mathbf{G}_{154}$.
c) Verifying that the resulting $\|\mathbf{T}_{yd}\|_\infty$ (without $\mathbf{W}_2$ and $\mathbf{W}_1$) $< \| \mathbf{G}_{154} \|_\infty$.

Due to the difference in the *hinfopt* and *hinfsyn* algorithms, it is found that a stable $\mathcal{K}_{28}$ designed using the method of *hinfopt* often fails step (b), whereas those designed with the *hinfsyn* more often than not pass step (b). Subsequently, all the design is done using the *hinfsyn* algorithm.

Using $\mathbf{W}_2$ with w given by (6.16), the resulting maximum singular value plot of the stable closed loop system using the $\mathcal{K}_{28}$ controller is given by Figure 6.4.

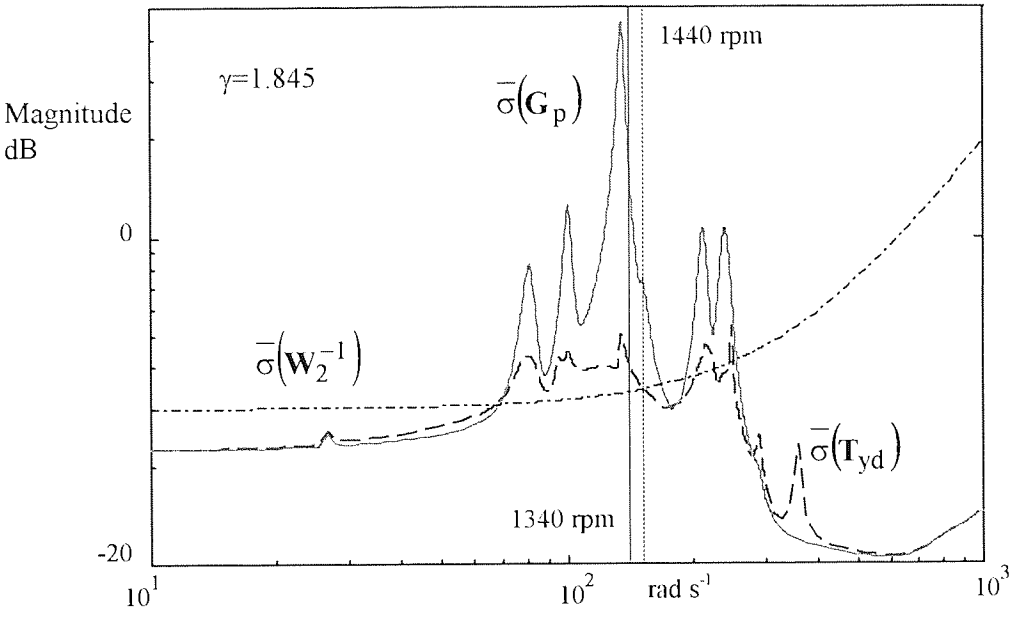

Figure 6.4 Maximum singular values of $\mathbf{G}_p$, and $\mathbf{T}_{yd}$

It is observed that the selected $\mathbf{W}_2$ results in $\bar{\sigma}(\mathbf{T}_{yd}(j\omega)) < \bar{\sigma}(\mathbf{G}_p(j\omega))$ between 70 rad s^{-1} and 280 rad s^{-1}. With $\gamma>1$, $\bar{\sigma}(\mathbf{T}_{yd}(j\omega)) \le \gamma \cdot \bar{\sigma}(\mathbf{W}_2^{-1}(j\omega))$ for some values of ω. At about 110 rad s^{-1}, $\bar{\sigma}(\mathbf{T}_{yd}) = \gamma \cdot \bar{\sigma}(\mathbf{W}_2^{-1})$. Higher attenuation is achieved at 140 rad s^{-1} (1340 rpm) than at 150.8 rad s^{-1} (1440 rpm). As shown later, the designed $\mathcal{K}_{28}$ is quite effective when used on the actual system for frequencies below 140 rad s^{-1} (1340 rpm).

The single weighting function is simple, but when plotted against the g_{ii} of $\mathbf{G}_p$, it turns out to be a poor weighting function for g_{11} and g_{22}. Hence as a next step, different weighting function w_{ii} are selected for each g_{ii} - only diagonal elements of $\mathbf{G}_p$ have w_{ii} specified. The weighting functions for these two design cases, called case I and case II are shown in Figures 6.5 and Figure 6.7. The resulting controllers are $\mathcal{K}_{28\_I}$ and $\mathcal{K}_{28\_II}$ respectively and the closed loop performance as measured by the maximum singular values of $\mathbf{T}_{yd}$ are shown on Figure 6.6 and Figure 6.8 respectively. In comparison with $\mathbf{G}_p$ and that of $\mathbf{T}_{yd}$ using the $\mathcal{K}_{28}$, no improvements were observed. Similarly experimental results using these $\mathcal{K}_{28\_I}$ and $\mathcal{K}_{28\_II}$ do not show any substantial improvements over the $\mathcal{K}_{28}$ in the operating speed of 1440 rpm (150.8 rad s^{-1}). Furthermore compared with that using

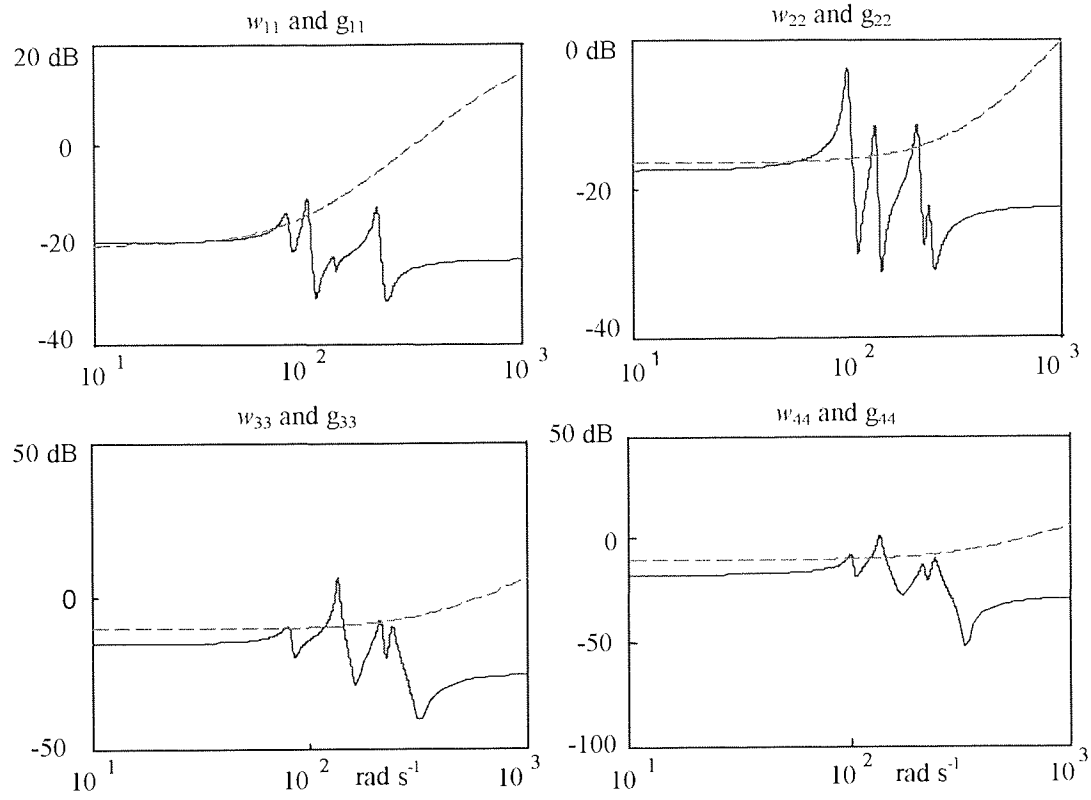

Figure 6.5 Weighting function w_{ii} of $\mathbf{W}_2^{-1}$ against g_{ii} of $\mathbf{G}_p$ for case I

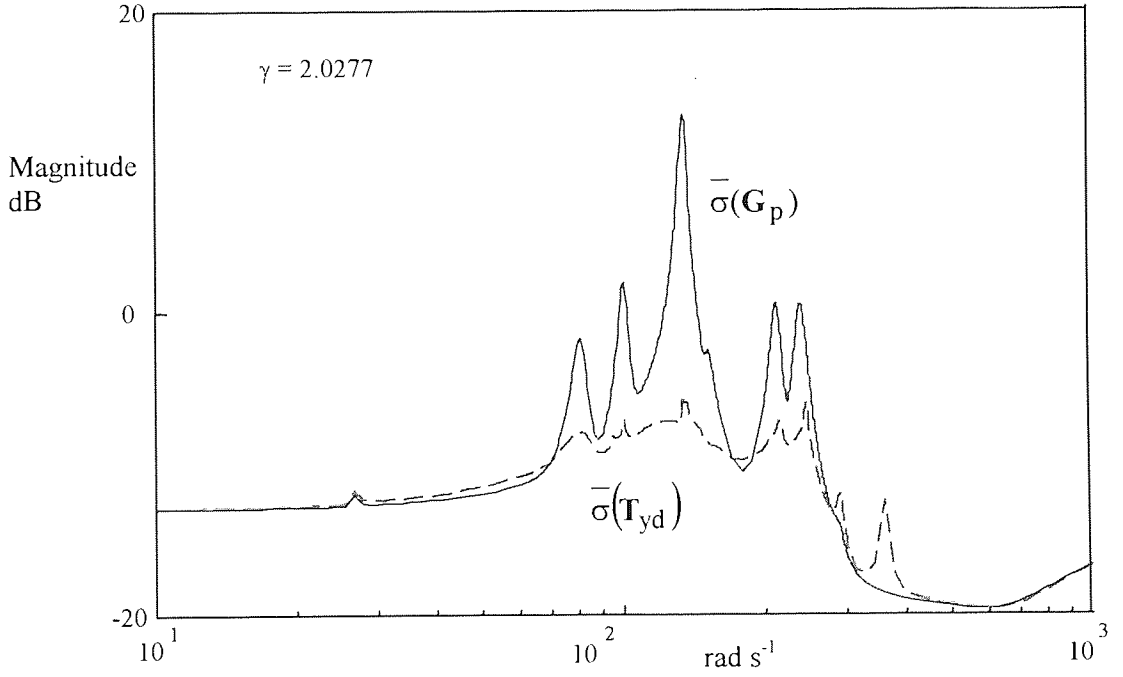

Figure 6.6 Maximum singular value of $\mathbf{G}_p$ and $\mathbf{T}_{yd}$ using $\mathcal{K}_{28\_I}$

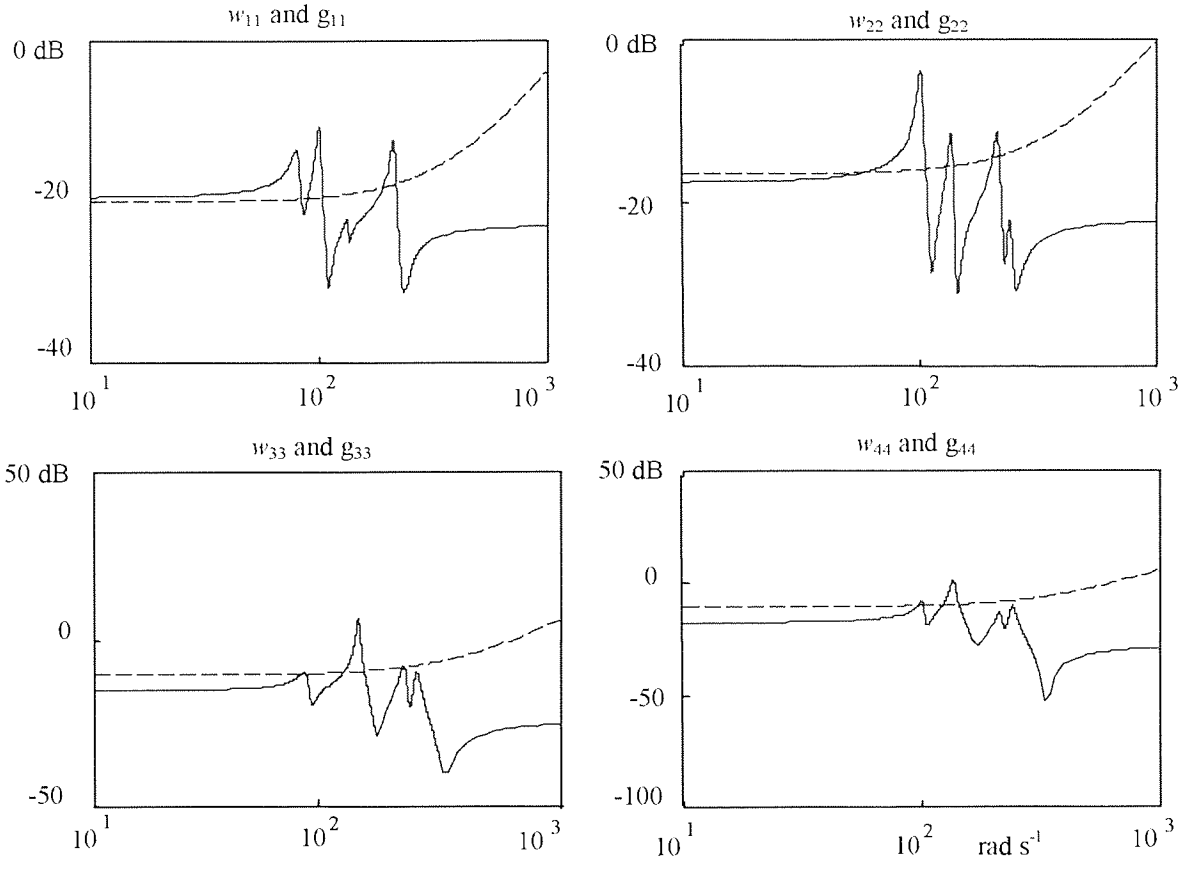

Figure 6.7 Weighting function w_{ii} of $\mathbf{W}_2^{-1}$ against g_{ii} of $\mathbf{G}_p$ for case II.

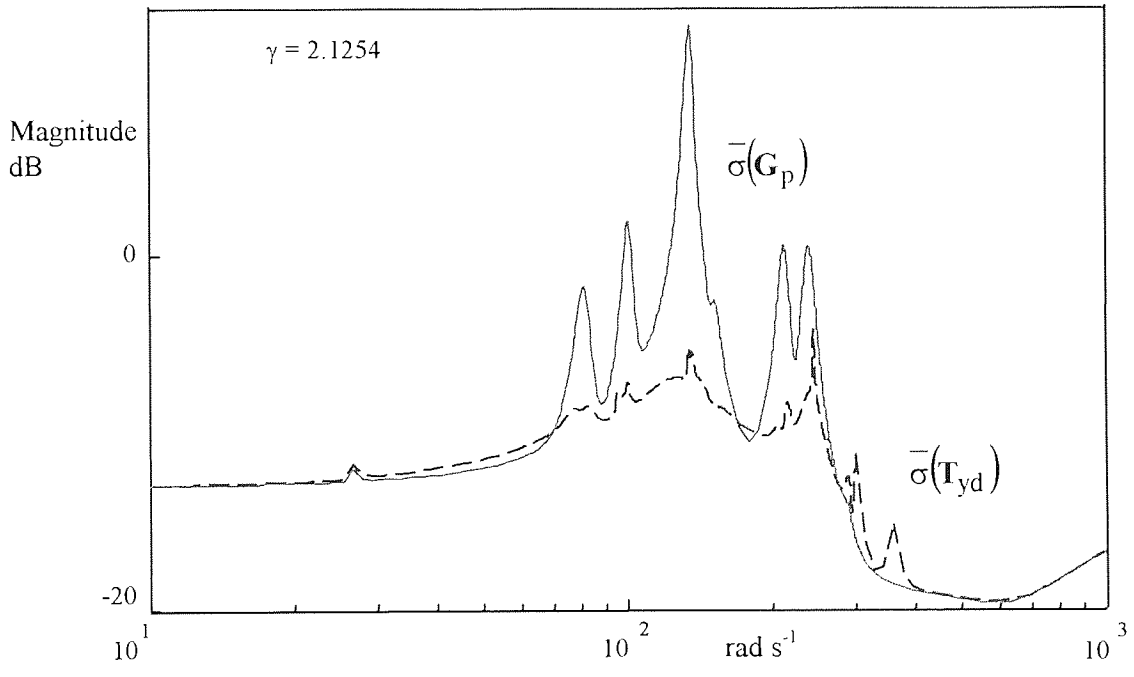

Figure 6.8 Maximum singular value of $\mathbf{G}_p$ and $\mathbf{T}_{yd}$ using $\mathcal{K}_{28\_II}$

equal w_{ii} for all the diagonal elements of $\mathbf{W}_2$, case I and case II are more involved. Hence only the experimental results of the $\mathcal{K}_{28}$ will be discussed subsequently.

6.6 The design of a $\mathcal{K}_8$ controller using the $\mathbf{G}_{154}$ model

One of the key objections to the approach adopted above is that a low order controller designed using $\mathbf{G}_{12}$ as a plant model may not stabilise a full order system model which has an order greater than 12. As the error between the reduced model and the full model that is not embedded in the $\mathcal{H}_\infty$ optimal problem formulation such situation can arise. So even if an internally stabilising controller $\mathcal{K}$ can be found using $\mathbf{G}_{12}$, there is no guarantee that this is a solution for the actual system. In a report on the control design for Large Space Structure, Balas, Young and Doyle (1992) used the sub-optimal $\mathcal{H}_\infty$ method on a reduced order model of the Minimast Facility at Caltech to design a (low order) controller. When applied to the full order model, this controller resulted in an unstable closed loop system. Nevertheless this low order controller provided them with an upper limit on the (disturbance) performance level. The *μ-synthesis* (structured singular value) approach was used to design the controller for eventual implementation. The use of the *μ-synthesis* method will improve the robust stability and the robust performance of the system. However, it is also a more complicated method involving an iterative procedure called the D-K iteration.

Instead of using the more involved *μ-synthesis*, a simpler approach is adopted. What has been done and presented is an iterative search for a design and test for a low order $\mathcal{K}$ designed using a reduced order system model but which also stabilises the full order system model. This has proved to be successful in simulation and in physical operation of the motor in some operating speed. Hence there is no need to use of *μ-synthesis* method. Alternatively, a $\mathcal{K}$ can be designed using the full order $\mathbf{G}_{154}$ to represent the full order in $\mathcal{P}$ and then a model reduction on the controller model is done next. This will provide some of the other poles or modes neglected in the $\mathbf{G}_{12}$ model. The resulting high order $\mathcal{K}$ can be reduced by the method discussed above of residualising the balanced realisation of the controller. This will facilitate implementation.

With $\mathbf{G}_p$=$\mathbf{G}_{154}$, $\mathbf{G}_a$ and $\mathbf{W}_2$ in $\mathcal{P}$, the resulting controller has a state vector of dimension 170x1. Two cases of $\mathcal{K}_{170\_1}$ and $\mathcal{K}_{170\_2}$ using different $\mathbf{W}_2$ are presented here. For $\mathcal{K}_{170\_2}$, $\mathbf{W}_2$ has the same diagonal elements as that used to design the $\mathcal{K}_{28}$. For $\mathcal{K}_{170\_1}$, the w_{ii} are given in Table 6.1. The w_{ii} are selected through trial and error. The orders of both controllers are subsequently reduced, and are respectively labelled as $\mathcal{K}_8$ and $\mathcal{K}_{12}$. These are the lowest order that give reasonably good disturbance rejection using the $\mathcal{H}_\infty$ norm as the criteria.

	α_i^2	$1/\tau_{i1}$ (rad s^{-1})	$1/\tau_{i2}$ (rad $^{-1}$)
i=1	0.1	300	1000
i=2	0.12	300	1000
i=3	0.19	300	3000
i=4	0.185	300	3000

Table 6.1 Values of w_{ii} defined for $\mathbf{W}_2$

The resulting maximum singular value plots of $\mathbf{G}_p$ and $\mathbf{T}_{yd}$ (using $\mathcal{K}_8$ and $\mathcal{K}_{12}$ respectively) are shown in Figure 6.9 and Figure 6.10. The figures indicate that the $\mathcal{K}_8$ has a better disturbance attenuation performance than the $\mathcal{K}_{12}$, but with a higher value of γ. The controller $\mathcal{K}_8$ also appears to give a better attenuation than the controller $\mathcal{K}_{28}$ for frequencies of $\omega \in [70, 250]$ rad s^{-1}. Since $\mathcal{K}_8$ is derived from $\mathcal{K}_{170\_1}$ which is designed using $\mathbf{G}_p$ = $\mathbf{G}_{154}$ with w_{ii} specifically selected for the respective g_{ii}, a better simulation result is expected. This is very likely due to the fact that more information about the system is available to the design algorithm. The additional effort of selecting w_{ii} for each g_{ii} is justified.

Subsequently, only the $\mathcal{K}_8$ will be implemented and the experimental results compared with that of the $\mathcal{K}_{28}$ discussed above.

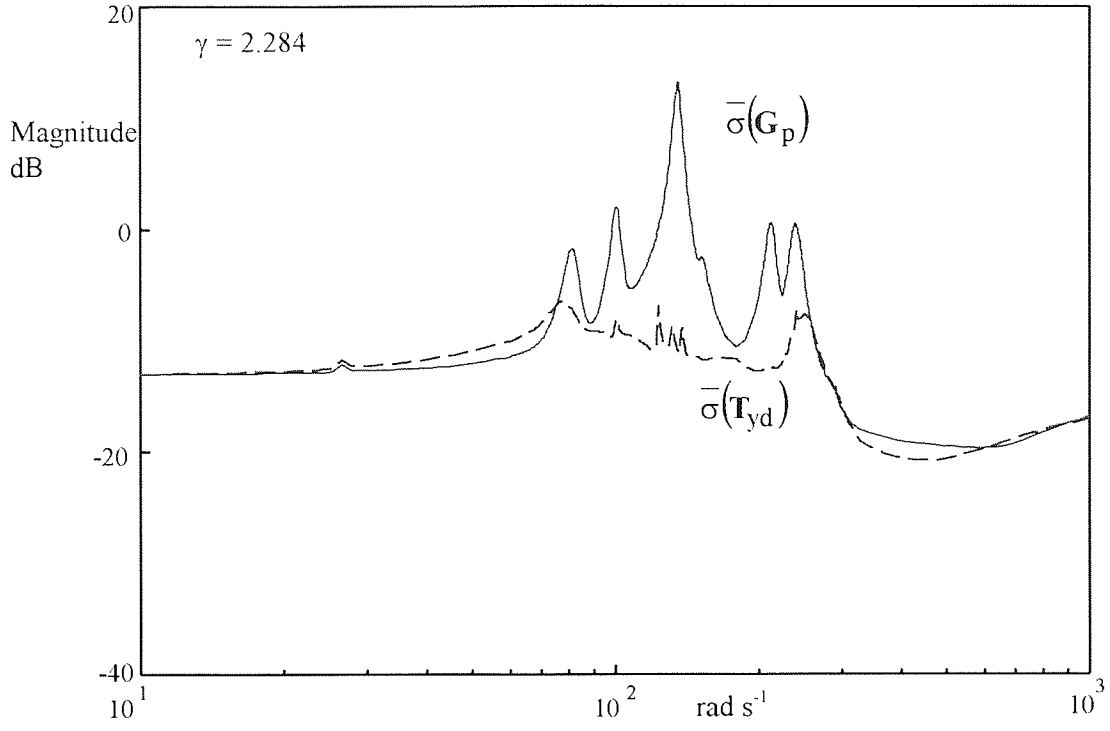

Figure 6.9 Maximum singular value of $\mathbf{G}_p$ and $\mathbf{T}_{yd}$ using $\mathcal{K}_8$

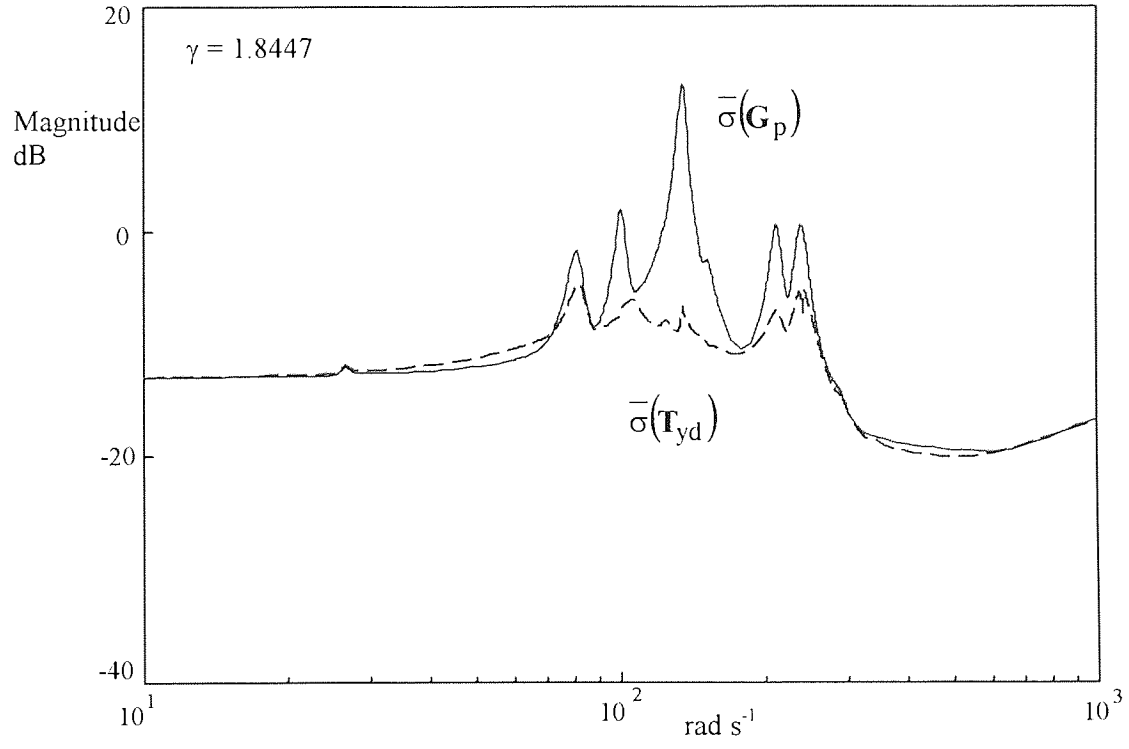

Figure 6.10 Maximum singular value of $\mathbf{G}_p$ and $\mathbf{T}_{yd}$ using $\mathcal{K}_{12}$

6.7. Static Output Feedback design

The most direct approach to the design of controllers for large-order systems such as this flexible system is to implement direct proportional gain between the input and the output. The design of such static output feedback (SOF) controller is stated as follows: given a linear time-invariant system, find a static gain feedback controller so that the closed loop system has certain characteristics, such as providing internal stability and satisfying some desired specifications. Although many approaches and numerical methods exist to design such controllers, the problems (Syrmos *et al*, 1997) with static output feedback designs are that:

i. there are no testable efficient necessary and sufficient conditions to check for stability;
ii. numerical algorithms do not in general converge;

Furthermore, with the given system, improvement in performance is achieved with a reduction in the stability margin. Nevertheless, the case for such a controller is quite strong. Firstly, as a 4x4-static gain controller it is easier to implement compared with the full 170x170-state controller or even the 28x28-state controller. Secondly in the presence of modelling error, there will be a need to perform some degree of manual tuning. With a smaller number of elements in the controller, such manual tuning is quite feasible. The stated primary purpose is to find a way to design such a controller specific to the system.

If the actuator dynamics is ignored for the present time, the control problem can be posed as a simple output feedback problem. Given the plant, $\mathbf{G}_p=\{\mathbf{A}_p,\mathbf{B}_p,\mathbf{C}_p,\mathbf{D}_p\}$ defined by

$$\begin{aligned}\dot{\mathbf{x}} &= \mathbf{A}_p\mathbf{x} + \mathbf{B}_p\mathbf{u}\\ \mathbf{y} &= \mathbf{C}_p\mathbf{x} + \mathbf{D}_p\mathbf{u}\end{aligned} \tag{6.17}$$

The objective is to find a controller $\mathcal{K}$ such that

(a) $(\mathbf{I}-\mathcal{K}\cdot\mathbf{D}_p)$ is non-singular
(b) the closed loop system is stable and possesses certain desirable characteristics

For disturbance rejection, the controller equation can take the form

$\mathbf{u} = \mathcal{K}\cdot\mathbf{y} + \nu$; where ν is the disturbance entering the system.

Substituting for the output, the controller equation becomes

$$\begin{aligned}\mathbf{u} &= \mathcal{K}\cdot\mathbf{C}_p\mathbf{x} + \mathcal{K}\cdot\mathbf{D}_p\mathbf{u} + \nu \\ &= \left(\mathbf{I} - \mathcal{K}\cdot\mathbf{D}_p\right)^{-1}\cdot\left(\mathcal{K}\cdot\mathbf{C}_p\mathbf{x} + \nu\right) \\ &= \mathbf{E}\cdot\mathcal{K}\cdot\mathbf{C}_p\mathbf{x} + \mathbf{E}\nu\end{aligned} \tag{6.18}$$

Where $\mathbf{E}=(\mathbf{I}-\mathcal{K}\cdot\mathbf{D}_p)^{-1}$. Consequently, the system equation becomes

$$\begin{aligned}\dot{\mathbf{x}} &= (\mathbf{A}_p + \mathbf{B}_p\cdot\mathbf{E}\cdot\mathcal{K}\cdot\mathbf{C}_p)\cdot\mathbf{x} + \mathbf{B}_p\cdot\mathbf{E}\cdot\nu = \mathbf{A}_{cl}\cdot\mathbf{x} + \tilde{\mathbf{B}}_p\cdot\nu \\ \mathbf{y} &= (\mathbf{C}_p + \mathbf{D}_p\cdot\mathbf{E}\cdot\mathcal{K}\cdot\mathbf{C}_p)\cdot\mathbf{x} + \mathbf{D}_p\cdot\mathbf{E}\cdot\nu = \tilde{\mathbf{C}}_p\cdot\mathbf{x} + \tilde{\mathbf{D}}_p\cdot\nu\end{aligned} \tag{6.19}$$

Where $\tilde{\mathbf{B}}_p = \mathbf{B}_p\cdot\mathbf{E}$, $\tilde{\mathbf{D}}_p = \mathbf{D}_p\cdot\mathbf{E}$, $\tilde{\mathbf{C}}_p = \left(\mathbf{C}_p + \tilde{\mathbf{D}}_p\cdot\mathcal{K}\cdot\mathbf{C}_p\right)$ and let

$\tilde{\mathbf{A}}_p = (\mathbf{A}_p + \tilde{\mathbf{B}}_p\cdot\mathcal{K}\cdot\mathbf{C}_p)$ represents the closed loop system A-matrix.

A stabilising controller $\mathcal{K}$ is one that give $\mathrm{Re}(\lambda_i(\tilde{\mathbf{A}}_p)) < 0$ for all eigenvalues of $\tilde{\mathbf{A}}_p$.

Assuming that $\mathbf{D}_p$ is non-singular, a possible design choice is to select $\mathcal{K} = -\mathbf{D}_p^{-1}$. This will make $\mathbf{E}=0.5\cdot\mathbf{I}$, and $\tilde{\mathbf{B}}_p=0.5\cdot\mathbf{B}_p$, and $\tilde{\mathbf{C}}_p=0.5\cdot\mathbf{C}_p$. The consequence is that the input and output matrix directions are unchanged but the magnitudes are scaled by a factor of 0.5. If this is stabilising, then the amount of disturbance is reduced at the input to the system by closing the loop, and the amount of output is correspondingly reduced by the same factor.

The controller gain, $\mathcal{K}$ can be parameterised as follows:

$$\mathcal{K} = -\alpha \mathbf{D}_p^{-1},\ 0 < \alpha \le \overline{\alpha} \tag{6.20}$$

Where $\overline{\alpha}$ is the maximum value of α that will not destabilise the system when $\mathcal{K}$ is given by (6.20). Then

$$\mathbf{E} = \frac{1}{1+\alpha}\mathbf{I},\quad \tilde{\mathbf{B}} = \frac{1}{1+\alpha}\mathbf{B}_p,\quad \tilde{\mathbf{C}} = \frac{1}{1+\alpha}\mathbf{C}_p,\quad \text{and } \tilde{\mathbf{D}} = \frac{1}{1+\alpha}\mathbf{D}_p$$

$$\tilde{\mathbf{A}}_p = \left(\mathbf{A}_p - \frac{1}{1+\alpha}\mathbf{B}_p \cdot \mathbf{D}_p^{-1} \cdot \mathbf{C}_p\right) \tag{6.21}$$

For the given model $\mathbf{G}_p$, $\mathcal{K} = (-\mathbf{D}_p^{-1})$ exists and results in $\tilde{\mathbf{A}}_p$ having two eigenvalues on the right half plane. This is due the d_{ij} values of $\mathbf{D}_p^{-1}$ being relatively high. The bisection method is used to find $\overline{\alpha}$ such that $\mathrm{Re}(\lambda_i(\tilde{\mathbf{A}}_p)) < 0$ for all i. For given $\mathbf{G}_p$, $\overline{\alpha} \approx 0.7235$.

Any $\alpha \le \overline{\alpha}$ will reduce the loop-gain of the system, and hence increase the relative stability of the system. Similar to the SISO case, the larger $\mathcal{K}$ is, the faster is the response. Hence there has to be a balance between stability and response. For α=0.72 a stable closed loop system is obtained with responses at the four mounts as shown by Figure 6.11. Like in the actual experiment, disturbance at location #1 is hard to reduce whereas mount location #3 has the largest reduction.

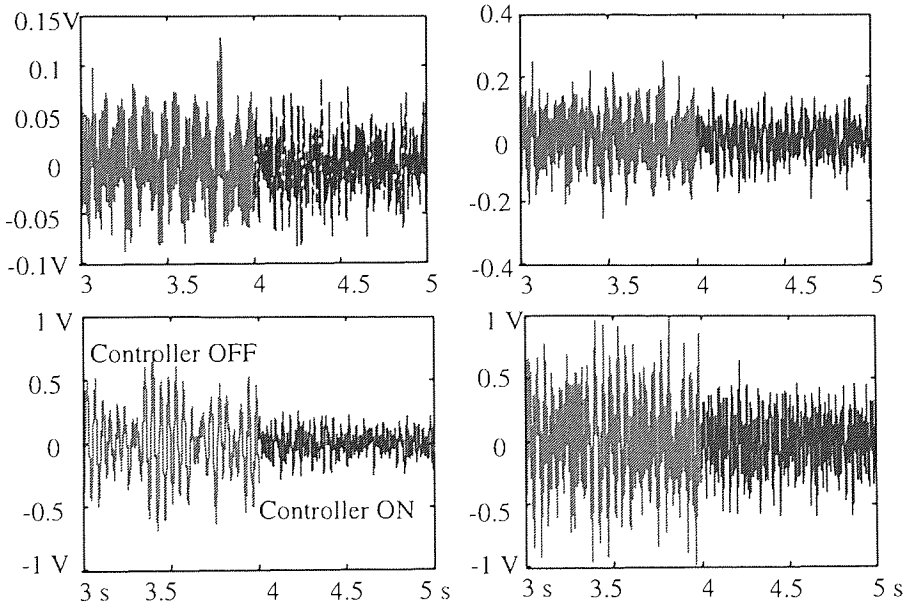

Figure 6.11 Responses at 1440 rpm with $\mathcal{K} = -0.72\mathbf{D}_p^{-1}$ w/o actuators' dynamics

When the actuators' dynamics are included, a higher upper limit can found. This is based on the observation that the actuators are force actuators with positive phase over the frequency range of interest (Figure 5.24). In a manner similar to the analysis of a SISO system, larger gain values can be used when lead compensators are added around the region of the cross over frequency since they provide phase stabilisation. Using the same bisection method it is found that $\overline{\alpha}=1.034$.

The dynamics of the actuators can be coupled to the static gain controller and what appears to be a dynamic feedback system can be brought back to the static output feedback case as follows. Let $\mathbf{G}_a = \{\mathbf{A}_a,\mathbf{B}_a,\mathbf{C}_a,\mathbf{D}_a\}$ represents the actuators transfer function matrix. The coupled transfer function matrix $\{\mathbf{G}_a\cdot\mathcal{K} : \mathbf{y} \rightarrow \mathbf{u}\}$ is given as

$$\mathbf{G}_a \cdot \mathcal{K} = \begin{bmatrix} \mathbf{A}_f & \mathbf{B}_f \\ \mathbf{C}_f & \mathbf{D}_f \end{bmatrix} : \mathbf{A}_f = \mathbf{A}_a,\ \mathbf{B}_f = \mathbf{B}_a\cdot\cdot\mathcal{K},\ \mathbf{C}_f = \mathbf{C}_a \text{ and } \mathbf{D}_f = \mathbf{D}_a\cdot\mathcal{K}. \tag{6.22}$$

Define new states: $\mathbf{u}_f = \dot{\mathbf{x}}_f$ and $\mathbf{y}_f = \mathbf{x}_f$.

$$\begin{Bmatrix} \mathbf{u}_f \\ \mathbf{u} \end{Bmatrix} = \begin{Bmatrix} \dot{\mathbf{x}}_f \\ \mathbf{u} \end{Bmatrix} = \begin{bmatrix} \mathbf{A}_f & \mathbf{B}_f \\ \mathbf{C}_f & \mathbf{D}_f \end{bmatrix} \begin{Bmatrix} \mathbf{x}_f \\ \mathbf{y} \end{Bmatrix} = \begin{bmatrix} \mathbf{A}_f & \mathbf{B}_f \\ \mathbf{C}_f & \mathbf{D}_f \end{bmatrix} \begin{Bmatrix} \mathbf{y}_f \\ \mathbf{y} \end{Bmatrix} = \tilde{\mathcal{K}} \begin{Bmatrix} \mathbf{y}_f \\ \mathbf{y} \end{Bmatrix} \tag{6.23}$$

Then the gain $\tilde{\mathcal{K}}$ matrix is given by (6.22). Its elements are real numbers and hence it is an equivalent static gain controller. An augmented system matrix given by (6.24) can then be constructed comprising the system $\mathbf{G}_p$ and the static gain controller $\tilde{\mathcal{K}}$.

$$\begin{Bmatrix} \dot{\mathbf{x}} \\ \dot{\mathbf{x}}_f \end{Bmatrix} = \begin{bmatrix} \mathbf{A}_p & \mathbf{0} \\ \mathbf{0} & \mathbf{0} \end{bmatrix} \begin{Bmatrix} \mathbf{x} \\ \mathbf{x}_f \end{Bmatrix} + \begin{bmatrix} \mathbf{0} & \mathbf{B}_p \\ \mathbf{I} & \mathbf{0} \end{bmatrix} \begin{Bmatrix} \mathbf{u}_f \\ \mathbf{u} \end{Bmatrix}$$

$$\begin{Bmatrix} \mathbf{y}_f \\ \mathbf{y} \end{Bmatrix} = \begin{bmatrix} \mathbf{0} & \mathbf{I} \\ \mathbf{C}_p & \mathbf{0} \end{bmatrix} \begin{Bmatrix} \mathbf{x} \\ \mathbf{x}_f \end{Bmatrix} + \begin{bmatrix} \mathbf{0} & \mathbf{0} \\ \mathbf{0} & \mathbf{D}_p \end{bmatrix} \begin{Bmatrix} \mathbf{u}_f \\ \mathbf{u} \end{Bmatrix} \tag{6.24}$$

Define input and output variables: $\tilde{\mathbf{u}} = \{\mathbf{u}_f \quad \mathbf{u}\}^T$ and $\tilde{\mathbf{y}} = \{\mathbf{y}_f \quad \mathbf{y}\}^T$. The static output feedback control law becomes $\tilde{\mathbf{u}} = \tilde{\mathcal{K}}\cdot\tilde{\mathbf{y}} + \tilde{\nu}$ where $\tilde{\nu} = [\mathbf{0} \quad \mathbf{I}]^T \nu$. Now substituting the

controller $\mathcal{K}=\mathbf{D}_p^{-1}$ would give a stable closed loop system unlike the previous case. The maximum singular value plot for closed loop and open loop is in Figure 6.12.

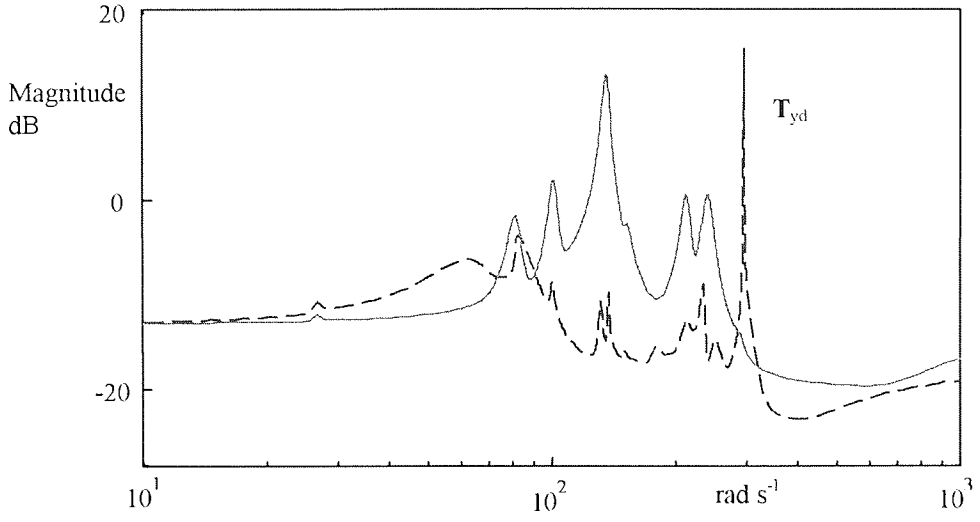

Figure 6.12 Maximum singular values of $\mathbf{G}_p$ and $\mathbf{T}_{yd}$ using $\mathcal{K}=-\mathbf{D}_p^{-1}$

The closed loop system without the weighting function $\mathbf{W}_2$ is now given by $\mathbf{T}_{yd}$. The transmitted disturbance is small over a range of frequency. However the peak of $\overline{\sigma}(\mathbf{T}_{yd})$ in Figure 6.12 means that at this frequency the disturbance is increased. This is undesirable. Such peaks are less likely to occur using the $\mathcal{H}_\infty$ method. The simulated time responses at all the mount locations for 1440 rpm are about the same as that without actuator dynamics. Selecting $\alpha<1$ can reduce the sharp peak at around 300 rad s^{-1}.

The limit on the magnitude of $\mathcal{K}$ is due to the presence of some unstable transmission zeros of the system $\mathbf{G}_p$. The further these are from the origin of the s-plane, the lower is the upper limit of the gain for the system to remain stable. This is obvious from a root locus plots of these two SISO systems with unity feedback. The first system is stable for all values of k whilst the second has an upper limit on k.

$$G(s) = k\frac{s+1}{s+2} \text{ versus } G(s) = k\frac{s-1}{s+2}$$

Although a pair of actuator-sensor is located at each mount location, they are not collocated because a hard mount separates them. This has three implications: (a) as discussed in chapter five, the Reciprocity theorem would not be applicable; (b) it gives

rise to a non-minimum phase system and (c) the system is not strictly proper. The farthest unstable pair of zeros of $\mathbf{G}_p = \mathbf{G}_{12}$ is at 23.1±j290.85. The zeros are as far from the imaginary axis as the complex poles of $\mathbf{G}_p$. Hence this limits the magnitude of $\mathcal{K}$.

The use of a system **D** matrix for the design of $\mathcal{K}$ can be explained by observing that its input is directly available on its output. In this case, the machine disturbance entering via the hard mount into the support structure is measured directly by the sensors. In addition, the sensors also measure the response of the system to the disturbance, and this part of the measurement is given by the dynamics of the system. If the closed loop system is able to make use of such information, and reduce or attenuate the direct disturbance the transmitted disturbance can be reduced.

In general, the use of inverse of **D** is not appropriate for strictly proper systems, i.e. for systems with **D=0**, or for systems with **D** that is not square nor is singular. Even if **D** is square and non-singular this method does not provide an idea about how good the disturbance rejection performance will be in terms of the % increase in damping of some selected closed loop eigenvalues or poles. The most commonly used analytical methods in the literature addressing such an issue are pole placements/assignment (Kimura, 1975) and (Srinathkumar, 1978), and eigenstructure assignment (Alexandrisdis & Paaraskevopoulos, 1996)

For example, in Independent Modal-Space Control, (Meirovitch, 1987), the pole assignment method is used on a set of equation in natural co-ordinates, $\{q_r\}$, in order to change a selected set of eigenvalues but not the eigenfunctions. Closed loop gains can be found by a set of equations to improve the damping or the response decay rates of the selected eigenvalues. Gawronski (1996) defined another set of co-ordinates called the balanced co-ordinates. Under the special case of collocation of sensors and actuators, shows that desired closed loop poles can be achieved using a diagonal controller $\mathcal{K}$ with the diagonal elements given by the vector $\underline{\kappa} = [\kappa_1, \kappa_2, \ldots, \kappa_p]^T$. The controller gain is

$$\underline{\kappa} = \mathbf{H}^{+} \cdot \underline{\delta\beta} \tag{6.25}$$

Where $\mathbf{H}$ is the matrix of the system's Hankel singular values for each actuator and sensor location and $\mathbf{H}^{+}$ is the pseudo-inverse. The vector $\underline{\delta\beta}$ is the desired amount of poles' shifting.

Syrmos, Abdallad, Dorato and Grigoriadis (1997) provided a brief survey and description of these and other analytical methods. They concluded that except for systems with special properties, the output feedback problem is hard to solve analytically and "*that exploitation of the special structure of the particular problem seems to be the only promising approach*", (Syrmos *et al.*, 1997). Some of these special properties include (a) minimum phase system, (b) collocated sensor and actuator i.e. $\mathbf{B}=\mathbf{C}^{T}$ and (c) strictly proper system i.e. $\mathbf{D}=\mathbf{0}$.

Lacking any special structure, a possible approach is to use non-linear optimisation programmes. Syrmos *et al.* (1997) cited the work of Davison (1965) who used such a method to minimise the real part of the dominant eigenvalues of the closed system. As $\mathbf{G}_p$ was used in a performance function in the $\mathcal{H}_\infty$ control design method, it again be used to find a static gain controller $\mathcal{K}$ using static output feedback. A cost function can be defined basing on $\mathbf{T}_{yd} = \mathbf{S}\cdot\mathbf{G}_p$ or on the sensitivity function $\mathbf{S} = (\mathbf{I}+\mathbf{G}_p\cdot\mathbf{G}_a\cdot\mathcal{K})^{-1}$. A search is done to find some $\|\mathcal{K}\|\in[\mathcal{k}_{min},\mathcal{k}_{max}]$ that gives a stable closed loop system and minimises the cost function or satisfies (6.5) i.e. $\overline{\sigma}(\mathbf{T}_{yd}(j\omega)) < \overline{\sigma}(\mathbf{G}_p(j\omega))$ for $\omega\in[\omega_1,\omega_2]$.

Given $\mathbf{G}_p$, whether (6.5) can be realised or not depends on $\overline{\sigma}(\mathbf{S}(j\omega))$. Any peaks in $\overline{\sigma}(\mathbf{S}(j\omega))$ will be reflected in $\overline{\sigma}(\mathbf{T}_{yd}(j\omega))$. Unlike the $\mathcal{H}_\infty$ control design case, ω can be limited to [80, 300] rad s^{-1} as $\overline{\sigma}(\mathbf{G}_p(j\omega))$ is relatively small outside this range. Non-linear optimisation algorithm can be applied to design $\mathcal{K}$, using $\|\mathbf{S}\|_\infty \le \alpha$ as the cost function. The problem is formulated as follows:

Find $\mathcal{K}$ such that $\| \mathbf{S} \|_\infty \le \alpha$;

Subject to

$\omega \in [80, 300]$

$\mathrm{Re}(\lambda_i(\tilde{\mathbf{A}}_p)) < 0$

It is not possible to have $\alpha = 1$ because $\mathcal{K}$ either de-stabilises the system or $\mathcal{K} = \mathbf{0}$ in the defined interval. Furthermore as the magnitude of the actuator dynamics is very small for $\omega \rightarrow 0$, and the band limited identified $\mathbf{G}_p$ becomes small as $\omega \rightarrow 50$ Hz, the singular values of $\mathbf{S}$ approach 1 at these two extremes. So solutions are sought for α arbitrary close to 1 for $\omega \in [80, 300]$ rad s^{-1}.

The approach involves defining the sensitivity function $\mathbf{S}=(\mathbf{I}+\mathbf{G}_p\mathbf{G}_a\mathcal{K})^{-1}$ for each choice of $\mathcal{K}$, and then the closed loop system eigenvalues are calculated to determine if the selected $\mathcal{K}$ gives a stable closed loop system or not. If it does, then the $\mathcal{H}_\infty$ norm of $\mathbf{S}$ is computed. From the set of candidates that produces a stable closed loop system, the candidate that gives the smallest $\| \mathbf{S} \|_\infty \leq \alpha$ within the specified frequency band is selected.

A constraint optimisation algorithm is used to find such a set of $\mathcal{K}$. Due to the different possible values of α and the range of $[\omega_1, \omega_2]$ used, no unique solutions can be found. Different sets of $\mathcal{K}$ are obtained and tested. One of the candidates $\mathcal{K}$ with $\alpha=1.5$ is given as:

$$\mathcal{K}_{optim1} = \begin{bmatrix} 4.4631 & 2.3507 & 1.4059 & 2.4793 \\ 1.6284 & 2.8443 & 1.5641 & 0.3236 \\ 0.0782 & 0.5509 & 2.4353 & 0.8430 \\ 0.0943 & 0.0376 & 0.3506 & 2.2472 \end{bmatrix}$$

The resulting sensitivity function $\mathbf{S}$ is shown on Figure 6.13 followed by a plot of the maximum singular values of $\mathbf{T}_{yd}$ and $\mathbf{G}_p$ in Figure 6.14. It can be observed that $\bar{\sigma}(\mathbf{S}(j\omega))$ is smaller than 1.5, and is almost flat. The resulting maximum singular value of the closed loop force transmissibility matrix, $\mathbf{T}_{yd}$ is lower than the open loop plot over the frequency range specified.

Such an approach will result in a set of $\mathcal{K}$ for actual controller design. For the physical system, some manual adjustments of k_{ij} are required to fine-tune the controller against modelling errors.

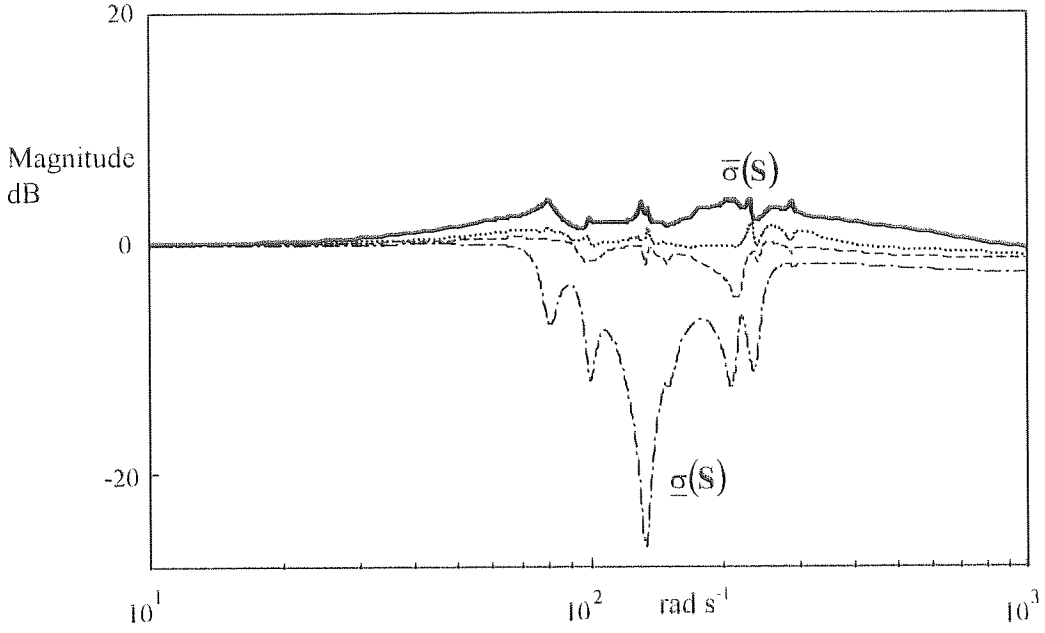

Figure 6.13 Singular values of the sensitivity function S for α=1.5

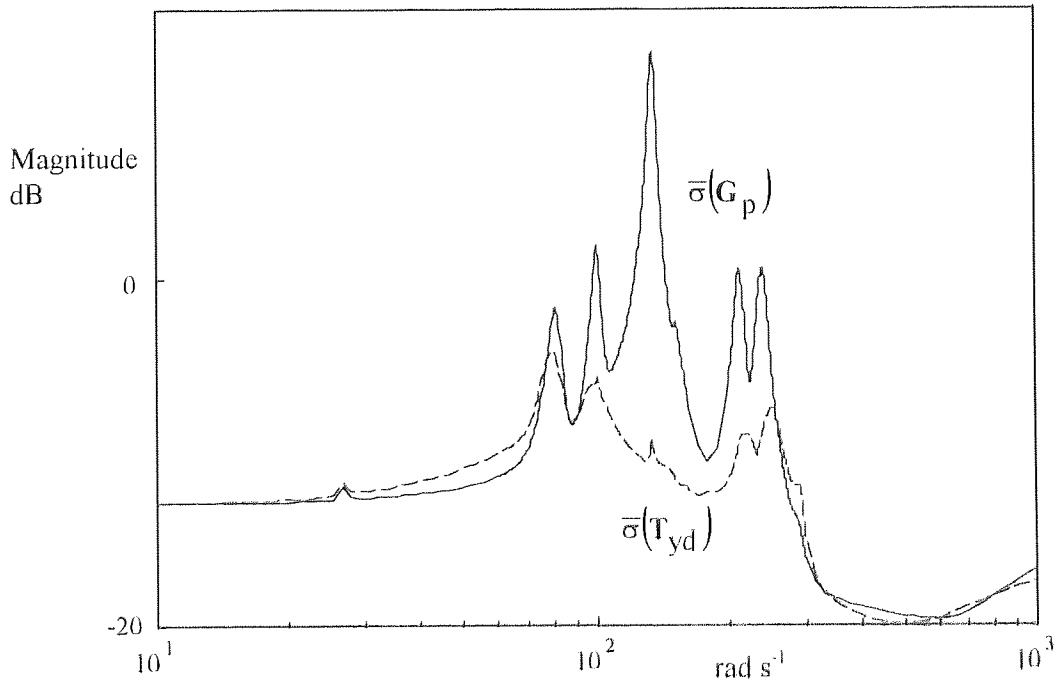

Figure 6.14 Maximum singular value of G_p and T_{yd} using $\mathcal{K}_{optim1}$

6.8 Controller Implementation

The controllers designed above were implemented on a DSP PC-AT bus board. The DSP board has a Texas Instrument's floating point TMS320C32 Digital Signal Processor and 4 Burr Brown 16-bit 100 kHz Analogue to Digital Converters and 4 16-bit 200 kHz Digital to Analogue Converters. The TMS runs on 50 MHz clock cycles. All controllers were implemented with *C*-routines.

Three type controller designs were implemented on the DSP and will be discussed here. These are listed below.

a) $\mathcal{K}_{28}$ is the 28-state controller designed using $\mathbf{G}_{12}$ model and the $\mathcal{H}_\infty$ method.

b) $\mathcal{K}_8$ is the 8-state controller designed using $\mathbf{G}_{154}$ model and the $\mathcal{H}_\infty$ method and subsequently reduce to 8 states.

c) $\mathcal{K}_4$ is a 4x4 static gain controller derived from $\mathcal{K}_{optim1}$ that is designed using the constraint optimisation method.

Both the $\mathcal{K}_{28}$ and the $\mathcal{K}_8$ controllers were designed in the continuous time domain and subsequently discretised by Tustin's transformation to the equivalent discrete time state space controller. Tustin's transformation retains the stability characteristics in both domains and is frequency invariant. Since the controllers were designed using frequency-weighted functions, the frequency invariant property is important to retain the response in the frequency domain (as least for ratio of sampling frequency to bandwidth frequency greater than 10 times). From the frequency plots of the weighting functions used, the system bandwidth is no greater than 50 Hz. Any sampling frequency greater than 500 Hz would preserve frequency invariance of the transformation.

In any discrete implementation of a controller, delay in the control loop invariably exists. This could be due to time for data conversion, computation and memory access time and processor latency. The overall time delay can be minimised and estimated so that a sufficiently high sampling frequency can be maintained. With the $\mathcal{K}_{28}$ and $\mathcal{K}_8$ controller,

matrix access and operations are done using pointers to reduce the time of computation. For the $\mathcal{H}_{28}$ controller which potentially has the longest computation time, a simple clocking function is used in a routine to estimate the delay. The total time for the interrupt routine to read the inputs, scale them as 16-bit data, update the state matrix, compute and scale the outputs, and write the output data is about 750 μs. This includes the Analogue to Digital conversion of about 10 μs per channel. The reciprocal of this delay of 750 μs is 1330 Hz. A sampling frequency of 1 kHz was selected and found to be suitable.

Similar tests were done on the $\mathcal{H}_8$ and $\mathcal{H}_4$. For the $\mathcal{H}_8$, a sampling frequency of 8 kHz was used, and since the computation associated with implementing $\mathcal{H}_4$ static gain controller is much shorter, a sampling frequency of 50 kHz was used.

In addition to the digital controllers, another set of tests was done using analogue controllers. These are phase shifters that can be tuned and were used in a local loop i.e. output from a sensor is fed back only to the actuator at its mount location.

6.9 Experimental Results

The experimental rig used to test the effectiveness of each controller is shown in Photo 5.1 and Photo 5.2. For each controller, the motor was operated at two speeds of the motor: 1340 and 1440 rpm. The control schematic is given in Figure 6.15.

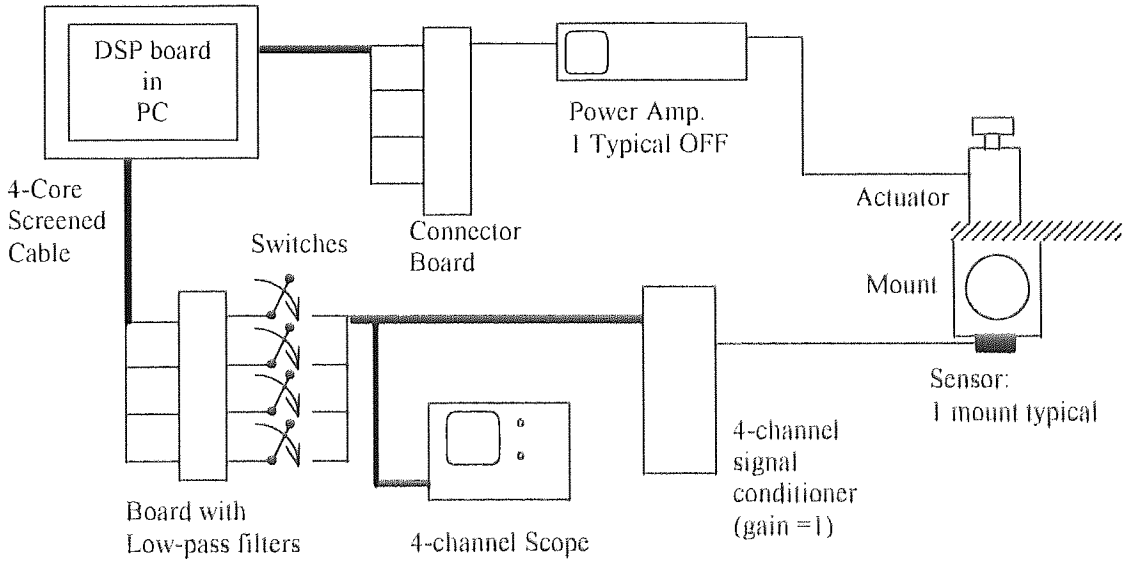

Figure 6.15 Control Loop schematic

Measurements were taken with controller turned OFF and then with controller turned ON. This was done using a bank of 4 toggle switches as shown in Figure 6.15. The controller outputs to each of the four power amplifier driving the respective actuators, and all the quartz force sensors are conditioned with unity gain before being converted and transmitted to the controller. A 4-channel oscilloscope simultaneously records measurements of all channels. However the 4-channel scope makes a sweep using 2 channels at a time. Most of the measurements on the oscilloscope is transmitted to a PC as HP Bench Link files and converted either to bit map files or to data image files.

6.9.1 Experimental results using the $\mathcal{K}_{28}$ controller.

The results are shown in Figures 6.16 and 6.17. Figure 6.16 shows that the $\mathcal{K}_{28}$ controller is very effective in attenuating disturbances at all mount locations for motor operating at 1340 rpm. At 1440 rpm, from Figure 6.17, a small degree of attenuation is observed at only two locations. This better performance at 1340 rpm is predicted by the simulation result of Figure 6.4 where the difference between $\bar{\sigma}(\mathbf{G}_p(j\omega))$ of the open loop system and $\bar{\sigma}(\mathbf{T}_{zd}(j\omega))$ of the controlled closed loop system is greater at 1340 rpm than at 1440 rpm. For 1340 rpm, this reduction is from 1.8 to 0.4 i.e. about 78% and is reflected at all four mount locations. At 1440 rpm, it is from about 0.7 to 0.3 i.e. 50%, but this is not reflected at all the mount locations except at mount #3, and very little at mount #2.

On examination of the measured signals (with control action turned OFF), it is observed that for the motor running at 1320 rpm, for example, the principal motor disturbance components at 22 Hz and 33 Hz are dominant; at 1340 rpm, only the 22.3 Hz is dominant. Since $\mathcal{K}_{28}$ is designed for the plant up to 50 Hz, it is quite effective in attenuating these disturbances. With the motor running at 1440 rpm, the plate on the supporting structure responds much more than at 1340 rpm. Frequencies higher than 50 Hz have amplitudes larger than that measured when it was running at 1340 rpm. The $\mathbf{G}_{12}$ model neglects resonant frequency beyond 40 Hz. The $\mathcal{K}_{28}$ controller is not effective to disturbance beyond 40 Hz. More significantly is the fact the system model was not identified with the motor running at 1440 rpm, in which case the entire disturbance spectra will be identified. Instead the system model was identified with the motor shaft stationary and a simulated spectrum of the machine disturbance was injected at each mount location.

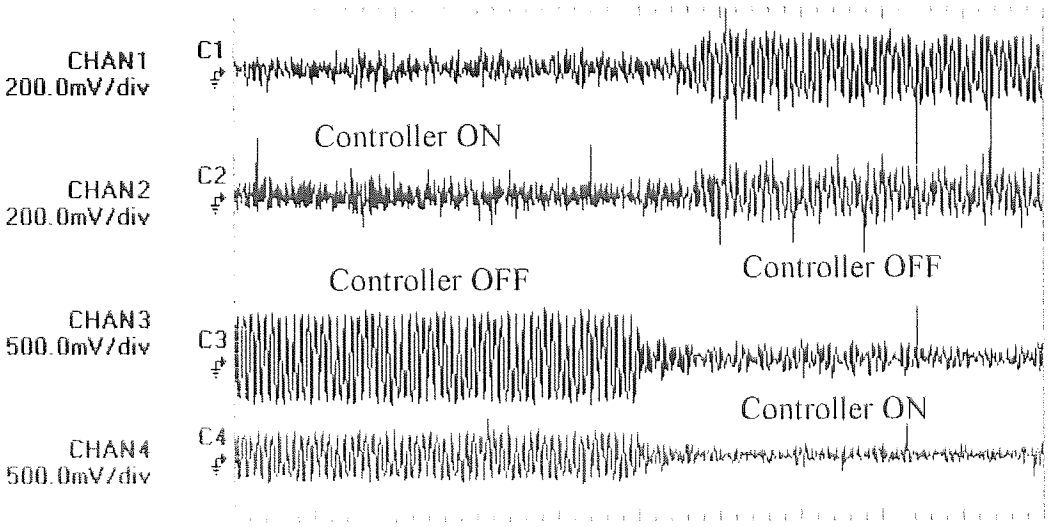

Figure 6.16 Responses using $\mathcal{K}_{28}$ for motor running at 1340 rpm

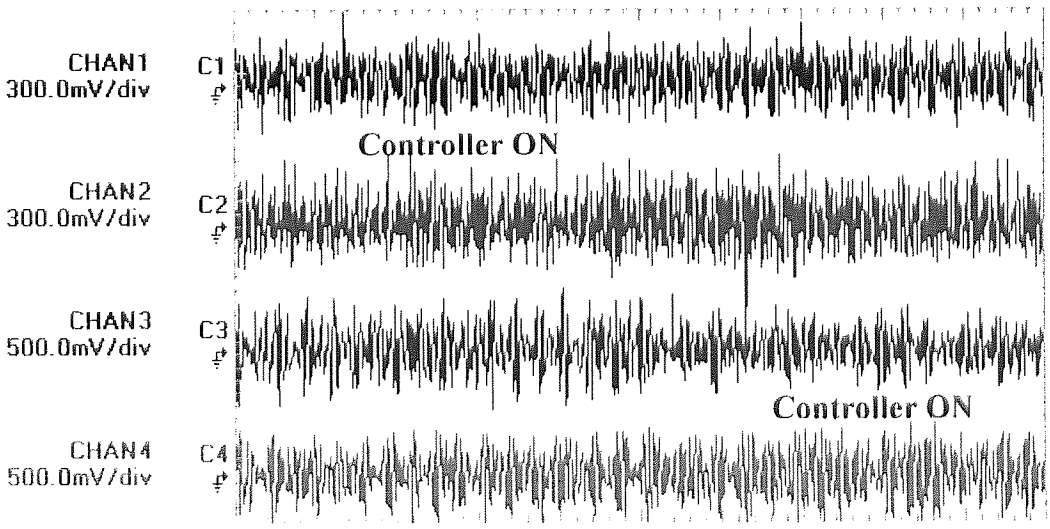

Figure 6.17 Responses using $\mathcal{K}_{28}$ for motor running at 1440 rpm

Hence the weakness is in the model representation of the system for the case when the motor is operating at 1440 rpm rather than in the design method itself. Nevertheless, this same model gives a $\mathcal{K}_{28}$ controller that is effective for motor running at 1340 rpm.

Robust controllers can be designed to take into account the effect of the neglected dynamics by including a model of higher frequency dynamics as unstructured uncertainty. Including the model of the uncertainty will result in a higher order controller model, and reduce the sampling frequency. This is discussed in detail below.

6.9.2 Experimental results using the $\mathcal{K}_8$ controller

The controller routine is essentially the same, but sampling frequency can be increased to 8000 Hz with fewer states to compute. Figures 6.18 and 6.19 respectively show the responses for motor speed at 1300 and 1340 rpm. These are no better than obtained using the $\mathcal{K}_{28}$. Performance or disturbances rejection when the motor is running at 1440 rpm is not better than that of $\mathcal{K}_{28}$. As G_{154}, which is used in the design of $\mathcal{K}_8$, itself is poorly fitted beyond 40 Hz, it may be unrealistic to expect $\mathcal{K}_8$ to work better. The main advantage of using the $\mathcal{K}_8$ lies only in the reduction in computational time allowing for a higher sampling speed.

6.9.3 Experimental Results using the $\mathcal{K}_{optim1}$ and the $\mathcal{K}_4$ controller

The controller routine for $\mathcal{K}_{optim1}$ is much simpler than the $\mathcal{K}_{28}$. One can ignore the use of pointers, and input and output scaling, and use a higher sampling frequency. The value of $\mathcal{K}_{optim1}$ is given again below as:

$$\mathcal{K}_{optim1} = \begin{bmatrix} 4.4631 & 2.3507 & 1.4059 & 2.4793 \\ 1.6284 & 2.8443 & 1.5641 & 0.3236 \\ 0.0782 & 0.5509 & 2.4353 & 0.8430 \\ 0.0943 & 0.0376 & 0.3506 & 2.2472 \end{bmatrix}$$

The k_{1j} values or the first row are relatively "higher" as the model underestimated the magnitude of the response of mount #1, and to some extent mount #2.

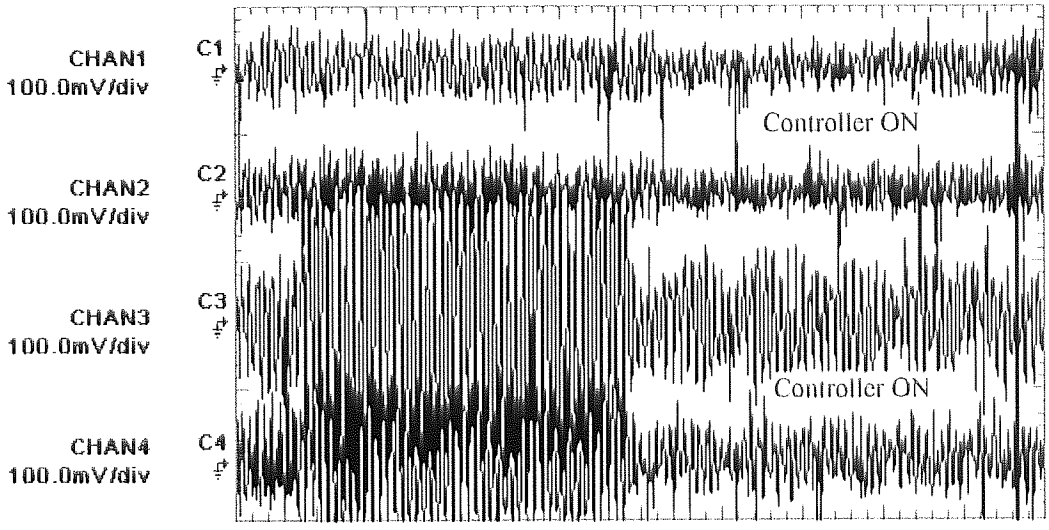

Figure 6.18 Responses using $\mathcal{K}_8$ for motor running at 1300 rpm

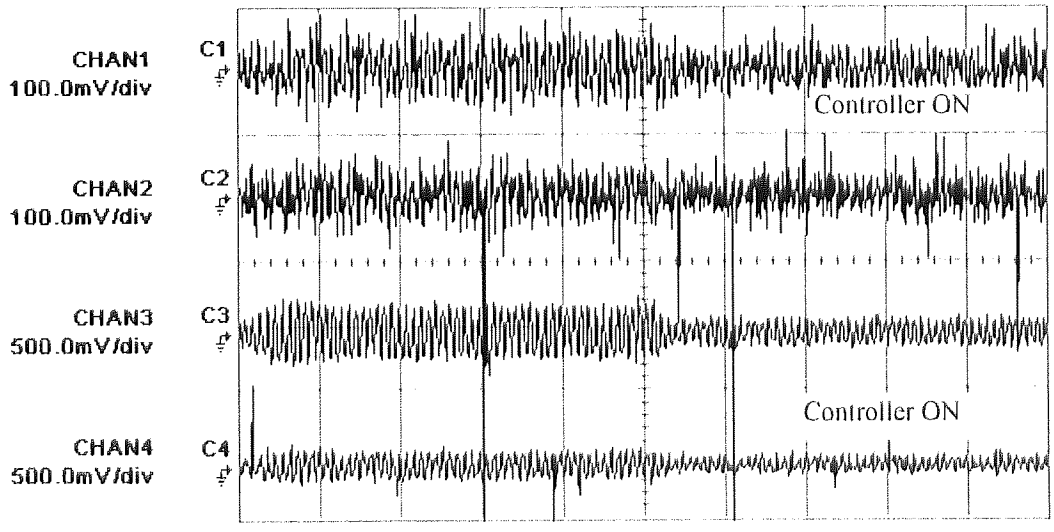

Figure 6.19 Responses using $\mathcal{K}_8$ for motor running at 1340 rpm.

Hence on implementing this controller, the response at mount #1 is much higher than required and the system becomes unstable. Subsequently, the values of row 1 are modified, with k_{12} and k_{13} set to zero. The other k_{1j} values are set to nearest integer values.

After a series of manual tuning, the resulting $\mathcal{K}_4$ controller is given by:

$$\mathcal{K}_4 = \begin{bmatrix} 5 & 0 & 0 & 3 \\ 1 & 3 & 3 & 0 \\ 0 & 0 & 3 & 0 \\ 0 & 0 & 0 & 3 \end{bmatrix}$$

The diagonal values are quite close to the $\mathcal{K}_{optim1}$. On analysing the closed loop performance, the maximum singular value plot is much better than that obtained using $\mathcal{K}_{28}$ and is about as good as $\mathcal{K}_{optim1}$ as shown in Figure 6.20 below.

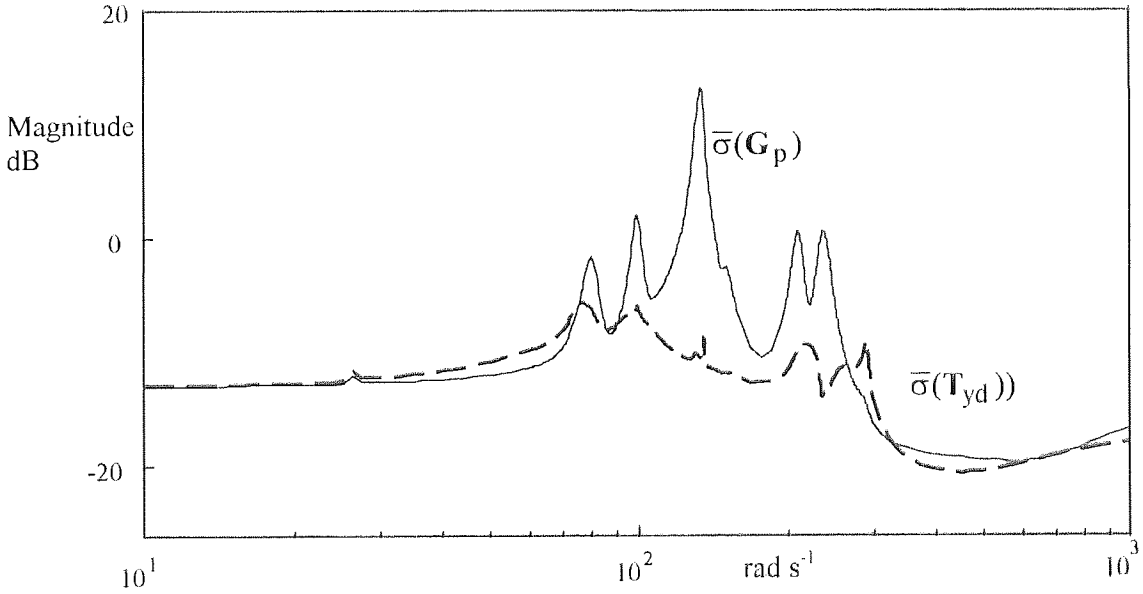

Figure 6.20 Maximum singular values of $\mathbf{G}_p$ and $\mathbf{T}_{yd}$ using $\mathcal{K}_4$

The time for computation is further reduced with some zeros in $\mathcal{K}_4$. The sampling frequency could be as high as 50 kHz. The results for the two operating speeds are given in Figure 6.21. As with the other controllers, the $\mathcal{K}_4$ is more effective for motor operating at 1340 rpm than at 1440 rpm. Unlike the $\mathcal{K}_{28}$, it is able to attenuate disturbance for motor running at 1440 rpm.

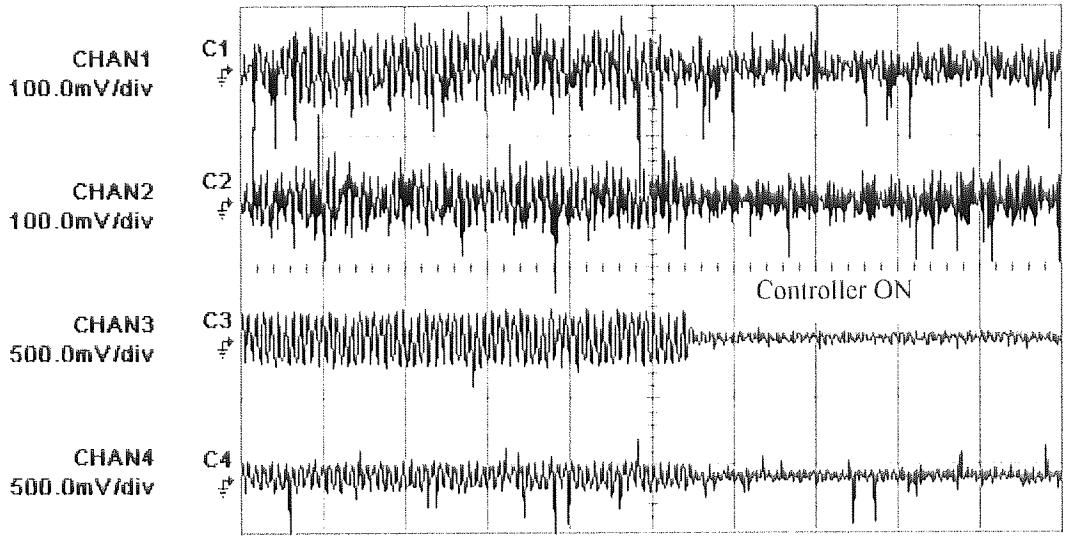

Motor running at 1340 rpm

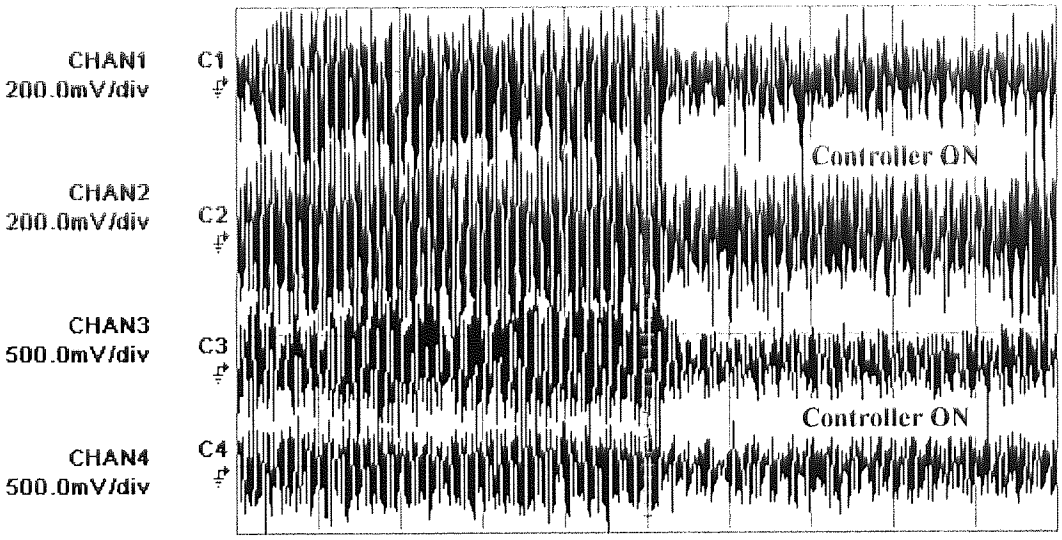

Motor running at 1440 rpm

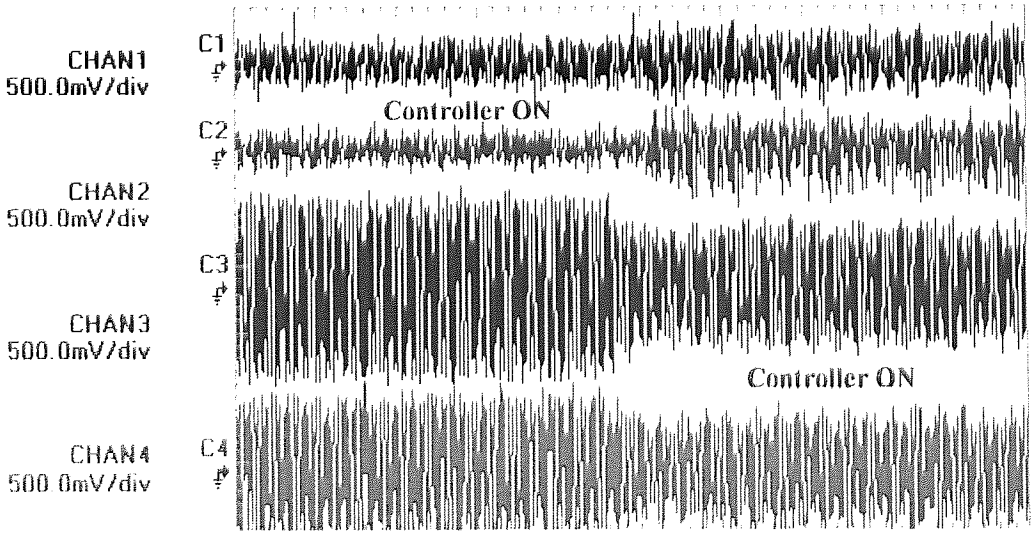

Motor running at 1700 rpm

Figure 6.21 Responses using $\mathcal{K}_4$ for various speed

When tested at motor speed of 1700 rpm, there is still attenuation although less effective. It is slightly more robust than the others are. Hence it is observed that the $\mathcal{K}_4$ (indirectly) designed from static output feedback gives better results than that designed from the $\mathcal{H}_\infty$ method. It has a much lower order too.

6.10 Discussions

It should be noted that the model $\mathbf{G}_p$, used for the controller designs is valid only for a frequency range up to 40 Hz and with the motor not operating. Beyond that frequency, the model is not representative of the real system. Furthermore, $\mathbf{G}_p$ is itself an element of a set of possible representation $\mathcal{S}$ of the true system. And it therefore has degree of uncertainty even within the frequency range for which the estimation is made. This uncertainty can be reduced but not totally removed. For example, using a stiffer and more damped structure and removing the plate that was artificially introduced in the experiment. The uncertainty can also be quantified by means of some function bound and be included in the model. Of the two methods described above, the $\mathcal{H}_\infty$ method has a formal structure that can include a model of the uncertainty in the design of a robust controller. To account for neglected higher frequency dynamics, model identification using an input with an upper frequency limit of 1000 Hz (beyond this value, the response of the plant starts to roll off) has to be done. The neglected dynamics can then be modelled by frequency response function covering the part of the plant response being ignored. An example of such approach is given by Balas *et al* (1992). The reason for not attempting to use such an approach is that the resulting uncertainty model Δ will be a full 4x4 complex block adding at least 64 states (assuming at least 4 states that will added by each δ_{ij} of Δ) to the nominal generalised plant $\mathcal{P}$. The use of the D-K iteration to solve the resulting structure singular value problem can be quite involved for practical applications. The order of the controller will be higher.

The selection of weights for the design of the $\mathcal{H}_\infty$ controllers requires much effort. If weighting functions are applied to all of the 16 transfer functions, the order of the controller will be very high. Hence in spite of the fact that $\mathbf{G}_p = \mathbf{G}_{12}$ or $\mathbf{G}_{154}$ is not diagonal dominance, the first step involves the use of a single weighting function based on $\bar{\sigma}(\mathbf{G}_p(j\omega))$. The best that was attempted was to apply weighting functions to g_{ii} of $\mathbf{G}_{12}$.

In the end, it is found that the simplest case of selecting a single weighting function based on $\bar{\sigma}(\mathbf{G}_p(j\omega))$ is more effective. However, the one selected may not be the best as there is no way to test this except to search over a large set of w_{ii} for $\mathbf{W}_2$.

Numerical results for the $\mathcal{H}_\infty$ designed controllers $\mathcal{K}_{28}$ and $\mathcal{K}_8$ are given in Table 6.2

	Mount #1 RMS values		Mount #2 RMS values		Mount #3 RMS values		Mount #4 RMS values	
	Control OFF	Control ON	Control OFF	Control ON	Control OFF	Control ON	Control OFF	Control ON
$\mathcal{K}_{28}$	0.065	0.033	0.046	0.038	0.179	0.058	0.101	0.050
	49.7%		17.1%		67.8%		50.2%	
$\mathcal{K}_8$	0.034	0.026	0.039	0.036	0.144	0.068	0.074	0.048
	21.0%		7.7%		52.9%		35.3%	

Table 6.2 Results of $\mathcal{K}_{28}$ and $\mathcal{K}_8$ at the four mounts for motor speed of 1340 rpm

These values are taken over a time interval of the measured signals. The % reduction from uncontrolled to controlled are all shown as positive numbers. Between $\mathcal{K}_8$ and $\mathcal{K}_{28}$, the latter provides higher overall attenuation at all locations at motor speed of between 1320 and 1340 rpm. An average reduction of 50% is achieved for all locations. At 1440 rpm the $\mathcal{H}_\infty$ designed controllers are not so effective as already explained in §6.9.1.

On the other hand, the static output feedback provides a more direct and less involved solution although there is no way to prove or ascertain robustness analytically. It also is easier to tune the elements of $\mathcal{K}_{optim1}$ using some knowledge about the response of the model in relation to the actual responses.

Results for the static output feedback controller $\mathcal{K}_4$ are shown in Table 6.3. A more uniform performance with about 50% attenuation achieved in terms of RMS values at 1440 rpm is observed. This is in spite of having signals higher than 50 Hz in the measured disturbance spectrum. At about 1340 rpm, $\mathcal{K}_4$ is as good as $\mathcal{K}_{28}$ at three locations but has a higher attenuation at location #3.

	Mount #1 RMS values		Mount #2 RMS values		Mount #3 RMS values		Mount #4 RMS values	
	Control OFF	Control ON	Control OFF	Control ON	Control OFF	Control ON	Control OFF	Control ON
1340	0.0331	0.0227	0.0285	0.0196	0.1347	0.0241	0.0772	0.0431
	31.5%		31.3%		82.1%		44.2%	
1440	0.162	0.075	0.178	0.102	0.284	0.143	0.206	0.139
	54.1%		42.5%		49.4%		32.5%	

Table 6.3 Results of $\mathcal{K}_4$ at two speeds for the four mounting locations.

The better performance of the Static Output Feedback controller $\mathcal{K}_4$ at 1440 rpm compared with the $\mathcal{K}_{28}$ is also shown by the simulation results.

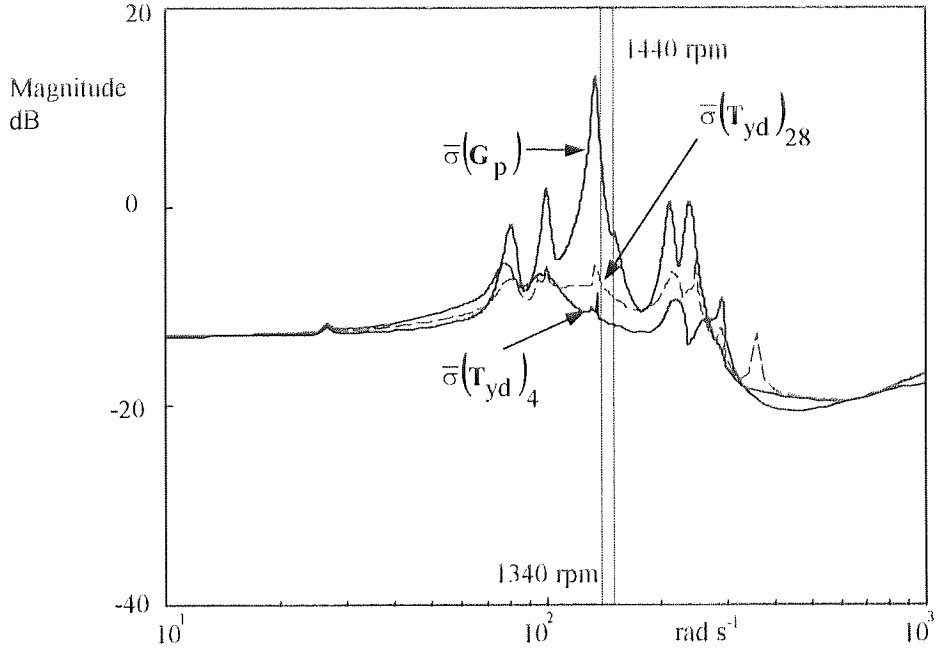

Figure 6.22 Maximum singular values of G_p, $(T_{yd})_4$ for $\mathcal{K}_4$ and $(T_{yd})_{28}$ for $\mathcal{K}_{28}$

Figure 6.22 shows plots of $\bar{\sigma}(T_{yd}(j\omega))$ of $\mathcal{K}_{28}$ and $\mathcal{K}_4$ against $\bar{\sigma}(G_p(j\omega))$. It shows that there is a greater reduction using the $\mathcal{K}_4$ compared with the $\mathcal{K}_{28}$ controller at both 1340 and 1440 rpm. However, the predicted better performance by $\mathcal{K}_4$ is observed only for 1440 rpm. At 1340 rpm both controllers have an average RMS reduction of about 46%.

It is assumed, here, that the actuators are rigidly attached and hence the disturbance model and the plant model can be the same. The actuator model is then identified separately. Otherwise it would be necessary to determine $\mathbf{G}$ as the transfer function matrix from actuator command to measured output and $\mathbf{G}_p$ as the transfer function matrix from machine disturbance to measured output. As discussed in chapter five, with $\mathbf{G} \approx \mathbf{G}_p \cdot \mathbf{G}_a$ $\mathbf{G}_p$ and $\mathbf{G}_a$ can be determined separately. This requires less data collection and processing. It also suits the use of static output feedback design. A suitable set of static gain controllers can be found using some search optimisation routine basing on $\mathbf{G}_p$. The $\bar{\sigma}(\mathbf{S}(j\omega))$ plot obtained is flatter than that obtained using the $\mathcal{K}_8$ or the $\mathcal{K}_{28}$ over the selected interval and hence the resulting $\bar{\sigma}(\mathbf{T}_{yd}(j\omega))$ has fewer and smaller peaks. The hard work is in the tuning the controller. However once it is tuned, the $\mathcal{K}_4$ controller is able to function quite consistently even with the motor running intermittently daily.

Although the results show that $\mathcal{K}_4$ is the preferred controller, it is not the intention of this thesis to conclude that all static gain controllers using static output feedback are better than $\mathcal{H}_\infty$ controllers are. There are no theoretical justifications to support such a conclusion. It could that the performance weighting functions used in the $\mathcal{H}_\infty$ design is not ideal.

The performance of all the controllers presented here can be compared with the results obtained by others in similar type of applications. For example, Dyke *et al.* (1994), using acceleration feedback control strategies for an m-DoF, 10-state structure, achieved an average of 60% reduction in RMS values for band limited white noise excitation. This is higher than what is currently achieved. However, tower-like truss structures typically have well defined poles-zeros pattern and hence well separated resonant and anti-resonant peaks.

In other studies, effectiveness is given in terms of peak reduction of chosen natural frequencies. Consider the spectrum of the signals at mount #3 for controller OFF and ON shown on Figure 6.23 for $\mathcal{K}_{28}$, Figure 6.24 for $\mathcal{K}_8$ and Figure 6.25 and Figure 6.26 for $\mathcal{K}_4$. An average of 10 to 15 dB reductions can be achieved for frequencies below 50 Hz. From Figure 6.25, the $\mathcal{K}_4$ gives the largest attenuation of 30 dB at the peak frequency of about 22 Hz.

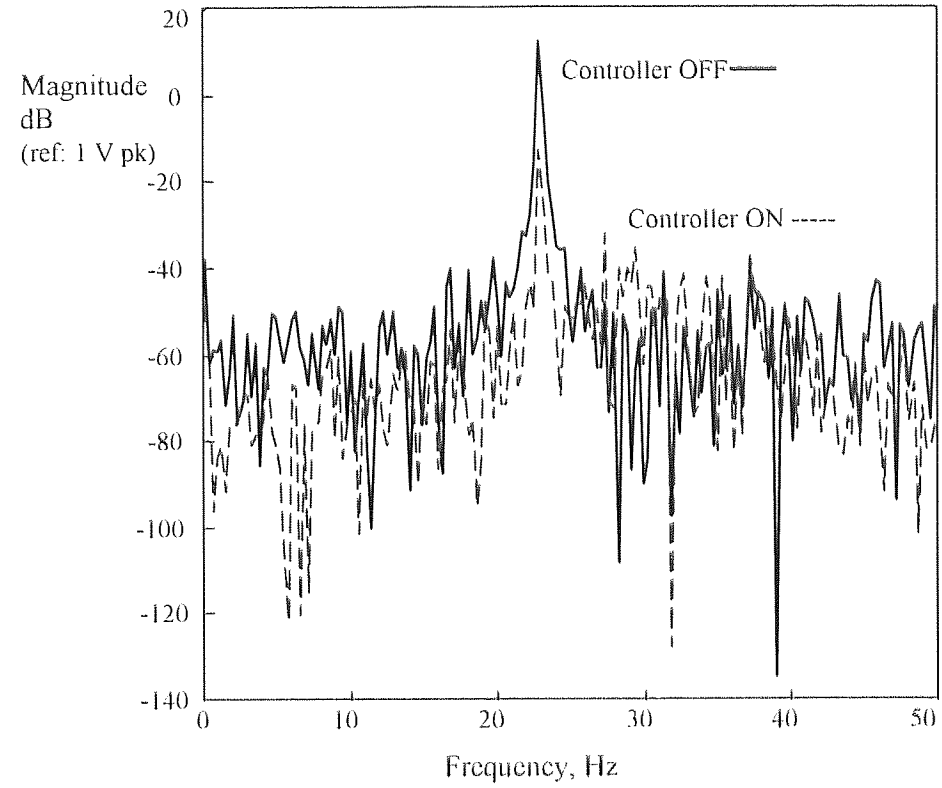

Figure 6.23 Power spectrum of mount #3 using $\mathcal{K}_{28}$ at 1340 rpm

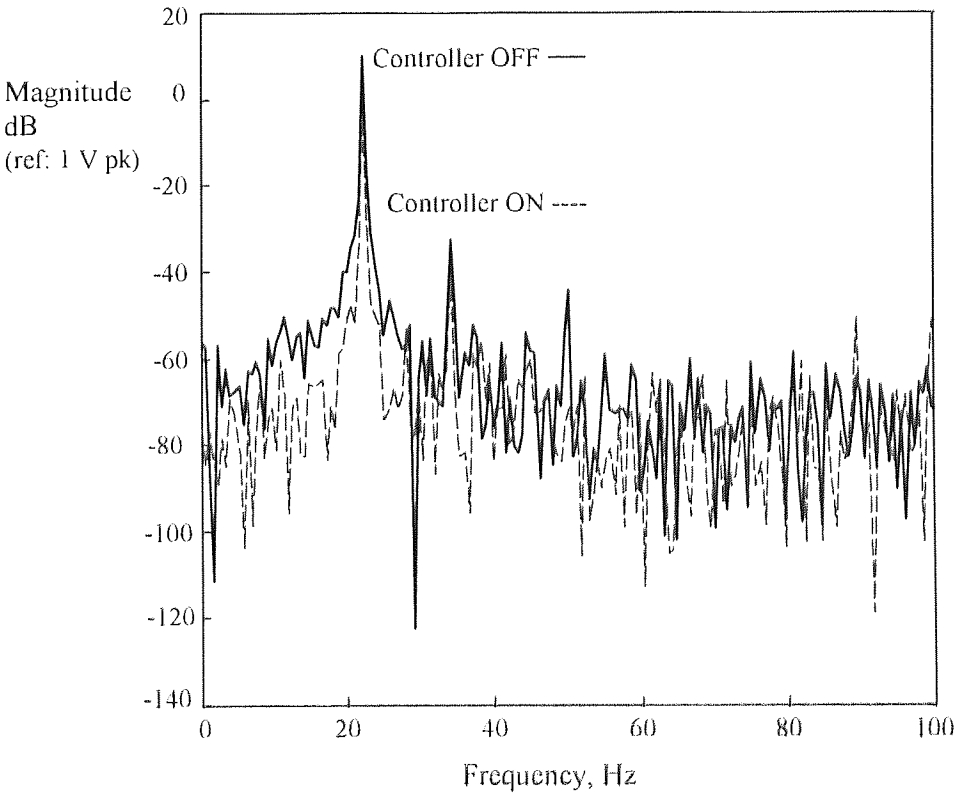

Figure 6.24 Power spectrum of mount #3 using $\mathcal{K}_8$ for 1320 rpm

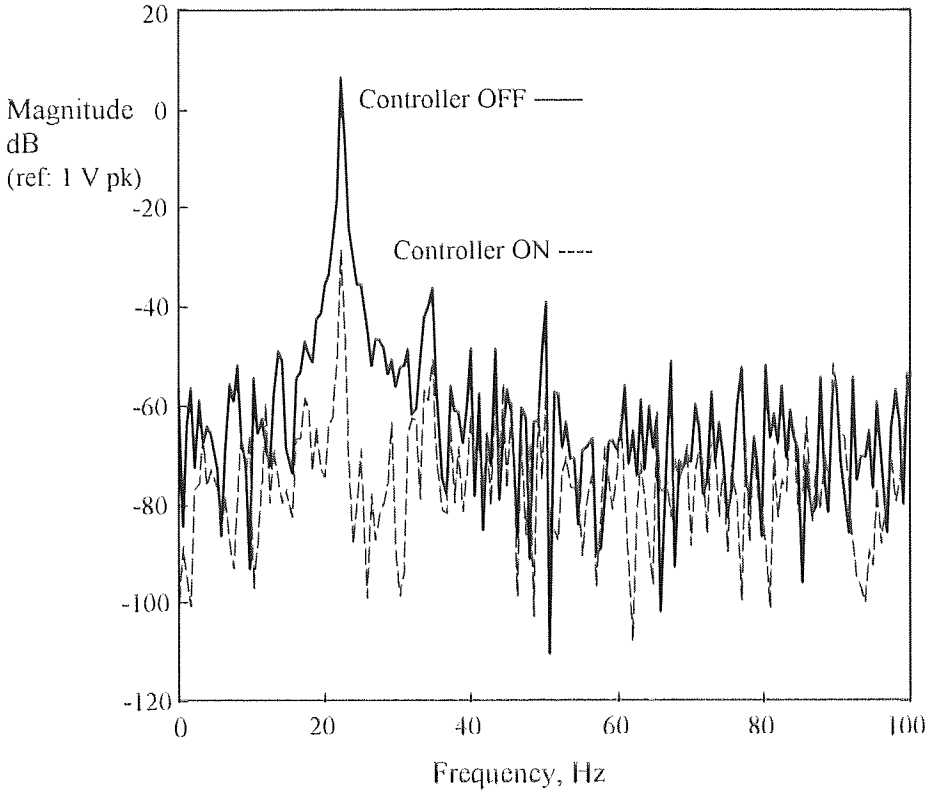

Figure 6.25 Power spectrum of mount #3 using $\mathcal{K}_4$ at 1320 rpm

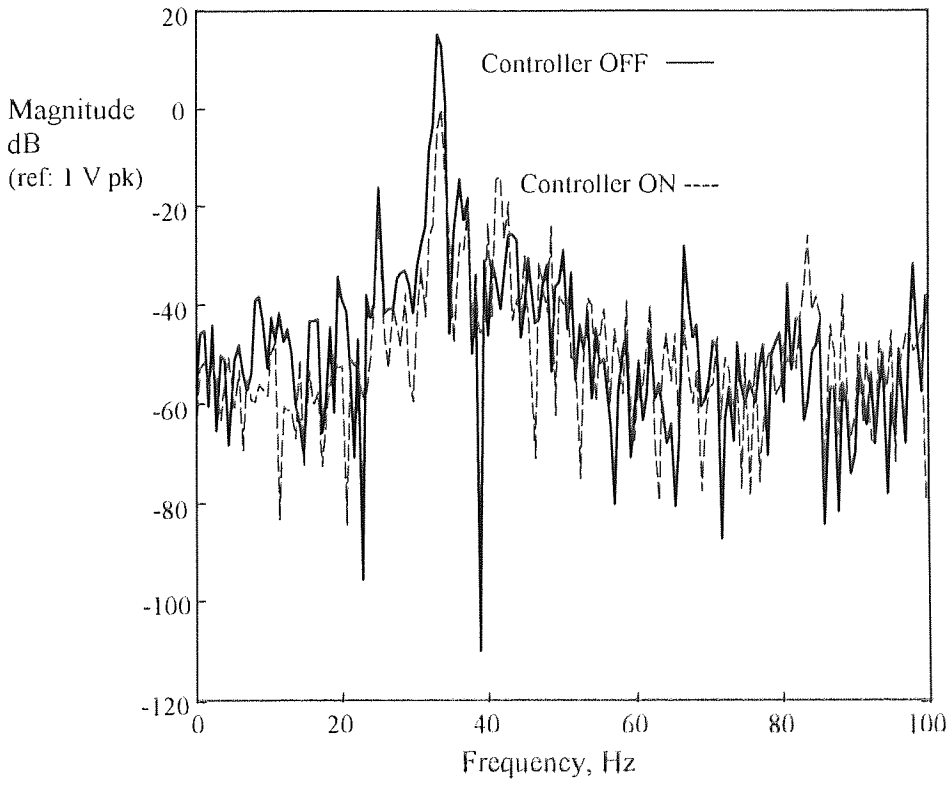

Figure 6.26 Power spectrum of mount #3 using $\mathcal{K}_4$ at 1440 rpm

This is better than that achieved by Tanaka and Kikushima (1988) who managed a 10 dB reduction in the transmitted force over a frequency range of 2 to 20 Hz on a forge hammer. For machine vibration, Watters *et al.*, (1988) using force feedback achieved a 20 dB uniform broadband reduction for a single active mount of a ship diesel engine. Spanos *et al.* (1993) managed a good 40 dB improvement (at the natural frequencies) on a flexible structure using nine second-order filters. In both works by Watters and Spanos, the actuator is installed in parallel with a passive isolator to control a single output. In comparison with motion feedback, the results are quite compatible with that achieved at a single location on the car body frame (15 to 30 dB) by Shoureshi and Knurek, (1996) using active engine mounts.

One of the limiting factors in getting performance from the controllers discussed here is the available actuator force. The inertia mass that can be added is a compromise between the inertia force to be provided and the stroke length of the movable mass in the actuator. The higher the inertia mass used, the greater is the static deflection and the shorter is the available stroke length. This means that the high acceleration specified for the actuator cannot be attained, and the maximum force generated is still limited. The highest force obtained is 10 N compared with the specified maximum of 18 N. The experiment was performed without any load attached to the motor. If a pulley were to be attached to the shaft, the magnitude of the disturbance force to be cancelled will be higher. Obviously a larger actuator will be needed.

6.11 Analogue controllers

It is useful to compare the performance of the digital implementation of the controller with that of analogue controllers. Four phase shifters were built and each is used as a SISO controller for each mount sensor and actuator pair. At motor operating speed of 1340 rpm and below, they perform better than the digital controllers do. This is because the phase of each circuit has been adjusted to drive the actuator in anti-phase to the respective measured signal at 1340 rpm. At this speed, only the 22.3 Hz is dominant.

When the motor speed is increased to 1440 rpm and if the phase shift of each controller was not adjusted, the attenuation is marginal - hardly perceptible except when viewed in the frequency domain. As with previous experiments with the $\mathcal{Z}_{2R}$ and the $\mathcal{Z}_{R}$, the

transmitted spectrum contains other frequency components with different phase angles. The circuit and the results are shown in Appendix E.

The analogue controllers provided only narrow band vibration isolation unless it is re-tuned. So phase readjustment of each controller was necessary, but with the forces at each mount affecting the other mounts, tuning of all the controllers was relatively difficult. Figure 6.27 shows the result of mount location #4 with only controller at location #4 re-tuned. When the controller is turned ON, there is about 50 % reduction in the peak amplitude. However, the attenuation at other mount locations did not increase.

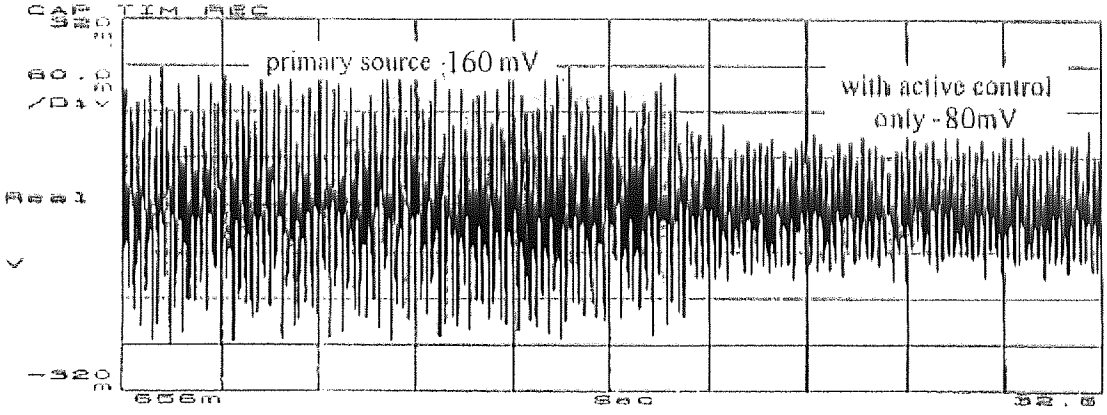

Figure 6.27 Active (analogue controller) at mount #4 for motor at 1440 rpm

6.12 "Hybrid" implementation - the use of thermoplastic material as a passive element

By combining active control with a (passive) damping material - hybrid control - a higher degree of vibration isolation should be achievable (Beard *et al.*, 1994). In addition it had been shown by Sievers *et al.* (1990) that closed loop relative stability could be improved using soft mounts (with damping) in series with hard mounts.

A hybrid approach was attempted for motor speed of 1440 rpm at mount location #4. A 3 mm piece of damping material (ISODAMP C-1000 series) was sandwiched between the motor base plate and hard mount #4. This material composed of energy absorbing thermoplastic alloys with a loss factor of about 0.9 at 24 Hz and 30 °C.

Figure 6.27 shows an average amplitude value of about 160 mV with the controller turned OFF. With the thermoplastic material inserted, this is reduced to about 80 mV as shown in Figure 6.28 giving a reduction of 50% in the vibration measured even without active control. When the controller is activated, another 50% reduction is further achieved. Hence the hybrid system comprising the thermoplastic material and the active controller achieved about 75 % reduction in the peak amplitude.

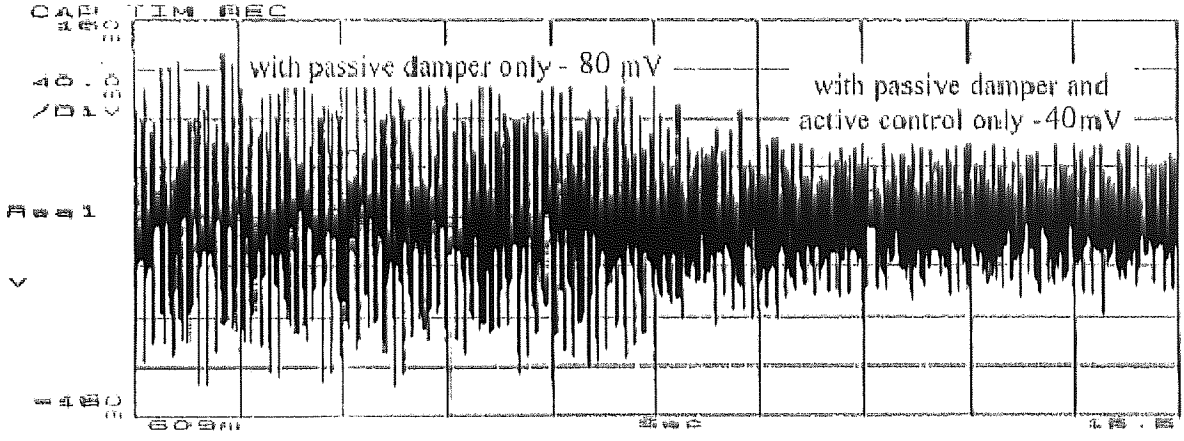

Figure 6.28 Active plus passive element at mount #4 for motor at 1440 rpm

The thermoplastic material provides some element of soft "spring" in series with a hard mount. It can also be used to reduce shear force transmission onto the mount.

6.13 Summary

The methods and their theory for the design of suitable controllers have been briefly presented. The results of the implementation of three selected controllers were given and the effectiveness of each was discussed. The static gain controller turned out to be more effective in general than the two types of $\mathcal{H}_\infty$ controllers designed. It is able to attenuate (between 32 and 54%) the force measured at the base when the motor is running at its rated speed of 1440 rpm. The $\mathcal{H}_\infty$ controllers were less effective. Between 1300 and 1340 rpm, all three types of controllers are very effective and the order of effectiveness is: $\mathcal{K}_4$, $\mathcal{K}_{28}$ and $\mathcal{K}_8$. And for all cases, mount location #3 is the most (output) controllable.

One outcome of the experiment is the demonstration that simple design such as a gain controller using static output feedback is quite as effective. However, it lacks any formal

structure to analyse for stability. It has been showed that instead of using eigenvalues as performance specifications, it is possible to use frequency dependent function as a cost function in an optimisation routine to obtain a controller design. In both cases, a model of the system is needed and "brute force" approach is used to determine if the controller is stabilising or not by checking the eigenvalues of the closed loop system. The implementation is simpler and avoids the limitation imposed by sampling limit on the performance of the $\mathcal{H}_\infty$ controllers on a DSP board. Different static gain values have been also tried. As long as the structure of the controller remains similar to the $\mathcal{K}_4$ presented above (but with different values) the results are about the same. They differ only in the improvements at different mount locations. However, no formal proof has been given nor attempted to show that the static output feedback approach in general gives a better performance in rejecting disturbance than that of the $\mathcal{H}_\infty$ method.

The $\mathcal{H}_\infty$ method has a very formal structure for analysis of stability and performance. The design goal of reducing the system RMS gain can be related to the goal of reducing the RMS values of the transmitted disturbance at each mount location and has been shown to be a minimisation problem that can solved using the $\mathcal{H}_\infty$ method. The disturbances need not be well defined except that the RMS of the vector of disturbances at all mount locations is to be bounded. The framework also provides the means to predict if an internally stabilising controller can be found that will minimise the system RMS gain value. The simulation result is able to predict quite well the relative overall performance at various motor speeds but not the performance at individual mount location. The existence of the formal structure and analytical framework are the primary reasons for experimenting with the $\mathcal{H}_\infty$ controllers.

In all cases considered, there is, however, a limitation imposed by the actuator. The small travel range and the mass of the inertia element will limit the amount of active force cancellation. Once again this constraint can be formulated in the design of the $\mathcal{H}_\infty$ controllers, something which the SOF method discussed in this chapter cannot.

CHAPTER SEVEN

CONCLUSION AND RECOMMENDATIONS

7.1 Conclusion

The test results in Chapter six show that vibration control of transmitted vibration from machine hard-mounted to a supporting structure is possible using active force cancellation at the feet of the machine. This involves measuring the net transmitted force between the bottom of a mount and the structure and applying inertia forces opposite to the disturbing forces. With the responses at each of the mount location being coupled to one another, direct local feedback to the actuator from the same mount sensor location itself is not effective. So non-diagonal controllers are needed. Two types of non-diagonal controllers are used: (a) dynamic compensators, $\mathcal{K}_{28}$, and $\mathcal{K}_8$ designed from $\mathcal{H}_\infty$ method and (b) static gain controller, $\mathcal{K}_4$, using Static Output Feedback. Both types are implemented on a digital signal processor.

Between these two types of controllers, it is found that the static gain controller performed better than the $\mathcal{H}_\infty$ controller at the machine rated speed of 1440 rpm. Both controllers are equally effective at speeds at and below 1340 rpm. For the $\mathcal{K}_{28}$, starting from 1340 rpm, the effectiveness of the attenuation deteriorates in varying degree amongst the various mounting locations until at 1440 rpm there is no attenuation of the disturbances at all mounting locations. This can be attributed to the presence of disturbances with frequencies higher than the frequency range used to estimate the model. Since the uncertainty pertaining to disturbances beyond the range is not incorporated in the model, it is not expected that $\mathcal{H}_\infty$ method will be capable of providing a design that is robust to the higher frequency disturbances. A possible alternative is to incorporate frequency-weighted functions to model the higher frequency response and use the μ-synthesis method. The order of the generalised model is already relatively high - 12 states plus 8 states due to the actuators and 8 states due to the performance weighting function $\mathbf{W}_2$. The use of μ-synthesis method will result in controller model of even higher order.

There are two ways in which the $\mathcal{H}_\infty$ controller design method can be used. A set of internally stabilising controllers, $\mathcal{K}_{170s}$, can be designed using the full $\mathbf{G}_p = \mathbf{G}_{154}$ and a suitable $\mathcal{K}_{170}$ can be reduced by for example balanced residualisation method to a $\mathcal{K}_8$ controller. The design of $\mathcal{K}_{170s}$ should be done using different weighting functions, w_{ij} for the respective transfer functions, g_{ij}, of the system. More appropriately, the $\mathbf{G}_{12}$ model

should be used in the controller design to obtain a set of $\mathcal{K}_{28}$ controllers. It is prudent to check that a selected, $\mathcal{K}_{28}$, controller obtained from a suitable $\mathbf{W}_2$ function also stabilises the $\mathbf{G}_{154}$ model. With $\mathbf{G}_p = \mathbf{G}_{12}$, there is no advantage in trying to select different weighting functions, w_{ij} for the respective transfer functions, g_{ij}, of the system as some of the designed $\mathcal{K}_{28s}$ may not stabilise $\mathbf{G}_{154}$ model. It would simpler and more efficient to design using a single w (i.e. $\mathbf{W}_2 = w \cdot \mathbf{I}$) as a specification basing on the $\bar{\sigma}(\mathbf{G}_p(j\omega))$ plot. Although the $\mathcal{K}_8$ is of lower order than the $\mathcal{K}_{28}$, it does not give a better performance than the $\mathcal{K}_{28}$. Also there is no substantial saving in computation speed using the $\mathcal{K}_8$. Considering that the design cycle time is faster using the $\mathbf{G}_{12}$ model, it is adequate to use to use $\mathcal{K}_{28}$ designed basing on $\mathbf{G}_p = \mathbf{G}_{12}$.

There is an advantage using Static Output Feedback design method. The controller, in this case, is 4x4 regardless of the order of the model of the plant. It is also easier to tune the gain parameters to accommodate any modelling error. Analytical solution to compute static gain controller is available only for certain classes of system models, but the model studied does not fit into any of these classes. A solution was proposed that uses the Sensitivity function, $\mathbf{S}(j\omega)$, as a cost function over a selected frequency range in an iterative search routine to find a controller that minimises $\|\mathbf{S}(j\omega)\|_\infty$ and at the same stabilises the plant model. The proposed method seeks to keep the closed loop response i.e. the closed loop (net) force transmissibility matrix small. With a 4x4 controller, and an understanding of the estimated model responses, fine-tuning to improve the measured responses is easier than using the $\mathcal{H}_\infty$ controller. The static gain controller turns out to be more effective at motor operating speed of 1440 rpm only after the controller has been tuned. In fact it still provides some degree of attenuation for the machine operating at 1700 rpm. It has already been demonstrated in §6.7 that a higher gain matrix is possible with Static Output Feedback when the actuators' dynamics are included. The actuators provide a near constant amplitude and a near zero or relatively small positive phase over a range of frequency higher than that used to estimate the model. This coupled with the constant gain values has some positive effect on attenuating the disturbances. The $\mathcal{K}_{28}(j\omega)$ on the other hand starts to roll off at around 50 Hz as the identified model has very little dynamics beyond this range. So although the actuators have constant gain, the controller itself does not. However this in no way suggests that the Static Output Feedback method is more superior to the $\mathcal{H}_\infty$ method in controller design for disturbance rejection. There is

insufficient data and a lack of experiment results to support such a suggestion. However the $\mathcal{K}_4$ is preferred in this case over the $\mathcal{K}_{28}$ at machine operating at rated speed and for its simplicity.

Although the $\mathcal{K}_{28}$ is not effective at motor speed of 1440 rpm, the control loops for both $\mathcal{K}_4$ and $\mathcal{K}_{28}$ are robust to modelling errors within the frequency range of $\mathbf{G}_p$. The issue of robustness is important, as more often than not errors of some sort are present in the models that are used in the design of a control system. In Chapter Three, a model suitable for the design of an active control system when little is known about the base flexibility i.e. the ability to design robust controller despite the presence of base resonance had been discussed. The uncertainty associated with base flexibility has been derived for the case of machine soft-mounted onto a structure and is embedded into the force transmissibility matrix. In Chapter Four a method is presented to estimate (a variant) of the force transmissibility function matrix for a machine hard-mounted onto a structure. Such a force transmissibility function matrix was identified for an experimental rig presented in Chapter Five. This matrix can be used to formulate a disturbance rejection performance specification for the purpose of controller design for both methods and was demonstrated in Chapter Six. Hence (both) the controllers designed, have in a sense, been shown to be robust to the modelling errors within the frequency range. They are also robust to the modelling errors in the actuators' dynamics as only a nominal model of one actuator has been determined and that is used to model all the actuators in the design of the controllers. However when disturbances beyond the frequency range are excessively dominant, the controller may or may not be robust to such neglected dynamics. In the case of $\mathcal{K}_{28}$ it is not robust in the presence frequencies beyond 40 Hz. Without any representation of the high frequency dynamics, the $\mathcal{H}_\infty$ algorithm will not be able to design a robust controller.

One notable benefit arising from the use of the $\mathcal{H}_\infty$ method is the use of the $\mathcal{H}_\infty$-norm. It permits the specification of a cost function that is suitable for the iterative design of a Static Output Feedback static gain controller. The use of singular values is quite established in modal analysis, and placing a penalty on the maximum singular values over a frequency range is a useful performance metric in controller design.

Although models for active force cancellation have been developed for both soft and hard-mounts, active control is implemented only for the case of a machine hard-mounted to a structure. These represent situations where machine alignment and dimensional accuracy are needed. The use of hard-mounts minimises any vibratory motion that may arise if soft-mounts are used instead and avoids machine motion in response to the actuators in active vibration isolation. Such motion has been observed in preliminary investigations where it is found that coil springs tend to cause the machine to vibrate and rock in response to any control effort. So a demonstration of active force cancellation is better served using hard-mounts.

When soft-mounts are preferred or necessary, a suitable model for active force cancellation for a machine on multiple mounting locations is given in Chapter Three. This model fits quite well into the current robust control theory and $\mathcal{H}_\infty$ optimal control theory framework. The effects of base flexibility modes are given as a multiplicative uncertainty to the nominal model of a machine soft-mounted onto a rigid base. This means that a control engineer can design and test a control system on a test-rig that is dissimilar to the actual structure that has some flexibility. The performance of the control system can then be evaluated against the multiplicative error introduced by the flexible modes of the base structure.

This decoupling of base flexibility from machine-on rigid base characteristics using soft mounts is a general knowledge and is known qualitatively. In Chapter Three a norm or magnitude condition of the product of two coupled dynamics has been presented to serve as a quantitative check on when decoupling is effective and useful. A simple simulation was given to demonstrate an instance of the validity of the model. Although the multiple-DoF model is motivated from the 1-DoF model of Blackwood and von Flotow (1992), the derivation and condition for decoupling are not the same. Using combined dynamic stiffness, a condition for decoupling for a 1-DoF case (for comparison) was obtained. This differs from that given by Blackwood and von Flotow (1992) by a multiplication factor. The method proposed is more consistent with the derivation of mass-spring-damper equation than that of combined Receptance (or Mobility) used by Blackwood and von Flotow.

7.2 Recommendations and suggestions for future work

For continuous or persistent excitation in the presence of uncertainty due to base flexibility, feedback control scheme is recommended. With current robust control design methods, the active vibration control system can be designed to be robust to high frequency dynamics. In most practical applications, the base structure is relatively stiffer than that used in the experiment. The force transmissibility matrix of some order can then incorporate unmodelled higher frequency dynamics as part of the generalised plant model. With a little more effort the $\mathcal{H}_\infty$ control design method can be used to give a controller that is robust to both modelling errors in the frequency range of the estimation and errors to higher frequencies disturbance. Such control paradigms are useful for MIMO problems and can be applied to a machine mounted at multiple points on a structure.

Since singular values are commonly used in vibration analysis, they are a useful link between robust controller design methods and vibration control techniques. For $\mathcal{H}_\infty$ design method, the frequency plot of the maximum singular values of the force transmissibility matrix can be used to define a disturbance rejection performance function $\mathbf{W}_2$. If a reduced plant order is used in the design, it is simpler and more efficient to define $\mathbf{W}_2 = w \cdot \mathbf{I}$, and to select w as a specification for the desired attenuation of the force transmissibility matrix. For the Static Output Feedback method, it is preferred to use $\overline{\sigma}(\mathbf{S}(j\omega))$ as a cost function in an iterative search for a stabilising controller. The full order plant model should be used since $\mathrm{Re}(\lambda_i(\mathbf{A}_{cl}))<0 \quad \forall i = 1,\ldots n$ is a necessary constraint function.

Attenuation basing on the suggested performance weighting functions discussed above is limited by the output of the actuators. One may specify a $\mathbf{W}_2$ or $\overline{\sigma}(\mathbf{S}(j\omega))$ that cannot be achieved using the present set of actuators. Higher inertia masses can be added to the actuators but that will limit its dynamic travel stroke and results in actuators' saturation. Larger actuators with higher inertia masses can be used but this will increase the weights of the actuators relative to the weight of the machine. A practical alternative as demonstrated in §6.12 is to use thermoplastic damping material inserts at the top of the hard-mounts between the mounts and the actuators. This would provide shear stiffness

while reducing the vertical stiffness, and would provide a better attenuation of the disturbances as demonstrated. It means also a lower requirement for secondary force actuation. Such a hybrid approach preserves the primary purpose of using hard-mounts to limit the motion of the machine and to maintain the necessary alignment and yet at the same time introduce some passive isolation elements. As to how much an increase in damping and a reduction in vertical stiffness are provided by the thermoplastic material can be investigated.

It is proposed that for the purpose of design, the thermoplastic inserts should be not used during the identification process of the force transmissibility matrix. A controller is to be designed subject to the weighting function $\mathbf{W}_1$ to prevent actuators' saturation. The inserts should then be introduced when the control system is implemented. Further work can be done to investigate how much improvement can be achieved from implementing this suggestion, and the amount of trade-off that is necessary between actuators' requirement and thickness of the thermoplastic or any other suitable material.

Whether the Static Output Feedback or active force cancellation at the feet of the machine is effective or not when soft-mounts are used remains to be investigated. The assumption used to develop the equations in Chapter Three is that a force is applied as if a shaker is hung in the air and is not coupled to the system. The mass of the actuators may not be too much of a problem to the model as they can be included into the mass of the machine. It is the coupling between the actuators and the soft-mounts that is of concern. In this case it is very likely that the (disturbance) force transmissibility matrix has to be separately identified from the command input to actuators to base structure transfer function matrix. Since improvements for soft-mounts active vibration isolation are always sort after, it is certainly worth an experimental investigation.

For this particular case, the use of the Static Output Feedback method has provided us with a simple static gain controller that is relatively effective. It is recommended for use in active vibration isolation using hard-mounts. It is a low order controller and has simple codes and hence the controller can be implemented on a lower cost processor rather than a digital signal processor.

REFERENCES

REFERENCES

Abu-Akeel, A.K. (1967), "The Electrodynamic Vibration Absorber as a Passive or Active Device", *Journal of Engineering for Industry (Transaction of ASME)*, **Nov.**, 741-740

Adcock, J and Potter, R. (1985), "A Frequency Domain Curve Fitting Algorithm with Improved Accuracy", *Proceedings of the 3rd International Modal Analysis Conference*, Florida, USA, pp. 541-547.

Agrawal, B.N. and Bang, H. (1993), "Active Vibration Control of Flexible Structures by using Piezoelectric Sensors and Actuators", *Proceedings of the ASME Conference on Vibration and Controlof Mechanical Systems*, **DE-61**, pp 169-179.

Alexandridis, A.T. and Paraskevopoulos, P.N. (1996), "A New Approach to Eigenstructure Assignment by Output Feedback", *IEEE Transactions of Automatic Control* **41**(7), 1046-1050.

Anderson, E.H., Leo, D.J. and Holomb, M.D. (1994), "UltraQuiet Platform for Active Vibration Isolation", *SPIE* **2717**, 436-451.

Auburn, J.N. (1980), "Theory of the Control of Structures by Low-Authority Controllers", *AIAA Journal of Guidance and Control*, **3**(5), 444-451.

Balas, M.J. (1979) "Direct Velocity Feedback Control of Large Flexible Structures", *AIAA Journal of Guidance & Control*, **3**(2), 252-253.

Balas, G.J. and Doyle, J.C. (1989), "Identification for Robust Control of Flexible Structure", *Proceedings of the American Control Conference*, Pennsylvannia, USA, pp 2566-2571.

Balas, G.J., Doyle, J.C., Glover, K., Packard, A. and Smith, R. (1991), *μ-Analysis and Synthesis Toolbox*, Massachusetts: Mathworks Inc. and MuSyn Inc.

Balas, G.J., Young, P.M. and Doyle, J.C. (1992), *μ Based Control Design as Applied to Large Space Structur: Control Design for the Minimast Facility*, NASA CSI/GI report.

Beard, A.M., Schubert, D.W., and von Flotow, A.H. (1994), "A Practical Product Implementation of an Active/Passive Vibration Isolation System", *Proceedings of ASME Conference on Active Control of Vibration and Noise*, USA, pp 485-492.

Blackwood, G and v. Flotow, A.H. (1992), "Active Control for Vibration Isolation Despite Resonant Base Dynamics", *Proceedings of the ASME Winter Annual Meeting on Active Control of Noise and Vibration*, Ca, USA, pp. 285-294.

BS 4675: Part 1: 1976, "Mechanical Vibration in Rotating Machinery: Basis for Specifying Evaluation Standards for Rotating Machines with Operating Speed from 10 to 200 revolutions per second".

BS6897:Part 5: 1995, "Experimental Determination of Mechanical Mobility: Measurement using Impact Excitation with an Exciter which is not attached to the Structure".

Burke, M., and Abdelhamid, M.K. (1991), "Force Requirements of an Active Isolation Mount", *Proceedings of Conference on Recent Advances in Active Control of Sound and Vibration*, Virginia, USA, pp. 430-447.

Cannon, R.H. Jr. and Schmitz, E., 1984, "Initial Experiments on the End-Point Control of a Flexible One-Link Robot", *Journal of Robotics Research* **3**(3), 62-75.

Chait, Y. and Radcliffe, C.J. (1989), "Control of Flexible Structurs, with Spillover using an Augmented Observer", *AIAA Journal of Guidance, Control and Dynamics* **12**(2), 155-161.

Chaplin, B. (1983), "Anti-noise – the Essex breakthrough", *Chartered Mechanical Engineer* **30**, 41-47.

Chiang, R.Y. and Safonov, M.G. (1992), *Robust Control Toolbox*, Massachusetts: Mathworks Inc.

Cremer, L., Heckl, M., and Ungar, E.E. (1988), *Structure-borne sound* (2nd edition), Berlin: Springer-Verlag.

DeJong, R.G., (1983), "The Role of Dynamic Structural Stiffness in Successful Vibration Isolation", *Proceedings of Noise-Con'83*, Massachusetts, USA, pp. 143-152.

DeJong, R.G. and Quartararo, L.R. (1987), "Resonance Evaluation of Machinery Foundation Designs", *Proceedings of Noise-Con'87*, Pennsylvania, USA, pp. 507-512.

Den Hartog, J.P. (1956), *Mechanical vibrations*, (4th edition), N.Y.: Dover Publication.

Desoer, C.A. and Vidyasagar, M. (1975), *Feedback Systems: Input-Output Properties*, New York: Academic Press.

Dyke, S.J., Spencer Jr, B.F., Kaspari Jr, D.C., Quast, P. and Sain, M.K. (1994), "Experimental verification of acceleration feedback control strategies for MDOF structures", *Proceedings of the 2nd International Conference on Computational Stochastic Mechanics*, Athens: Greece, pp.137-148.

Eghtesadi, Kh., and Chaplin, G.B.B. (1987), "The Cancellation of Reptitive Noise and Vibration by Active Methods", *Proceedings of Noise-Con'87*, Pennsylvania, USA, pp. 347-352.

Elliot, S.J. and Nelson, P.A., (1986), "Algorithm for multichannel LMS adaptive Filtering", *Electronics Letters*, **21**, 979-981.

Fernando, K.V., and Nicholson, H. (1982), "Singular Perturbation model reduction of balanced systems", *IEEE Transaction of Automatic Control* **AC-27(2)**, 466-468.

Fuller, C.R., Elliot, S.J., and Nelson, P.A. (1996), *Active Control of Vibration*, London:Academic Press.

Garcia, J.G., Sievers, L.A., and v. Flotow, A.H. (1990), "Broadband Positioning Control of Small Payloads Mounted on a Flexible Structure", *Proceedings of the ASME Winter Annual Meeting on Active Noise and Vibration Control*, Texas:USA, pp. 83-93.

Garvey, S.D. , 1996, personal communcation

Gawronski, W. (1996), *Balanced Control of Flexible Structures*, Lecture Notes in Control and Information Series 211, London: Springer.

Goh, C.J. and Caughey, T.K. (1985), "On the Stability Problem Caused by Finite Actuator Dynamics in the Collocated Control of Large Space Structures", *International Journal of Control* **41**(3), 787-802.

Goh, C.J., and Yan, W.Y. (1994), "Robust Acceleration Feedback Vibration Control of Large Space Structures", *presented in NTU internal seminar* (unpublished)

Goyder, H.G.D. and White, R.G. (1980), "Vibrational Power Flow from Machines into Built-up Structures, Part I: Introduction and Approximate Analyses of Beam and Plate-like Foundations", *Journal of Sound and Vibration* **68**(1), 59-75.

Goyder, H.G.D. and White, R.G., 1980, "Vibrational Power Flow from Machines into Built-up Structures, Part III: Power Flow through Isolation Systems", *Journal of Sound and Vibration*, **68**(1), 97-117.

Guigou, C., Wagstaff, P.R. and Fuller, C.R. (1991), "Active Vibration Isolation using Smart Structures", *Proceedings of the American Control Conference*, USA pp 1372-1377.

Hughes, P.C. (1982), "Space Structure Vibration Modes: How Many Exist? Which Ones are Important", *A reprint in IEEE Control Systems Magazine*, Feb.1987, 22-28.

Jenkins, M.D., Nelson, P.A., and Elliot, S.J. (1990), "Active Isolation of Periodic Machinery Vibration on Resonant Substructures", *Proceedings of the ASME Winter Annual Meeting on Active Noise and Vibration Control*, Texas, USA, pp 95-99.

Junger, M.C., and Feit, D. (1986) *Sound, structures and their interaction*, (2nd Edition) Massachusetts: MIT Press.

Kimura, H. (1975), "Pole Assignment by Gain Feedback", *IEEE Transactions on Automatic Control* **AC-20**, 509-516.

Kollár, I. (1994), *Frequency Domain System Identification Toolbox*, Massachusetts: Mathworks Inc.

Korenev, B.G, and Reznikov, L.M. (1993), *Dynamic Vibration Absorbers: Theory and Technical Applications*, England: John Wiley & Sons.

Lau, W.S.M, Garvey, S.D. and Penny, J.E.T. (1997), "Testing Machines for Vibration Levels on a Test-Bed Mounting which is not similar to the Application Mounting", *Proceedings of ASME Design Technical Conferences,* California, USA, VIB4197 (CD)

Lau, W.S.M., Sundararajan, N., Garvey, S.D. and Penny, J.E.T. (1998) "Active Vibration Control at the Feet of a Machinery", *Proceedings of the 5th International Conference on Control, Automation,Robotics and Vision, Singapore*, pp 381- 385.

Liao, J.Y. and Tse, C.C. (1993), "An algebraic approach for the modal analysis of synthesised structures", *Mechanical Systems and Signal Processing*, **7**(1), 89-104.

Liu, Y. and Anderson, B.D.O. (1989), "Singular Perturbation approximation of balanced Systems", *International Journal of Control*, **50**(4), 1379-1405.

Lublin, L., and Athans, M. (1994), "An Experimental Comparison of H2 and H∞ Designs for an Interferometer Test-Bed", *Proceedings of the Conference in Honour of Professor George Zames (60th Birthday)*, Montreal, Canada, 150-172.

Luenberger, D.G. (1971), "An Introduction to Observers", *IEEE Transactions on Automatic Control* **AC-16**(6), 596-602.

Lyons , R. (1987), *Machinery Noise and Diagnostics*, Boston: Butterworths pp. 17-23.

MacFarlane, A.G.J. (1970), "Return Difference and Return Ratio Matrices and their Use in Analysis and Design of Multivariable Feedback Control Systems", *Proceedings of IEE* **117**(10), 2037-2049.

McKinnell, J.R. (1989), "Active Isolation of Vibration", *PhD Thesis*, Cambridge, UK.

Meirovitch, L. and Baruh, H. (1982), "Control of Self-Adjoint Distributed Parameter Systems", *AIAA Journal of Guidance and Control*, **5**(1), 60-66.

Miller, L.R., Ahmadian, M., Nobles, C.M., & Swanson, D.A. (1992), "Modelling and Performance of an Experimental Active Vibration Isolator", *Proceedings of ASME Winter Annual Meeting on Active Control of Noise and Vibration, California:USA*, pp. 157-163

Moorhouse, A.T. and Gibbs, B.M. (1993), "Prediction of the Structure-Borne Noise Emission of Machines: Development of a Methodology", *Journal of Sound and Vibration* **167**(2), 223-237.

Moore, B.C. (1981), "Principal Component analysis in linear systems: controllability and observability and model reduction", *IEEE Transactions on Automatic Control* **AC-26**(1), 17-32.

Mottershead J.E. and Friswell, M.I. (1993), "Model Updating in Structural Dynamics: A Survey", *Journal of Sound and Vibration* **167**(2), 347-375.

Nelson, P.A., Jenkins, M.D., and Elliot, S.J., (1987), "Active Isolation of Periodic Vibrations", *Proceedings of Noise-Con'87*, Pennsylvannia, USA, pp. 425 - 430.

Nelson, P.A. (1991), "Active Vibration Isolation", in Hansen, C.H. (ed), *Active Control of Noise and Vibration*, University of Adelaide, Australia, pp. 13-41.

Nicholson, J.W. and Bergman, L.A. (1986), "Vibration of Damped Plate-Oscillator Systems", *ASCE Journal of Engineering Mechanics*, **112**(1), 14-30.

Nishimura, H and Kojima, A. (1997), "Active Vibration Isolation Control for a Multi-Degree-of-Freedom Structure with Uncertainties of its Base", *Proceedings of the ASME Design Engineering Technical Conference*, California, USA, DETC97/VIB-3800 (CD-ROM)

Norwood, C. (1989), "Vibration Isolator Properties and Performance Prediction", *Proceedings of the 1st Noise and Vibration Conference*, Singapore, pp I-1 to I-8.

Packard, A. and Doyle J.C. (1993), "The Complex Structured Singular Values", *Automatica*, **29**(1), 71-109.

Pan, J., Pan Jiaqiang, and Hansen, C.H. (1992), "Total Power Flow from a Vibrating Rigid Body to a Thin Panel through Multiple Elastic Mounts", *Journal of Acoustics Society of America*, **92**(2), Pt 1, 895 - 907.

Pan Jiaqiang, Hansen, C.H., and Pan, J. (1993a), "Active Isolation of a Vibrating Source from a Thin Beam using a Single Active Mount", *Journal of Acoustics Society of America*, **94**(3), Pt 1, 1425-1434.

Pan Jiaqiang and Hansen, C.H. (1993b) "Active Control of Power Flow from a Vibrating Rigid Body to a Flexible Panel through Two Active Isolators", *Journal of Acoustics Society of America* **93**(4), Pt 1, 1947-1953.

Pintelon, R. and Schoukens, J. (1990) "Robust Identification of Transfer Functions in the s- and z-Domains", *IEEE Transactions on Instrumentation and Measurement*, **39**(4), 565-573.

Plunkett, R. (1954), "Interaction between a Vibratory Machine and Its Foundation", *Noise Control*, **4**(1), 18-22.

Preumont, A., and Loix, N. (1994) "Active Damping of a Stiff Beam-like Structure with Acceleration Feedback", *Journal of Experimental Mechanics* **Mar**, 23-26.

Plunkett, R. (1958), "Interaction Between a Vibratory Machine and Its Foundation", *Noise Control Engineering Journal*, **4**(1), 18-22.

Raju, P.K. and Sun, S.P. (1989), "Modal Control of a Flexible Beam with Multiple Sensors and Actuators", *Proceedings of the ASME Design Technical Conference*, Quebec, Canada, pp. 245-252.

Rider, E and Hodson, W.R. (1991) , "Multi-degree of Freedom Vibration Detuners: the potential offered by active techniques", *Proceedings of the Conference on Recent Advances in Active Control of Sound and Vibration*, Virginia, USA, pp. 464-484.

Rosenbrock, H.H. (1974), *Computer-Aided Control System Design*, London: Academic Press.

Sanathanan, C.K. and Koerner, J. (1963), "Transfer Function Synthesis as a Ratio of Two Complex Polynomials", *IEEE Transactions on Automatic Control*, **AC-8**, 56-58.

Schoukens, J. and Renneboog, J. (1986) "Modelling the Noise Influence on the Fourier Coefficients After a Discrete Fourier Transform", *IEEE Transactions on Instrumentation and Measurement*, **35** (3), 278-286.

Schoukens, J., Pintelon, R, and Renneboog, J. (1988) "A Maximum Likelihood Estimator for Linear and Non-Linear Systems - A Practical Application of Estimation Techniques in Measurement Problems", *IEEE Transactions on Instrumentation and Measurement*, **37** (1), 10-17.

Schroeder M.R. (1970), "Synthesis of Low Peak FactorSignals and Binary Sequences with Low Autocorrelation", *IEEE Transaction on Information Theory* **16**, 85-89.

Schubert, D.W. (1991), "Characteristics of an Active Vibration Isolation System using Absolute Velocity Feedback and Force Actuation", *Proceedings of the Recent Advances in Active Control of Sound and Vibration*, Virginia, USA, pp. 448 - 463.

Sciulli, D. and Inman, D.J. (1997), "Active Isolation Design for a Flexible Base", *Proceedings of the ASME Design and Technical Engineering Conferences*, California, USA, DETC97/VIB-4117 (CD-ROM).

Seto, K, & Furuishi, Y. (1991), "A Study of Active Dynamic Absorber", *Proceedings of the ASME Confereneces on Modal Analysis, Modelling, Diagnostics and Control - Analytical and Experimental*, USA, **DE-38**, pp. 263-270.

Scribner, K.B., Sievers, L.A., and von Flotow, A.H., (1993), "Active Narrow-band Vibration Isolation of Machinery Noise from Resonant Substructures", *Journal of Sound and Vibration* **167**(1), 17-40.

Shoureshi, R. and Knurek, T., (1996), "Automative Applications of a Hybrid Active Noise and Vibration Control", *IEEE Control Systems* **16**(6), 72-77.

Sievers, L.A., and von Flotow, A.H. (1988), "Linear Control Design for Active Vibration Isolation of Narrow-band Disturbances", *Proceedings of the 27th Conference on Decision and Control*, Texas, USA, pp. 1032 - 1037.

Sievers, L.A., and von Flotow, A.H. (1989), "Comparison of Two LQG-based Methods for Disturbance Rejection", *Proceedings of the 28th Conference on Decision and Control*, Florida, USA, pp. 483 - 485.

Sievers, L.A., and von Flotow, A.H. (1990), "Comparison and Extension of Control Methods for Narrow-band Disturbance Rejection", *Proceedings of the ASME Winter Annual Meeting on Active Noise and Vibration Control*, Texas, USA, pp. 11-22.

Skogestad, S. and Postlethwaite, I. (1996), *Multivariable Feedback Control: Analysis and Design*, Chichester: Wiley, pp. 363-364.

Sommerfeldt, S.D. and Tichy, J. (1988), "Adaptive Control of a Two-Stage Vibration Mount", *Proceedings of the 27th Conference on Decision and Control*, Texas, USA, pp. 2039-2044.

Southward, S.C., Ivers, D.E. and Nicholson, G.C. (1997), "Commercialisation of Active Isolation for Jet Aircraft", *Proceedings of the ASME Design Technical Engineering Conference*, California, USA, DETC97/VIB-4115 (CD-ROM).

Spanos, J., Rahman, Z. and von Flotow, A.H. (1993), "Active Vibration Isolation on an Experimental Flexible Structure", *SPIE Smart Structures and Intelligent System*, **1917**, 674-680.

Srinathkumar, S. (1978), "Eigenvalue/Eigenvector Assignment Using Output Feedback", *IEEE Transactions on Automatic Control* **AC-23**(1), 79-81.

Stanway, R. and O'Reilly, J. (1984), "State-variable Feedback control of Rotor-bearing Suspension Systems", *Proceedings of the 3rd International ImechE Conference on Vibration in Rotating Machinery*, University of York, UK, pp 515-524.

Stein, G. and Doyle, J.C. (1991), "Beyond Singular Values and Loop Shapes", *AIAA Journal of Guidance and Control*, **14**(1), 5-16.

Swinbanks, M.A., (1984), "The Active Control of Noise and Vibration and Some Applications in the Industry", *Proceedings of ImechE* **198A**(13) 281-288

Su, J.H. (1997), "Robust Passive-Active Mounts for Machinery and Equipment", *Proceedings of the ASME Designe Engineering Technical Conferences*, California, USA, DETC97/VIB-3774 (CD-ROM).

Syrmos, V.L., Abdallah, C.T., Dorato, P. & Grigoriadis, K. (1997), "Static Output Feedback - A Survey", *Automatica* **33**(2), 125-137.

Tanaka, N. and Kikushima, Y. (1985), "A Study of Active Vibration Isolation", *Journal of Vibration, Acoustics, Stress and Reliability in Design (Transactions of ASME)*, **107**(Oct) 392- 397.

Tanaka, N. and Kikushima, Y. (1988), "Rigid Support Active Vibration Isolation", *Journal of Sound and Vibration*, **125**(3), 539 - 553.

Tanaka, N. and Kikushima, Y. (1988), "Optimal Design of Active Vibration Isolation System", *Journal of Vibration, Acoustics, Stress and Reliability in Design (Transactions of ASME)*, **110**(Jan), 42-48.

Tøffner-Clausen, S. (1996), *System Identification and Robust Control: A Case Study Approach*, Berlin: Springer-Verlag.

von Flotow, A.H. (1988), "An Exposition Overview of Active Control of Machinery Mounts", *Proceedings of the 27th Conference on Decision and Control*, Teaxs, USA, pp. 2029-2032.

von Flotow, A.H., and Vos D.W. (1991), "The Need for Passive Damping in Feedback Controlled Flexible Structures", *Proceedings of the Recent Advances in Active Control of Sound and Vibration*, Virginia, USA, pp. 593-603.

Watters, B.G., Coleman, R.B. (1988), Duckworth, G.L., & Berkman, E.F.,1988, "A Perspective on Active Machinery Isolation", *Proceedings of the 27th IEEE Conference on Decision and Control*, Texas, USA, Dec. pp. 2033-2038.

Wei, B. and Bryson, A.E., Jr. (1981), "Modelling and Control of Flexible Space Structures", *Proceedings of 3rd VPI&SU/AIAA Symposium on Dynamics and Control of Large Flexible Spacecraft*, Virginia,USA, pp. 153-172.

Wei, B. and Byun, K.W. (1989), "New Generalised Structural Filtering Concept for Active Vibration Control Synthesis", *Journal of Guidance, Control & Dynamics* **12**(2), 147-154.

Whitfield, A.H. and Williams, N.G. (1988), "Integral Least-square Techniques for Frequency Domain Model Reduction", *International Journal of Systems ScienceI,* **19**(8), 1355-1373.

Yang, J., Suemastu, Y., and Gotou, K. (1996), "Active Vibration Control of the Vehicle Engine-Body System Using Filtered-X LMS Algorithm", *Proceedings of the 4th International Conference on Control, Automation, Robotics and Vision*, Singapore, pp. 2111-2115.

Yeong, W. (1988), "Demonstration of Active Vibration Control of the Hughes Cryocooler Testbed", *Proceedings of the 31st Conference on Decision and Control*, Texas, USA, pp. 2580-2585

Wilkinson, J.H. (1965), *The Algebraic Eigenvalue Problem*, Oxford University Press.

Zimmerman, D.C., Horner, G.C., AND Inman, D.J. (1988), "Micro-processor Controlled Force Actuators", *AIAA Journal of Guidance, Control and Dynamics*, **11**(3), 230-236.

Zimmerman, D.C., and Inman, D.J., 1990, "On the Nature of the Interaction between Structures and Proof-Mass Actuators", *AIAA Journal of Guidance, Control and Dynamics*, **13**(1), 82-88.

APPENDIX A

MODEL OF A PASSIVE ISOLATOR

A.1 Introduction

When a machine or an engine is soft-mounted onto a base structure, the isolators determine the amount of force transmitted to the base structure. The isolator effectiveness is dependent upon its stiffness or mobility function. This is typically given by its 4-pole parameters. Under certain circumstances, the 4-pole parameters can be approximated by blocked-transfer impedance, and an isolator can be approximately modelled as a stiffness element.

A.2 A mount 4-pole parameters

A.2.1 General Case

The forces and velocities of an isolator are shown in Figure A.1.

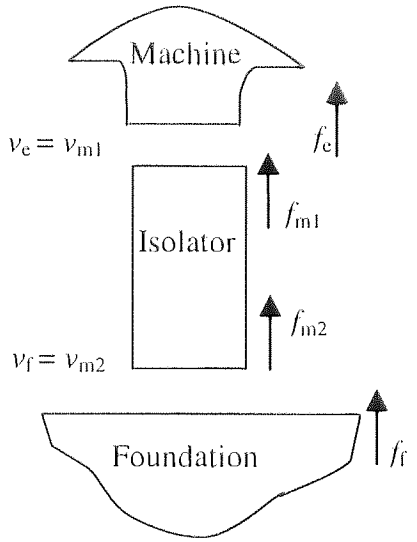

Figure A.1 Forces and displacements of an isolator

The four pole parameters {A,B,C,D} relate the pairs $\{v_{m1}, f_{m1}\}$ with $\{v_{m2}, f_{m2}\}$ by

$$\begin{bmatrix} f_{m1} \\ v_{m1} \end{bmatrix} = \begin{bmatrix} A & B \\ C & D \end{bmatrix} \begin{bmatrix} f_{m2} \\ v_{m2} \end{bmatrix} \tag{A.1}$$

with $f_{m1} = Af_{m2} + Bv_{m2}$ and $v_{m1} = Cf_{m2} + Dv_{m2}$. The constraint is that AD-BC=1. Hence,

$$A = \left.\frac{f_{m1}}{f_{m2}}\right|_{v_{m2}=0} \qquad B = \left.\frac{f_{m1}}{v_{m2}}\right|_{f_{m2}=0}$$

$$C = \left.\frac{v_{m1}}{f_{m2}}\right|_{v_{m2}=0} \qquad D = \left.\frac{v_{m1}}{v_{m2}}\right|_{f_{m2}=0} \tag{A.2}$$

A and C are called the blocked parameters, $v_{m2} = 0$; and B and D are called the free parameters, $f_{m2}=0$. Experimental determination of A, B, C, and D can be found in (Norwood, 1989).

A.2.2 Special cases

a. If the isolator is symmetric, then

$$A = \left.\frac{f_{m1}}{f_{m2}}\right|_{v_{m2}=0} = D = \left.\frac{v_{m1}}{v_{m2}}\right|_{f_{m2}=0} \tag{A.3}$$

b. If the isolator is massless or very light weight, A=D=1 and B=0. This is true at low frequencies below the mount internal resonant frequency. In this case,

$$f_{m1}=f_{m2} \quad \text{and} \quad v_{m1}= Cf_{m2} + v_{m2}$$

giving,

$$f_{m2} = C^{-1} (v_{m2} - v_{m1})$$

Alternatively, the pairs $\{v_{m1},v_{m2}\}$ and $\{f_{m1},f_{m2}\}$ are related by

$$\begin{bmatrix} v_{m1} \\ v_{m2} \end{bmatrix} = \mathbf{Y}_m \cdot \begin{bmatrix} f_{m1} \\ f_{m2} \end{bmatrix} = \begin{bmatrix} Y_{11} & Y_{12} \\ Y_{21} & Y_{22} \end{bmatrix} \cdot \begin{bmatrix} f_{m1} \\ f_{m2} \end{bmatrix} \tag{A.4}$$

where $\mathbf{Y}_m$ is the mount mobility function. The transfer function or the blocked transfer impedance of the mount can be defined as

$$Z_{21} = \left.\frac{f_{m2}}{v_{m1}}\right|_{v_{m2}=0} = \frac{Y_{12}}{Y_{12}^2 - Y_{11}Y_{22}} = \frac{1}{C} \tag{A.5}$$

At frequencies below the mount internal resonance, and assuming that the mount is almost massless, the mount equation is given by

$$f_{m2} = C^{-1}(v_{m2}-v_{m1}) = Z_{21}(v_{m2} - v_{m1}) \tag{A.6}$$

or

$$f_{m2} = k(x_{m2}-x_{m1})$$

Where k is the stiffness of the isolator. This will be the model for the isolators used through-out the thesis.

A.3 A general model of a mount or isolator with 6-DoF

A 6-DoF isolator with linear and angular displacements can be modelled as a cylinder with its longitudinal axis along the z-axis. The translational displacements and angular displacements are indicated in Figure A.2. For each i[th] mount, $q_{m1i}=q_{ei}$, and $q_{m2i}=q_{fi}$.

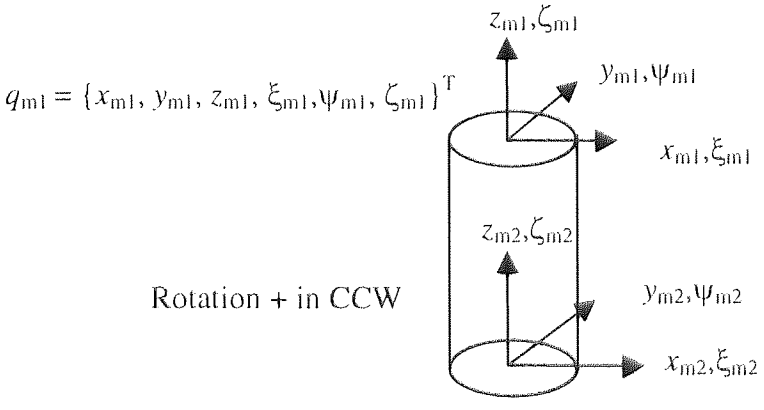

Figure A.2 Displacements and angular displacements of an isolator

The general stiffness matrix, with respect to the principal axis of the cylinder is given as

$$\underline{\mathbf{k}}_i = \begin{bmatrix} \underline{k}_{xi} & 0 & 0 & 0 & 0 & 0 \\ 0 & \underline{k}_{yi} & 0 & 0 & 0 & 0 \\ 0 & 0 & \underline{k}_{zi} & 0 & 0 & 0 \\ 0 & 0 & 0 & \underline{G}_{xi} & 0 & 0 \\ 0 & 0 & 0 & 0 & \underline{G}_{yi} & 0 \\ 0 & 0 & 0 & 0 & 0 & \underline{G}_{zi} \end{bmatrix} \tag{A.7}$$

The diagonal elements are the complex elastic constants of a mount where $\underline{k}_{xi} = k_{xi} + jk_{xi}'$ where k_{xi} and k_{xi}' are the resistive and dissipative spring rates respectively. For an isotropic mount, the resistive components $k_{xi}=k_{yi}$, and $G_{yi}=G_{xi}$.

The stiffness coefficients for a cylindrical isolator of radius, a, and length l are given in the following Table A.1 (ν is the Poisson ratio, and E the Young's Modulus).

k_X	k_Z	k_Y	G_X	G_Z	G_Y
$3\pi Ea^4 \div (4l^3)$	$\pi Ea^2 \div l$	$3\pi Ea^4 \div (4l^3)$	$\pi Ea^4 \div (4l)$	$\pi Ea^4 \div \{4(1+\nu)l\}$	$\pi Ea^4 \div (4l)$

Table A.1 Values of stiffness of an isotropic isolator

A.4 Model of a 3 DoF isolator

A 3-DoF model of the isolator considers only the linear displacements. The complex stiffness matrix is given by a 3x3 matrix of the form,

$$\underline{\mathbf{k}}_i = \begin{bmatrix} \underline{k}_{xi} & 0 & 0 \\ 0 & \underline{k}_{yi} & 0 \\ 0 & 0 & \underline{k}_{zi} \end{bmatrix} \tag{A-8}$$

Without dissipative stiffness, the stiffness and damping matrix of each isolator is given by,

$$\mathbf{k}_i = \begin{bmatrix} k_{xi} & 0 & 0 \\ 0 & k_{yi} & 0 \\ 0 & 0 & k_{zi} \end{bmatrix} \tag{A.9}$$

A.5 Summary

A simple model of the isolator is a cylinder, and its property is given in terms of the spring stiffness when the frequency of excitation is below its internal resonant frequency.

APPENDIX B

MODEL OF A MACHINE MOUNTED ON A FLEXIBLE BEAM AT TWO POINTS

B.1 Example model

The condition shown below can be modelled as a rigid machine on a flexible beam at two points:

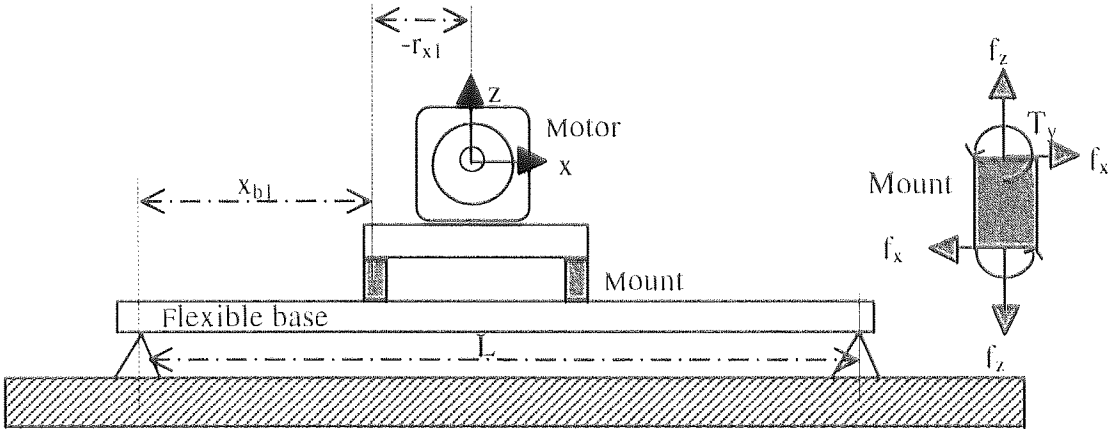

Figure B.1 A model of a machine mounted at two points on a flexible beam

B.2 Model Parameters

Machine and mount parameters	Mild steel beam parameters
Mass, m= 3.7 kg Moment of inertia J_{yy} =0.53 kg-m^2	Density, ρ=7800 kg m^{-3} Elastic modulus E=220*10^9 N m^{-2}. L, length =1.5 m h, height of the beam =0.01 m A_b, cross-section area = 0.0015 m^2 Ib_{yy} = 1.25 * 10^{-8} m^4
Machine c.g. location r_{x1}= -0.23 m; r_{x1} = 0.23 m r_{z1}= -0.08 m; r_{z1} = -0.08 m	Mount locations #1 $x_{b1}=(L+r_{x1})/2$ m #2 $x_{b2}=(L+r_{x2})/2$ m
Mount property: Loss factor, nz = 0.07 Stiffness coefficients, k_{zo} Case (1): k_{zo}= 1 kN m^{-1}. Case (2): k_{zo} = 5 kN m^{-1}.	mode shapes loss factor, nb=0.05

Table B.1 Model parameters

B.3 Model Equations

The mount can be considered to be capable of transmitting three types of forces and moments as shown in Figure B.1. At each mount location, i, the mount location matrix, $\mathbf{P}_i$, mount complex stiffness matrix, $\mathbf{K}_i$ and the machine mass matrix, $\mathbf{M}$ are given by

$$\mathbf{P}_i = \begin{bmatrix} 1 & 0 & r_{zi} \\ 0 & 1 & -r_{xi} \\ 0 & 0 & 1 \end{bmatrix}; \quad \mathbf{K}_i = \begin{bmatrix} k_{xi} & 0 & 0 \\ 0 & k_{zi} & 0 \\ 0 & 0 & g_{yi} \end{bmatrix}; \quad \mathbf{M} = \begin{bmatrix} m & 0 & 0 \\ 0 & m & 0 \\ 0 & 0 & J_{yy} \end{bmatrix} \tag{B.1}$$

Where $k_{zi}=k_{zo}(1+jnz)$ and $k_{xi}=k_{xo}(1+jnx)$ where k_{zo} and k_{xo} are spring constants and nz and nx are the loss factors. The machine sub-system matrix can be written as

$$\mathbf{P} = \begin{bmatrix} \mathbf{P}_1 \\ \mathbf{P}_2 \end{bmatrix}; \quad \mathbf{K} = \begin{bmatrix} \mathbf{K}_1 & 0 \\ 0 & \mathbf{K}_2 \end{bmatrix}; \tag{B.2}$$

For disturbance, $\mathbf{Q}_d=\{F_x, F_z, T_y\}^T$ applied at the feet and the displacements measured also at the feet (assuming that the mounts are at the feet), the receptance matrix is given by

$$\mathbf{P}\,\mathbf{R}_c\,\mathbf{P}^T = \mathbf{P}\left[-\omega^2\mathbf{M} + \mathbf{P}^T\mathbf{K}\mathbf{P}\right]^{-1}\mathbf{P}^T \tag{B.3}$$

The flexible beam, assuming the Euler-Bernoulli model is given by

$$\rho.A_b \frac{\partial^2 w}{\partial t^2} + E.Ib_{yy} \frac{\partial^4 w}{\partial x^4} = \sum_{i=1,2} f_{bzi}\delta(x - x_{bi}) + \sum_{i=1,2}\left(\frac{h}{2} f_{bxi} + \tau_{byi}\right)\frac{\partial\delta(x - x_{bi})}{\partial x} \tag{B.4}$$

Where the force at a given location, x-x_{bi}, is given by delta function $\delta(x$-$x_{bi})$ and τ denotes the moment.

The boundary conditions for simply supported beam are used. By solving the equation using the matrix of eigenfunctions, Ψ, and assuming the modal complex amplitude to be given by the vector $\{w\}$, we have

$$w = \Psi^{T}\{\mathbf{w}\}; \quad \Psi^{T} = \{\Psi_r\} = \left\{\sin\left(\frac{\mathrm{r}\pi\mathrm{x}}{\mathrm{L}}\right)\right\} \tag{B.5}$$

The base coupling matrix at i^{th} location, P_{bi}, for N modes is given by

$$\mathbf{P}_{bi}{}^{T} = \begin{bmatrix} -\frac{h\pi}{2L}\cos(\frac{\pi x_{bi}}{L}) & \sin(\frac{\pi x_{bi}}{L}) & -\frac{\pi}{L}\cos(\frac{\pi x_{bi}}{L}) \\ \cdots & \cdots & \cdots \\ \cdots & \cdots & \cdots \\ -\frac{h\pi}{2L}\cos(\frac{N\pi x_{bi}}{L}) & \sin(\frac{N\pi x_{bi}}{L}) & -\frac{\pi}{L}\cos(\frac{N\pi x_{bi}}{L}) \end{bmatrix} \tag{B.6}$$

Defining the modal mass, r^{th} modal frequency and the r^{th} modal damping respectively with the usual notations (and adding the structure loss factor nb) as

$$m_b = \frac{1}{2}\rho.A_b.L; \; \omega_r = \left(\frac{\pi\, r}{L}\right)^2\sqrt{\frac{E.Ib_{yy}}{\rho.A_b}}; \; k_{br} = m_b\left(\omega_r{}^2\right)(1 + j\eta b); \tag{B.7}$$

The base structure system matrices are given as

$$\mathbf{M}_b = \mathrm{diag}(m_b...), \; \mathbf{K}_b = \mathrm{diag}(k_{b1}...k_{bN}) \text{ and } \mathbf{P}_b{}^{T} = [\mathbf{P}_{b1}{}^{T} \mid \mathbf{P}_{b2}{}^{T}] \tag{B.8}$$

From the system equation matrix, the uncoupled base receptance matrix for the coupled force at the mounting points to displacements at those points is found to be

$$\mathbf{D}_f{}^{-1} = \mathbf{P}_b\left[-\omega^2\mathbf{M}_b + \mathbf{K}_b\right]^{-1}\mathbf{P}_b{}^{T} \tag{B.9}$$

The coupled base receptance matrix is taken to be

$$\left[\mathbf{D}_f + \mathbf{K}\right]^{-1} = \mathbf{P}_b\left[-\omega^2\mathbf{M}_b + \mathbf{K}_b + \mathbf{P}_b{}^{T}\,\mathbf{K}\,\mathbf{P}_b\right]^{-1}\mathbf{P}_b{}^{T} \tag{B.10}$$

In this case the two matrices differ only by the stiffness term, and does not include the mass inertia effects of the mounts, and it can be shown that $[\mathbf{D}_f+\mathbf{K}]=\mathbf{D}_f{}^{-1}[\mathbf{I}+\mathbf{K}\,\mathbf{D}_f{}^{-1}]^{-1}$.

To simplify further for the case where the mounts transmit only a vertical force, although the machine is itself capable of 2-DoF disturbance $\{F_z, T_y\}^T$, we can write the respective coupling matrices as

$$\mathbf{P} = \begin{bmatrix} 1 & -r_{x1} \\ 1 & -r_{x2} \end{bmatrix}; \quad \mathbf{P}_b = \begin{bmatrix} \sin(\frac{\pi x_{b1}}{L}) & \dots & \dots & \sin(\frac{N\pi x_{b1}}{L}) \\ \sin(\frac{\pi x_{b2}}{L}) & \dots & \dots & \sin(\frac{N\pi x_{b2}}{L}) \end{bmatrix} \tag{B.11}$$

The base coupling matrix is now basically a matrix of the eigenfunctions evaluated at the two mounting points x_{b1} and x_{b2} for the first N modes. For control of a self-adjoint system, $\mathbf{P}_b$ is the modal measurement matrix of sensed motion that relates the complex modal amplitudes to the actual motions and is a function of the location of the sensors. For a collocated actuator-sensor pair, $\mathbf{P}_b^T$ is the modal control matrix (and is a function of the location of the actuator).

The results shown in Chapter 3 uses the $\mathbf{P}$ and $\mathbf{P}_b$ matrices given by (B.11)

B.3 Summary

A simple beam equation is used in the model of the example given in §3.6 of chapter three. The results of the simulation are shown in Figure 3.4 and 3.5. They have been used to demonstrate the relevance of the model equation developed in chapter three.

APPENDIX C

TRANSFER FUNCTIONS FREQUENCY REPONSE

PLOTS OF ESTIMATED AND MEASURED G_p

(Estimated plots given by solid lines)

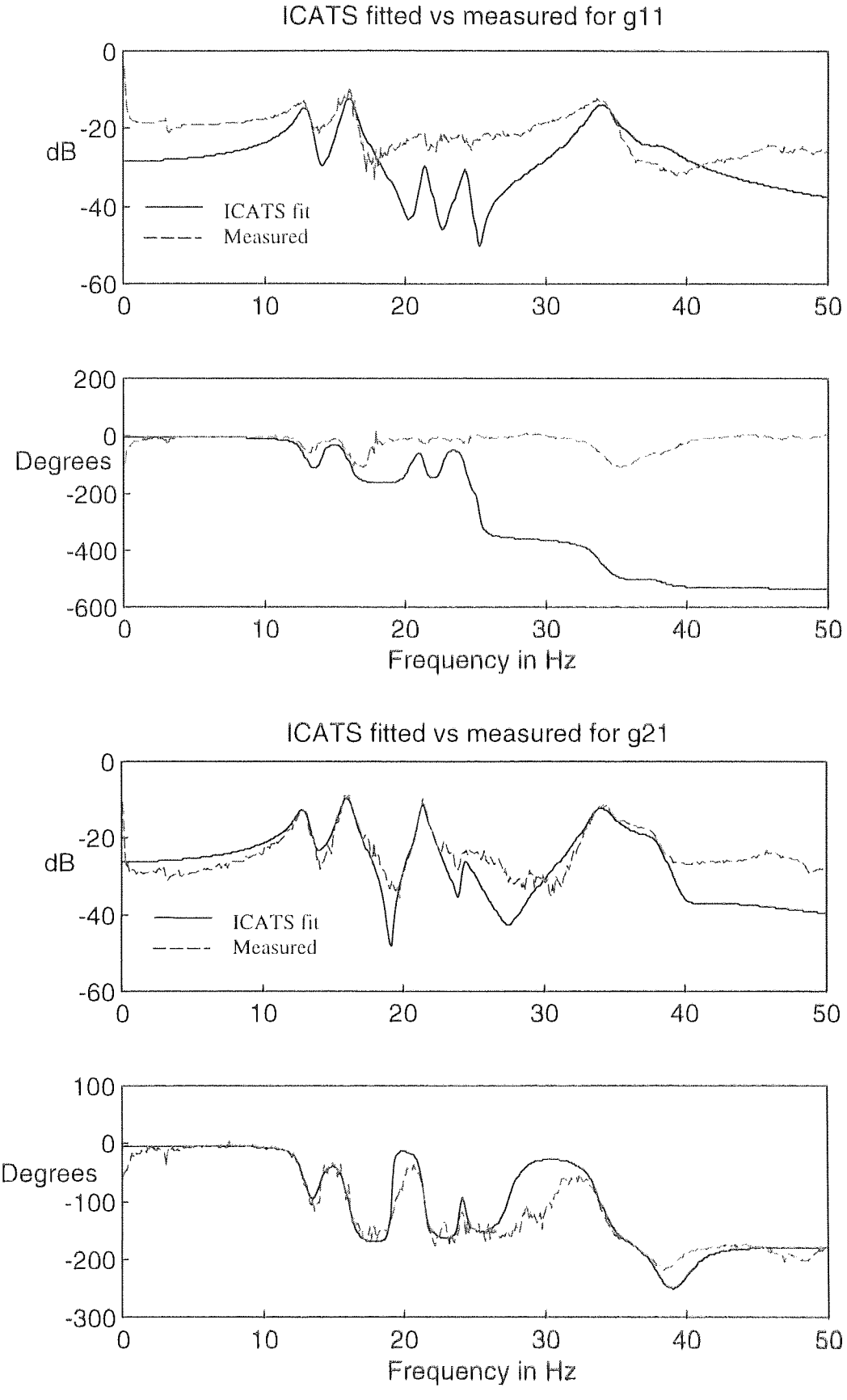

Figure C.1a Bode plots of g_{11} and g_{21} of measured and ICATS fit

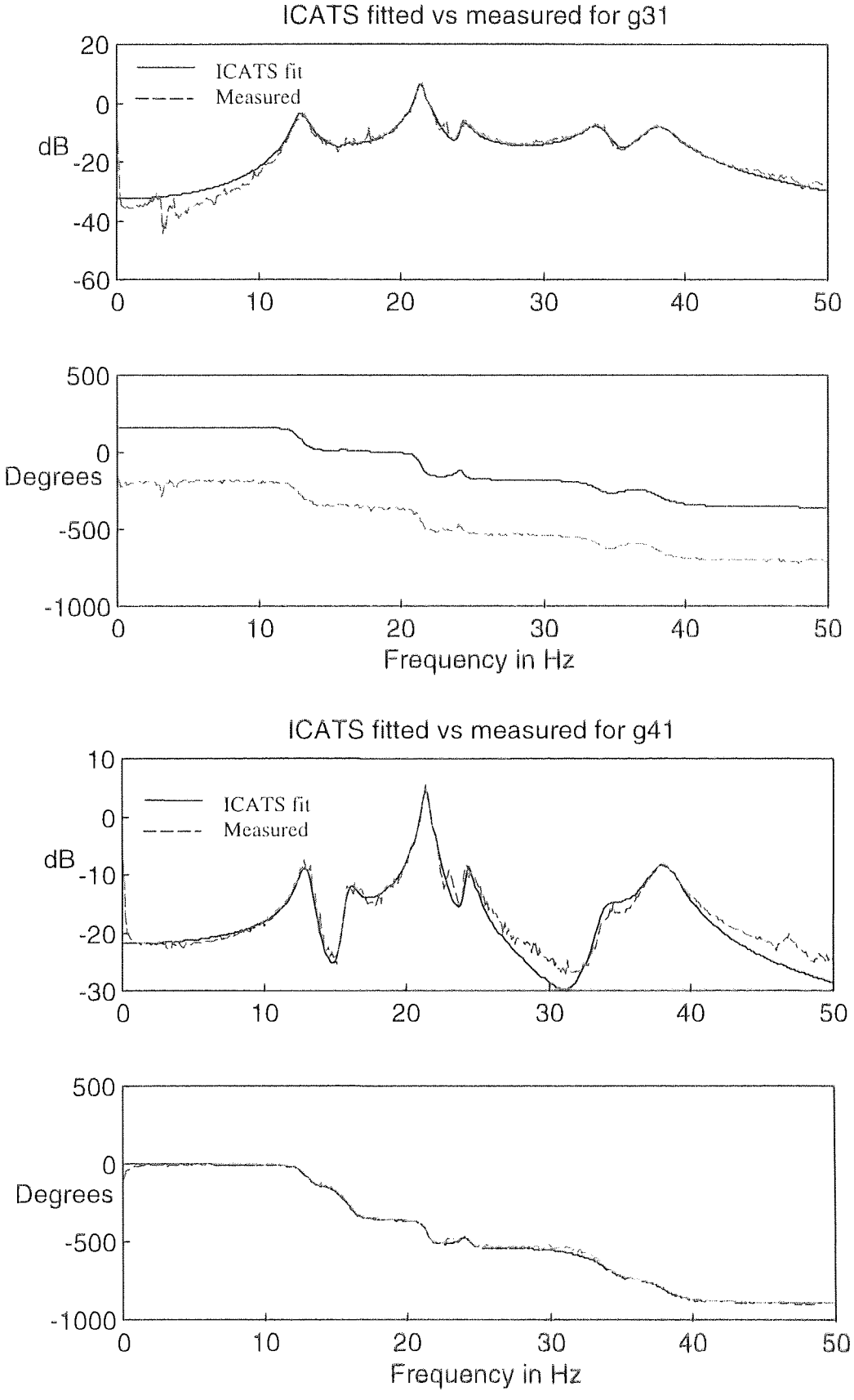

Figure C.1b Bode plots of g_{31} and g_{41} of measured and ICATS fit

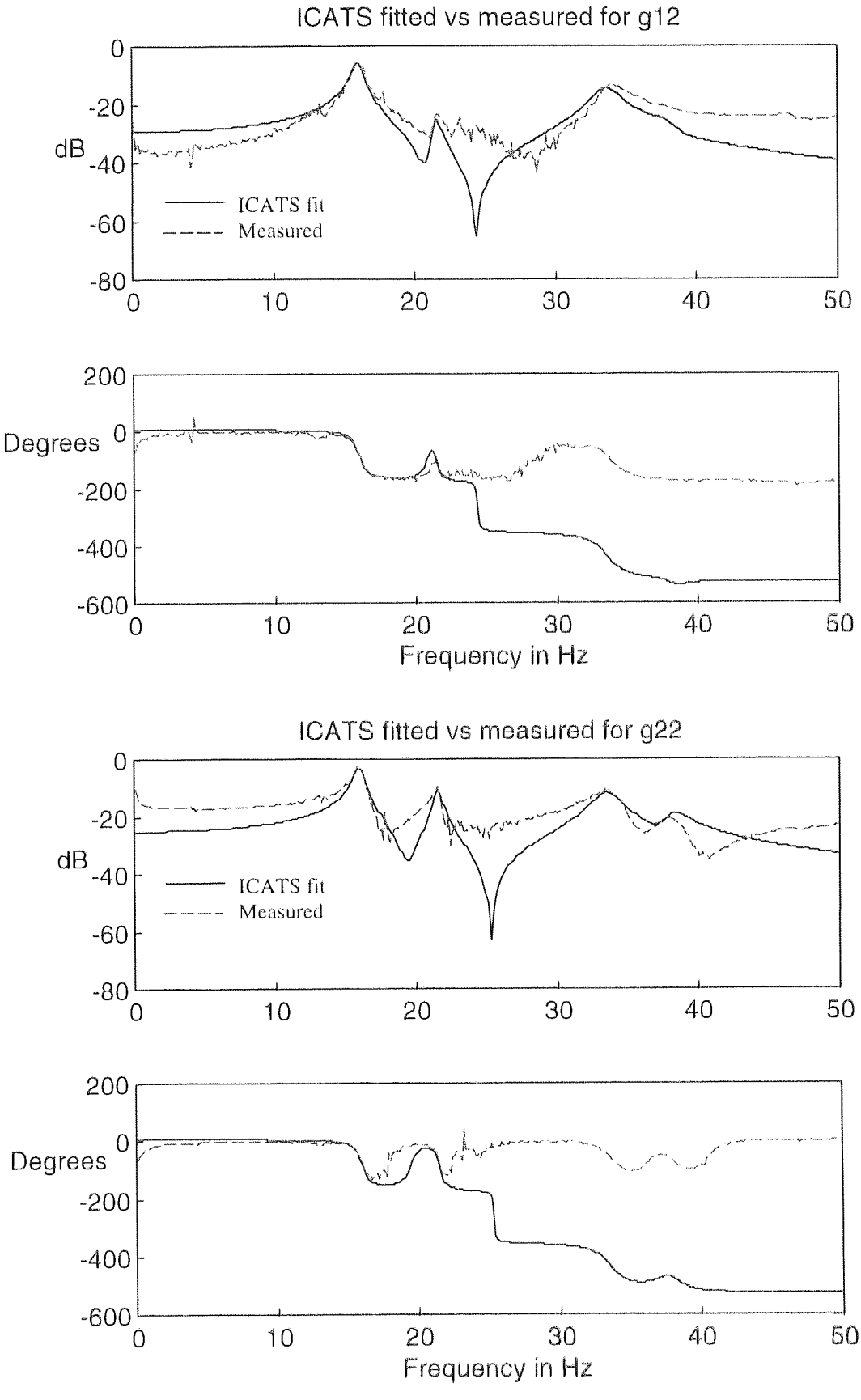

Figure C.2a Bode plots of g_{12} and g_{22} of measured and ICATS fit

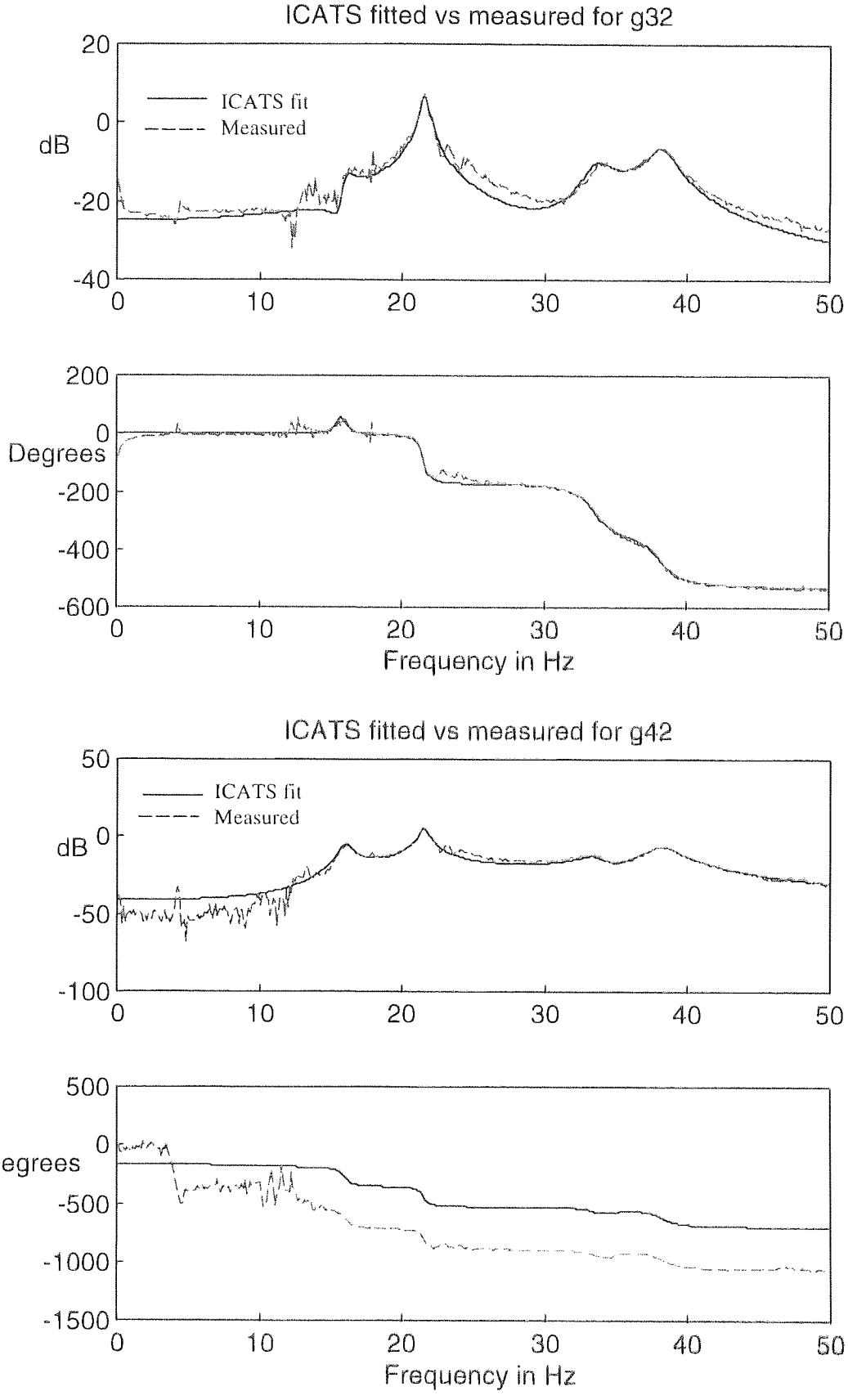

Figure C.2b Bode plots of g_{32} and g_{42} of measured and ICATS fit

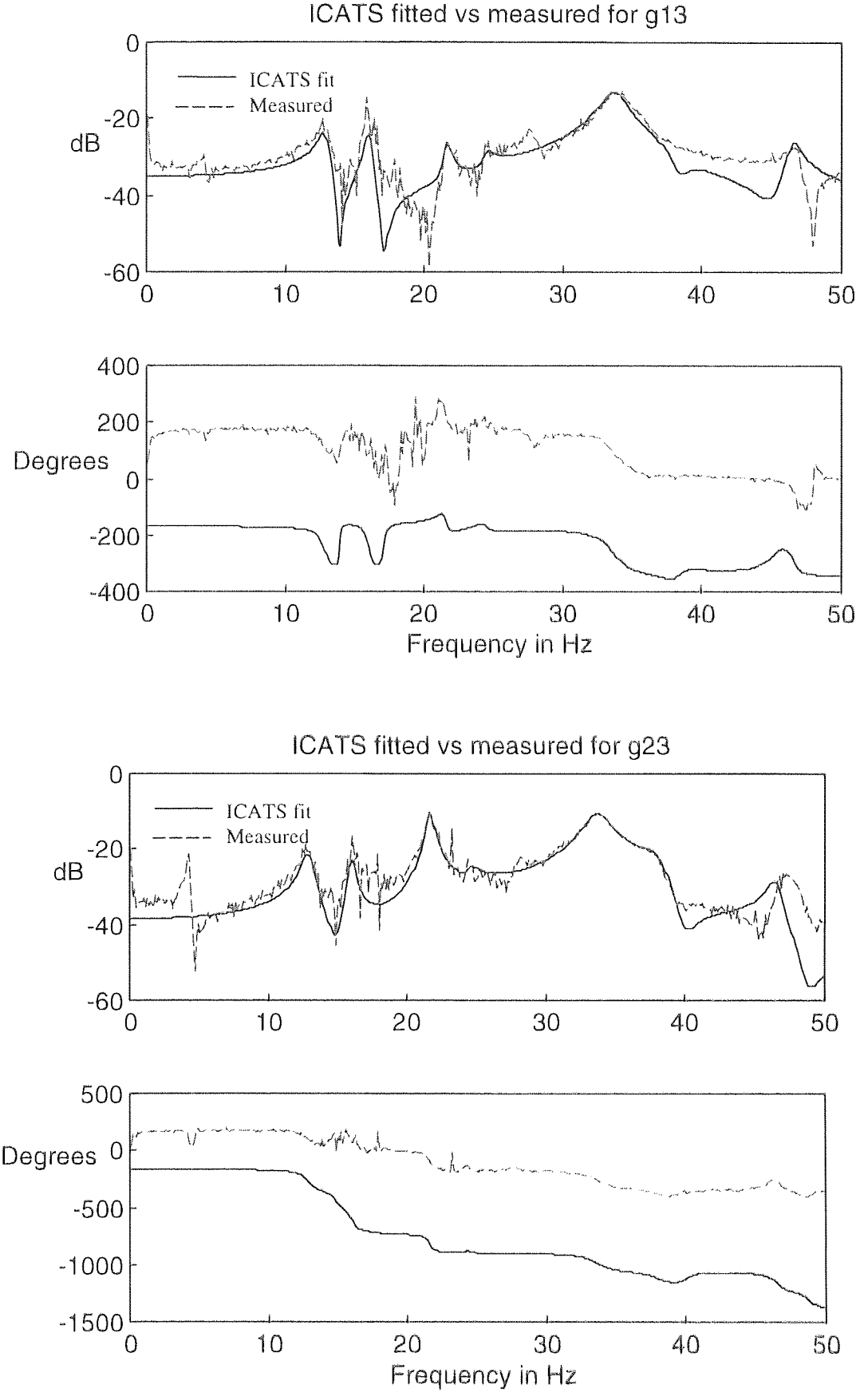

Figure C.3a Bode plots of g_{13} and g_{23} of measured and ICATS fit

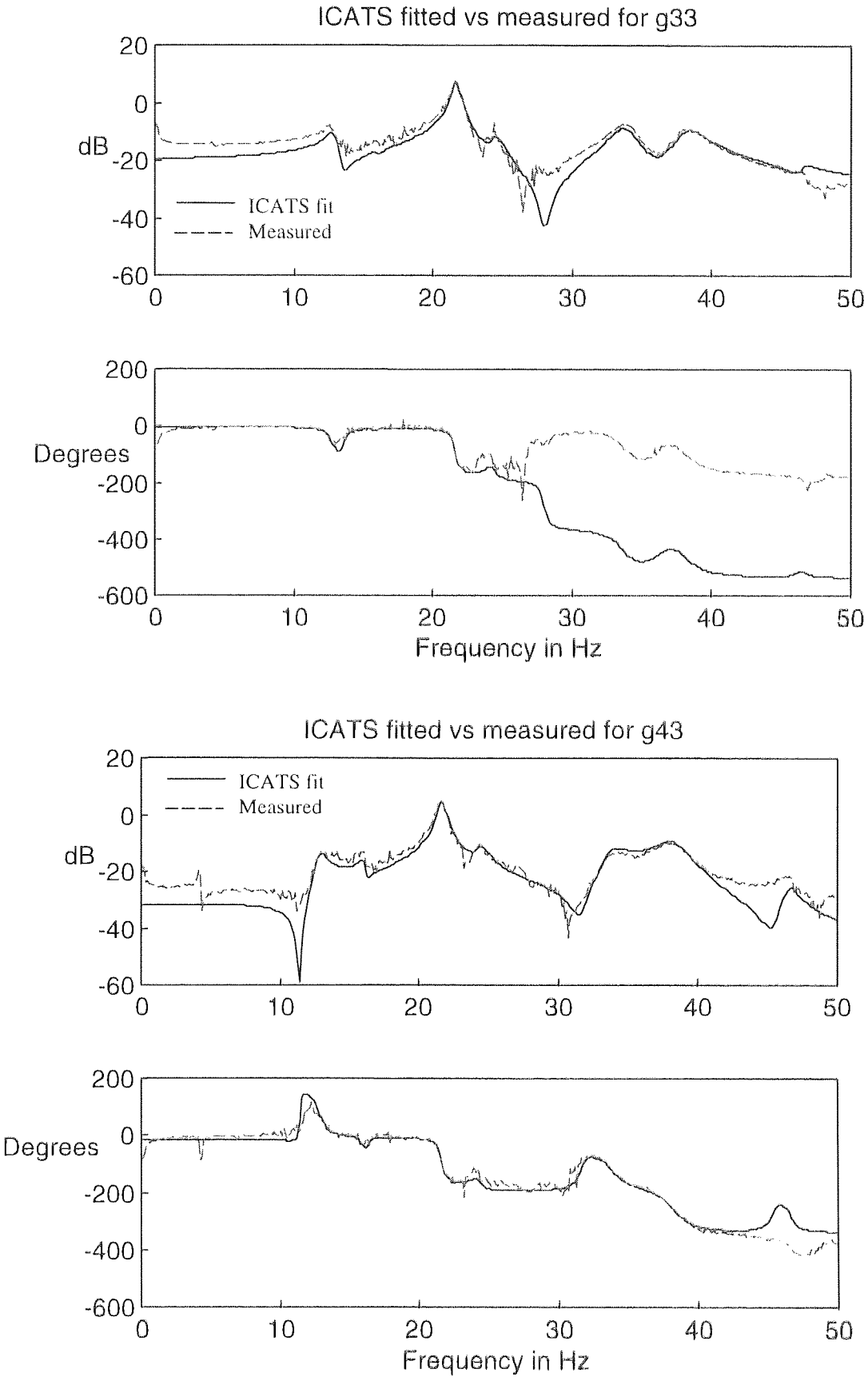

Figure C.3b Bode plots of g_{33} and g_{43} of measured and ICATS fit

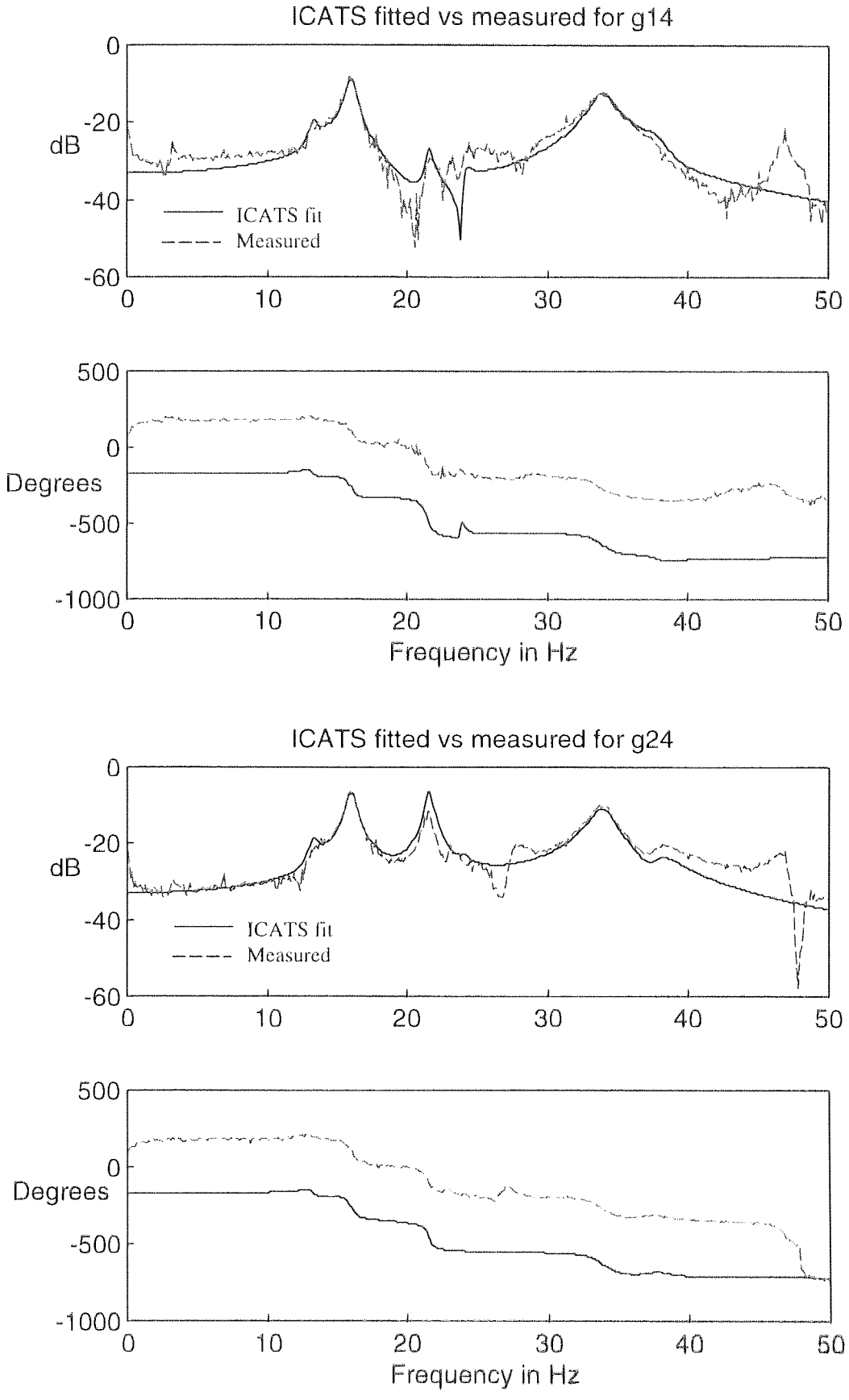

Figure C.4a Bode plots of g_{14} and g_{24} of measured and ICATS fit

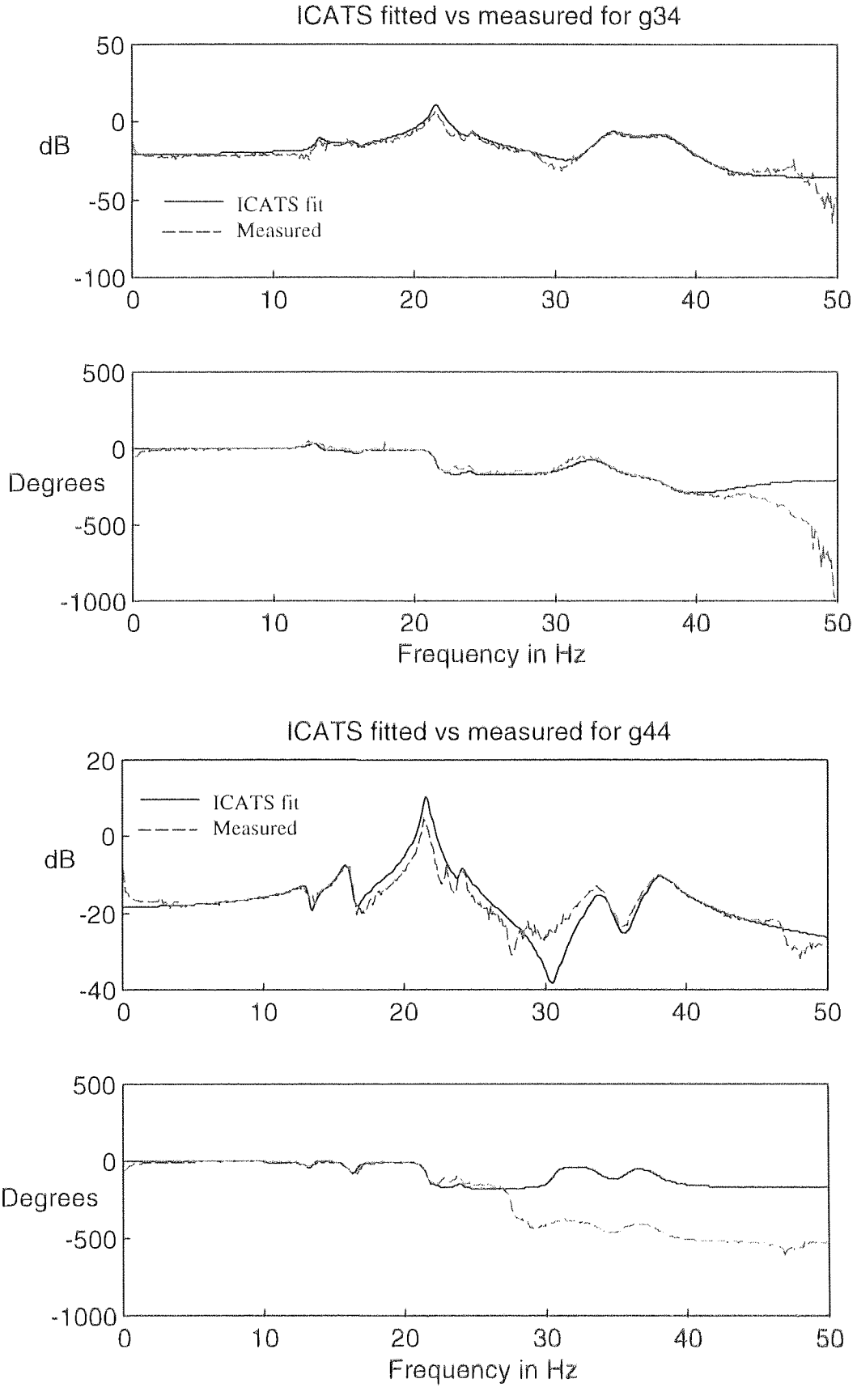

Figure C.4b Bode plots of g_{34} and g_{44} of measured and ICATS fit

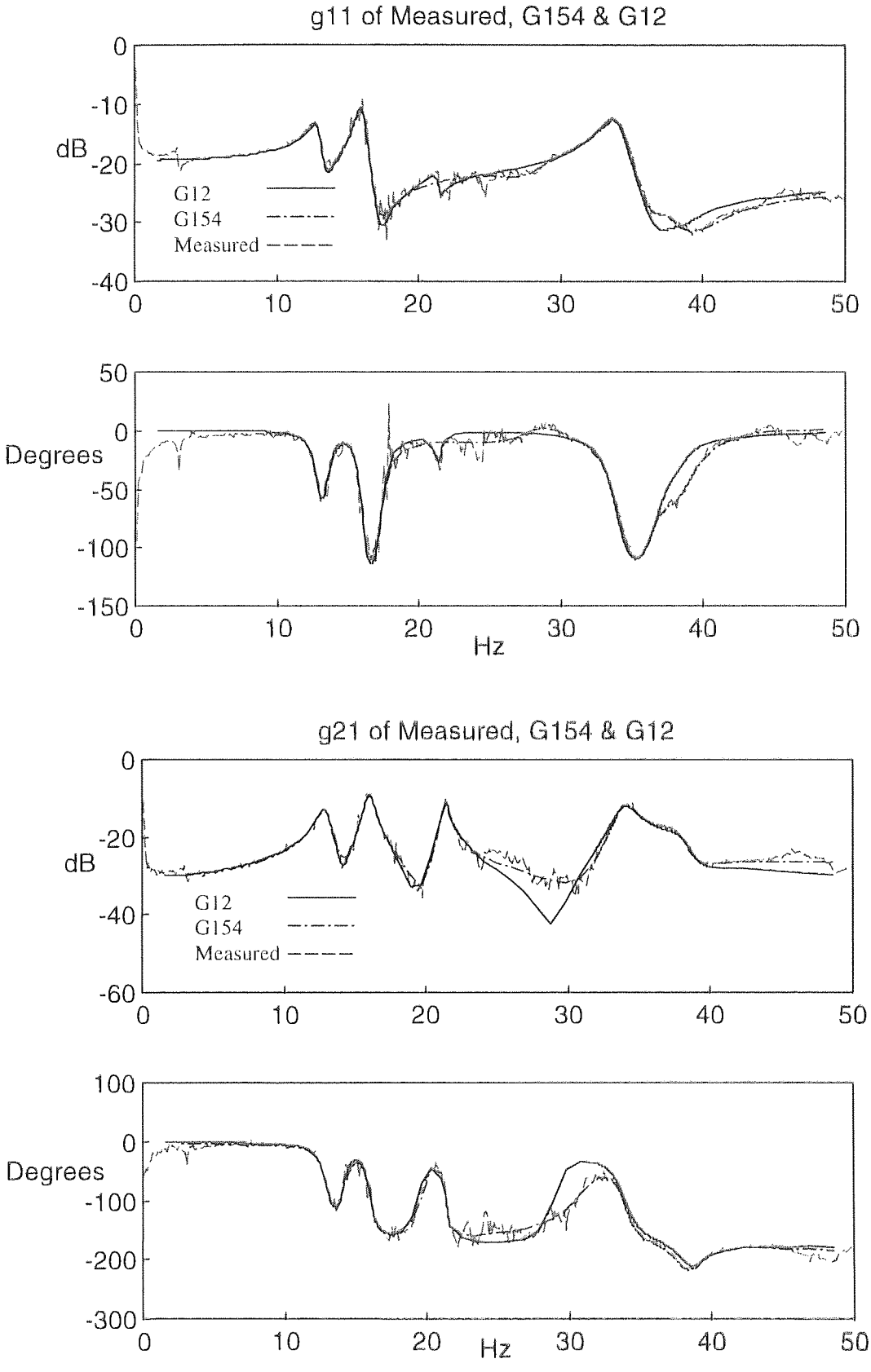

Figure C.5a Bode plots of g_{11}, g_{21} of Measured, $\mathbf{G}_{154}$ and $\mathbf{G}_{12}$

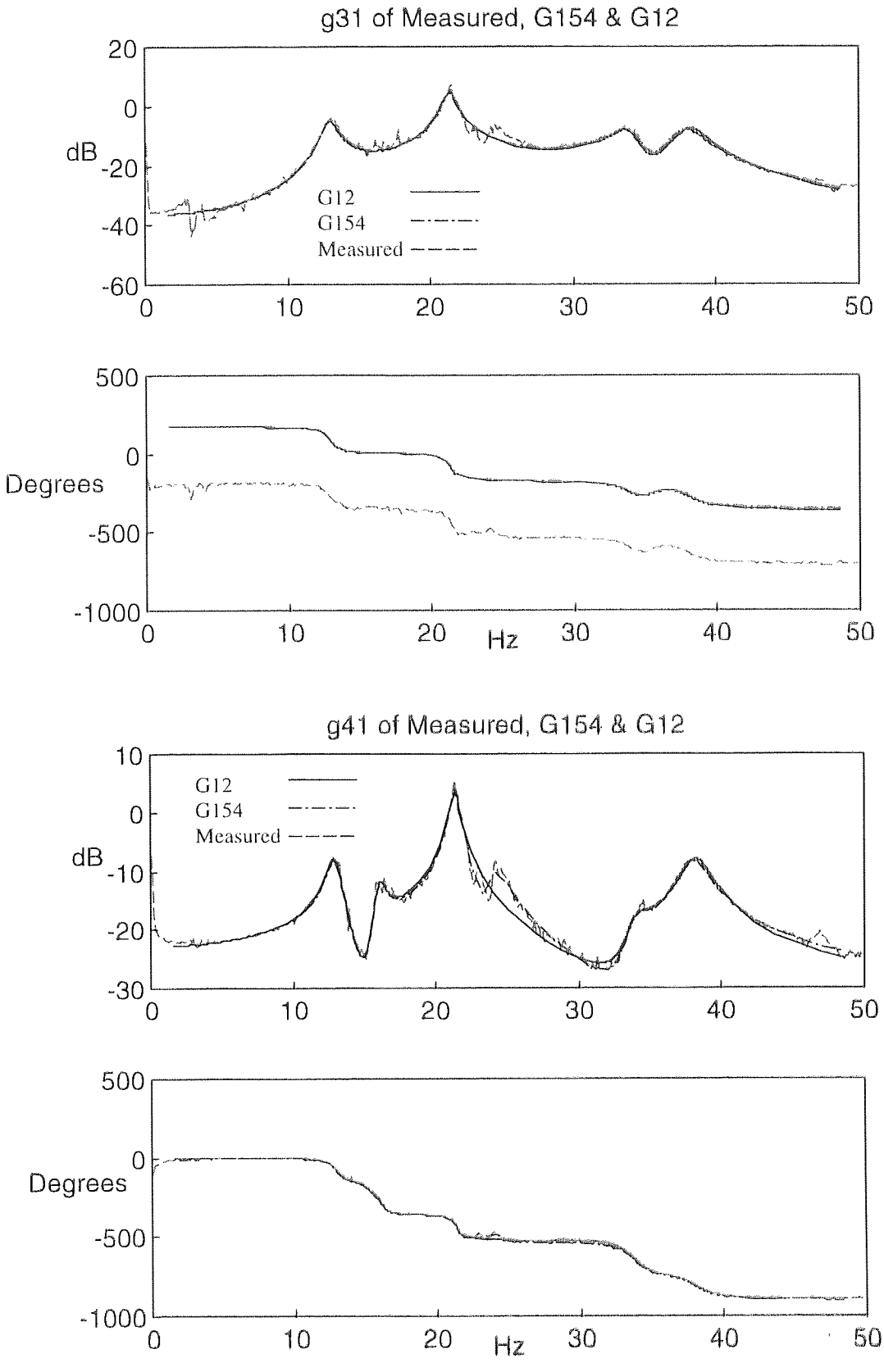

Figure C.5b Bode plots of g_{31}, g_{41} of Measured, G_{154} and G_{12}

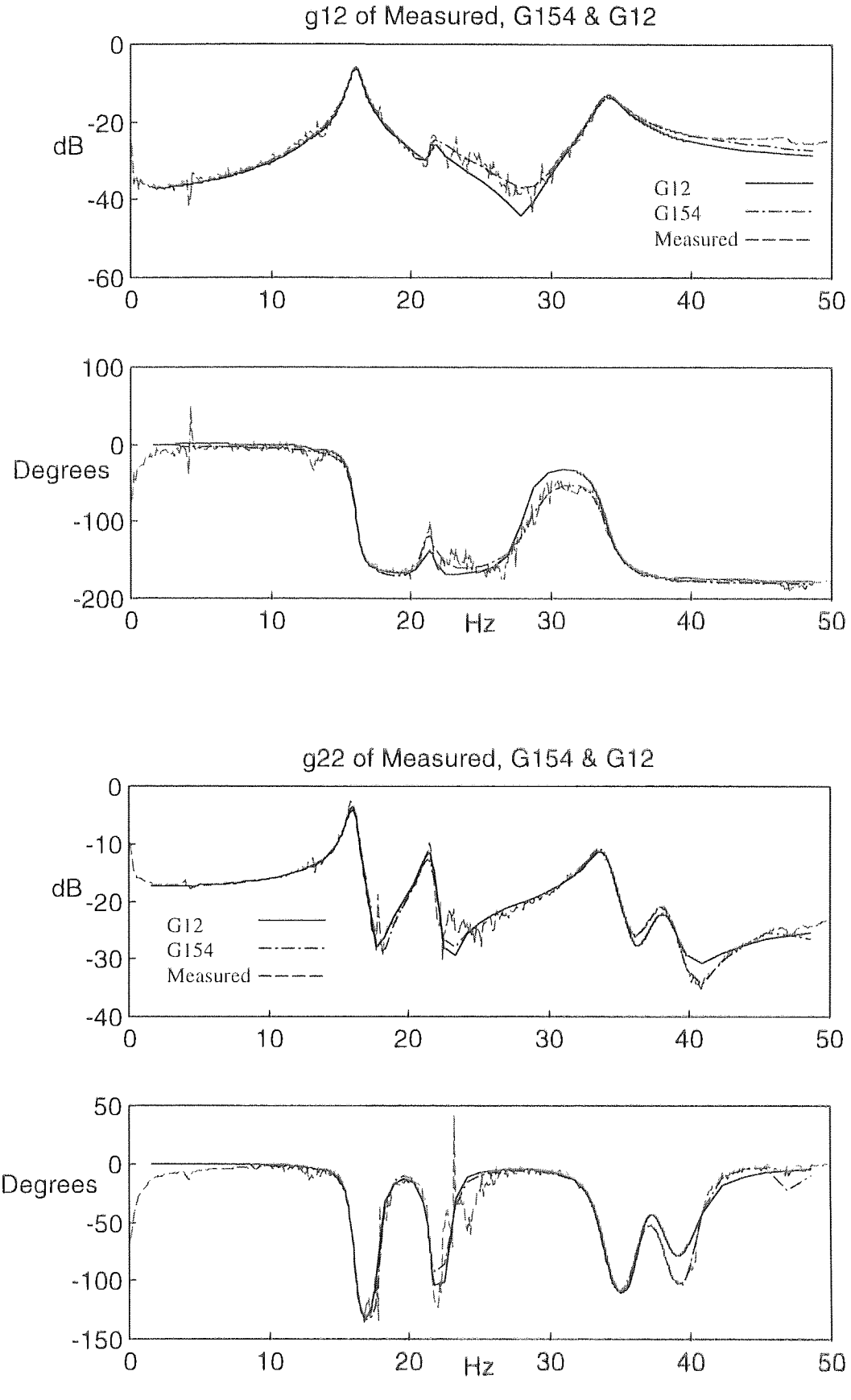

Figure C.6a Bode plots of g_{12}, g_{22} of Measured, G_{154} and G_{12}

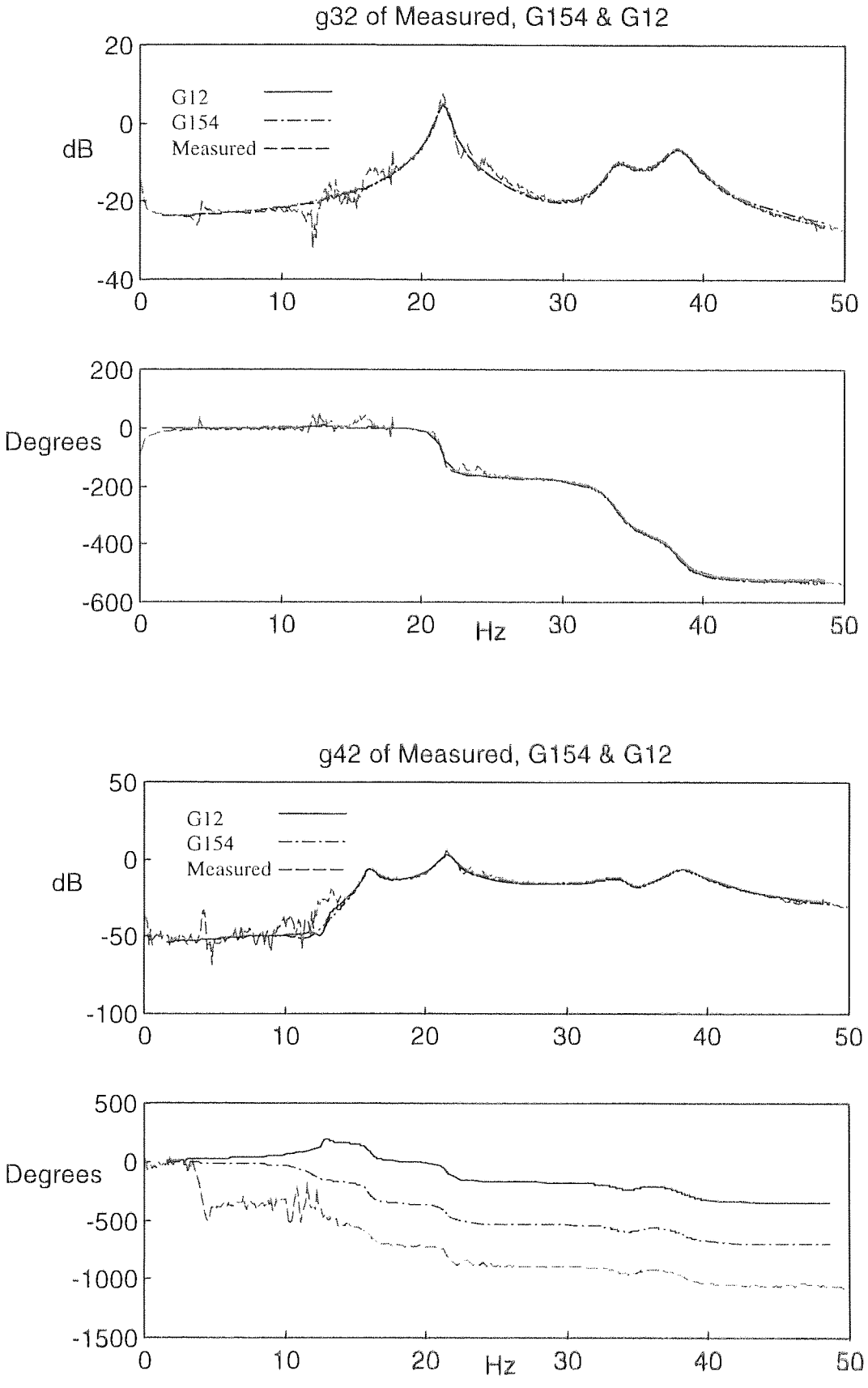

Figure C.6b Bode plots of g_{32}, g_{42} of Measured, $\mathbf{G}_{154}$ and $\mathbf{G}_{12}$

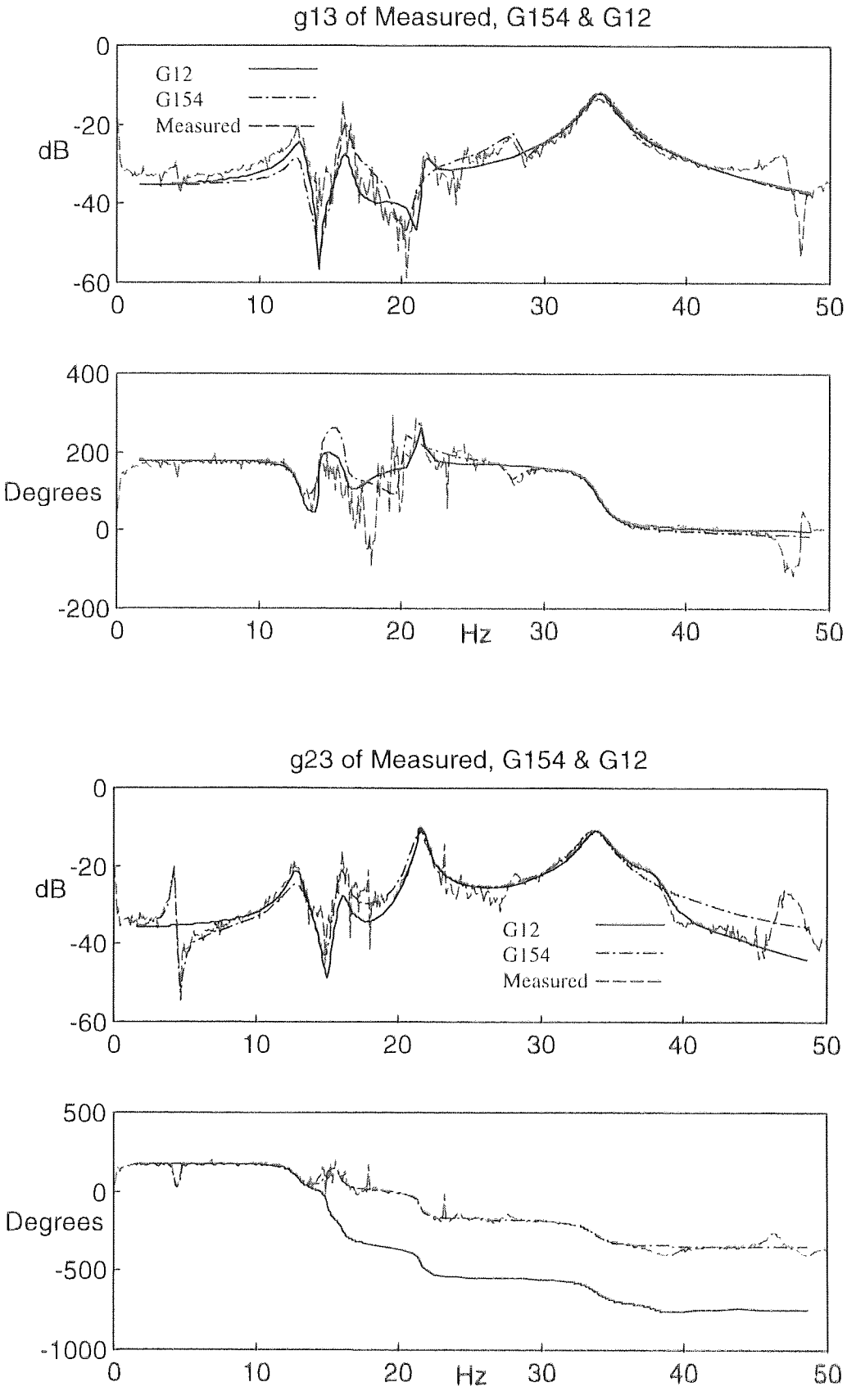

Figure C.7a Bode plots of g_{13}, g_{23} of Measured, $\mathbf{G}_{154}$ and $\mathbf{G}_{12}$

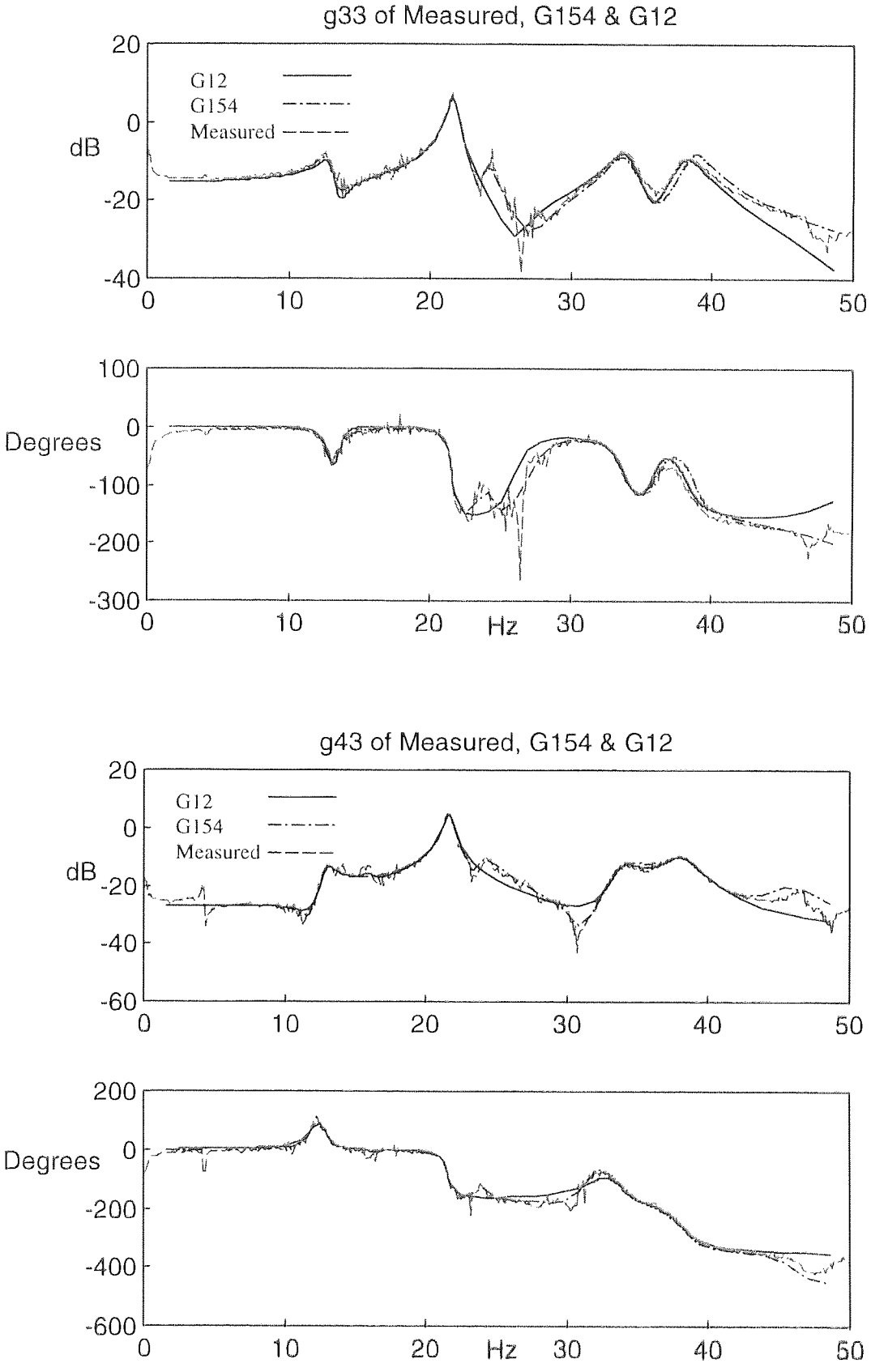

Figure C.7b Bode plots of g_{33}, g_{43} of Measured, $\mathbf{G}_{154}$ and $\mathbf{G}_{12}$

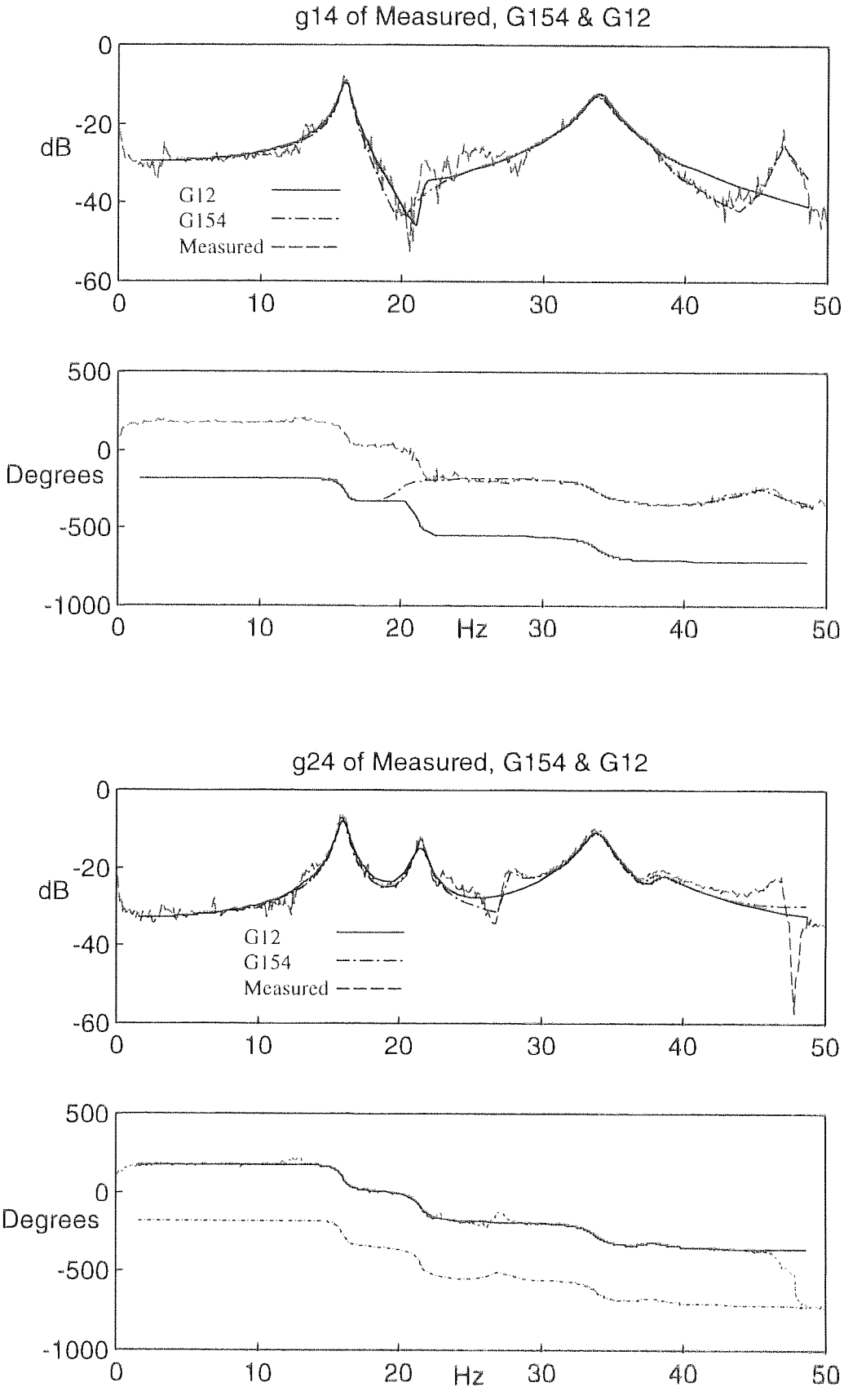

Figure C.8a Bode plots of g_{14}, g_{24} of Measured, G_{154} and G_{12}

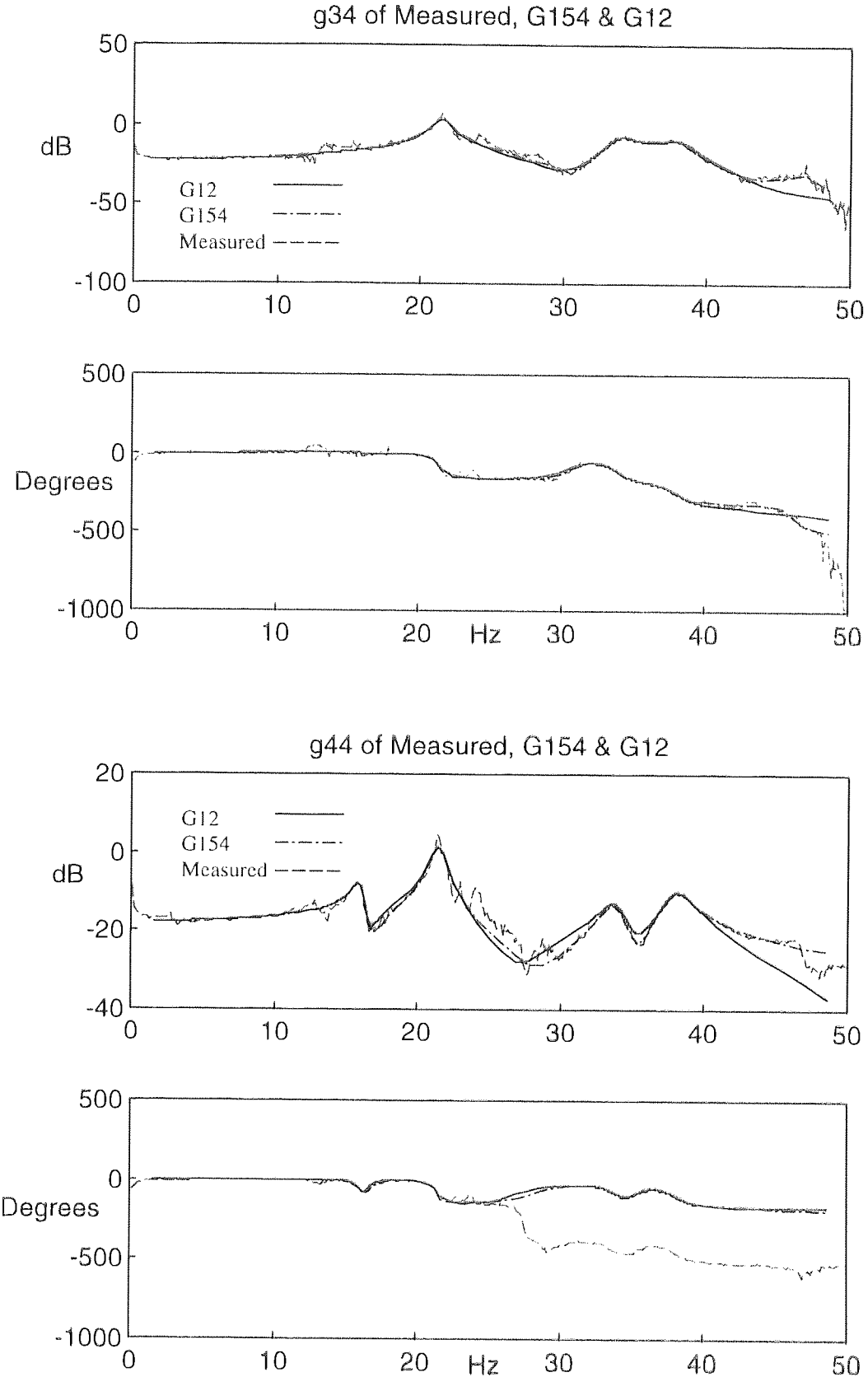

Figure C.8b Bode plots of g_{34}, g_{44} of Measured, $\mathbf{G}_{154}$ and $\mathbf{G}_{12}$

APPENDIX D

SMALL GAIN THEOREM

D.1 Introduction

The General Nyquist (Stability) Theorem and the Small Gain Theorem are included for completeness. The former is needed in the proof of the latter and the latter to show the common framework relating "classical" $\mathcal{H}_\infty$ (Tøffner-Clausen, 1996) robust control theory and the more current μ-synthesis robust control theory. Its use in vibration will also be highlighted.

The MIMO Nyquist theorem is an extension of the classical Nyquist stability theorem. Let $\mathbf{L}(s)$ represent the Loop transfer function as shown in Figure D.1.

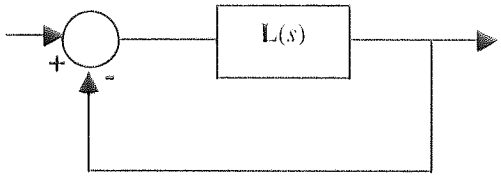

Figure D.1 A unity feedback system

The Return Difference is given in (D.1) and its determinant is given by MacFarlane (1970) in (D.2).

$$\mathbf{F}(s) = (\mathbf{I} + \mathbf{L}(s)) \tag{D.1}$$

$$|\mathbf{F}(s)| = \frac{\text{closed loop characteristic polynomial}}{\text{open loop characteristic polynomial}} \tag{D.2}$$

As s traverses clockwise along the closed D-contour in the closed Right-Half s-plane, the Nyquist plot of $|\mathbf{F}(s)|$ can be generated.

D.2. Theorem D.1 Generalised (MIMO) Nyquist Theorem

Let P_{ol} represents the number of open loop unstable poles of $\mathbf{L}(s)$. The closed loop system given in Figure D.1 is stable if and only if the Nyquist plot of $|\mathbf{F}(s)|$

i) makes P_{ol} anti-clockwise encirclements of the origin, and

ii) does not pass through the origin.

In the simple case of $P_{ol} = 0$, if the Nyquist plot of $|\mathbf{F}(s)|$ does not encircle or pass through the origin means that RHP of the s-plane enclosed by D-contour does not contain zeros of the closed loop characteristic polynomial. And hence from (D.2), $|\mathbf{F}(s)| \neq 0$.

The Small Gain Theorem is a very general theorem that gives sufficient conditions for which a bounded input will give a bounded output (Desoer and Vidyasagar, 1975). However it is used very often to derive robust stability tests for different uncertainty models. The most basic (small gain) theorem is given in terms of the spectral radius $\rho(L(j\omega))$, which is defined for each frequency as the maximum magnitude of the eigenvalue

$$\rho(L(j\omega)) = \max_i | \lambda_i (L(j\omega)) | \qquad (D.3)$$

D.3 Theorem D.2 The Small Gain Theorem (one version)

Assume that a system given by $\mathbf{L}(s)$ is stable. Then the closed loop system is stable if

$$\rho(\mathbf{L}(j\omega)) < 1 \qquad \forall\omega \qquad (D.4)$$

Proof. Let the closed loop system be unstable and (D.4) be true. From Theorem D.1, an unstable closed loop system will have $|\mathbf{F}(s)|$ encircling the origin. Then there exists a gain $\varepsilon \in (0,1]$, and a frequency ω^* such that

$$|\mathbf{I} + \varepsilon\, \mathbf{L}(j\omega^*)| = 0.$$

$$\Leftrightarrow \prod \lambda_i(\mathbf{I} + \varepsilon\, \mathbf{L}(j\omega^*)) = 0$$

$$\Leftrightarrow 1 + \varepsilon\, \lambda_i(L(j\omega^*)) = 0 \qquad \text{for some i.}$$

$$\Leftrightarrow \lambda_i(L(j\omega^*)) = -\frac{1}{\varepsilon} \qquad \text{for some i.}$$

$$\Rightarrow | \lambda_i(L(j\omega^*)) | \geq 1 \qquad \text{for some i.}$$

The last statement contradicts the condition given in (D.4). So the spectral radius less than one is a sufficient condition. It is quite intuitive when one considers that if all the

eigenvalues are less than one for all frequencies, then any signal perturbation will eventually die off and the system will be stable.

A more general requirement can be obtained from the relationship

$\rho(\mathbf{L}) \leq \| \mathbf{L} \|$ for any matrix norm $\|\bullet\|$ satisfying the $\|\mathbf{A}\cdot\mathbf{B}\| \leq \|\mathbf{A}\|\cdot\|\mathbf{B}\|$

Hence for any stable system $\mathbf{L}(s)$, the closed loop system is stable if

$$\| \mathbf{L} \| < 1 \qquad \forall\omega \qquad (D.5)$$

Since any induced norm also satisfies the above two conditions, it can be used in lieu of the spectral radius.

D.4 Equivalence of robust stability and $\mathcal{H}_\infty$ control problem

We can examine the structure shown in Figure 3.8 and how see the robust stability problem and the $\mathcal{H}_\infty$ control problem are equivalent through the use of the Small Gain Theorem. Part of the figure is redrawn here as Figure D.2, without the subscript 'M' for Δ.

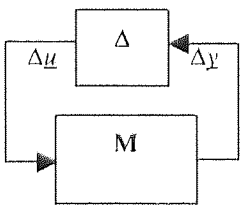

Figure D.2 The M-Δ block problem

The loop transfer function $\mathbf{L} = \mathbf{M}\cdot\Delta$. A version of the Small Gain Theorem can be applied to the system shown in Figure D.2.

Let $\mathbf{M}(s)$ be a stable system and $\gamma>0$. Then the system given in Figure D.2 is physically realisable and internally stable for the set of all stable complex matrices $\Delta(s)$ with

i. $\|\Delta\|_\infty \leq 1/\gamma$ if and only if $\|\mathbf{M}\|_\infty < \gamma$

ii. $\|\Delta\|_\infty < 1/\gamma$ if and only if $\|\mathbf{M}\|_\infty \leq \gamma$

Both norms of Δ and $\mathbf{M}$ cannot be equal to 1 at the same time as this violates (D.5). So if the product $\|\mathbf{M}\|_\infty \cdot \|\Delta\|_\infty < 1$, the closed loop system will be stable. In a sense the above theorem gives a margin of stability. In most cases, $\Delta(s)$ is normally scaled so that $\|\Delta\|_\infty \leq 1$, and the necessary and sufficient condition for closed loop stability is $\|\mathbf{M}\|_\infty < 1$.

The general LFT framework given by Figure 3.7 can be redrawn as Figure E.3.

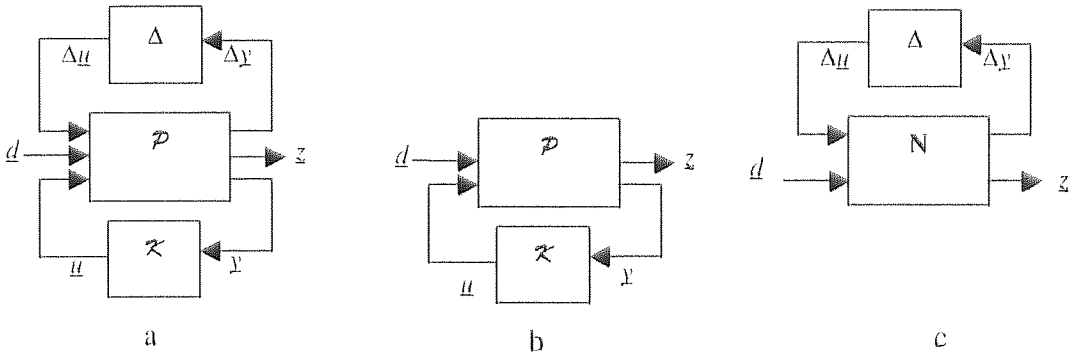

Figure D.3 General LFT framework

In Figure D.3(a) if $\Delta=0$, we have the standard $\mathcal{H}_\infty$ control problem as shown in Figure D.3(b). In Figure D.3(a), let $\mathbf{N} = F_l(\mathcal{P},\mathcal{K})$, and hence in Figure D.3(c), if $\underline{d}=0$ we have the standard robust stability problem. If $\Delta(s)$ is a full complex block, the two problems are equivalent as far as the Small Gain Theorem is concerned. Thus a solution to the $\mathcal{H}_\infty$ control problem is the key to robust stability problem.

D.5 Application to the vibration problem of Chapter Three

For the model derived in chapter three and represented by Figure 3.7, the closed system with controller $\mathcal{K}$, is given by

$$\mathbf{M}(s)=(I+\mathbf{G}_0\cdot\mathcal{K})^{-1}\cdot\mathbf{G}_0\cdot\mathcal{K}$$

It is possible to evaluate the stability of the closed loop system for a set of designed controllers against the uncertainty introduced by the flexible dynamics of the base structure. This uncertainty can be regarded as a perturbation to the nominal system $\mathbf{M}(s)$.

The perturbation is given by $\Delta_M = (\mathbf{G}_o\text{-}\mathbf{I})\cdot\mathbf{K}\cdot\mathbf{R}_{mf}$, where $\|\Delta_M\|_\infty \leq \gamma$. Applying the small gain theorem the closed loop system given by $\mathbf{M}(s)$ will stable if and only if $\|\mathbf{M}\|_\infty < 1/\gamma$.

Since the machine on the test bed dynamics, $\mathbf{G}_o$, is known, the condition $\|\Delta_M\|_\infty \leq \gamma$ can be translated to finding a bound on $\|\mathbf{K}\cdot\mathbf{R}_{mf}\|_\infty$ or $\|\mathbf{R}_{mf}\|_\infty$. For example, if $\|\mathbf{G}_o\text{-}\mathbf{I}\|_\infty < \beta$, then $\|\mathbf{K}\cdot\mathbf{R}_{mf}\|_\infty \leq \gamma/\beta$, subject to an upper bound of 0.5 as discussed in chapter 3.

D.6 Summary

The thesis considers the $\mathcal{H}_\infty$ control problem as part and parcel of robust control theory. With this framework it will be difficult, though, to efficiently test for robust stability using the Small Gain Theorem in the form given. One would have to search through an infinite set of allowable Δ. On the other hand, for the model discussed in chapter three, one could check the design of the flexible base structure and ascertain the value of $\|\Delta_M\|_\infty$ and then determine if the designed controller has robust stability or not.

For the general case, recent developments in μ-synthesis had made available testable methods using the structured singular value (Stein and Doyle, 1991). This approach is not adopted in the thesis as a simpler and more direct approach was used to design the required controller.

APPENDIX E

ANALOGUE CONTROLLER CIRCUIT AND THE

RESPONSES AT 1330 AND 1440 RPM

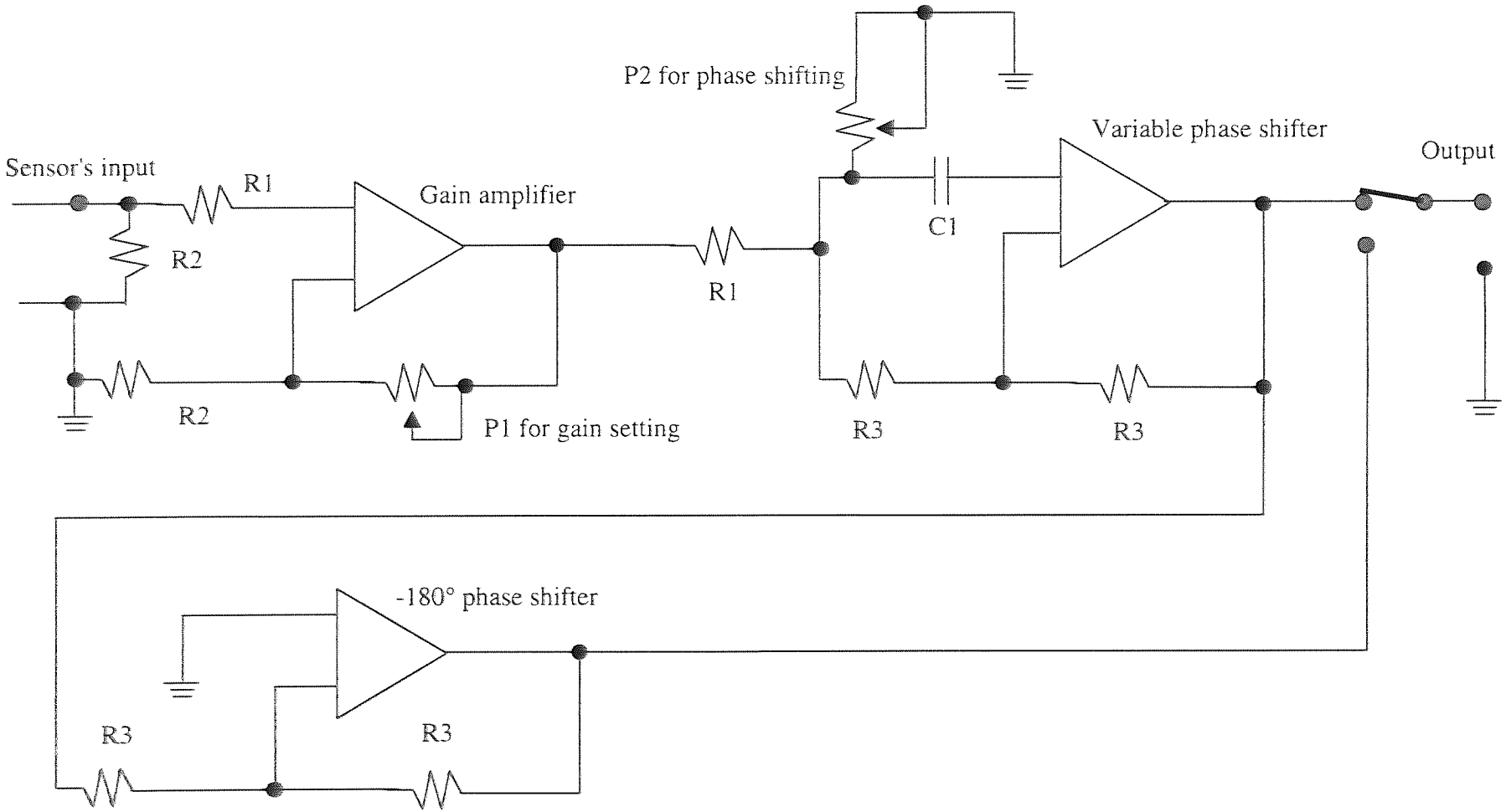

Figure E.1 The variable phase shifter circuit used as a local analogue controller in active vibration isolation experiment

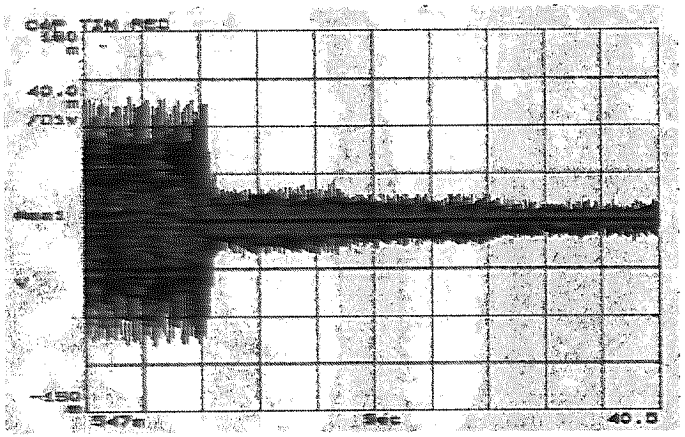

Mount #1 response for 1340 rpm

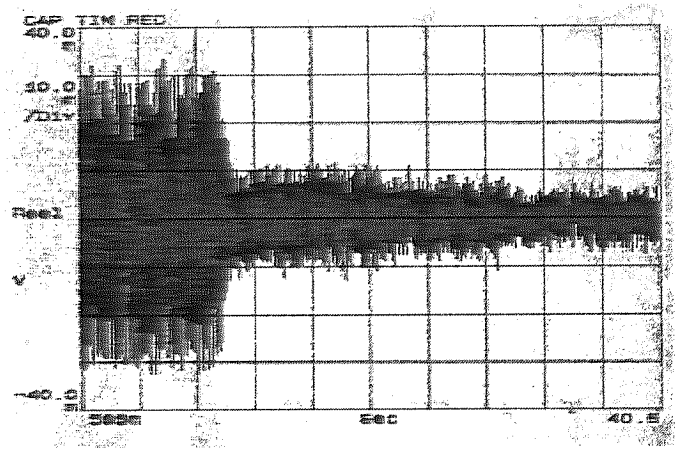

Mount #2 response for 1340 rpm

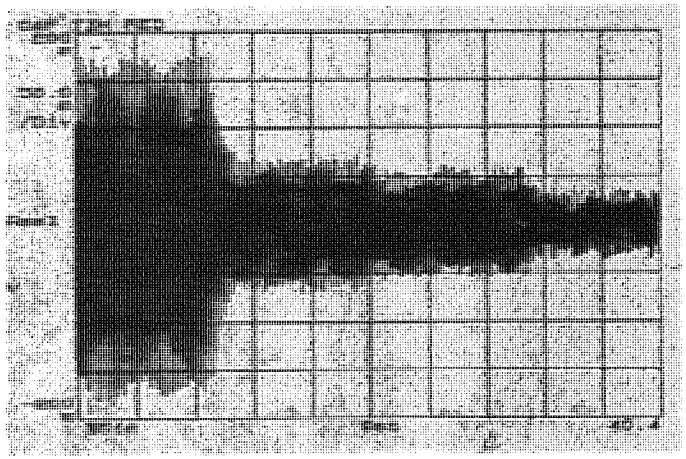

Mount #3 response for 1340 rpm

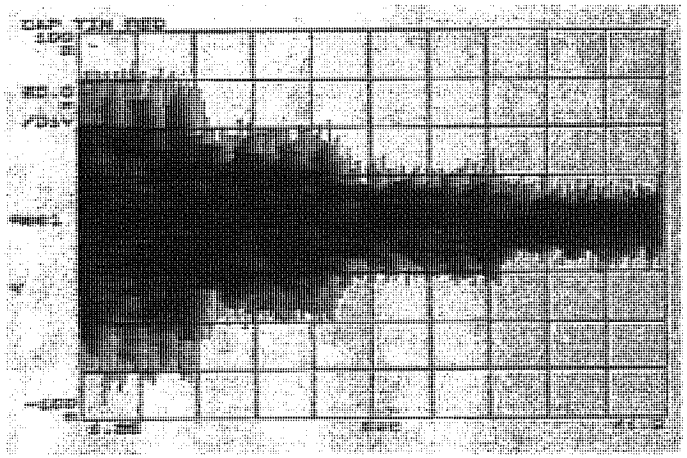

Mount #4 response for 1340 rpm

Figure E.2 Responses at the mount locations using analogue controller at 1340 rpm

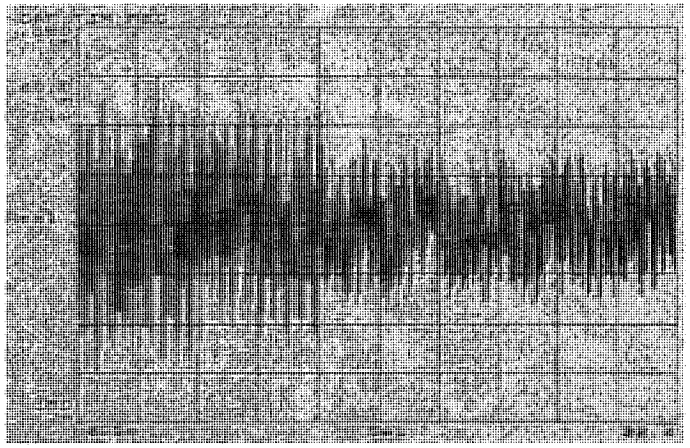

Mount #1 response at 1440 rpm

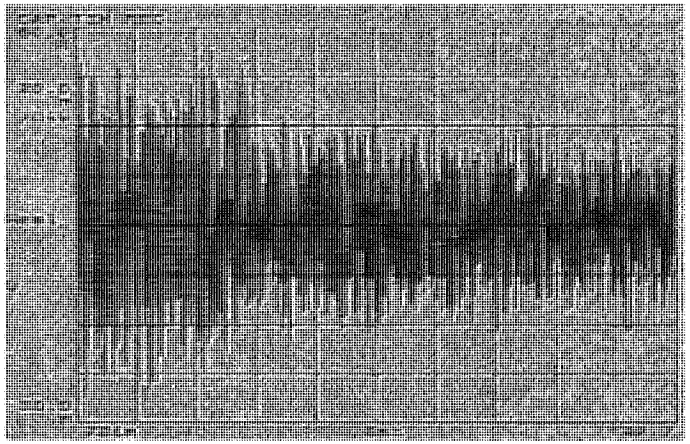

Mount #2 response at 1440 rpm

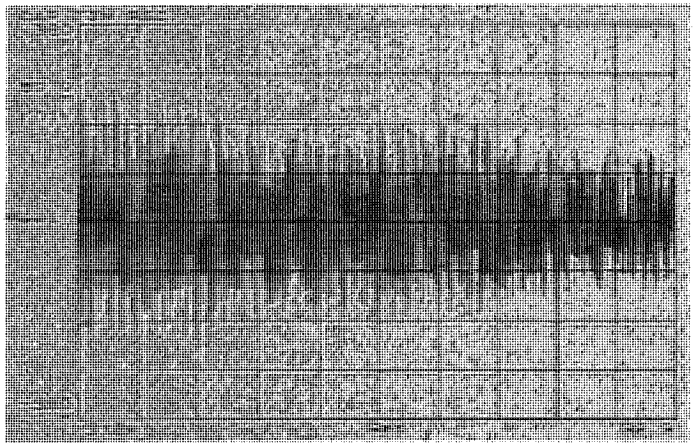

Mount #3 response at 1440 rpm

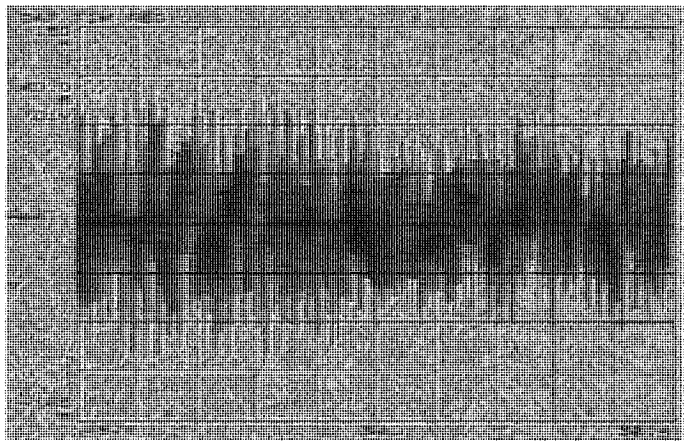

Mount #4 response at 1440 rpm

Figure E.3 Responses at mount locations using analogue controllers at 1440 rpm